Vol. 62 September, 1958 No. 9

THE JOURNAL OF PHYSICAL CHEMISTRY

(Registered in U. S. Patent Office)

CONTENTS

NOTES

THE JOURNAL OF PHYSICAL CHEMISTRY

(Registered in U. S. Patent Office)

Published monthly by the American Chemical Society at 20th and Northampton Sts., Easton, Pa.

Second-class mail privileges authorized at Easton, Pa.

The *Journal of Physical Chemistry* is devoted to the publication of selected symposia in the broad field of physical chemistry and to other contributed papers.

Manuscripts originating in the British Isles, Europe and Africa should be sent to F. C. Tompkins, The Faraday Society, 6 Gray's Inn Square, London W. C. 1, England.

Manuscripts originating elsewhere should be sent to W. Albert Noyes, Jr., Department of Chemistry, University of Rochester, Rochester 20, N. Y.

Correspondence regarding accepted copy, proofs and reprints should be directed to Assistant Editor, Allen D. Bliss, Department of Chemistry, Simmons College, 300 The Fenway, Boston 15, Mass.

Business Office: Alden H. Emery, Executive Secretary, American Chemical Society, 1155 Sixteenth St., N. W., Washington 6, D. C.

Advertising Office: Reinhold Publishing Corporation, 430 Park Avenue. New York 22, N. Y.

Articles must be submitted in duplicate, typed and double spaced. They should have at the beginning a brief Abstract, in no case exceeding 300 words. Original drawings should accompany the manuscript. Lettering at the sides of graphs (black on white or blue) may be pencilled in and will be typeset. Figures and tables should be held to a minimum consistent with adequate presentation of information. Photographs will not be printed on glossy paper except by special arrangement. All footnotes and references to the literature should be numbered consecutively and placed in the manuscript at the proper places. Initials of authors referred to in citations should be given. Nomenclature should conform to that used in *Chemical Abstracts*, mathematical characters marked for italic, Greek letters carefully made or annotated, and subscripts and superscripts clearly shown. Articles should be written as briefly as possible consistent with clarity and should avoid historical background unnecessary for specialists.

Notes describe fragmentary or incomplete studies but do not otherwise differ fundamentally from articles and are subjected to the same editorial appraisals as are articles. In their preparation particular attention should be paid to brevity and conciseness. Material included in Notes must be definitive and may not be republished subsequently.

Communications to the Editor are designed to afford prompt preliminary publication of observations or discoveries whose value to science is so great that immediate publication is imperative. The appearance of related work from other laboratories is in itself not considered sufficient justification for the publication of a Communication, which must in addition meet special requirements of timeliness and significance. Their total length may in no case exceed 500 words or their equivalent. They differ from Articles and Notes in that their subject matter may be republished.

Symposium papers should be sent in all cases to Secretaries of Divisions sponsoring the symposium, who will be responsible for their transmittal to the Editor. The Secretary of the Division by agreement with the Editor will specify a time after which symposium papers cannot be accepted. The Editor reserves the right to refuse to publish symposium articles, for valid scientific reasons. Each symposium paper may not exceed four printed pages (about sixteen double spaced typewritten pages) in length except by prior arrangement with the Editor.

Remittances and orders for subscriptions and for single copies, notices of changes of address and new professional connections, and claims for missing numbers should be sent to the American Chemical Society, 1155 Sixteenth St., N. W., Washington 6, D. C. Changes of address for the *Journal of Physical Chemistry* must be received on or before the 30th of the preceding month.

Claims for missing numbers will not be allowed (1) if received more than sixty days from date of issue (because of delivery hazards, no claims can be honored from subscribers in Central Europe, Asia, or Pacific Islands other than Hawaii), (2) if loss was due to failure of notice of change of address to be received before the date specified in the preceding paragraph, or (3) if the reason for the claim is "missing from files."

Subscription Rates (1958): members of American Chemical Society, $8.00 for 1 year; to non-members, $16.00 for 1 year. Postage free to countries in the Pan American Union; Canada, $0.40; all other countries, $1.20. Single copies, current volume, $1.35; foreign postage, $0.15; Canadian postage $0.05. Back volumes (Vol. 56-59), $15.00 per volume; (starting with Vol. 60) $18.00 per volume; foreign postage $1.20, Canadian, $0.40; $1.75 per issue, foreign postage $0.15, Canadian postage $0.05.

The American Chemical Society and the Editors of the *Journal of Physical Chemistry* assume no responsibility for the statements and opinions advanced by contributors to THIS JOURNAL.

THE JOURNAL OF PHYSICAL CHEMISTRY

(Registered in U. S. Patent Office) (© Copyright, 1958, by the American Chemical Society)

VOLUME 62 SEPTEMBER 24, 1958 NUMBER 9

PRECIPITATION FROM SUPERSATURATED SOLUTIONS OF INSOLUBLE AND SPARINGLY SOLUBLE METAL SALTS. PART I. THE PARTICLE SIZE OF CRYSTALLINE PRECIPITATES

BY A. PACKTER

106 Howberry Road, Middlesex, England

Received June 20, 1956

The factors that determine the crystal size of precipitates from supersaturated insoluble metal salt solutions at different supersaturation are discussed. The experimental data are best explained by a two-stage consecutive nucleation and condensation mechanism for precipitation, rather than by a sol coagulation mechanism. Duke and Brown's analysis for such a former process has been extended to take into account those factors other than interfacial energy, that may determine the rate of the nucleation process. At any supersaturation, the crystal size of precipitates of salts of widely different solubilities is mainly determined by the solute concentration, rather than by the rate constants for nucleation or crystal growth.

Introduction

The properties of insoluble metal salt precipitates from supersaturated aqueous solution have been studied by von Weimarn, Odén, Kolthoff and Balarev,[1-4] and more recently by Težak.[5] The factors that determine the stability of such solutions—*i.e.*, the induction period that generally precedes precipitation—also have been investigated very extensively; and Nielsen recently has reviewed all the data on this subject. Two main theories have been developed to explain the precipitation of insoluble metal salts. Balarev[4] has suggested that growth of the precipitate crystals occurs by the coalescence of "submicrons" of colloidal size present in the supersaturated solution, by a coagulation mechanism; and many other workers, although less explicitly, have also assumed a colloidal nature for supersaturated metal salt solutions.[1,3,6-7] On the basis of this theory, the final crystal size would depend mainly on the degree of aggregation or "polymerization," which in turn would be determined by the rate of coagulation of the submicrons.[8,9]

On the other hand, van Hook,[10a] La Mer[10b] and Dunning[10c] have proposed that the crystal growth takes place by condensation of the ions of the metal salt onto small nuclei that are first formed in the supersaturated solution. The rate determining step for nucleation is the formation of a "cluster" or "embryo" that consists of a small number of reacting ions. The kinetics of such a consecutive and autocatalytic reaction have been analyzed by several workers,[11-15] who showed that the average crystal size of the precipitate depends on the relative rates of the nucleation and growth processes, and as some high power of the concentration of reacting ions. The rate of nucleation in turn varies with the supersaturation according to the Volmer–Weber theory.

(1) (a) P. P. von Weimarn, *Chem. Revs.*, **2**, 71 (1926); (b) *Kolloid Z.*, **2**, 199, 230, 275 (1908); (c) **3**, 282 (1909); (d) **42**, 305 (1927).

(2) S. Odén, *Arkiv. Kemi. Min. Geol.*, **9**, 25 (1926).

(3) (a) I. M. Kolthoff, *et al.*, *J. Am. Chem. Soc.*, **56**, 1264, 1658 (1934); **57**, 597 (1935); **58**, 121 (1936); **60**, 39, 197, 499, 505, 508 (1938).

(4) (a) D. I. Balarev, *Kolloid-Beih.*, **50**, 1 (1939); (b) *C. A.*, **49**, 12910ef (1955).

(5) (a) B. Težak, *et al.*, *Z. physik. Chem.*, **A175**, 284 (1936); (b) **A190**, 257 (1942); (c) THIS JOURNAL, **57**, 301 (1953); (d) *J. Colloid Sci.* (Suppl.), 18 (1954).

(6) A. Packter and R. Matalon, *Disc. Faraday Soc.*, **18**, 161 (1955).

(7) (a) E. N. Gapon, *J. Russ. Phys. Chem.*, **61**, 512 (1929); (b) E. Pozner, *J. Phys. Chem. U.S.S.R.*, **13**, 889 (1939); (c) W. Takami. *Kagaku*, **23**, 428 (1953); (d) F. Brescia, *et al.*, *J. Am. Chem. Soc.*, **76**, 9946 (1954).

(8) H. Dorstal, *Monats.*, **70**, 334 (1937).

(9) F. C. Collins and G. E. Kimball, *J. Colloid Sci.*, **4**, 425 (1949).

(10) (a) A. van Hook, THIS JOURNAL, **45**, 422, 879, 1194 (1941); (b) V. La Mer and R. H. Dinegar, *J. Am. Chem. Soc.*, **76**, 2124 (1951); (c) W. J. Dunning, *Disc. Faraday Soc.*, **5**, 79 (1949).

(11) F. R. Duke and L. M. Brown, *J. Am. Chem. Soc.*, **76**, 1443 (1954).

(12) R. A. Johnson and J. D. O'Rourke, *ibid.*, **76**, 2124 (1954).

(13) (a) O. M. Todes, *Acta Physicochem. U.S.S.R.*, **13**, 617 (1940); (b) *Problem Kinetiki, Akad. Nauk, S.S.S.R.*, **7**, 91 (1949); *C. A.*, **48**, 13323i (1954).

(14) M. Roginskii, *Acta Physicochem. U.S.S.R.*, **10**, 825 (1939).

(15) S. H. Brausom and W. J. Dunning, *Disc. Faraday Soc.*, **5**, 96 (1949).

Although the particle size of a "crystalline" precipitate can be determined accurately by simple techniques over a far wider range of concentrations than can induction period, less quantitative experimental data had been presented on this property. (Von Weimarn studied only barium sulfate, lead halides and a few insoluble silver salts.) However, Duke and Brown[11] recently have extended these studies to metal chelates, Jonkers[16] and van Schulenburgh[17] have discussed the properties of microcrystalline silver bromide and ferric hydroxide precipitated at very low supersaturation, while the author[18] has presented new data on a series of crystalline "peptized" insoluble silver, copper and lead salts. It is therefore now possible to test these two theories with data on the variation of crystal size with supersaturation of precipitating solution for metal salts of a wide range of solubility.

Earlier studies on stability of supersaturated solutions are also rather unsatisfactory from a theoretical viewpoint, since most workers (including the author) have estimated rates of nucleation and of coagulation as the reciprocal of induction periods,[7-10a,10c,19] without any theoretical basis for this assumption. Johnson and O'Rourke,[12] however, have recently proved that stability depends on the rates of both nucleation and crystal growth; and it would thus be valuable to re-examine earlier data in the light of their theory,

This series of papers presents such a quantitative analysis of previous studies on crystal size and supersaturated solution stability. Earlier work on the effect of additives also will be re-evaluated. In the first paper we have studied the variation of particle size of crystalline precipitates with supersaturation. The theoretical analyses of Duke and Brown for a consecutive two-stage condensation process for precipitation has been developed further to include those factors, other than surface energy, that may affect the rate of the nucleation process: a semi-quantitative analysis of a precipitation process that occurs according to Balarev's theory also has been presented. The experimental data are best explained by the former theory.

Theoretical

We first discuss the relations between crystal number (and size) of precipitates from supersaturated solutions, and the absolute solute concentration, predicted by the two main theories proposed by previous workers.

I. Growth by Nucleation and Condensation onto Nuclei. (a) **Number of Crystals.**—Duke and Brown[11] have noted that the number N_c of precipitate crystals deposited from supersaturated metal salt solutions rises rapidly with the solute concentration (C) at intermediate and high supersaturations. For precipitation from equivalent solutions prepared by rapid mixing of the reactants, they have proposed the equation

$$N_c = \frac{0.3\rho^{4/9}}{M^{4/9}}\left(\frac{k_1}{k_2}\right) C^{m-m'} = K\left(\frac{k_1}{k_2}\right) C^{m-m'} \text{ particles/l.} \qquad (1)$$

(16) G. H. Jonkers and H. R. Kruyt, *ibid.*, **18**, 170 (1955).
(17) J. van Schulenburgh, *et al.*, *Rec. trav. chim.*, **68**, 999 (1949).
(18) A. Packter, *Z. physik. Chem.*, **207**, 210 (1957).
(19) A. E. Nielsen, *J. Colloid Sci.*, **11**, 520 (1955).

k_1 and k_2 are the rate constants for nucleation and growth onto nuclei, K is a function of M and ρ (molecular weight and specific gravity of the solute); m and m' are the orders of reaction in the nucleation and growth processes.

These workers, however, did not consider the effect of decreasing rates of nucleation (predicted by the Volmer–Becker theory on crystal growth at *low* supersaturation). We have therefore extended their analysis to take this and other factors into account.

(i) Duke and Brown assumed that the rate of nucleation at equivalent ion concentration C, $+ dN/dt = k_1C^m$ since nucleation is determined by supersaturation rather than by absolute ion concentration,[10b,15,19,20] we propose that the equation $+ dN/dt = k_1s^m$, would be more appropriate in the above analysis, where s is the supersaturation constant. [$s = (C - Cs)/C_s$, where C_s is the saturation solubility in distilled water.]

Similarly, for the rate of crystal growth, we would substitute the relation $- dN/dt = k_2a(s + 1)^{m'}.C_s^{m'}$ in place of $- dN/dt = k_2aC^{m'}$, where a's are the total surface area of the nuclei.

Equation 1 then will become

$$N_s = \frac{Kk_1s^m}{k_2C_s^{m'}(s+1)^{m'}} \text{ particles/l.} \qquad (2)$$

(ii) Recent work[10b,20] on the kinetics of crystal growth onto seeds of insoluble metal salts has confirmed that $m = 2$; *i.e.*, (2) becomes

$$N_s = \frac{Kk_1s^m}{k_2C_s^2(s+1)^2} \text{ particles/l.} \qquad (3)$$

For larger values of s, (3) then becomes

$$N_s = \frac{Kk_1s^{m-2}}{k_2C_s^2} \text{ particles/l.} \qquad (3A)$$

(iii) Earlier workers[10c] had considered that the value of k_1 was determined by the interfacial energy per unit surface area of the nucleus. Recent studies have indicated that more generally[15,21-23]

$$\log k_1 = \phi_1 - \frac{(\Delta A_1)_\sigma}{R\theta} - \frac{(\Delta A_1)_{non\sigma}}{R\theta} \qquad (4)$$

where ϕ_1 is a constant that depends on the physical properties of the salt, $(\Delta A_1)_\sigma$ is the energy of activation required to overcome the interfacial forces, and $(\Delta A_1)_{non\sigma}$ is the energy of activation required to overcome electrostatic and steric effects. (In unstirred systems the $(\Delta A_1)_{non\sigma}$ term will also include a diffusion term $(\Delta A)_{visc.}$)[24] (ΔA_1) in turn equals $\gamma\sigma r_k^2$, and varies with the supersaturation (s), while $(\Delta A_1)_{non}\sigma$ is independent of the supersaturation. (σ represents the solid–liquid surface energy per unit surface energy of the nucleus, r_k is the critical radius of the nucleus; and γ is a geometrical constant depending on the shape of the nucleus.) r_k in turn varies with s, according to the relation

(20) C. W. Davies and A. L. Jones, *Trans. Faraday Soc.*, **41**, 802 (1955).
(21) R. S. Srikantan, *J. Ind. Chem. Soc.*, **30**, 469 (1950).
(22) K. Hirano, *Busseiron i Kenkyo Fukushima*, **5**, 100 (1953); *C. A.*, **47**, 3667i (1953).
(23) R. Gopal, *J. Ind. Chem. Soc.*, **20**, 62 (1943).
(24) A. van Hook and A. J. Bruno, *Disc. Faraday Soc.*, **5**, 112 (1949).

$$\frac{2\sigma}{r_k} = \frac{\rho R\theta}{M} \ln (s + 1) \quad (5)$$

where M,ρ are the molecular weight and specific gravity of the metal salt, and θ is the absolute temperature of the supersaturated solution.

r_k falls rapidly from infinity at very low supersaturations to a limiting value of $r_k - 10$ Å. at high supersaturations,[24,25] and $(\Delta A_1)\sigma$ varies accordingly. k_1 also falls rapidly with s at low s values, but we may note that at high s values, k_1 will approach some asymptotic value, according to the relation

$$(\log k_1)_{s\to\infty} = \phi_1 - \frac{(\Delta A_1)_{\text{non}\sigma}}{R\theta} \quad (6)$$

Similarly, k_2 varies with (ΔA_2), the activation energy for crystal growth onto nuclei, according to the relation where ϕ_2 is another constant.

$$\log k_2 = \phi_2 - \frac{(\Delta A_2)}{R\theta} \quad (7)$$

To take into account the variation of k_1, with both $(\Delta A_1)\sigma$ and $(\Delta A_1)_{\text{non}}\sigma$, and the variation of the former with s, equation 2 is best expressed in a general logarithmic form (to the base 10)

$$\log N_s = \log \frac{K}{C_s^2} + \log \frac{k_1}{k_2} + \log \frac{s^m}{(s+1)^2} = (\phi_1 - \phi_2) + \log \frac{K}{C_s^2} - \frac{(\Delta A_1)\sigma}{R\theta} - \frac{(\Delta A_1)_{\text{non}}\sigma}{R\theta} + \frac{(\Delta A_2)}{R\theta} + \log \frac{s^m}{(s+1)^2} \quad (8)$$

At high s values, this relation becomes

$$\log N_s = (\phi_1 - \phi_2) + \log \frac{K}{C_s^2} + \frac{\Delta A_2}{R\theta} - \frac{(\Delta A_1)_{\text{non}}\sigma}{R\theta} + \log s^{m-2} \quad (8A)$$

In Fig. 1, curve I represents graphically the variation of $(\Delta A_1)\sigma/R\theta$ with s, according to the equation

$$P(s) = \phi_1 - \left[\frac{(\Delta A_1)\sigma}{R\theta}\right]_\sigma$$

and curve II represents the variation of the function

$$\left[\frac{(\Delta A_1)_{\text{non}}\sigma - \Delta A_2}{R\theta}\right] s^{m-2}$$

with s_1 according to the equation

$$Q(s) = \phi_2 + \log \frac{K}{C_s^2} - \frac{(\Delta A_1)_{\text{non}}\sigma}{R\theta} + \frac{\Delta A_2}{R\theta} + (m-2)\log s$$

Curve III, the sum of I and II, then represents graphically the variation of the function $\log N_s = R(s) = P(s) + Q(s)$ with s, according to equation 8. N, the extrapolated value of $Q(s)$ at $s = 1$, may be expressed by the relation

$$\log N' = \phi_2 + \log \frac{K}{C_s^2} - \frac{[(\Delta A_1)_{\text{non}}\sigma - (\Delta A_2)]}{R\theta} \quad (9)$$

(b) Size and Size Distribution.—The modal average diameter, d_{mode}, varies with N_s, according to the simple relation

$$d^3_{\text{mode}} = \frac{M(C - C_s)}{\rho N_s} = \frac{MC_s s}{\rho N_s} \quad (10)$$

where d represents the diameter of the cube of volume equivalent to that of the crystal.[21]

The size distribution of a precipitate deposited from a supersaturated solution according to a nucleation and condensation process has been analyzed by several workers.[20,21,23,25] For "autocatalytic" growth where no appreciable number of new nuclei are formed after the induction period, the size distribution will be "left-skewed": and with fall in k_1/k_2Cs^2 values, the mode value of d^3 may rise from about 0.5 to >0.9 $d^3_{\max}$, where $d_{\max}$ is the diameter of the largest crystal. The mean deviation of the final crystal crop corresponds to that of the original nuclei, on which these crystals have grown, and will thus decrease with decrease in k_1/k_2Cs^2.

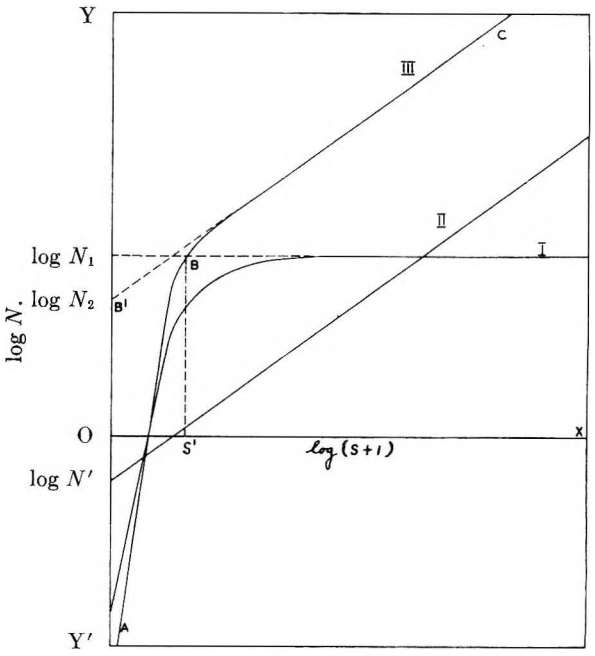

Fig. 1.

(II) Growth by Coagulation.—The shape of the rate of growth—time curves for precipitation of insoluble metal salts would indicate that a prolonged "induction period" is followed by a rapid utilization of micelles.[7,10b,12] Therefore, if precipitation does occur by a coagulation process, this must be largely *autocatalytic*,[26] *i.e.*, after the induction period, coagulation must occur predominantly by growth (of micelles) onto the aggregations of largest surface area that have already formed.

(a) Number of Crystals.—We have applied Duke and Brown's method of analysis to such an autocatalytic coagulation. The rate of nucleation now varies as $k_1a_mC^2$ where a_m is the average surface area of the sol micelles, and k_2 now equals k_1; whence equation 3 becomes

$$N = \frac{Kk_1d_mC^2}{k_1C^2} = K\alpha^m \text{ particles/l.} \quad (11)$$

More exactly, substituting in the Duke and Brown analysis, the rate of formation of new nuclei per unit weight of precipitate, dN/dw now equals A (*cf.* ref 11), and $dN/dw = a_m/A = \frac{\rho^{2/3}a_m}{M^{2/3}W^{2/3}N^{1/3}}$ (where W is the weight of nuclei).

(25) J. Harbury, THIS JOURNAL, **51**, 382 (1947).

(26) E. F. Burton, "The Physical Properties of Colloidal Solutions," Longmans, Green & Co., London, 1938, Ch. 12, p. 210.

$$N^{1/3}dN = \alpha_m(\rho/M)^{2/3}W^{-2/3}dW$$

$$N^{1/3}dN = \alpha_m(\rho/M)^{2/3}W_0^{1/3} \quad (12)$$

i.e.

$$N = (\rho/M)^{1/3}W^{1/4}\,\alpha_m^{3/4}$$

$$= \frac{\alpha_m^{3/4}\rho^{1/3}C_s^{1/4}s^{1/4}}{M^{1/4}} \text{ particles/l.} \quad (13)$$

The number of crystals would here thus be independent of k_F, and vary only to a small extent with metal salt concentration, but would depend on $(a_m)^{3/4}$.

Generally, for any coagulation process mainly autocatalytic, we might therefore expect that N will vary with C, according to a relation N_s = constant $\times$ $s^{\beta'}$, where $\beta'<1$.

(b) **Size and Size Distribution.**—Autocatalytic slow coagulation will lead to the same type of left-skewed distribution expected for growth by condensation. The mean particle size deviation will correspond to that of the aggregations onto which the rapid growth has taken place.

We may note that coagulation theories do not include any explanation of the very high stabilities of insoluble metal salt systems at low supersaturation.

Discussion of Published Data

We have next tested the theoretical equations derived, with the available experimental data for variation of crystal size and size distribution (of sparingly soluble salts) with supersaturation, from papers by von Weimarn, Duke and Brown, and the author. The experimental methods used to determine crystal size, etc., were essentially the same in all cases.

(a) **Crystal Size and Number.**—For a supersaturated solution of metal salt concentration, C, the final crystal size d_s, is determined by the number N_s, of crystals, according to equation 10.

$$d_s{}^3{}_{\text{mode}} = \frac{M(C - C_s)}{\rho N_s}$$

According to either equations 1, 8 or 13, N_s should in turn vary with s, at higher supersaturations, according to a relation of the general form, N_s = constant $\times$ s^β. We have therefore studied the variation of d_s and N_s with s, for a series of silver, copper, nickel and lead salts, by plotting log N_s against log s. Some typical graphs have been presented in recent work.[11,18]

These log N_s–log s graphs in all cases show the general form proposed in Fig. 1 for an autocatalytic condensation process; and consist of two or in some cases three portions. A rapid rise in N_s with s at low s values along AB is followed by a straight line portion BC; and this in turn may be followed by a further section CD, along which the increase of N_s with s gradually falls off.

As we have demonstrated above, AB represents the rapid rise of k_1, and thence N_s, with s at low supersaturations according to the Volmer–Becker theory.

As the critical nucleus radius approaches its minimum value in the range of higher supersaturations represented by BC, N_s then varies with s according to the relation

$$\log N_s = \log N_2 + \beta \log s \quad (14)$$

where N_2 is the extrapolated value of N_s at $s = 1$. The inflection at B is generally observed at s values of 2 to 10. For metal salts of molecular weights within the range 200 to 300, and of specific gravity of 3 to 5, these values would correspond to σ values of the order of 12 to 50 ergs/cm.^{2}; *i.e.*, r_k values of the order of 8 to 20 Å.

We have found that $\beta > 3$ for all the systems examined. This fact is further evidence for the condensation character of the precipitation process; since a coagulation mechanism would require that $\beta<1$.

(b) **Crystal Size Distribution. Technique.**—Size distribution of a precipitate is generally expressed in terms of the standard deviation for weight (D), and of the maximum weight function (fn); while orderliness of growth is represented by the skewness (Δm) of the crystal weight distribution curve.[15,19,27,28]

The "skewness" of the crystal weight distribution curve Δm is positive for all the systems examined up to high supersaturations; and the crystal weight distribution is of the type predicted for an "autocatalytic" growth process. For a particular salt, the size distribution generally becomes narrower with increasing supersaturation and reduced number of crystals.

However, whereas $D < 0.2$ for precipitates of the very insoluble salts such as barium sulfate even at high N (*i.e.*, k_1/k_2Cs^2) values, the precipitates of more soluble salts such as lead iodide, silver benzoate, copper pyridine thiocyanate, etc., show far higher D values at similar N values.[18] The far wider size distribution about the mode in such systems indicates that growth to "crystalline" size has occurred on nuclei of a correspondingly wide size distribution.

(c) **The Energies of Activation for Nucleation and Crystal Growth.**—It would be of interest to compare the $(\Delta A_1)_{\text{non }\sigma}$ and ΔA_2 values of series of metal salts, but individual values of these activation energies cannot be obtained from crystal size data alone. However, k_1/k_2 ratios for different salts in solution of a high supersaturation depend on the function $f_1(A) = (\Delta A_1)_{\text{non }\sigma} - \Delta A_2$; and we might expect that this function would vary significantly with the solubility of the metal salt.[5,16,18] Such variations would be of some theoretical interest. We have therefore subdivided these simple sparingly soluble metal salts, whose precipitation behavior has been quantitatively described to date into various series according to their chemical characteristics, and have compared the $f_1(A)$ values of salts in each series with solubility (C_s).

Technique. Comparison of $f_1(A)$ Values.—It follows from equation 9 that if as a first approximation the constant ϕ_2 is considered constant for any series of metal salts of similar molecular weight and specific gravity, then the values of $f_1(A)$ of the members of such a series can be compared by comparing values of the function. Log $N'Cs^2$. N' the extrapolated value of $Q(s)$ at $s = 1$ (refer to Fig. 1) may in turn be estimated from log N_s – s curves. In Fig. 1 we note that as $s \to \infty$, $P(s) \to \log N_1$:

(27) A. Packter, THIS JOURNAL, 59, 1140 (1955).
(28) J. Turnbull, *Acta Metallurgica*, 1, 684 (1953).

and to a first approximation, for values of s greater than s (the point of inflection of the curve III (ABC))

$$R(s) = Q(s) + \log N_1$$

i.e.

$$Q(s) = R(s) - \log N_1 \qquad (15)$$

The line BC extrapolated back cuts OY at β'; and

$$\log N_2 = R_s = 1 \qquad (16)$$

Therefore

$$\log N' = Q_{s=1} = R_{s=1} - \log N_1 = \log N_2 - \log N_1$$

C_s values have been taken from the literature.

We have reported our results in earlier work. Although the values of C_s in a particular metal salt series may vary by a factor of 10^{20}, neither the values of $f_1(A)$, nor of $f_2(A) = f_1(A) - \log C_s^2$, show such a wide variation: N_s values at any supersaturation have not varied by a factor of more than 10^3 to 10^5 for crystalline salts of widely different physical and chemical properties. In other words, although $(\Delta A_1)_{\text{non }\sigma}$, ΔA_2 and C_s values may individually vary appreciably from salt to salt, the over-all values of $f_1(A)$ and $f_2(A)$ show far smaller variations.

Discussion. General

Two main concepts have been proposed to explain the precipitation of sparingly soluble metal salts from supersaturated solution, the nucleation theory and the coagulation theory. The detailed kinetics for a precipitation process that occurs according to Balarev's[4] theory have still to be completely developed; but it is clear from the growth-time curves for all the systems examined to date, that should precipitation of insoluble metal salts occur by some slow coagulation process, then this must be autocatalytic in character. The rate of coagulation would hence depend at any instant on the surface area of the growing aggregates, and the crystal number in such systems would only vary to a small extent with supersaturation over a wide range of solute concentrations. This has not been noted. Furthermore, the coagulation theory does not include any explanation for the exceptionally high stability of metal salt systems at very low supersaturation—or for the large size of crystals deposited from systems of the "slightly soluble" metal salts that show no specific colloidal characteristics.

The experimental data discussed in this work are indeed best explained by the extension of Duke and Brown's "theoretical analysis" for an autocatalytic condensation growth onto nuclei. There is no sharp differentiation in the kinetics of precipitation between colloidal salts, "peptized" crystalline salts of low solubility, and those crystalline salts such as lead chloride and potassium chlorate, the solubility of which approaches that of the so-called "soluble" salts. A complete analysis of precipitation of sparingly soluble metal salts must, however, take into account colloidal phenomena, since at all supersaturations, the growing particles at some stage pass through the 100 to 1000 Å. size range. Even although their adsorbed charge may only stabilize this phase transiently, such a "peptization" may modify the kinetics of the precipitation. One phenomenon that requires explanation, for example, is the narrow size distribution noted in barium sulfate precipitates[19]; since it would appear from a careful analysis[10c,11,13] that this salt is more the exception than the rule in this effect. Precipitates of larger average particle size show a wide size distribution that corresponds to the wide size distribution of the nuclei onto which crystal growth has occurred; and narrow size distribution must therefore be due to the absence of smaller particles of colloidal size amongst such nuclei. A suitable explanation of the adsorption phenomena associated with "peptized" crystalline[3,4,10b,18,29] salts is also still lacking.

The number (N_s) of crystals deposited from unit volume of a supersaturated metal salt solution varies with the supersaturation constant (s), according to equation 3. (Refer to Figs. 1 and 2.) The very rapid rise in N_s with s at low supersaturations corresponds to the increase in rate of nucleation with decreasing cuticle nucleus radius r_k predicted by the Volmer–Becker theory.[10c] At higher supersaturations, r_k falls to its minimum value, $(\Delta A_1)\sigma$ becomes progressively less significant and the rate of nucleation depends mainly on the term $(\Delta A_1)_{\text{non}\sigma}$. N_s then varies with s according to the mass-action equations 10 and 14.

The individual values of the activation energies $(\Delta A_1)_\sigma$ $(\Delta A_1)_{\text{non}\sigma}$ and ΔA_2 cannot be determined directly from crystal size data[30]; but the function $f_1(A) = [(\Delta A_1)_{\text{non}\sigma} - \Delta A_2]$ may be estimated. In the series of simple crystalline metal salts that have been studied to date, however, we have not noted any appreciable variation of this function with solubility (C). It follows then from our analysis that the main factor that determines crystal size and number at any supersaturation is the actual value of $(1/C_s^2)$, rather than that of k_1/k_2, the ratio of the rate coefficient of nucleation to that of crystal growth.

In supersaturated solutions of very insoluble salts, the number of nuclei formed immediately after mixing is generally so great that the solution is rapidly exhausted of solute. Further growth onto the nuclei is limited, and only results in particles of colloidal size. In solutions of salts of higher solubility, on the other hand, even if k_2 is small, the high value of the $(1/C_s^2)$ factor will lead to rapid growth onto the smallest nuclei, immediately they are formed. This effect may rapidly deplete the solution of solute, and a small number of larger crystals of size greater than 1 micron is generally deposited.

(29) J. Herak, *et al.*, *Arkiv. Kem. (Zagreb)*, **27**, 117 (1955).

(30) The determination of activation energies from crystal size and induction period data will be the subject of a later paper.

HOMOGENEOUS CATALYSIS FOR HOMOGENEOUS REACTORS. CATALYSIS OF THE REACTION BETWEEN HYDROGEN AND OXYGEN[1]

By H. F. McDuffie, E. L. Compere, H. H. Stone, L. F. Woo and C. H. Secoy

Contribution from the Chemistry Division of the Oak Ridge National Laboratory, Oak Ridge, Tennessee

Received August 14, 1957

The reaction between hydrogen and oxygen, dissolved in aqueous solutions at elevated temperatures, is catalyzed homogeneously by dissolved cupric salts. The rate of consumption of hydrogen, dy/dt, is given by the equation $dy/dt = V_l(P/\alpha)[Cu^{++}]^1 k_{Cu}$. When no vapor phase is present, or when there is no mass transfer of hydrogen to the liquid phase during the reaction, this equation reduces to $-d[H_2]/dt = [H_2][Cu^{++}]^1 k_{Cu}$. The specific reaction rate constant for cupric perchlorate in dilute perchloric acid solution at 250° is 1.4 M^{-1} sec.$^{-1}$; for cupric sulfate in 0.16 M uranyl sulfate solution the specific reaction rate constant is given by the expression $k_{Cu} = 2 \times 10^{10} \exp(-24{,}140/RT)\ M^{-1}$ sec.$^{-1}$

Introduction

Disposal of the 2:1 mixture of hydrogen and oxygen created by the radiolytic decomposition of water in fissioning aqueous solutions presents a substantial technical and engineering problem in connection with the development of aqueous homogeneous reactors. The magnitude of the problem may be illustrated by reference to the operation of the Homogeneous Reactor Experiment (HRE) at 1000 kw. which was accompanied by a gas evolution of 10.5 cfm. (STP).[2] As this gas was released from the reactor core, mixed with saturated steam at 250°, the composition of the gas–steam mixture was well within the explosive range. In the operation of the HRE, as it was originally designed, the gas–steam mixture was throttled to atmospheric pressure and the gas burned to water in a flame recombiner; the condensed water was returned to the system by injection pumps. The operation of full-scale homogeneous reactors would be accompanied by the production of much larger amounts of explosive gas (10,000 cfm. for a 1,000 Mw. reactor).

It has been discovered that dissolved hydrogen and oxygen will react smoothly at elevated temperatures to form water if dissolved copper is present in the solution. The copper acts as a homogeneous catalyst for the reaction. The present paper discusses the kinetics of this reaction as elucidated through laboratory experiments; other reports have extended the application of the reaction to the recombination of hydrogen and oxygen generated *in situ* by action of fission fragments formed by the exposure of enriched uranyl sulfate solutions to reactor-induced neutron fluxes[3] and, finally, to the use of copper sulfate as a catalyst for the internal recombination of hydrogen and oxygen formed during the operation of the HRE.[4] The performance of the catalyst in suppressing net gas formation was found to be consistent with the kinetic picture developed in this paper and the engineering characteristics of the reactor system. It is planned that homogeneous catalysis of the hydrogen–oxygen reaction will be used in advanced types of aqueous homogeneous reactors now under development.

(1) Presented before the ACS Southwide Chemical Conference, Memphis, Tennessee, December 6, 1956.

(2) S. E. Beall and C. E. Winters, *Chem. Eng. Progr.*, **50**, 256 (1954).

(3) D. M. Richardson, H. F. McDuffie, C. H. Secoy, F. H. Sweeton, L. F. Woo and J. W. Boyle, "In-Pile Studies of Homogeneous Reactor Solution Stability and Hydrogen-Oxygen Recombination," presented at the Southwide Chemical Conference, Memphis, Tennessee, December 6, 1956.

(4) S. Visner, P. N. Haubenreich and R. E. Aven, "Internal Recombination of Radiolytic Gas with a Homogeneous Catalyst in the Homogeneous Reactor Experiment," presented at the Southwide Chemical Conference, Memphis, Tennessee, December 6, 1956.

Experimental Techniques

Small stainless steel or titanium autoclaves (bombs) of 10 to 30-ml. capacity were charged with measured amounts of the catalyst solution to be tested, connected to a pressure gauge through a length of capillary tubing by means of a conical fitting and placed in an aluminum block furnace. Convenient pressures of hydrogen and oxygen gas were charged to the vapor space above the test solution from regular high pressure cylinders of these gases through reducing valves and a gas-charging manifold (for safety reasons the hydrogen and oxygen supply cylinders were never both connected to the manifold at the same time). Usually 600 p.s.i. of hydrogen and 400 p.s.i. of oxygen were charged so that there would always be an excess of oxygen over that required for reaction with all the hydrogen. Then the furnace was heated rapidly to the desired temperature, at which time the rocking mechanism was started to maintain equilibrium between the gas phase and the liquid phase. The progress of the reaction was indicated thereafter by a decreasing total pressure, recorded for subsequent analysis.

Thus the experimental data available for subsequent interpretation were temperature, solution composition at room temperature, fractional filling of the bomb at room temperature, the partial pressures of gases charged at room temperature, and the decrease in total pressure with time, observed at the reaction temperature.

Interpretation of Experimental Data

It was first established that the reaction occurred only in the liquid phase. Hydrogen and oxygen brought together in the absence of any liquid phase did not react, nor did they react in the presence of distilled water. As discussed later, large variations in the type or amount of surface area of metal exposed did not alter the reaction rate; thus the reaction was not occurring at the surface. Finally, it was found that some agitation was necessary to provide reproducible experimental results; this would logically be the case if gaseous reactants dissolved in the liquid phase were consumed in the reaction, since it would be necessary to replace them by mass transfer from the gas phase.

It was next established that the observed rate of reaction (pressure decrease) was directly proportional to the partial pressure of hydrogen gas and independent of the partial pressure of oxygen gas (as long as there was even a very small amount of oxygen present). Experiments in which the partial pressures of hydrogen and oxygen were varied over wide ranges, while the temperature and the composition of the test solution were held

constant, revealed that the pressure always decreased exponentially from its initial value toward a final value which corresponded to the total of steam pressure plus any excess oxygen and/or inert gas present. The first-order rate constant for this pressure decrease, k_π, obtained conveniently by measuring the slope of the linear relationship between $\Delta P/\Delta t$ and $(P - P_\infty)$ on a plot of $\Delta P/\Delta t$ *vs.* P, is equal to the first-order rate constant relating $\Delta P_{H_2}/\Delta t$ to P_{H_2}, since both $\Delta P/\Delta t$ and $P - P_\infty$ are 3/2 the corresponding values for hydrogen. This is a consequence of the fact that hydrogen and oxygen combine in a 2:1 ratio and both obey Henry's law quite well in the range of pressures studied.

When systems were tested which had an excess of hydrogen over that required for reaction with the available oxygen, the linear relationship between pressure decrease and total pressure was followed until essentially all the oxygen was consumed, after which the copper catalyst ultimately was reduced to metallic copper powder. Since only a small amount of oxygen was necessary to ensure the normal reaction rate and to maintain the catalyst in the cupric state, it was inferred that the rate-determining step cannot be the reaction of oxygen with some reduced species. Since the observed rate of pressure decrease was directly proportional to the hydrogen pressure it was inferred that the rate-controlling reaction in solution must be first order in dissolved hydrogen. The over-all reaction thus appears to be a slow reduction of the cupric catalyst by dissolved hydrogen, followed by a rapid regenerative oxidation of the reduced species.

The experimental arrangement which was utilized provides an example of the general case of two immiscible phases with a solute distributed between them but reacting in only one. It has been shown, in the analogous liquid–liquid systems, that the observed rate of reaction may be slowed down by providing a large excess of the liquid in which the solute does not react.[5] The magnitude of the distribution coefficient of the solute and the relative volumes of the two phases combine to determine just how much the reaction will be slowed down. In the present work the two phases were vapor and liquid, and the distribution coefficient was expressed as the solubility of hydrogen in the liquid phase.

Values for the solubility of hydrogen in water at elevated temperatures have been presented[6] from which the distribution coefficients shown in Table I were calculated. It is important to be consistent in the use of solubility values, and the work in this paper has been based on the assumption that the values given in Table I are valid for uranyl sulfate solutions, acidified copper sulfate solutions and water. Any improvement[7] in our knowledge of these solubilities will require corresponding changes in the rate constants assigned in this paper.

TABLE I

SOLUBILITY OF HYDROGEN IN WATER AT ELEVATED TEMPERATURES

Temp., °C.	α[a]	Temp., °C.	α[a]
149	17,560	250	7,300[b]
174	16,720	260	6,720
199	14,640	316	5,000
224	11,000	343	2,680

[a] $\alpha = p_{H_2}$(p.s.i.)/[H_2] (moles/l.). [b] Interpolated.

Quantitative application of the relationship between the slowing down of the observed reaction rate and the amount of the immiscible inert phase which is present requires first of all that the reactive solute be distributed between the two phases in accordance with its distribution coefficient. In the present case this means that the solution must be kept saturated with hydrogen so that the concentration of dissolved hydrogen everywhere in the solution is (within the limits of our experimental measurements) that called for by the distribution coefficient definition

$$[H_2] = \frac{P_{H_2}}{\alpha}$$

where

[H_2] = concn. of hydrogen in the liquid phase, M
[α] = hydrogen solubility constant, p.s.i./M

In early experiments it was found that the observed rates of reaction, for a given gas-to-liquid ratio, were lower when the bombs were mounted vertically than when they were mounted horizontally. In the horizontal position there was much more interfacial area across which the hydrogen could diffuse, and the depth of liquid under the interface was much smaller. Rocking the bombs through an arc of 15° above and below the horizontal at a rate of 30 cycles per minute provided a slight additional increase in rate. Further increases in the intensity of agitation (up to reciprocal shaking in a horizontal position with a 1/4-in. stroke at a rate of 240 cycles per minute) did not result in further increases in the observed rate, from which it was inferred that the rocking agitation was keeping the hydrogen satisfactorily distributed throughout the solution.

Having established a basis for the assumption that the hydrogen distribution equilibrium is maintained throughout the course of our reaction, the the relationship used by Goldschmidt and Messerschmidt[5] and by more recent workers[8] can be applied to the determination of the true rate of the reaction in solution.

Since it was shown that the reaction occurs only in the liquid phase, with the rate of pressure decrease proportional to the partial pressure of hy-

(5) H. Goldschmidt and A. Messerschmidt, *Z. physik. Chem.*, **31**, 235 (1899), discussed in Taylor's "Treatise on Physical Chemistry," Vol. 2, 2nd Ed., D. Van Nostrand Co., Inc., New York, N. Y., 1936, p. 1053.

(6) H. A. Pray, C. E. Schweickert and B. H. Minnich, *Ind. Eng. Chem.*, **44**, 1146 (1952); also Battelle Memorial Institute Report BMI-T-25 (May 15, 1950).

(7) E. F. Stephan, N. S. Hatfield, R. S. Peoples and H. A. Pray, Battelle Memorial Institute Report BMI-1067 (January 23, 1956).

(8) While this paper was under review our attention was called to the paper by Klein, McKelvey and Webre, "The Simultaneous Measurement of Distribution Coefficients and Hydrolysis Rates," presented at the ACS Meeting in New York City on September 12, 1957, published in THIS JOURNAL, **62**, 286 (1958), which shows a similar relationship between the phase volume ratio and the observed rate of change of concentration of solute in the inert phase. An analogous treatment by Levy, *et al.*, *J. Am. Chem. Soc.*, **73**, 3792 (1951), was noted by one of their referees and kindly brought to our attention by Dr. Klein.

drogen, it was inferred that the consumption of hydrogen could be expressed as

$$\frac{dy}{dt} = V_l \frac{P_{H_2}}{\alpha} k_{sol} = V_l[H_2]k_{sol}$$

where

y = no. of moles of hydrogen which have been consumed by the reaction at time t
V_l = vol. of the liquid phase, l.
k_{sol} = rate constant for the soln., hr.$^{-1}$

Since

$$y = N_0 - N_t, \text{ where}$$

N_0 = total moles of hydrogen in the system originally
N_t = total moles of hydrogen in the system at time t

then

$$dy/dt = -dN_t/dt$$

and

$$dN_t/dt = -V_l \times \frac{P_{H_2}}{\alpha} \times k_{sol}$$

Mass balance considerations and the perfect gas law give a relationship between the consumption of hydrogen and the change in pressure of the system

$$N_t = N_g + N_l = \frac{P_{H_2}V_g}{RT} + \frac{P_{H_2}V_l}{\alpha} = P_{H_2}\left(\frac{V_g}{RT} + \frac{V_l}{\alpha}\right)$$

where

N_g = moles of hydrogen in the gas phase
N_l = moles of hydrogen in the liquid phase
R = gas constant

and

$$\frac{dN_t}{dt} = \frac{dP_{H_2}}{dt}\left(\frac{V_g}{RT} + \frac{V_l}{\alpha}\right)$$

Equating now the two expressions for dN_t/dt we have

$$\frac{dP_{H_2}}{dt}\left(\frac{V_g}{RT} + \frac{V_l}{\alpha}\right) = -V_l \times \frac{P_{H_2}}{\alpha} \times k_{sol}$$

which, on rearranging terms, gives

$$\frac{\frac{-dP_{H_2}}{dt}}{P_{H_2}}\left(\frac{V_g}{V_l} \times \frac{\alpha}{RT} + 1\right) = k_{sol}$$

As previously noted, the term $(-dP_{H_2}/(dt)/P_{H_2}$ is equal to the experimentally measured rate constant for pressure decrease, k_r. The term in parentheses

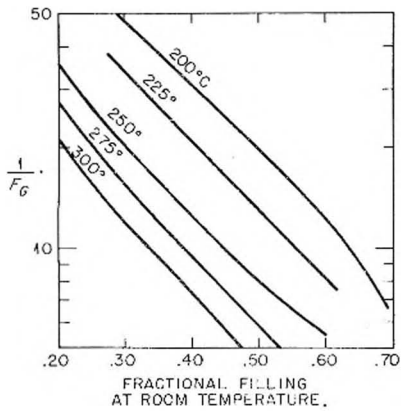

Fig. 1.—Geometry factors at elevated temperatures.

contains all the geometry and distribution factors which are necessary to correct the observed rate of pressure decrease to the true rate constant for the solution; this term is referred to as the geometry factor, $1/F_g$. Thus $k_{sol}F_g = k_r$ and

$$k_{sol} = k_r\left(\frac{1}{F_g}\right) = k_r\left(\frac{V_g}{V_l} \times \frac{\alpha}{RT} + 1\right) \quad (1)$$

Equation 1 is the form in which the relationship is commonly used for the interpretation of our experimental data.

Under certain conditions the term dN_g/dt can be made to equal zero; this can occur when no gas phase is present (as is the case for solution in the core region of an aqueous homogeneous reactor) or when the pressure of hydrogen in the gas phase is in a steady state (as is the case when hydrogen is being introduced into the system at a rate just matching the rate of its consumption in the liquid phase). Then, since $N_t = N_g + N_l$ and $dN_t/dt = dN_g/dt + dN_l/dt$, we find that

$$\frac{dN_t}{dt} = 0 + \frac{dN_l}{dt} = -V_l \frac{P_{H_2}}{\alpha} k_{sol}$$

or

$$\frac{1}{V_l} \times \frac{dN_l}{dt} = \frac{-P_{H_2}}{\alpha} k_{sol} = -[H_2]\, k_{sol}$$

But

$$\frac{1}{V_l} \times \frac{dN_l}{dt} = \frac{d[H_2]}{dt}$$

whence

$$\frac{-d[H_2]}{dt} = [H_2]k_{sol}$$

This is the form of the kinetic equation which is most useful for comparison with the results of other kinetic studies reported in the literature, since all the complications arising from the presence of two phases and the mass transfer from the gas phase to the liquid phase have been eliminated. The value of k_{sol} is of course, the same, whether calculated from equation 1 or determined from experiments in which dN_g/dt is zero.

Since aqueous solutions expand considerably between room temperature and the test temperature, and since there is transfer of water from the liquid phase to the vapor phase as the temperature is raised, it is necessary to allow for both these factors in calculating the correct gas-to-liquid volume ratios for the various test temperatures. Figure 1 illustrates the relationships between the fractional filling of a container at room temperature and the geometry factor which must be applied at several elevated temperatures.

The change in gas-to-liquid ratio upon heating of course affects the ultimate concentration of the catalyst. A number of additional factors, such as external cold volumes, effect of gas pressure on water vapor pressure, effect of water formed during the reaction, effect of pressure on the volume of the system, compressibility of water in cold external volumes, etc., have been considered but are of relatively minor importance except for the influence of the cold external volume. In the present work this volume was minimized by filling the pressure cell with water and by using short lengths of small diameter (0.020-in. i.d.) capillary tubing to connect the bomb to the pressure cell and charging valve. Corrections for the densities of the solu-

tions were applied in determining the geometry factors for solutions containing uranyl sulfate as an added solute. Except as otherwise indicated the catalyst concentrations were corrected for the expansion of the solution.

Test for Surface Effects.—The dependence of the observed reaction rate upon the fractional filling of the container in a manner established by the geometry factor was strong evidence that the reaction was occurring only in the liquid phase. However, to test for additional surface effects which might be due to catalytic reactions on the walls of the bombs, two types of experiments were performed.

1. Hydrogen and oxygen were charged to bombs partially filled with distilled water but containing no catalyst; when heated to 250° with rocking agitation no substantial amount of reaction was observed. This test was used subsequently when any question of contamination of the interior of the bombs was raised; any bombs which showed the ability to catalyze the reaction were discarded or etched until they no longer were catalytically active.

2. The bombs were packed with pieces of stainless steel rod, enough to treble the surface area; no substantial change in the reaction rate was observed when the proper corrections were made for the volume occupied by the added metal. Stainless steel and titanium turnings were packed into some bombs for tests with the thus greatly increased surface; no increases in the reaction rate were noted.

Dakers and Halpern[9] have reported, in connection with a study of the reaction between cupric acetate and hydrogen in aqueous solution at 130°, that the addition of stainless steel powder to their systems failed to affect the reaction rate.

Dependence on Catalyst Concentration.—The reaction appears to be first order in dissolved copper at 250° as indicated by experiments in which varying concentrations of copper sulfate were added to dilute sulfuric acid to form test solutions with results shown in Fig. 2. A similar first-order dependence on added copper sulfate was noted when the catalyst was added to a typical reactor fuel solution (0.17 M uranyl sulfate) and tested at 250° as shown by the data in Fig. 3. Based on the finding of first-order dependence on the dissolved cupric concentration, which means that $k_{sol} = k_{Cu}[Cu^{++}]^1$, expressions for the reaction involving the specific reaction rate constant, k_{Cu}, now can be written

$$\frac{dy}{dt} = V_1 [H_2][Cu^{++}]k_{Cu}$$

or, when $dN_g/dt = 0$

$$\frac{d[H_2]}{dt} = -[H_2][Cu^{++}]k_{Cu} \qquad (2)$$

Dependence on Anion and Acidity.—In order to determine the activity of the copper catalyst under conditions which would tend to minimize any complexing of the cupric ion by anions of the solution tests were made of solutions containing only cupric perchlorate and perchloric acid. Hydrolytic precipitation was noted in solutions of 0.001 M cupric perchlorate at 250°; the presence of 0.005 M perchloric acid suppressed phase instability at this temperature. Tests of solutions containing 0.001 M cupric perchlorate plus 0.005, 0.010 and 0.050 M perchloric acid gave values for k_{Cu} of 5000 M^{-1} hr.$^{-1}$ for each solution.

The constancy of k_{Cu} suggests that this may be the correct value for the catalytic activity of uncomplexed cupric ion. The data suggest further that no complexing by perchlorate is taking place and that there is no direct participation of hydrogen ions in the reaction (except for the suppression of hydrolytic precipitation). The experiments with perchlorate were limited to short times in order to avoid excessive corrosion of apparatus by the traces of chloride and hydrochloric acid released upon slight decomposition of perchlorate at the elevated temperatures.

When copper sulfate solutions plus varying concentrations of sulfuric acid were tested similarly

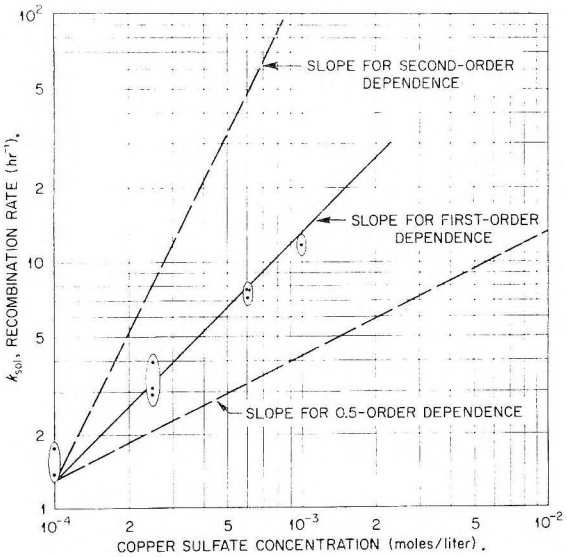

Fig. 2.—Effect of copper sulfate concentration upon recombination rate in 0.005 M sulfuric acid solution at 250°.

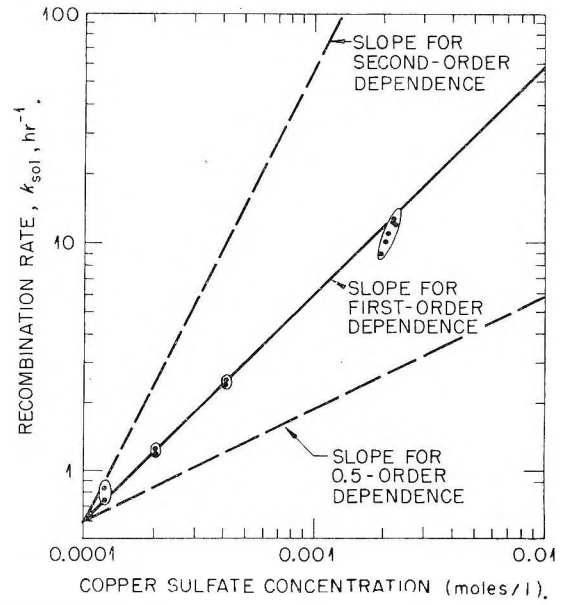

Fig. 3.—Effect of copper sulfate concentration upon recombination rate in 0.166 M uranyl sulfate solution at 250°.

(9) R. G. Dakers and J. Halpern, *Can. J. Chem.*, **32**, 969 (1954).

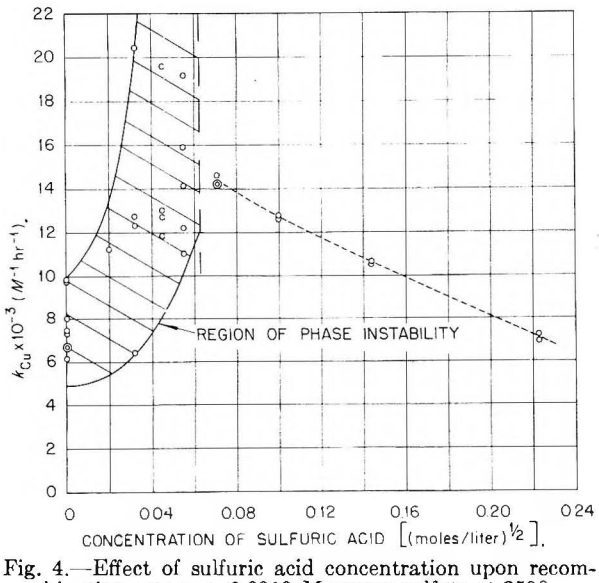

Fig. 4.—Effect of sulfuric acid concentration upon recombination rate over 0.0010 M copper sulfate at 250°.

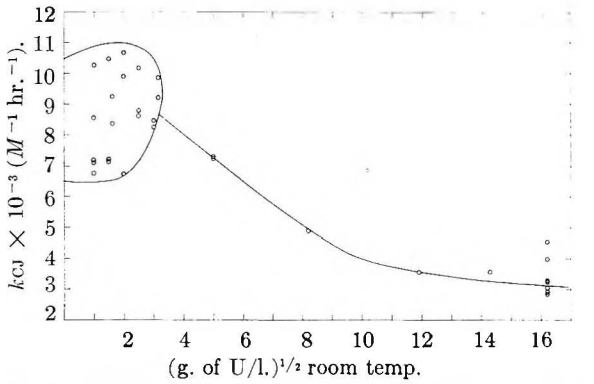

Fig. 5.—Effect of uranyl sulfate concentration upon recombination rate in 10^{-3} M copper sulfate solution at 250°.

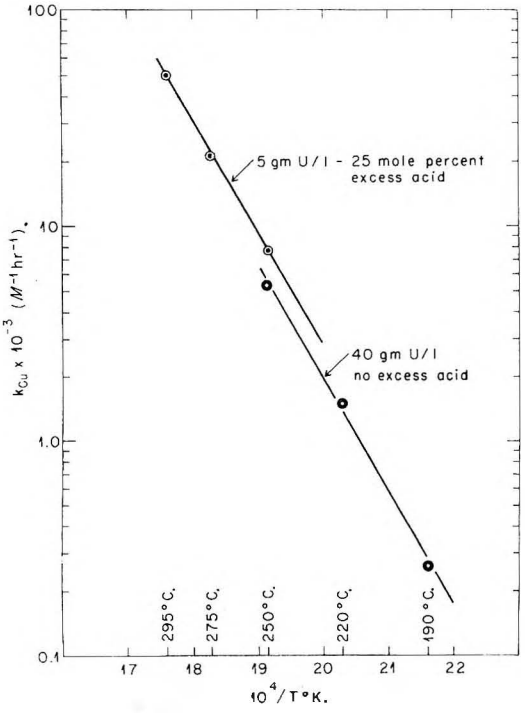

Fig. 6.—Effect of temperature on the recombination rate.

the results were quite different. The experiments illustrated by Fig. 4 indicate that, after hydrolytic phase instability is overcome, the addition of more sulfuric acid causes a substantial drop in the activity of the catalyst.

Dependence upon Uranyl Sulfate Concentration and Acidity.—When uranyl sulfate was added to a solution containing 0.001 M copper sulfate the catalytic activity decreased after a region of phase instability was passed. Figure 5 illustrates this decrease.

Temperature Coefficient of the Reaction.—The influence of temperature is shown by the lines in Fig. 6, a conventional Arrhenius plot of log k_{Cu} *vs.* $1/T$, for two different solutions, based on data from Tables II and III. The activation energy is indicated to be 24,140 cal./mole, and the best expression for the specific reaction rate constant for cupric sulfate in 0.16 M uranyl sulfate is

$$k_{Cu} = 2 \times 10^{10} \exp(-24{,}140/RT') \frac{1}{M} \frac{1}{\text{sec.}} \quad (3)$$

The combined effects of temperature, uranium concentration, copper concentration and excess acid upon the reaction rate, for solutions of interest as potential homogeneous reactor fuel systems, are shown by the data in Table III.

Table II

Temperature Dependence of Recombination Rate in 0.166 M Uranyl Sulfate Plus 0.0025 M Copper Sulfate Solution

Temp., °C.	190	220	250
Av. $k_{Cu} \times 10^{-3}$, M^{-1} hr.$^{-1}$	0.261	1.59	5.35

Table III

Effects of Uranium Concentration, Copper Concentration, Excess Sulfuric Acid and Temperature Upon Recombination Rate

Temp., °C.	Excess acid,[b] mole %	U concn., g./l.[a]	Av. values of $k_{Cu} \times 10^{-3}$, M^{-1} hr.$^{-1}$ CuSO$_4$, M[a] 0.001	0.005
250	25	2.5	9.6	9.1
		5	9.0	8.6
		10	6.3	7.6
	50	2.5	8.8	
		5	6.6	
		10	6.1	
275	25	2.5		20.5
		5		22.9
		10		21.2
	50	2.5	24.2	
		5	20.9	
		10	17.6	
295	25	2.5	51.9	
		5	50.7	
		10	47.0	
	50	2.5	60.6	
		5	50.9	
		10	40.1	

[a] Measured at room temperature. [b] The concentration of sulfuric acid added to stoichiometric uranyl sulfate, based upon the molarity of the uranyl sulfate, *e.g.*, a solution of 0.25 M sulfuric acid and 1.00 M uranyl sulfate would represent 25 mole % excess acid.

Reaction Rate with Deuterium.—In a reactor system based on the use of heavy water as the sol-

vent for a uranium salt the decomposition products of the water will be deuterium and oxygen rather than hydrogen and oxygen. Therefore it was of reactor interest as well as kinetic interest to ascertain the rates of reaction when deuterium was used in place of hydrogen. A test solution was chosen (0.005 M sulfuric acid and 0.001 M cupric sulfate in light water) for which considerable data concerning the reaction rate with hydrogen gas at 250° were available. The rate of reaction of deuterium gas, at 250°, inferred from the rate of change of pressure at a particular ratio of gas volume to liquid volume, was about 60% of the rate of reaction of hydrogen. The difference is believed to be due to a combination of the difference in reaction rate and the difference in gas solubility, but these effects have not been separated since the solubility of deuterium in the test solution is not known accurately. Experiments with heavy-water solutions are planned in which the differences between hydrogen and deuterium reactivity will be measured under a variety of environmental conditions.

Discussion

The important feature of this reaction is that molecular hydrogen, dissolved in an aqueous solution, reacts homogeneously with the dissolved catalyst. The regeneration of the catalyst by subsequent reactions with oxygen appears to be of lesser kinetic interest. Early references in the literature provide indications of reactions between dissolved hydrogen and molecularly dispersed species in aqueous solutions.[10,11] The use of hydrogen for the reduction of copper ions to large microcrystals of metallic copper was described by Ipatieff and Werchowsky.[12] Other papers of Ipatieff[13,14] and the later paper by Ipatieff, Corson and Kurbatov[15] have established that under proper conditions Cu, Ni, Co, Pb and Bi can all be reduced and precipitated. More recently Halpern and his co-workers have reported detailed kinetic studies of the reaction of hydrogen with dissolved copper salts in aqueous solutions; these studies have been reviewed by Halpern.[16]

The results reported in the present paper are generally in agreement with the findings reported by Halpern although our investigations were made at temperatures of 190–300° while Halpern's were in the 80–140° range. The closeness of agreement between our results and those of Halpern can be seen best upon comparison of data for the simplest system, cupric perchlorate in relatively dilute acid. Peters and Halpern[17] reported that the kinetics were represented by equation 2 with the bimolecular rate constant given by the expression $k = 1.0 \times 10^{13} \exp(-26{,}600/RT)$ l. mole^{-1} min.$^{-1}$. Extrapolation of their data to 250° by means of this rate constant and conversion from minutes to hours gives a value for k_{Cu} of 4.6×10^{3} which is within 10% of our experimental value of 5.0×10^{3} M^{-1} hr.$^{-1}$.

Peters and Halpern noted that the value for the apparent activation energy, 26.6 ± 0.8 kcal., was about 2 kcal. higher than that which they had previously reported for the reaction between hydrogen and cupric acetate, and that this was consistent with the greater catalytic activity of the cupric acetate. The value reported in the present paper for cupric sulfate in dilute uranyl sulfate, 24.1 kcal., is in good agreement with this concept.

Halpern, Macgregor and Peters[18] recently have reported that the addition of substantially more perchloric acid to solutions containing cupric perchlorate (up to 1 M acid) decreased the reaction rate at 110°. They have interpreted their data in terms of these reactions and rate constants

$$Cu^{++} + H_2 \underset{k_{-1}}{\overset{k_1}{\rightleftharpoons}} CuH^+ + H^+ \qquad (4)$$

$$CuH^+ + Cu^{++} \xrightarrow{k_2} 2Cu^+ + H^+ \qquad (5)$$

$$2Cu^+ + \text{oxidant} \xrightarrow{\text{fast}} 2Cu^{++} \qquad (6)$$

From their data they concluded that the values for k_1 and the ratio (k_1/k_2) were 9.5×10^{-5} l. mole^{-1} sec.$^{-1}$ and 0.26, respectively, at 110°. Their hypothesis appears very attractive when applied to the 110° data, but a possible inconsistency becomes evident when the results of experiments at 250° are considered; in the perchlorate system there was no indication that the addition of up to 0.050 M perchloric acid to 0.001 M cupric perchlorate affected the reaction rate. Although the concentration of acid used was not so great as in the 110° experiments, the concentration of cupric perchlorate was also much lower, more than enough to compensate for the lower acid concentrations as is evident when the kinetic expressions are resolved into the form

$$\frac{1}{\text{rate}} = \frac{1}{k_2[Cu^{++}][H_2]}\left[1 + \frac{k_{-1}[H^+]}{k_2[Cu^{++}]}\right] \qquad (7)$$

The importance of the ratio of copper to acid in determining the ratio of k_{-1} to k_2 (rather than the total concentration of either) is apparent. It could be concluded from our data that the reaction between H^+ and CuH^+ to regenerate Cu^{++} and H_2 has effectively disappeared at 250°. This is not yet inconsistent with Halpern's hypothesis that the intermediate CuH^+ exists, based on his 110° data, since no information has been provided concerning the effect of temperature on the component reactions.

Application of the same kinetic analysis to the data from Fig. 4, which illustrate the suppressing effect of sulfuric acid upon the reaction, supports the conclusion that the ratio (k_{-1}/k_2) might have a value of 0.0258, *i.e.*, the reaction between the postulated CuH^+ and H^+ is relatively unimportant compared with the reaction between the postulated CuH^+ and another Cu^{++} ion. Further

(10) M. N. Beketoff, *Compt. rend.*, **48**, 442 (1859).

(11) G. Tammann and W. Nernst, *Z. physik. Chem.*, **9**, 1 (1892).

(12) W. Ipatieff and W. Werchowsky, *Ber.*, **42**, 2078 (1909).

(13) W. Ipatieff, *et al.*, *ibid.*, **62**, 356 (1929).

(14) W. Ipatieff, *et al.*, *ibid.*, **60**, 1982 (1927).

(15) V. Ipatieff, B. Corson and I. Kurbatov, THIS JOURNAL, **43**, 589 (1939).

(16) J. Halpern, "Homogeneous Catalytic Activation of Molecular Hydrogen by Metal Ions," Presented at the International Congress on Catalysis, Philadelphia, Pa., Sept. 10–14, 1956, to appear in *Advances in Catalysis*, Vol. IX.

(17) E. Peters and J. Halpern, THIS JOURNAL, **59**, 793 (1955).

(18) J. Halpern, E. R. Macgregor and E. Peters, *ibid.*, **60**, 1455 (1956).

studies of the effect of sulfuric and perchloric acid on the reaction rate at intermediate temperatures between 110 and 250° are being carried out to provide additional information concerning this phase of the kinetic picture of the reaction.

The slower rate of reaction with deuterium than with hydrogen represents the combination of solubility and reaction rate effects. It will be necessary to obtain measurements of the solubility of deuterium under the reaction conditions before these two effects can be separated, but it seems reasonable to find that the heavier deuterium is less reactive than hydrogen.

A large number of other materials were tested as possible catalysts for the hydrogen–oxygen reaction in solution; these tests usually were made with the element or compound dissolved in 0.16 *M* uranyl sulfate, and the tests usually were carried out at 250°. No attempt was made to test all the oxidation states of the species examined, since it was believed that the combination of hydrogen, oxygen and acidic uranyl sulfate solution at elevated temperatures would dictate the oxidation state of the species. In many cases the interpretation of the results was clouded by the question whether the material remained in solution at the elevated temperature. No significant activity was found for Ni, Co, Zn, Cd, Pb, As, Li, Rb, Cl, K, Br and Mg. No significant activity can be attributed to sulfate ions *per se*. Uranyl solutions showed slight activity which is attributed to the uranyl ions. Fe, Tl, Ce, Sn, Mn, V, and Ti were found to have slight activity in the presence of uranyl sulfate. In one experiment an acidified pertechnetate solution showed moderate activity, but interpretation was made difficult by the formation of a large amount of black precipitate during the run. The metals Pt, Pd, Os, Ir, Rh and Ru, added as ionic species, were reduced to the metallic state in which they acted as extremely effective heterogeneous catalysts, usually initiating explosions of the confined gas. Silver and iodine, added to uranyl sulfate solutions as silver sulfate and potassium iodide, were found to confer substantial activity upon the system. At the end of these experiments, however, the silver appeared as a gray fog of apparently precipitated silver and the iodine as elemental iodine; these appearances raised questions as to the homogeneous nature of the reaction, but, nevertheless, the kinetic expressions were developed for the specific rate constants as

$$k_{\text{solAg}} = [H_2][A_g]^{2.46} \times 2.2 \times 10^{10} \exp(-9{,}000/RT) \pm 20\% \text{ (7 expt.)} \quad (8)$$

$$k_{\text{solI}} = [H_2][I]^{1.0} \times 1.2 \times 10^{11} \exp(-18{,}500/RT) \pm 20\% \text{ (5 expt.)} \quad (9)$$

The relatively small number of experimental determinations with silver solutions, and the uncertainty arising from the appearance of solid, do not suggest any inconsistency with the assignment of order (second) or the rate constants for the reaction of silver with hydrogen as reported by Webster and Halpern.[19]

Acknowledgment.—The authors wish to express their indebtedness to J. W. Boyle, S. F. Clark, D. M. Richardson and F. H. Sweeton for valuable suggestions and assistance preliminary to and during the course of this work and to the United States Atomic Energy Commission for support of the work.[20]

(19) A. H. Webster and J. Halpern, *ibid.*, **60**, 280 (1956).

(20) This paper is based upon work performed at Oak Ridge National Laboratory, which is operated by Union Carbide Nuclear Company for the Atomic Energy Commission.

NITROGEN ADSORPTION ON SOLVENT-EXCHANGED WOOD CELLULOSE FIBERS: INDICATIONS OF "TOTAL" SURFACE AREA AND PORE SIZE DISTRIBUTION[1]

BY EDWARD F. THODE, JOHN W. SWANSON AND JOSEPH J. BECHER

The Institute of Paper Chemistry, Appleton, Wisconsin

Received December 11, 1957

Nitrogen adsorption isotherms at −195.8° have been obtained on samples of wood cellulose prepared in the expanded state by a recently perfected solvent drying technique. Bleached sulfite cellulose (paper-making grade) was subjected to various degrees of beating in a ball mill, then the water displaced by methanol, the methanol displaced with *n*-pentane, and the pentane evaporated in an atmosphere of dry nitrogen at 35.5°. Interpretation of the isotherms indicates that the "total" surface area of the whole fibers increased from 100 to 200 sq. m. per g. of dry cellulose over 250 minutes of ball mill processing. The most common pore diameter of 38 Å. did not change with beating and the total volume of pores in the range 32–44 Å. was but slightly affected. The possible relation of these observations to the fine structure of cellulose is discussed.

Introduction

Reports of nitrogen adsorption studies on cellulose go back 25 years,[2] but it is only within the past few years that the necessity for total exclusion of atmospheric moisture during all steps in processing the sample has been appreciated. Building on an earlier work by Haselton,[3] Merchant[4] has critically examined the effect of conditions of solvent drying upon the figure for apparent total surface area of wood cellulose obtained from nitrogen adsorption

(1) Presented at the 134th National Meeting of the American Chemical Society, Chicago, Ill., Sept. 7–12, 1958.

(2) (a) N. H. Grace and O. Maass, THIS JOURNAL, **36**, 3046 (1932); (b) P. H. Emmett and T. DeWitt, *Ind. Eng. Chem., Anal. Ed.*, **13**, 28 (1941); (c) A. G. Assaf, R. H. Haas and C. B. Purves, *J. Am. Chem. Soc.*, **66**, 66 (1944); (d) C. M. Hunt, R. L. Blaine and J. W. Rowan, *J. Research Natl. Bur. Standards*, **43**, 547 (1949).

(3) (a) W. R. Haselton, *Tappi*, **37**, 404 (1954); (b) **38**, 716 (1955).

(4) M. V. Merchant, *ibid.*, **40**, 771 (1957).

data. This worker showed that polarity and molecular weight of the final solvent and the temperature of drying were all-important in determining the ultimate surface accessible to nitrogen. Merchant worked primarily with the sequence water–methanol–non-polar solvent and discovered that in this case the surface tension of the non-polar solvent determined the surface area available. As surface tension decreases, either by going down the homologous series in molecular weight or by increasing the temperature of drying, the total surface of the cellulose increases. Merchant found that atmospheric moisture must be rigorously excluded from the dried sample to prevent large decreases in the surface available to nitrogen.

For the present work, it was decided that the sequence water–methanol–*n*-pentane should be used with drying at 35.5°. This procedure yields a very large accessible surface with good reproducibility, but it is acknowledged that the choice is arbitrary and does not produce the "ultimate" surface which might be made available to nitrogen molecules. It was considered, however, that this technique and conditions represent a sufficient advance over those which were employed in previous investigations so that a definitive study could be made of the effect of beating on surface area and pore size distribution.

Experimental Procedure

Sample Preparation.—Bleached sulfite cellulose (primarily western hemlock) was obtained from the manufacturer in the undried state. Ninety grams of this pulp was thoroughly dispersed in 2000 g. of water and then charged to a ball mill with 4546 g. one-inch porcelain balls. The mill was of porcelain, 10.5 by 13 inches, and rotated at 60 r.p.m. After completion of the specified maceration time, the fiber charge was withdrawn from the ball mill and fractionated to remove debris. A device designed to separate fibers by length, the Bauer–McNett classifier, was used and only the fraction retained on a 150-mesh screen was saved for experimental use. The whole fibers retained for study were dewatered to about 30% solids and stored at low temperature in the presence of formaldehyde.

In preparing the sample for study, one to two grams of wet fiber was soaked in excess water for 24 hours, and then packed into the enlarged portion of a cylindrical sample holder. This holder was fashioned from a 25-mm. test-tube, with a capillary tube and stopcock with 1-mm. capillary bore attached to the bottom. After insertion of the sample, a top closure was fused in place connecting to a capillary with a 2-mm. bore stopcock and terminating in a 10/30 standard taper inner joint.

The anhydrous methanol employed for this study was specially dried by refluxing absolute methanol with magnesium turnings and iodine, and then distillation. The anhydrous pentane was prepared by distillation over sodium. Nitrogen required for the processing was dried by passing over phosphorus pentoxide and magnesium perchlorate.

For solvent displacement, the sample holder was connected to the solvent reservoir by means of the standard taper joint and the water displaced by slowly passing 600 ml. of anhydrous methanol through the packed bed of fiber; the methanol was then displaced with a like amount of anhydrous pentane. With the sample holder and its attached tubing full of pentane, the device was detached from the solvent reservoir and attached to the gas drying train. The sample holder was thermostated at 35.5° during the first four hours of drying. (Nitrogen flow rate was 50 cc./min.) For 12 hours succeeding, the flow of nitrogen was continued but the sample was permitted to cool to room temperature. At the completion of drying, both stopcocks were closed, the bottom connection was sealed off, and the sample holder transferred to the vacuum header of the gas adsorption apparatus where it was pumped down to a pressure of 10^{-4} mm.

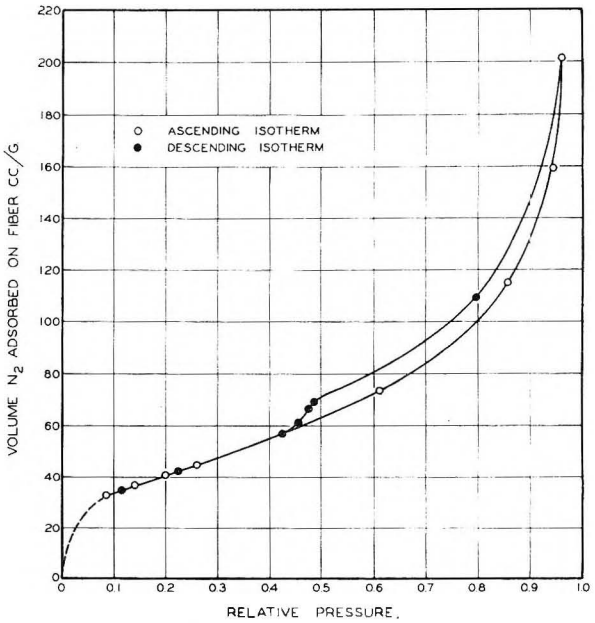

Fig. 1.—Representative isotherms: nitrogen adsorption on wood cellulose fibers dried from pentane.

Gas Adsorption.—The nitrogen adsorption apparatus was of the Harkins–Jura[5] type and is essentially the same one described by Haselton.[2]

After the sample had been thoroughly degassed by being connected to the vacuum header overnight, it was immersed in liquid nitrogen, dead space determinations were made with helium, and complete ascending and descending isotherms were obtained using conventional and careful technique. A typical isotherm is shown in Fig. 1. At the conclusion of the run, the dry weight of the sample was determined.

For each sample, the ascending and descending portions of the isotherm were always identical or essentially so below relative pressure 0.45. As a matter of routine, however, only data points on the ascending (adsorption) isotherm were used to calculate the surface area by the well-known method of Brunauer, Emmett and Teller.[6]

The highest relative pressure attainable with the particular apparatus was slightly over 0.97. Since this figure is a convenient starting point for the Pierce[7] method of computing pore size distributions, the adsorption isotherm terminated and the desorption isotherm began at or about 0.97 in all cases.

Surface Area of Cellulose.—The summarized data in Table I show surface areas computed from the lower part of the adsorption isotherm using the Brunauer–Emmett–Teller (BET) method and from the upper part of the desorption isotherm calculated by the Pierce method. Considering the great differences in the assumptions on which the respective calculations are based, the agreement is remarkable. However, since the assumptions on which the BET calculation rests have been better tested and validated, it is assumed that the BET "areas" are more likely to be the "correct" values for apparent surface.

Inspection of the comparative figures for surface area and time of ball mill beating shows that the apparent surface increment due to beating is a direct linear function of the time of beating. Since the power output characteristic of the ball mill is essentially constant with time, these results are consistent with Rittinger's law for size reduction, which states that new surface developed is directly proportional to energy input.

The correlation to be expected between water-vapor adsorption and nitrogen adsorption on cellulose is not yet clear. It would seem that nitrogen adsorption might never cover all the surface accessible to water, even if a 100% efficient

(5) G. Jura and W. D. Harkins, *J. Am. Chem. Soc.*, **66**, 1356 (1944).
(6) S. Brunauer, P. H. Emmett and E. Teller, *ibid.*, **60**, 309 (1938).
(7) G. Pierce, THIS JOURNAL, **57**, 149 (1953).

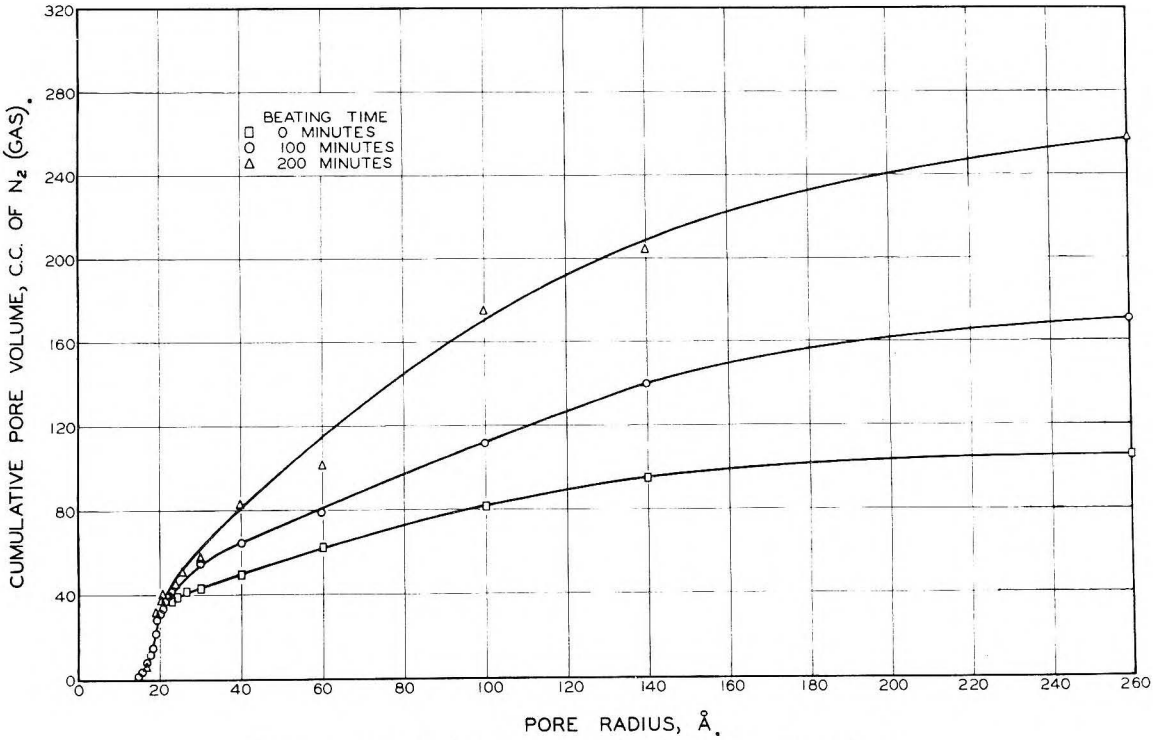

Fig. 2.—Influence of beating on pore distribution in cellulose fibers.

TABLE I

NITROGEN ADSORPTION RESULTS ON SOLVENT-DRIED FIBERS —B.E.T. AREAS AND PORE SIZE DISTRIBUTIONS

Time of ball mill beating, min.	Total area B.E.T. method, sq. m./g.	Area from Pierce calcd., sq. m./g.	Tot. vol. N_2 ads., cc./g., S.T.P. Exptl.	Tot. vol. N_2 ads., cc./g., S.T.P. Calcd.	Modal pore diam., Å.	Calcd. vol. pores 32–44 Å. diam., cc./g. (liq. N_2)	Calcd. vol. pores 80–200 Å. diam., cc./g. (liq. N_2)
0	100	95	121	116	38.0	0.0550	0.0499
20	110	108	142	143	38.2	.0542	.0584
50	123	115	157	155	37.8	.0546	.0601
100	149	128	195	191	38.0	.0542	.0735
150	164	159	250	242	37.5	.0647	.0926
200	185	170	285	294	37.4	.0607	.1447
250	202	178	280	275	38.5	.0657	.1153

solvent displacement technique were used in preparation. Comparison of the results of the present investigation with those of other workers is therefore not very revealing. The surface area reported here for nitrogen adsorption on unbeaten wood cellulose is considerably larger than some figures reported earlier,[1] where the final solvent was butanol or benzene. This is to be expected from the principles outlined by Merchant.[4] The surface area reported for unbeaten fiber is of the same order of magnitude as that calculated by Escard, Saulquin and Girardy[8] from water–vapor adsorption data on cotton cellulose. These workers reported an increase in area from 120 sq. m./g. at the start to 142 sq. m./g. after prolonged beating. The fact that Escard, *et al.*,[8] obtained a much smaller increase in accessible area on beating than we did is probably related to the higher crystallinity of the cotton cellulose. All that can be concluded is that the surface area available for adsorption in the samples as prepared for this study represents a large part of the porous structure existing in water-swollen cellulose.

A previous investigation in some ways close to the present one is the argon adsorption study of Grotjahn and Hess,[9] but comparison of their figures with those here presented is quite difficult. Firstly, it is not entirely clear what final solvent was used by these previous authors: they specify that the cellulose was dried by azeotropic distillation with butanol and then state that final displacement with and drying from ether is desirable. They do not state, however, whether or not ether was used actually in their procedure, a fact which would have considerable bearing on the apparent surface area obtained. Also while these authors comment on the decrease in surface area which occurs on exposure to atmospheric moisture, it appears that they considered it a question of many days at relatively high humidity to obtain a significant effect. There is no certainty that they completely excluded the atmosphere in handling and transferring their specimens, although they did carry out the final drying *in vacuo*. They further reported that their preparations were fine white powders, whereas we used only whole fibers with fines removed. Finally, the initial surface reported by them was quite low (*ca.* 40 m.²/g.), rose to a maximum of a little over 200 m.²/g. after two hours wet maceration in their beating device, and then leveled off at a slightly lower figure up to their maximum beating time of 5 hours.

Pore Size Distribution.—In addition to the surface area data just discussed, Table I also gives information of the volume of gas taken up by each sample and on the pore-volume and pore-size distribution as calculated by the Pierce method. As the original author explains in his paper,[7] one test of the validity of the pore-volume analysis is to check the calculated total volume of pores against the actual experimental amount of gas adsorbed. Pierce appears to believe that these figures should check within about 5% to show good agreement and a valid analysis. The seven runs shown in Table I all show the required agreement within 5% or less, for the most part less.

In Fig. 2, the cumulative pore volume (expressed in terms of cc. of nitrogen gas at standard conditions) is plotted as a function of pore radius for samples beaten 0, 100 and 200 minutes. It may be noted that the differences brought about by beating (increase in pore volume) begin to show up at about 22 Å. pore radius; below this value, beating does not make very much difference. This point is also illustrated in Table I, where it may be seen that the most common pore diameter (expressed as cc. of *liquid nitrogen*) in the diameter range below 44 Å. remains unchanged during the first 100 minutes of beating and is but slightly increased thereafter. On the other hand, the volume of pores in the

(8) J. Escard, A. Saulquin and E. Girardy, *Assoc. tech. ind. papetiere Bull.*, **7**, 366 (1951).

(9) H. Grotjahn and K. Hess, *Kolloid-Z.*, **129**, No. 2/3, 128 (1952).

larger diameter range of 80–200 Å. increases regularly with beating time.

Despite the theoretical uncertainties in Kelvin equation applications such as the Pierce calculation, the conclusion is inescapable that the ball-mill beating of wood cellulose creates additional pores or fissures in the amorphous regions of the fiber, or at least enlarges existing pores, all the way down to 50 Å. or so in pore diameter.

Relation to Fine Structure of Cellulose.—The break in the descending isotherm between relative pressure 0.50 and 0.45 (Fig. 1) appears consistently in all cellulose samples, beaten and unbeaten, and has been independently observed by four different experimenters in these laboratories, as well as by Hunt, Blaine and Rowan.[2d] Even though any present method of calculating the absolute value of the pore sizes and pore volumes concerned may be open to some criticism as to accuracy, the generalized conclusion from these facts is inescapable, *viz.*, wood and cotton cellulose in the native, swollen state contain a sizable volume (*ca.* 0.05 cc./g.) of pores rather narrowly distributed in a range with a median pore diameter of about 40 Å. The results of this particular investigation further indicate that the volume of these very small pores does not change appreciably with moderate amounts of wet maceration but does increase somewhat with severe and continued mechanical treatment in the wet state.

The inference from these observations and conclusions is that the 40 Å. diameter pore size is a characteristic of the fine structure of wood cellulose fibers and may be related to the basic structural unit in wood cellulose. It may be hypothesized, for example, that the elementary building blocks of "solid" cellulose are laid down in some sort of array (*e.g.*, hexagonal) permitting the regular occurrence of "holes" approximately the size of an elementary polymer unit. It is not difficult to imagine several possible combinations of structural units, consistent with the known X-ray identity periods of cellulose, which would permit such regular occurrence of holes. The elucidation of such possibilities should provide a fertile field for further research.

Conclusions

The increase in total (internal and external) surface of wood cellulose fibers upon wet maceration in a ball mill is a linear function of time and is principally accounted for by the increase in volume of submicroscopic pores in the range of 44-800 Å. diameter. The most common pore size of 38 Å. diameter is unaffected by beating and the total volume in the range about that pore size is but slightly affected. It is suggested that this most common pore diameter is a fundamental property of the cellulose and that it is structurally related to the elementary polymer unit of cellulose.

Acknowledgment.—The authors wish to acknowledge the financial assistance in carrying out this investigation of the thirty-seven pulp and paper manufacturing companies comprising the Pulp Evaluation Group and to thank them for permission to publish these results.

KINETICS OF THE FISCHER-TROPSCH SYNTHESIS ON IRON CATALYSTS. I. RATE DATA ON REDUCED AND NITRIDED CATALYSTS

BY F. S. KARN, B. SELIGMAN, J. F. SHULTZ AND R. B. ANDERSON

Branch of Coal-to-Oil Research, Division of Solid Fuels Technology, Bureau of Mines, Pittsburgh, Pa.

Received January 13, 1958

Kinetic data are presented for the Fischer–Tropsch synthesis on nitrided fused-iron catalysts at 21.4 atmospheres with feed gases varying from $2H_2 + 1CO$ to $0.25H_2 + 1CO$. Sufficient results are reported to demonstrate that the kinetics of the synthesis are qualitatively similar on both reduced and reduced-and-nitrided catalysts, despite major differences in selectivity. As nitrided catalysts maintained essentially constant activity for long periods of time compared with rapidly changing activity for reduced catalysts, the bulk of the experiments were made with nitrided catalysts. For nitrided-iron catalysts the over-all apparent activation energy determined by empirical methods increased with increasing carbon monoxide content of the feed gas, for example, by comparing the initial reaction rates activation energies of 19.5 kcal./mole for $2H_2 + 1CO$ and 23.7 for $0.7H_2 + 1CO$ were obtained. The initial reaction rate r_0 could be expressed by the equation $r_0 = ap_{H_2}^{0.65}p_{CO}^{0.34}$.

Introduction

Kinetic data for the Fischer–Tropsch synthesis on iron catalysts are meager. Early German experiments[1,2] were usually not designed to permit a simple interpretation of kinetic aspects of the synthesis. Some general features of the synthesis were described in recent papers from foreign laboratories,[3–5] and the Bureau of Mines.[6]

Synthesis studies[6] on reduced iron catalysts with $1H_2 + 1CO$ gas at principally 7.8 atmospheres showed that the rate data could be expressed by the empirical equation

$$-\log(1 - x) = \frac{A'Pe^{-E/RT}}{S}$$

where x is the conversion of $H_2 + CO$, S the space velocity, P the operating pressure and E has the value of 18–20 kcal./mole. The usage ratio, H_2/CO, was shown to decrease, pass through a minimum and increase as the conversion was increased.

The present paper extends this study to 21.4 atmospheres for both reduced and nitrided iron catalysts with a variety of feed gas compositions. Experiments with the reduced catalyst were difficult because of a rapid decrease in catalytic activity. The activity was checked at frequent intervals by short tests at "standard" conditions, and the catalyst was replaced when significant changes in activity were observed. The nitrided catalyst showed only minor variations in activity durin periods of operation as long as six months.

(1) A. Scheuerman, in report of H. Zorn, "The CO–H_2 Synthesis at I. G. Farben.," PB 79,368 (1949); FIAT Final Report 1267 (1949).

(2) H. H. Storch, N. Columbic and R. B. Anderson, "The Fischer–Tropsch and Related Syntheses," John Wiley and Sons, Inc., New York, N. Y., 1951.

(3) H. Tramm, *Brennstoff-Chem.*, **33**, 21 (1952).

(4) Fuel Research, 1953 and 1954, Department of Scientific and Industrial Research, London.

(5) H. Uchida, M. Kuraishi, H. Ichinokawa and K. Ogawa, *Bull. Chem. Soc. Japan*, **29**, 181 (1956).

(6) R. B. Anderson, B. Seligman, J. F. Shultz, R. Kelly and M. A. Elliott, *Ind. Eng. Chem.*, **44**, 391 (1952).

Experimental

The apparatus described previously was used with only minor changes.[6-8] The reactor held about 75 cc. of catalyst in a half-inch, schedule 40, steel pipe surrounded by an electrically heated bath of boiling Dowtherm. The temperature of the bath was maintained by regulating the pressure on the boiling Dowtherm. The flow of synthesis gas, which was premixed in cylinders, was controlled by a geared needle valve and measured by calibrated capillary flowmeters held at 35° in a thermostat. Synthesis gas was passed down through the catalyst bed, and most of the water and C_5^+ hydrocarbons were condensed in the wax trap and refrigerated trap. Pressure was reduced by a back-pressure regulator, and the gas was passed through a carbon dioxide scrubber,[9] a water-saturating vessel and measured in a water-filled wet test meter.

Gas samples were collected beyond the back-pressure regulator for Haldane carbon dioxide analyses and for mass spectrometric analyses. The latter samples were collected by withdrawing mercury from the sample bulb at a constant rate over a period of an hour or more. The mass spectrometric analysis for H_2, CO, CO_2, CH_4 and C_2 to C_4 saturated and unsaturated hydrocarbons accounts for all components except water present in sizable amounts in the gas phase at synthesis temperature. Water was estimated from an oxygen balance, assuming that all the oxygen in the products was present as carbon dioxide or water. An attempt was made to remove exit gas directly from the outlet of the reactor into an evacuated vessel at total pressure less than the vapor pressure of water. Mass spectroscopic analyses of these gases could not account for a substantial fraction of the water vapor, and hence the method was discontinued.

In this study, 6- to 8-mesh particles of fused ammonia synthesis catalyst D3001 were used. The raw catalyst contained Fe 67.2 weight %, SiO_2 0.71, Cr_2O_3 0.65, MgO 4.61, K_2O 0.67, and oxygen combined with iron 26.04. Physical properties and behavior of this catalyst during reduction, pretreatment and synthesis have been described in previous papers.[10-14] The catalyst was reduced in hydrogen at an hourly space velocity of 2,500 at 450° for 40 hours and at 500° for 8 hours in a metal-block reactor.[11] Nearly complete reduction (98.3 to 98.6%) was achieved in this treatment. Nitrides were prepared by treating the reduced catalyst with anhydrous ammonia at an hourly space velocity of 1,000 at 350° for 12 hours. This treatment converted the catalyst to an ϵ-nitride with an atom ratio N/Fe of about 0.47.

The pretreated catalysts were transferred to the synthesis unit by methods that prevent exposure to air,[11] and $1H_2 + 1CO$ gas was introduced at 21.4 atmospheres and an hourly space velocity of 300. For reduced catalysts the temperature was increased rapidly to 220° and then slowly increased to 255°; at this temperature the flow was adjusted to give an apparent contraction of 65%. This flow rate and temperature were used as reference conditions to test reproducibility of catalyst charges and variation of activity with time. For nitrided catalysts reference conditions were similarly established at 240°.

For each experimental point with a given feed, the temperature and flow were set at the desired values, and the reactor was operated long enough for the contraction to become constant, indicating that reaction products from the previous condition had been flushed from the system. The time required for reaching steady-state conditions varied inversely with space velocity. Flows of gas into and from the reactor were then determined over a 2-hour period, and a sample of exit gas was collected for mass spectrometric analysis. At the end of the test period, carbon dioxide was determined on an exit-gas sample with a Haldane apparatus.

Data were obtained at 21.4 atmospheres with synthesis gas having H_2/CO ratios of 1.0 and 2.0 at 240° and 255° for reduced catalysts and with H_2/CO ratios of 0.25, 0.7, 1.0 and 2.0 for nitrided catalysts at 225° and 240°. Gas flows were varied to obtain conversions of $H_2 + CO$ from about 0.05 to 0.85.

In the hydrocarbon synthesis, the principal reactions producing higher hydrocarbon may be represented by

$$(1 + y)H_2 + (2 - y)CO = \frac{1}{n}(CH_2)_n + yH_2O + (1 - y)CO_2 \quad (1)$$

where y may vary from -1 to $+2$. Thus 3 moles of $H_2 + CO$ produce $1/n$ moles of $(CH_2)_n$, and a useful measure of extent of reaction is the fraction of $H_2 + CO$ consumed x. The conversion x is defined as $x = 1 - E/I$, where I and E are, respectively, volumes (S.T.P.) of $H_2 + CO$ introduced into and passing from the reactor per unit time. This quantity is not influenced by the water–gas-shift reaction, which is apparently a secondary process. In this paper space velocity is defined as volumes (S.T.P.) per bulk volume of catalyst per hour.

Results

Data for a typical experiment with nitrided iron catalyst computed from the inlet and outlet flows are shown in Table I.[15] Plots of data of this type as a function of reciprocal space velocity, S^{-1}, for reduced catalysts with $1H_2 + 1CO$ feed gas at 240° are in Fig. 1. Similar graphs for nitrided catalysts with $2H_2 + 1CO$ and $1H_2 + 1CO$ are given in Figs. 2 and 3. The upper portions of these graphs show plots of conversion of $H_2 + CO$, x; space-time-yield, xS; and differential reaction rate, $r = dx/d(1/S)$ as determined by two graphical differentiation methods. The lower portions of these graphs show plots of mole fractions of the major components of the exit gas as a function of reciprocal space velocity. To demonstrate the influence of gas composition and the general consistency of experimental results from tests with nitrided catalysts, all of the rate data are plotted on a double logarithmic scale in Fig. 4. This plot expands the scale to show the relationship of experimental points at low values of S^{-1} more clearly.

The data in Figs. 1 and 2 indicate that the kinetics of the Fischer–Tropsch synthesis are qualitatively similar for reduced and nitrided catalysts despite large differences in selectivity. Results for tests with $0.25H_2 + 1CO$ gas are probably complicated by the carbon-forming reaction, $2CO = CO_2 + C$, as the conversion exceeds the maximum allowable according to equation 1. Figure 4 indicates that the rate of synthesis increases with hydrogen content of the feed gas, possibly to a maximum between 50 and 67% hydrogen.

The differential reaction rates at zero conversions r_0 were estimated by extrapolating the xS-curves to $S^{-1} = 0$, and by empirical equations.

(7) R. B. Anderson, A. Krieg, B. Seligman and W. E. O'Neill, *Ind. Eng. Chem.*, **39**, 1548 (1947).

(8) H. H. Storch, R. B. Anderson, L. J. E. Hofer, C. O. Hawk, H. C. Anderson and N. Golumbic, U. S. Bureau of Mines Tech. Paper 709, 1948.

(9) A. Krieg, A. Dadash and R. B. Anderson, *Ind. Eng. Chem.*, **41**, 1508 (1949).

(10) W. K. Hall, W. H. Tarn and R. B. Anderson, *J. Am. Chem. Soc.*, **72**, 5436 (1950); THIS JOURNAL, **56**, 688 (1952).

(11) R. B. Anderson, J. F. Shultz, B. Seligman, W. K. Hall and H. H. Storch, *J. Am. Chem. Soc.*, **72**, 3502 (1950).

(12) J. F. Shultz, B. Seligman, L. Shaw and R. B. Anderson, *Ind. Eng. Chem.*, **44**, 397 (1952).

(13) R. B. Anderson, L. J. E. Hofer, E. M. Cohn and B. Seligman, *J. Am. Chem. Soc.*, **73**, 944 (1951).

(14) J. F. Shultz, B. Seligman, J. Lecky and R. B. Anderson, *ibid.*, **74**, 637 (1952).

(15) Detailed data similar to Table I for tests of nitrided catalysts with $2H_2 + 1CO$, $1H_2 + 1CO$ and $0.7H_2 + 1CO$ gas at 225 and 240° are presented as Document number 5593 with the ADI Auxiliary Publications Project, Photoduplication Service, Library of Congress, Washington 25, D. C. A copy may be secured by citing the Document number and by remitting $1.25 for photoprints, or $1.25 for 35 mm. microfilm in advance by check or money order payable to: Chief, Photoduplication Service, Library of Congress.

TABLE I

BASIC DATA AS COMPUTED FROM GAS FLOWS AND COMPOSITIONS. NITRIDED CATALYST WITH $1H_2 + 1CO$ GAS AT 240°

Space velocity, hr.$^{-1}$	Se/S[a]	Conversion, %	Reaction[b] rate, hr.$^{-1}$	Partial pressures of exit gas (atm.) p_{H_2}	p_{CO}	p_{CO_2}	p_{H_2O}[c]	p_{CH_4}	p_{C_2}	$p_{C_3+C_4}$
Feed gas[d]	1.00	(0)	293	10.68	10.68	0.02	0	0.02	0	0
1834	0.904	16.3	264	10.16	9.60	.77	0.46	.19	0.10	0.12
1177	.870	22.6	247	9.86	9.14	1.25	.51	.31	.13	.20
903	.831	28.4	233	9.54	8.89	1.70	.60	.38	.13	.13
607	.766	38.5	204	8.97	8.35	2.50	.85	.52	.18	.08
325	.610	64.9	126	8.02	4.78	5.43	1.39	1.14	.31	.31
222	.530	79.2	49	6.84	1.99	8.42	1.40	1.70	.56	.47
112	.472	88.2	..	5.41	0.50	10.12	1.96	2.32	.67	.44

[a] Ratio of outlet flow S_e to inlet flow S. Outlet flow includes H_2O, CO_2 and C_1–C_4 hydrocarbons. [b] Computed using the half-order empirical equation. [c] Computed by difference from oxygen balance assuming that no oxygenated molecules other than CO_2 and H_2O are formed. [d] Corresponds to infinite space velocity or zero conversion.

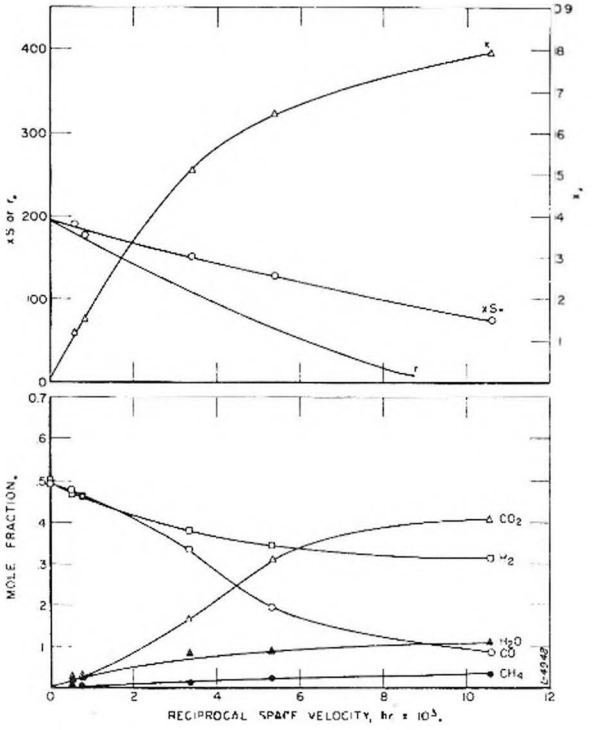

Fig. 1.—Evaluation of data for 1 H_2 + 1 CO feed gas at 240°, reduced catalyst.

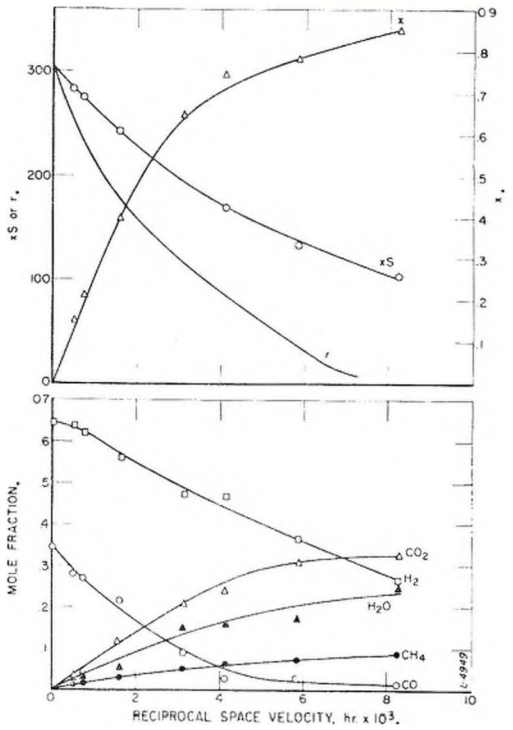

Fig. 2.—Evaluation of data for 2 H_2 + 1 CO feed gas at 240°, nitrided catalyst.

First or half order equations of the type $r = k(1 - x/x_e)^n$, where $n = 1$ or $1/2$, $k = r_0$, and x_e is a constant, were used. As previously reported[6] the first-order empirical equation with $x_e = 1$ in the integrated form, $-\ln(1 - x) = k/S$, fits the kinetic data satisfactorily up to $x = 0.4$, as shown in Fig. 5, and in some cases up to $x = 0.6$ or 0.7. If x_e is taken as an adjustable constant, the half-order empirical integrated equation

$$xS - k - k^2/(4x_eS)$$

does provide a satisfactory representation of the data up to conversions of 0.7 or 0.8.[16] This equation also was used to compute the differential reaction rate r. These values, shown in Table I, are in good agreement with those obtained by graphical differentiation. Values of r_0 obtained by various methods and over-all activation energies computed by the Arrhenius equation are given in Table II.

Activation energies of the over-all synthesis may also be obtained by comparing values of xS at constant conversion; activation energies computed in this way are given in Table III for conversions of 0, 0.15, 0.30, 0.45 and 0.60.

Discussion

The experimental results indicate that the kinetics of the synthesis are essentially the same for reduced and reduced- and nitrided-fused iron catalysts despite the rather large differences in selectivity of these catalysts. As the activity of nitrided catalysts remained essentially constant for long periods, the results from nitrided catalysts will be largely used to interpret the kinetics of the Fischer–Tropsch synthesis. Although the experiments were carefully made and the best available

(16) The fact that first- and half-order empirical equations give reasonably good descriptions of the same data is not surprising. Plots of x against S^{-1} for first- and half-order equations deviate less than the usual experimental errors up to values of x of 0.3 or 0.4. *cf.*, C. D. Prater and R. M. Lago, "Advances in Catalysis," Vol. VIII, Academic Press, Inc., New York, N. Y., 1956, pp. 295–301.

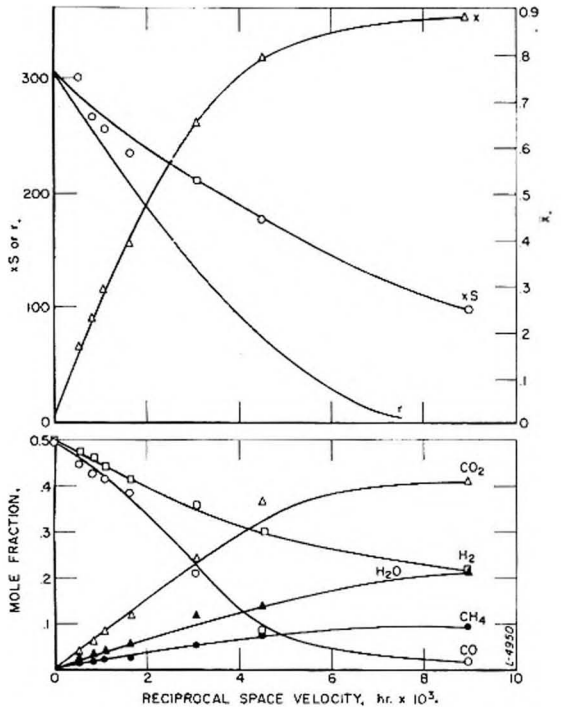

Fig. 3.—Evaluation of data for 1 H_2 + 1 CO feed gas at 240°, nitrided catalyst.

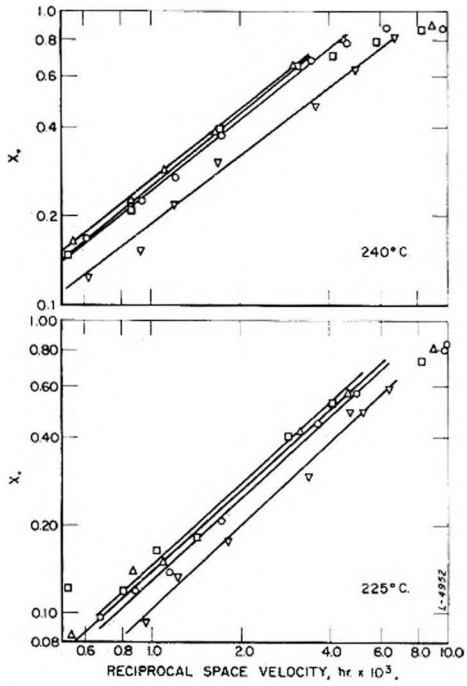

Fig. 4.—Double logarithmic plot of rate data for nitrided catalysts: □, 2 H_2 + 1 CO; △, 1 H_2 + 1 CO; ○, 0.7 H_2 + 1 CO; ▽, 0.25 H_2 + 1 CO.

analytical methods were employed, the final kinetic results have a moderate degree of uncertainty. Data for tests with 0.25H_2 + 1CO gas at moderate to high conversions should not be regarded as significant, as carbon forming and other reactions probably occur.

The simple first-order type rate equation $r = k(1 - x)$, is very useful for examining the over-all characteristics of the synthesis and for evaluating

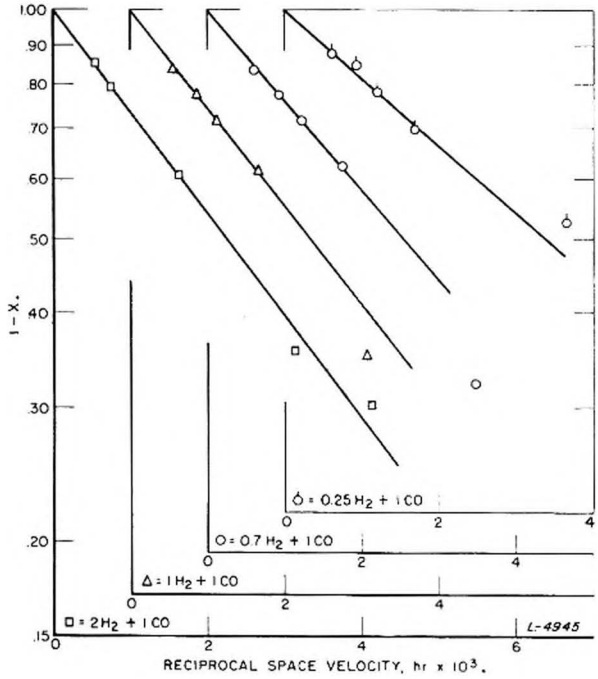

Fig. 5.—Data for nitrided catalysts at 240° according to empirical equation.

TABLE II

VALUES OF INITIAL REACTION RATE, r_0

A. Reduced catalysts

Synthesis gas H_2/CO	r_0 at 240° by method A[a]	B[b]	C[c]	Av.	r_0 at 255° by method A[a]	B[b]	C[c]	Av.
2/1	191	182	186	186	324	330	..	327
1/1	193	190	190	191	315	314	..	314

B. Nitrided catalysts

	225°				240°			
2/1	181	161	161	168	315	289	291	298
1/1	169	146	157	157	303	282	293	293
0.7/1	134	130	140	135	279	272	262	271
0.25/1	114	98	112	108	207	205	204	205

C. Activation energies from Arrhenius equation using average values of r_0

	Reduced catalysts	Nitrided catalysts
2/1	20.4	19.5
1/1	17.9	21.2
0.7/1	..	23.7
0.25/1	..	21.8

[a] From equation $-\ln(1 - x) = k/S$. [b] Extrapolation of values of xS to $S^{-1} = 0$. [c] From half-order empirical equation.

TABLE III

ACTIVATION ENERGIES FROM RATIOS OF xS VALUES AT CONSTANT VALUES OF x FOR NITRIDED-IRON CATALYSTS

Conversion, x	Activation energies for different feed gases, kcal./mole: 2H_2 + 1CO	1H_2 + 1CO	0.7H_2 + 1CO	0.25H_2 + 1CO
0	19.5	21.2	23 7	21.8
0.15	21.5	21.7	22 4	19.2
.30	17.6	20.0	20.8	19.9
.45	18.8	19.5	20.9	..
.60	17.8	19.5	18.6	..

and correlating data of catalyst testing experiments and studies in larger reactors. It must be inferred that the over-all reaction is greater than first order

with respect to partial pressures of H_2 + CO, as these partial pressures decrease less rapidly with increasing x than the quantity $(1 - x)$. Equally good or better representation of the data is obtained by a half-order equation.

For nitrided catalysts the apparent over-all activation energies computed from the variations of r_0 increase with carbon monoxide content of the feed gas up to $0.7H_2 + 1CO$, and the magnitude of the increase seems to be greater than experimental uncertainties. This trend is also shown by activation energies computed by comparing values of xS at constant x in Table III. The fact that relatively constant activation energies are obtained by this method, as well as by the empirical equation suggests that the rate equation can, to at least a first approximation, be separated into the form $r = f(T)g(x)$. Activation energies for reduced iron catalysts reported by British workers[4] varied in the same way with gas composition. Their values were 14.5, 18, 22.3 and 27.5 kcal./mole for feed gases with H_2/CO ratios of 3, 2, 1.12 and 0.67, respectively.

If the extrapolation to zero values of S^{-1} is correct, values of r_0 may be properly related to the feed gas composition. A rate equation

$$r_0 = a p_{H_2}^{1-n} p_{CO}^{n} \qquad (2)$$

which will be considered in detail in a subsequent paper, was rearranged to

$$r_0 = a P_t f^{1-n} (1 - f)^n \qquad (3)$$

$$\frac{r_0}{f} = a P_t [(1 - f)/f]^n$$

where a is a constant, p_{H_2} and p_{CO} are the partial pressures of H_2 and CO, respectively, n is a constant less than 1, P_t is the system pressure, and f is the mole fraction of H_2 in the feed gas. A double logarithmic plot of r_0/f against $(1 - f)/f$ should give a straight line with a slope of n, and approximately linear plots were obtained as shown in Fig. 6. For nitrided catalysts, values of n of 0.32 and 0.36 were obtained at 225 and 240°, respectively, and the initial reaction rate can be represented by

$$r_0 = a p_{H_2}^{0.66} p_{CO}^{0.34}$$

This equation approximates the data for reduced catalysts to within the experimental uncertainties.

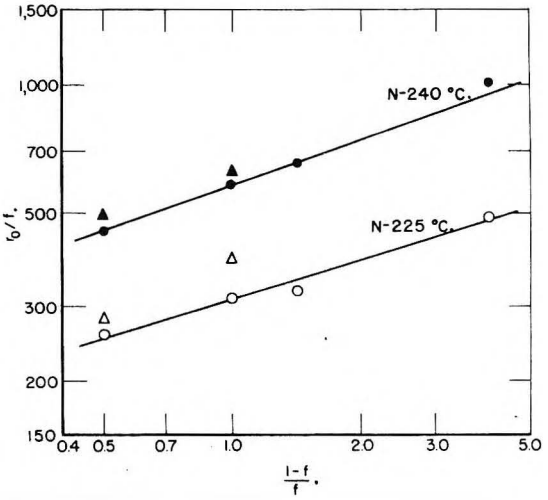

Fig. 6.—Plots of equation 3 for reduced catalysts at 240° ▲, and 255° △, and nitrided catalysts at 225° ○ and 240° ●.

THE HEATS OF FORMATION OF CHF_3 AND CH_2F_2[1]

BY CONSTANTINE A. NEUGEBAUER AND JOHN L. MARGRAVE

Contribution from the Department of Chemistry, University of Wisconsin, Madison, Wisconsin

Received February 8, 1958

The standard heats of formation at 298.15°K. of gaseous CHF_3 and CH_2F_2, have been determined in a rotating bomb calorimeter as -162.60 ± 0.65 and -105.50 ± 0.22 kcal./mole, respectively.

Introduction

Investigations on the properties of gaseous fluorocarbons have been carried out extensively in recent years, primarily because of the use which these gases find in the refrigerating and polymer fields and because of their great chemical stability. Nevertheless, not many quantitative data are available on their thermal stabilities and heats of formation, probably because of the difficulties involved in making the particular fluorocarbon undergo reaction. No measurements of the heats of formation of the fluoromethanes have been carried out hitherto, with the exception of CF_4, the most stable of all fluorocarbons. Six independent determinations of its heat of formation were reported prior to 1956, ranging from -161 to -231 kcal./mole. This spread illustrates the difficulties encountered in making precise calorimetric investigations on these compounds.

The four main problems which have to be solved in fluorocarbon calorimetry are: (1) many fluorocarbons are inert toward the common chemical reagents used in calorimetry, such as oxygen and hydrogen. (2) The thermodynamic state of the final products in the reaction whose heat is measured may be inadequately defined, such as gaseous HF, amorphous carbon, CO_2 dissolved in aqueous HF, etc. (3) The data needed to make the nonideality corrections are generally not available. (4) Since aqueous HF is a common product in combustion reactions involving fluorocarbons, corrosion problems arise.

An isothermal bomb calorimeter was used exclusively in this investigation since most of the reactions would not take place unless the reactants

(1) Abstracted in part from the thesis presented by Constantine A. Neugebauer in partial fulfillment of the requirements for the degree of Doctor of Philosophy at the University of Wisconsin in February, 1957.

were at pressures higher than atmospheric. This made a flow calorimeter, which is generally used for gas reactions, unsuitable.

In order to achieve the maximum accuracy and precision attainable with the bomb calorimeter if a solution phase is formed in the reaction, it proved advantageous to construct a device which would allow the bomb to rotate end over end. Thus it was possible to agitate the contents of the bomb after combustion had occurred. The need for this is fourfold: (1) the solution phase will rapidly become uniform in concentration throughout and will thus be in a well defined standard state. (2) The gas phase will reach equilibrium quickly with the dissolved species in solution. (3) Corrosion of the bomb is reduced by preventing the formation of very concentrated HF solutions. (4) The heat exchange between the pool of solution inside the bomb and the calorimeter water is greatly speeded up. This prevents interference in the after period in the measurement of the temperature rise.

Experimental

Design and Operation of the Rotating Bomb Calorimeter.—A stationary bomb calorimeter, which was used in the determination of the heats of formation of CF_2CF_2, CH_2CF_2 and CF_4, and of conventional design has been described previously.[2] This calorimeter has been modified to operate with a rotating bomb.

Sunner,[3] studied the combustion calorimetry of organic sulfur compounds in the first moving-bomb calorimetric system. A similar method was used at the Bureau of Mines[4,5] to measure the heats of combustion of various nongaseous sulfur and fluorine compounds.

A double valve Parr illium bomb of conventional cylindrical design and a capacity of 360 ml. was used in all experiments. The illium metal is quite resistant to attack by aqueous HF up to about 3 molar, provided the bomb is stationary. No metal ions were detectable when 100 ml. of a 3 *M* solution of HF was formed in the hydrogenation of tetrafluoroethylene, even though the solution was in contact with the metal for about one hour.

If the bomb is rotated, however, some corrosion will take place, the extent of which depends on the concentration of the acid produced and the length of the time of rotation. About 1% of the acid reacted during a run when the bomb was rotated for 15 min. and the acid strength was 2 *M*.

The conventional loop electrode for ignition of the bomb charge was employed only in the calibration experiments with benzoic acid. Two short straight electrodes were used to ignite a gaseous mixture by electrically heating either a short length of platinum wire or a thin carbon rod to incandescence.

The calorimeter can was constructed from copper sheet and plated with a heavy layer of bright nickel to minimize radiation loss to the jacket. The bomb was held in a 1 inch wide stainless steel ring and tightened into place with six brass screws. Rotation of the bomb was effected by turning a vertical brass drive shaft with an electric motor. Torque was transmitted through two bevel gears so that the bomb itself made 16 r.p.m. Details of the construction are given in reference 1.

During a calorimetric measurement the jacket temperature was kept constant at 24.800 ± 0.003° with a conventional mercury regulator in conjunction with a thyratron relay. A slow flow of water was maintained through a cooling coil to balance the heat input by the heater.

In preparation for a run, one placed the charged bomb into the bomb carriage either in an upright position (for calibration experiments) or upside down (for the fluorocarbon experiments). When the bomb was upside down, the water initially in the bomb covered the stainless steel valves and protected them from the initial blast of the combustion.

The can containing the bomb was positioned in the well by visual observation and 6.8 l. of distilled water was added carefully. The water had been weighed to ±0.05 g., and had a temperature somewhat lower than that of the desired initial temperature in the experiment. Three drops of light oil were placed on the surface of the water to prevent excessive evaporation during the run. The water level was always sufficiently high to cover the bomb completely in any position.

A calorimetric type platinum resistance thermometer, Leeds and Northrup serial no. 1132445, was used in all experiments to measure the temperature rise produced by the reaction. This thermometer was calibrated by the National Bureau of Standards in 1955. The resistance of the thermometer was measured with a Mueller type Wheatstone bridge, Leeds and Northrup designation G-2, which was thermostated in an oil-bath at 30.0 ± 0.1°. The sensing element of the bridge was a high sensitivity (0.05 μ v./mm.) galvanometer, Leeds and Northrup Cat. No. 2284-b, with a 12.8 ohm critical damping resistance. In actual use the galvanometer was somewhat underdamped which gave a more rapid response. The galvanometer was 3.5 m. distant from the scale and the reflection of the filament of the galvanometer lamp from the galvanometer mirror onto the Lucite scale was used as the deflection indicator. A change in resistance in the thermometer of 0.0001 ohm moved the light spot 3 mm. on the scale.

Calibration of the Rotating Bomb Calorimeter.—Benzoic acid, NBS standard sample 39g having an isothermal heat of combustion at 25° of 26.4338 kj./g. mass under certificate conditions[6] was used for determining the energy equivalent of the calorimeter.

In the combustion of both CH_2F_2 and CHF_3, concentrated HF solutions containing dissolved CO_2, O_2 and excess fluorocarbons were found. Since the solubility and heat of solution of CO_2 and O_2 in aqueous HF are not known, and aqueous HF causes some corrosion of the bomb walls, a calibration under certificate conditions does not reproduce actual bomb conditions in many respects.

This difficulty was overcome by designing comparison experiments in a manner such that the final state of the calibration bomb process was as nearly equal to that obtained in the experiments with fluorocarbons as possible. Thus, the initial pressure of O_2 was chosen to be the same as the initial pressure of O_2 in the combustion experiments; the quantity of benzoic acid burned was taken to be such that the final partial pressure of CO_2 would be nearly identical with that obtained in the combustion experiments. In addition, 50.0 ml. of 2 to 3 *N* HF was added initially to the bomb, so that the final conditions after the combustion of benzoic acid very closely resembled those met in the actual combustion experiments. Comparison experiments of this type were first used by Waddington,[7] *et al.*, in 1956.

In all, three series of calibration experiments were performed. In the first series the calorimeter was calibrated by burning benzoic acid under certificate conditions in order to find the correct energy equivalent of the system. Two grams of acid was burned in each experiment, rather than the one gram recommended on the NBS certificate, to achieve a greater temperature rise. The appropriate certificate corrections were applied. The bomb was rotated for only 1 min. (16 revolutions).

In the second series a procedure exactly like the one outlined above for the comparison experiments was followed, with the exception that 50.0 ml. of pure water, rather than HF solution, was added initially to the bomb. The bomb was rotated for 230 sec. or longer. Reductions to standard states were made, and, if properly applied, should give the same value for the energy equivalent as the first series of calibration experiments under certificate conditions. The third series of calibration experiments consisted of the comparison experiments with HF present.

When calibration experiments were carried out under certificate conditions, reductions to standard states did not have to be applied, since the value for the heat of combus-

(2) C. A. Neugebauer and J. L. Margrave, THIS JOURNAL, **60**, 1318 (1956).

(3) (a) S. Sunner, *Svensk. Kem. Tid.*, **58**, 71 (1946); (b) Thesis, Univ. of Lund, Sweden, 1950.

(4) W. N. Hubbard, C. Katz and G. Waddington, THIS JOURNAL, **58**, 142 (1954).

(5) W. D. Good, D. W. Scott and G. Waddington, *ibid.*, **60**, 1080 (1956).

(6) NBS certificate accompanying standard sample 39g.

(7) W. D. Good, D. W. Scott and G. Waddington, THIS JOURNAL, **60**, 1080 (1956).

TABLE Ia

CALIBRATION OF THE ROTATING BOMB CALORIMETER, NO HF PRESENT

(1) Lab. no.	R195	R196	R197	R212	R213	R216	R220
(2) m, benz. acid, g.	2.5559	2.0033	2.2552	2.12095	2.02201	0.89109	0.88936
(3) v, soln., ml.	1.00	1.00	1.00	1.00	1.00	50.0	50.0
(4) N (HF)	0.0	0.0	0.0	0.0	0.0	0.0	0.0
(5) ΔT, °C.	2.2097	1.7285	1.9390	1.8351	1.7389	0.7661	0.7660
(6) $(m/M)\Delta E_B$ (or ΔE^0_v) benz. acid, cal.	−16,150.6	−12,657.8	−14,249.9	−13,401.4	−12,776.1	(−5,625.4)	(−5,614.5)
(7) ΔE(fuse + HNO_3 + ign.), cal.	−102.2	−52.9	−27.3	−106.8	−28.4	−29.7	−28.2
(8) ΔE(rotation), cal.	−6.6	−1.2	−4.8	−0.6	−0.6	Continuous rotation −23.9	−6.5 −23.9
(9) ΔE, cor. to stand. states, cal.							
(10) $C_{cont}\ \Delta T$, cal.	+9.8	+7.6	+8.7	+7.9	+7.4	+40.3	+40.3
(11) Cor. heat evolved, cal.	−16,249.6	−12,704.3	−14,273.3	−13,500.8	−12,797.7	−5,638.7	−5,632.8
(12) C(calor. + water), cal./deg.	7,353.7	7,349.9	7,361.7	7,357.0	7,359.7	7,360.2	7,353.4
(13) C(water, cal./deg.)	6,780.4	6,780.0	6,789.3	6,782.8	6,785.4	6,783.5	6,783.1
(14) C(empty calor.), cal./deg.	573.3	569.9	571.8	574.2	574.3	576.7	570.3

TABLE Ib

CALIBRATION OF THE ROTATING BOMB CALORIMETER, HF PRESENT

(1) Lab. no.	R218	R219	R222	R235	R236
(2) m, benz. acid, g.	0.88870	0.89298	0.88835	0.89220	1.78880
(3) v, soln., ml.	50.0	50.0	50.0	50.0	50.0
(4) N (HF)	1.98	1.98	1.98	3.17	3.17
(5) ΔT, °C.	0.7647	0.7715	0.7631	0.7666	0.5333
(6) $(m/M)\Delta E_v^0$ benz. acid, cal.	−5,610.3	−5,637.3	−5,608.1	−5,632.4	−11,292.5
(7) ΔE(fuse + ign.), cal.	−30.8	−34.2	−28.2	−18.3	−21.8
(8) ΔE(rotation), cal.	−15.5	−32.9	−10.7	−20.0	−26.8
(9) ΔE, cor. to stand. states, cal.	−24.2	−24.2	−24.2	−24.2	−51.6
(10) $C_{cont}\ \Delta T$, cal.	+39.4	+39.8	+39.3	+39.5	+79.4
(11) Cor. heat evolved, cal.	−5,641.4	−5,688.8	−5,631.9	−5,655.4	−11,313.3
(12) C_{app}(calor. + water), cal./deg.	7,377.2	7,373.7	7,380.1	7,377.1	7,378.4
(13) C(water), cal./deg.	6,792.1	6,787.7	6,792.3	6,790.8	6,798.1
(14) C_{app} (empty calor.), cal./deg.	585.1	586.0	587.8	586.3	580.3

tion per gram of benzoic acid given on the certificate has also been derived under bomb, not standard conditions.

When the calibration was carried out with 50.0 ml. of HF present in the bomb, however, deviations from certificate conditions were so large that it was necessary to calculate all the reductions to the standard bomb process at unit fugacity and 25°, and, by also using the heat of combustion of benzoic acid under standard conditions, −6312.91 ± 0.62 cal./g., in these calculations, the apparent heat capacity of the calorimeter, C_{app}, was obtained.

A convenient step by step method for making these corrections can be found in the recent literature.[8] One starts with the reactants at unit fugacity at 25°, compresses and confines them to bomb conditions, lets the reaction occur at 25°, and then one decompresses the products to unit fugacity at 25°.

The results for the three series of calibration experiments are given below. In the Tables Ia and Ib the first four items give the initial conditions of the particular experiment; item (4) lists the concentration of the HF solution. Then five energy factors follow, the sum of which should add up to the corrected heat evolved, item (11). Here ΔE_B stands for the uncorrected heat of combustion of benzoic acid under bomb conditions, ΔE^0_v is the corrected heat under standard conditions, C_{cont} denotes the heat capacity of the bomb contents, the items (7) through (10) are energy corrections. The first five experiments (R195-213) in Table Ia (first series of calibration experiments) were carried out under certificate conditions, and the average for the heat capacity of the empty calorimeter was 572.7 ± 1.5 cal./deg. The last two experiments (R216, 220) in Table Ia (second series of calibration experiments), where 50.0 ml. of water was present during the reaction, give an average of 573.5 ± 3.2 cal./deg. Within experimental error these two values are identical, as they should be if the non-ideality corrections have been applied correctly. The greater average deviation from the mean in the second series must be expected since the sample size of benzoic acid was smaller. It should be noted at this point that the procedure followed in these two experiments was identical to that followed in all other experiments from here on. The conditions for the first three experiments (R218–222) in Table Ib (third series of calibration experiments) were practically identical. The average for the apparent heat capacity of the empty calorimeter from these runs is 586.3 ± 1.0 cal./deg. This indicates that the temperature rise measured for this set of comparison experiments was somewhat lower than expected, or (586.3 − 572.7) (0.76) = 10.6 cal. less than expected was evolved. This difference could be explained if the product of the solubility times the heat of solution per mole of CO_2 in HF at that pressure of CO_2 is less than that in pure water. It may also be partially due to an over correction for the heat of corrosion, which is necessarily somewhat ill defined.

Regardless of the source of this difference in apparent heat capacities, this factor is eliminated in the actual fluorocarbon combustion experiments. The conditions of the bomb processes are very nearly the same and it was

(8) W. N. Hubbard, D. W. Scott and G. Waddington, *ibid.*, 58, 152 (1954).

possible to apply a blanket correction of 10.6 cal. to each run.

Correction for the Heat of Rotation.—During the reaction period the bomb was rotated until the maximum temperature was reached (about 230 sec.) to make sure that the heat exchange between the pool of solution in the bomb and the rest of the calorimetric system was complete. To determine the magnitude of the heat of rotation correction, the bomb was again rotated for about 400 seconds at the end of the after period. The rate of cooling was slower since the loss of heat to the jacket was partially offset by the heat generated by the rotating bomb. The difference between the normal rate of cooling and the rate observed when the bomb was rotating gave the rate at which the rotating bomb generated heat while in operation. When 50.0 ml. of water was initially present, enough heat was produced on rotation to change the temperature at the rate of about 0.00000028°/sec., which corresponds to 0.022 cal./sec. When there was 50.0 ml. of 2 *N* HF solution present in the bomb while it rotated, the heat of rotation observed was somewhat greater, around 0.05 cal./sec. The difference between the two heats of rotation is the heat of corrosion.

Weighings and Definitions.—The water needed as the calorimetric fluid was weighed on a solution balance having a capacity of 5 kg. per pan and a sensitivity of 7 mg. per division with a 2 kg. load. Weighings for solid combustible samples (benzoic acid, the ignition wires, etc.), whose exact weight had to be known for calibration and analytical purposes, were done on a semi-micro Ainsworth balance to within 0.01 mg.

All weights used were calibrated and all weighings were corrected to "*in vacuo*." For this purpose the density of the brass weights was taken as 8.4 g./ml.

The atomic weights were those reported in the *J. Am. Chem. Soc.* in 1956. The energy unit is the calorie, defined as equal to 4.1840 abs. joules.

All reactions were referred to 298.15°K.

Uncertainties and Precision.—The uncertainty quoted for the final value of a particular heat of formation is composed of three parts.

The first is the deviation from the mean of the heats observed for the individual combustion experiments. The resulting uncertainty in the mean value of the heat of reaction is called the precision error, according to Rossini,[9] and is taken as twice the standard deviation

$$2\sqrt{(\Sigma\Delta)^2/n(n-1)}$$

where Δ denotes the deviation from the mean and n the number of trials.

The second is called the calibration error and reflects the uncertainty produced in the heat of formation by the average deviation from the mean of the heat capacity measurements in the calibration experiments of the calorimeter.

The third is the accuracy error and is an estimate of the effect, in calories, of various other factors on the final heat of formation: the purity of the reactants used, the quality of the estimates which were necessary in making the non-ideality corrections, the definiteness of the thermodynamic states, etc.

The final uncertainty quoted for a standard heat of formation is the square root of the sum of the squares of the precision error, the calibration error, and the accuracy error.

The Heat of Formation of Methylene Fluoride

The combustion reaction of gaseous CH_2F_2 with oxygen in the presence of water was used to determine its heat of formation

$$CH_2F_2(g) + O_2(g) = CO_2(g) + 2HF(aq., 2.4\ N) \quad (4)$$

By measuring the heat of reaction under bomb conditions, correcting it to the reactants and products in their respective standard states, and from the known values of the standard heats of formation of CO_2 and HF (aq.),[10] the value of the standard heat of formation was obtained. Mass spectrometric analysis of the products of the reaction showed that no other product was formed; in particular no CF_4 was produced. The reaction went essentially to completion, small amounts of CH_2F_2 in the product gas being due to appreciable solubility in water.

Purity of Methylene Fluoride.—The sample of CH_2F_2 used in these experiments, coded FCD-1592, was obtained through the courtesy of the Jackson Laboratory of E. I. du Pont de Nemours and Co. Mass spectrometric analysis showed 0.2 mole % fluoroform (CHF_3) and 0.1 mole % chlorodifluoromethane. The impurity due to CHF_3 is probably not serious, since, as will be seen later, it is not very reactive toward oxygen. A small CO_2 peak was observed in the mass spectrogram, but it was present in quantities too small to influence the final CO_2 analysis. No other impurities were detectable.

Procedure.—First, 50.0 ml. of pure water was added to the bomb which was then flushed 5 to 8 times with the same oxygen used for the calibration experiments. The bomb was then loosely connected to the methylene fluoride tank and any air which may have been in the connection was swept out. The connection was tightened and methylene fluoride was admitted to a pressure of 5 atm. Finally, the oxygen tank was connected again, the filling connection swept clear of air as before, and then oxygen was added to a total pressure of 25 atm.

In the calorimeter this charge was ignited by electrically heating (15 v., 5 amp.) a thin platinum wire, 1 cm. long and fastened to the two electrodes. An ignition energy of about 30 cal. generally sufficed to initiate the reaction. Rotation of the bomb was started as soon as practical after the ignition, to prevent the formation of very concentrated hydrofluoric acid on the bomb walls and continued for 200 to 250 sec. The procedure of measuring and correcting the temperature rise was identical to that described for the calibration experiments.

Analysis of the Bomb Products.—To fix the amount of CH_2F_2 which undergoes reaction, one must analyze the gas phase for CO_2 and titrate the aqueous phase with standard NaOH. The bomb gases were first passed through an acid scrubber to take out any HF which had vaporized and were then led through a tube filled with $Mg(ClO_4)_2$ for drying before the CO_2 present was absorbed on ascarite. Before the bomb pressure reached atmospheric pressure, the bomb was connected to a tank of high purity helium, and a helium sweep was continued for 1.5 hours to make sure that all the CO_2 in the aqueous phase was swept out. CO_2-free air was drawn by an aspirator through the ascarite bulb for another 30 min. to displace the light helium gas and make the bulb ready for reweighing. The weight gain was equal to the weight of CO_2 produced in the reaction.

For the analysis of the HF produced in the reaction, the bomb was rinsed carefully to ensure quantitative recovery of the solution; the acid was diluted to 1 liter; and 100-ml. aliquots were titrated to the phenolphthalein end-point with standard 0.1 *N* NaOH, which was standardized frequently against Bureau of Standards benzoic acid sample 39g. Shortly before the end-point the solution turned a faint green due to the precipitation as hydroxides of the metals dissolved in the corrosion of the bomb. Since the metal ions took the place of an equivalent number of hydrogen ions, the stoichiometry of the neutralization was preserved. The green color did not interfere with the end-point because of the intensity of the color change.

From the stoichiometry of the combustion of methylene fluoride, 1 mole of CO_2 and 2 moles of HF are produced from 1 mole of fluorocarbon. The results of the analyses are given in the third and fourth row of Table II. The CO_2 and HF analyses generally agreed within 0.25%, and within 0.44% at worst.

Corrections to Standard States.—The solubility of CH_2F_2 in 50 ml. of water at 5 atm. of gas pressure was taken as 0.0044 mole. This value was arrived at by interpolating values for the solubility of CF_4, CHF_3 and CH_4, and using the solubilities of the series CF_4, $CClF_3$, CCl_2F_2, CCl_4, and the series CCl_4, $CHCl_3$, CH_2Cl_2, CH_3Cl and CH_4,[11,12] as interpolation aids. The heat of solution was estimated in a similar manner, using the difference in the solubility at different temperatures to calculate the ΔH_{soln}, according to the relation

(9) F. D. Rossini, *Chem. Revs.*, **18**, 223 (1936).

(10) National Bureau of Standards Circular 500.

(11) H. M. Parmelee, *Refrigeration Eng.*, Dec., 1341 (1953).

(12) Solvay Process Division, Product Data Sheets on Chloromethanes.

TABLE II

THE HEAT OF FORMATION OF METHYLENE FLUORIDE

(1) Lab. No.	R223	R224	R225	R226	R227	R228
(2) ΔT, °C.	1.1323	0.9904	1.0006	1.0398	0.9907	1.0093
(3) n, moles CO_2	0.06024[a]	0.05298	0.05298	0.05533	0.05261	0.05343
(4) n, 1/2 moles HF	0.05999	0.05257	0.05322[a]	0.05513	0.05265	0.05350
(5) C(calor. + water), cal./deg.	7,363.8	7,370.1	7,360.7	7,369.5	7,365.9	7,357.5
(6) C(calor. + water), ΔT, cal.	−8,338.0	−7,299.3	−7,365.1	−7,662.8	−7,297.4	−7,425.9
(7) ΔE(ign.), cal.	+45.0	+35.9	+34.1	+23.3	+26.9	+26.9
(8) ΔE(rotation), cal.	+7.1	+4.6	+8.6	+7.2	+6.7	+8.4
(9) ΔE(cor. to stand. states), cal.	−6.5	−7.5	−7.5	−7.1	−7.5	−7.3
(10) $C_{cont}(-\Delta T)$, cal.	−58.8	−51.3	−51.9	−54.0	−51.4	−52.2
(11) $n\Delta E_c^0$, cal.	−8,351.2	−7,317.6	−7,381.8	−7,693.4	−7,322.7	−7,450.1
(12) ΔE_c^0, kcal./mole	−139.21	−139.09	−139.33	−139.30	−139.14	−139.36
(13) ΔH_f^0, kcal./mole			−105.50 ± 0.22 kcal./mole			

[a] Values were discarded.

$$\left(\frac{\partial \ln N_2}{\partial T}\right)_P = \frac{\Delta H_{soln}}{RT^2}$$

It was estimated as −4.30 kcal./mole. Interpolation is somewhat difficult since both the solubility and heat of solution are at a maximum for CH_2F_2, CH_2Cl_2 and CCl_2F_2, the middle members of all the three methane series mentioned above.

From calorimetric measurements Rossini and Frandsen[13] found that the dependence of $(\partial E/\partial P)_T$ on concentration for the two component system O_2–CO_2 may be represented empirically by a simple equation. In the absence of experimental data, for the systems O_2–CH_2F_2 and O_2–CO_2–CH_2F_2, the dependence of $(\partial E/\partial P)_T$ on concentration was assumed to be similar.

The steps involved in making the corrections to standard states differ somewhat from those used in the calibration experiments or other experiments where solids or liquids instead of gases are burned; the detailed procedure and solubility data for O_2, CO_2, etc., are found in references 1 and 8.

Results.—Six out of twelve reaction trials were successful (in the other six an insufficient rotation time was allowed) and essential data for each run are given in Table II. Row (2) gives the corrected temperature rise observed for the reaction, while the results for the analysis are given in rows (3) and (4). The value for the HF analysis is divided by two for comparison purposes: it should agree with the number of moles of CO_2 produced and also gives directly the number of moles of CH_2F_2 which took part in the reaction. The value for the sum of the heat capacity of the calorimeter and the calorimeter water multiplied by ΔT gives the number of calories evolved under bomb conditions. This value is then corrected for the ignition and rotation energy, the non-ideality of the system and the heat capacity of the bomb contents (the solution and gas phase). The sum of items (6) to (10) is then the standard internal energy change at 25° for the number of moles of CH_2F_2 that took part in the reaction (row 11), and in row (12) the same quantity is given per mole. From the stoichiometry of reaction 4 the standard heat of formation at 25° of CH_2F_2 can be calculated (row 13). The average value of the heat of formation is −105.50 kcal./mole. The precision error was 0.09 kcal./mole, the calibration error 0.03 kcal./mole and the accuracy error was estimated as 0.20 kcal./mole, giving a final value of

ΔH_f^0 [CH_2F_2(g)] at 298.15°K. = −105.50 ± 0.22 kcal./mole

(13) F. D. Rossini and M. Frandsen, *J. Research Natl. Bur. Standards*, **9**, 733 (1932).

The Heat of Formation of Trifluoromethane

The reaction used to determine the heat of formation is similar in principle to the one given for CH_2F_2

$$CHF_3(g) + {}^1/_2O_2(g) + H_2O(l) = CO_2(g) + 3HF(aq., 2.5\ N) \quad (5)$$

However, from mass spectrometric analysis of the product gases it was found that a small amount of CF_4 also was produced. CF_4 could be formed by either of two side reactions

$$CHF_3(g) + {}^1/_2O_2(g) = {}^1/_2CO_2(g) + {}^1/_2CF_4(g) + HF(aq.) \quad (6)$$

$$CHF_3(g) + {}^1/_2O_2(g) = {}^1/_4CO_2(g) + {}^3/_4CF_4(g) + {}^1/_2H_2O(l) \quad (7)$$

If the quantity of CHF_3 consumed in either of these side reactions is known, the standard heat of formation can be calculated from equation 5 by a method of successive approximations. It can be shown that the two side reactions 6 and 7 are actually identical, since from a combination of either equations 5 and 6 or equations 5 and 7, the same over-all equation can be derived.

Purity of the Sample of Trifluoromethane.—The sample of CHF_3 used in this investigation was obtained from the General Chemical Division of the Allied Chemical and Dye Corporation. Mass spectrometric analysis indicated that the sample was quite pure. In particular CH_2F_2 was completely absent; CO_2 was present only in traces; and no CF_4 was detectable. The only impurities were some oxygen and a small quantity of nitrogen.

Procedure and Analysis.—The procedure followed in charging the bomb was essentially that described in the previous section, except 7 atm. of CHF_3 and 23 atm. of O_2 were used, bringing the total pressure to 30 atm. The rather large quantity of CHF_3 was necessary in order to force the reaction to proceed 50% toward completion. The charge was ignited by electrically heating (10 v., 9 amp.) a thin, 1.5 cm. long pencil lead carbon rod, since the temperature reached with a hot platinum wire was insufficient to ignite the charge. The heat of combustion of the rod in the presence of HF was determined in separate experiments in which only carbon was burned. It was 5023 cal./g. with an evolution of 0.0528 mole of CO_2 per gram of rod. About 2% of the final number of moles of CO_2 produced in the combustion were due to this carbon fuse.

TABLE III

THE HEAT OF FORMATION OF TRIFLUOROMETHANE

(1) Lab. no.	R229	R230	R231	R232	R233
(2) ΔT, °C.	0.3813	0.5280	0.5468	0.5240	0.5503
(3) Moles CO_2	0.02967	0.04163	0.04295	0.04109	0.04313
(4) $^1/_3$ moles HF	0.02949	0.04142	0.04258	0.04058	0.04257
(5) Difference, moles	0.00018	0.00021	0.00037	0.00051	0.00056
(6) C(calor. + water), cal./deg.	7355.7	7364.3	7353.9	7365.3	7365.3
(7) C(calor. + water) ΔT, cal.	−2804.7	−3888.4	−4021.1	−3859.4	−4053.3
(8) ΔE(ign.), cal.	+17.4	+21.5	+32.1	+30.2	+24.4
(9) ΔE(fuse), cal.	+84.0	+73.8	+93.0	+96.0	+107.0
(10) ΔE(rotation), cal.	+5.8	+6.8	+6.9	+6.8	+6.9
(11) ΔE, cor. to std. states, cal.	−2.4	+6.7	+6.9	+6.5	+6.9
(12) $C_{cont}(-\Delta T)$, cal.	−19.7	−27.5	−28.5	−27.3	−28.7
(13) $n\Delta E_c^0$, cal.	−2719.6	−3807.1	−3910.7	−3747.2	−3937.4
(14) ΔH_f, kcal./mole	−161.88	−161.92	−162.80	−163.17	−163.15

The ashes from the rod did not affect the acidity of the solution. The electrical energy needed to cause ignition was about 20 cal.; the heat of combustion of the fuse per run was of the order of 90 cal.

The analyses for CO_2 and HF were performed as previously described. The difference between the CO_2 analysis and $^1/_3$ the HF analysis is a measure of the quantity of CF_4 produced according to reactions 6 or 7.

Results and Calculations.—The results for five runs are given in Table III. The third and fourth rows give the result of the analyses, the difference is given in row (5). The various energy factors, rows (7) through (12), are listed similarly to those in Table II. For the purpose of the $[\partial E/\partial P]_T$ correction, CHF_3 was treated in the same manner as CH_2F_2. The solubility of CHF_3 at 7 atm. was taken as 0.00457 mole in 50.0 ml. of water, and its heat of solution in water as −3.80 kcal./mole.

The corrections to standard states are given in row (11). The sum of items (7) through (12) gives the internal energy change had the reaction proceeded under standard conditions (row 13).

To calculate the heat of formation of CHF_3, it was assumed that the reactions which were involved were no. (5) and (7), and the number of moles of CHF_3 which reacted in both equations was calculated. Then, from an estimated heat of formation of CHF_3 the contribution to the total heat produced per run made by reaction 7 was calculated. The difference in the heats was due solely to reaction 5 and thus a more accurate determination of the heat of formation of CHF_3 was possible. The calculation was repeated until a consistent value for the heat of formation was obtained. Since the contribution of reaction 7 to the total heat evolved is small (about 4%), a consistent value was obtained after only 2 or 3 trials. The values thus derived are given in row (14).

The magnitude of the correction for the reaction producing CF_4 is essentially determined by the difference in the CO_2 and HF analyses. Since here the difference between two relatively large numbers is involved, its reliability is no more than 40%, which is magnified by a factor of 4. This is the reason why the results for the standard heat of formation consistently increase as the difference between the two analyses increases. If it were assumed that the average of the differences between the CO_2 and $^1/_3$ HF observed in all five runs is more accurate than that obtained in any one run separately, the precision error of the average heat of formation would be substantially lower, although the value for the average heat would stay the same. The values for the total heat observed under standard conditions (row 13), divided by the HF or CO_2 analyses alone, without making the correction for the production of CF_4, are consistent to within ± 0.25 kcal./mole, thus showing that the quantity of CF_4 produced did not vary as much from run to run as indicated by the analyses.

However, from the analyses as obtained, the precision error was 0.58 kcal./mole and the calibration error 0.02 kcal./mole, giving a final value for

$\Delta H_f^0[CHF_3(g)]$ at 298.15°K. =

-162.60 ± 0.65 kcal./mole

Acknowledgments.—The authors wish to acknowledge the financial support of the Wisconsin Alumni Research Foundation, the Minnesota Mining and Manufacturing Corporation, the E. I. du Pont de Nemours Company, and the Office of Ordnance Research. The sample of methylene fluoride was obtained through the courtesy of the Jackson Laboratory of the du Pont Company and the sample of trifluoromethane through the courtesy of the General Chemical Division of the Allied Chemical and Dye Corporation.

CARBON-OXYGEN BOND ENERGIES AND BOND DISTANCES[1]

BY GEORGE GLOCKLER

Contribution from the Department of Chemistry, Duke University, Durham, North Carolina

Received February 14, 1958

On the basis of earlier work on carbon–carbon and carbon–hydrogen bonds, it is possible to make a similar study of the relation between carbon–oxygen bond energies and bond distances. The following estimates were established: carbon monoxide, B(C≡O, 1.131 Å.) = 257.3 kcal.; carbon dioxide, B(C=O, 1.163 Å.) = 192.1 kcal.; ketene, B(C=O, 1.17 Å.) = 184.8 kcal.; aldehydes and ketones, B(C=O, 1.21 Å.) = 160.0 kcal.; carboxylic acids, B(C=O, 1.21 Å.) = 160.0 kcal. and B(C—O, 1.34 Å.) = 106.0 kcal.; alcohols, B(C—O, 1.427 Å.) = 81.5 kcal.; ethers, B(C—O, 1.420 Å.) = 83.4 kcal.; esters, B(C=O, 1.21 Å.) = 160.0 kcal., B(C—O, 1.34 Å.) = 106.0 kcal. and B(C—O, 1.42 Å.) = 81.8 kcal.; ethylene oxide, B(C—O, 1.486 Å.) = 67.45 kcal. A type of intramolecular hydrogen bonding is postulated to exist between protons and the oxygen atom of the carbonyl group in the aldehyde and carboxyl groups: B(··OH, ~2.0 Å.) ≐ 5.0 kcal.

Introduction

In an earlier paper[2] a relation between carbon–carbon and carbon–hydrogen bond energies and internuclear distances was derived. A similar analysis for carbon–oxygen bonds is described herewith. Large carbon–oxygen bond energies are found with bonds of short internuclear distances and *vice versa* (Fig. 1a). In general it is expected that the latter, obtained from physical measurements such as ultraviolet, infrared and microwave spectroscopy, electron diffraction and X-ray studies, are also the bond distances of chemical bonds. While this relation holds in a great number of instances, there are some exceptions (cyclopropane, ethylene oxide, boron hydrides, etc.) where the direction of the chemical bonds are not coincident with the internuclear distances. In the usual case it is possible to correlate bond energies of molecules, derived from thermochemical studies, with the internuclear distances of these molecules. In the exceptional cases, it is said that bonds are bent or that the maxima of given orbitals do not lie along the bond direction.

If a system of bond energies and bond distances has been established, then these quantities may be estimated for a new compound: (1) if Q(f) is known; (2) if Q(f) is not known, but the structure of the compound has been determined; (3) if the compound has not yet been prepared, but its structure can be surmised. Bond energies are also useful in deriving electronegativities and resonance energies. A given set of geometric parameters of a molecule must fit into its bond energy–bond distance picture. It would be desirable to be able to consider the problem of bond energies at 0°K. However, thermochemical quantities are usually determined at 25°. The latter differ only by about 2 kcal. from the former. In order to study carbon–oxygen bonds it is necessary to transfer carbon–carbon and carbon–hydrogen bond energies from other molecules. A similar process has necessarily been adopted in the case of force constants. The latter show the same dependence on internuclear distances as do bond energies: large force constants describe short bonds and *vice versa* (Fig. 1b). It is, of course, recognized that the transfer of bond energies, force constants and internuclear distances is an approximate process. Actually each species of molecule has its individual properties, which have distinctive values belonging to that particular molecule only.

Notation

(25°)

B(CC, 1.543 Å.) = CC-bond energy (kcal.) at R(CC) = 1.543 Å.
B(CO) = CO-bond energy in general (kcal.)
B(CO, H_2CO) = CO-bond energy in H_2CO (kcal.)
B(O..H) = electrostatic interaction between oxygen and hydrogen atoms (kcal.)
B(O..H, HCOOH = electrostatic interaction between oxygen and hydrogen atoms in HCOOH (kcal.)
δ = proton chemical shift in magnetic resonance ($\delta(H_2O)$ = 0)
I_α = moment of inertia of a molecule about the α-axis (α = X, Y, Z, A, B, C), (c.g.s. units)
Q(a, bond) = atomic heat of formation from bond energies alone (kcal.)
Q(a, m) = atomic heat of formation from internuclear distances and bond energy–bond distance relations (kcal.)
Q(a, th) = atomic heat of formation from thermochemical information (kcal.)
Q(comb) = heat of combustion (kcal.)
Q(ev) = heat of evaporation (kcal.)
Q(f) = heat of formation from the elements in their usual standard states (kcal.)
Q(fusion) = heat of fusion (kcal.)
R(C=O) = bond length of a C=O bond (Å.)
R(C=O, HCOOH) = bond length of a C=O bond in HCOOH (Å.)

The Carbon-Oxygen Bond Energies.—The bond energies of carbon monoxide and carbon dioxide can be determined directly. In other cases it is necessary to transfer bond energies and bond distances from other molecules. In order to carry out these calculations, the following relations are needed:

1. The carbon–carbon bond energies (B(CC)) as a function of bond lengths (R(CC)) are given in Fig. 2 (25°). No empirical equation has been derived as it is sufficiently accurate to obtain values from a graph based on B(CC,C_2H_2) = 186.0 kcal. at R(CC, C_2H_2) = 1.207 Å.,[3] B(CC, C_2H_4) = 134.0 kcal. at R(CC, C_2H_4) = 1.344 Å.,[4] B(CC, graphite) = 113.5 kcal.[5] at R(CC, graphite) = 1.421 Å.[6] and B(CC, C_2H_6) = 86.0 kcal. at R(CC, C_2H_6) = 1.543 Å.[7]

(1) This research is supported by the Office of Ordnance Research, U. S. Army, under contract No. DA-31-124-ORD-1535.

(2) G. Glockler, THIS JOURNAL, **61**, 31 (1957).

(3) G. Herzberg, "Infrared and Raman Spectra of Polyatomic Molecules," D. Van Nostrand Co. Inc., New York, N. Y., 1945.

(4) B. P. Stoicheff, private communication.

(5) G. Glockler, *J. Chem. Phys.*, **22**, 159 (1954).

(6) L. Pauling, "The Nature of the Chemical Bond," Cornell University Press, Ithaca, N. Y., 1940.

(7) G. E. Hansen and D. M. Dennison, *J. Chem. Phys.*, **20**, 313 (1952).

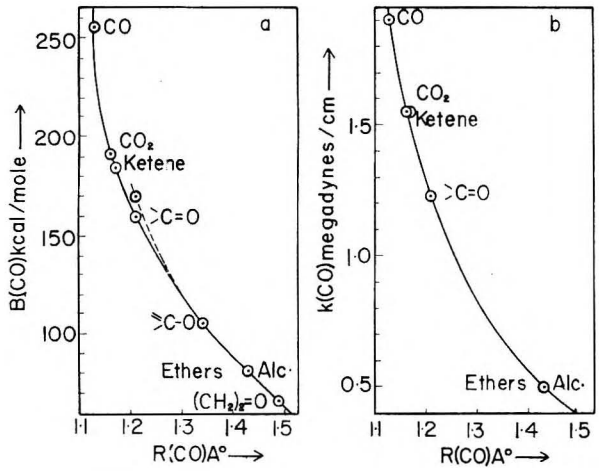

Fig. 1.—(a) Relation between carbon–oxygen bond energies and internuclear distances (at 25°); (b) relation between carbon–oxygen force constants and internuclear distances.

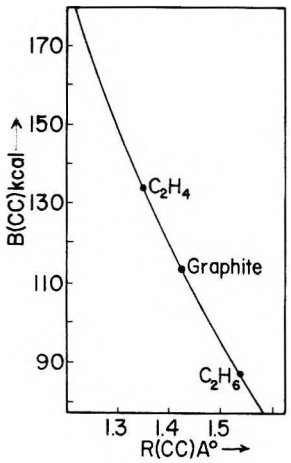

Fig. 2.—Relation between carbon–carbon bond energies and internuclear distances.

2. Carbon–carbon bond distances (R(CC)) and carbon–hydrogen bond lengths (R(CH)) in hydrocarbons are related by

$$R(\mathrm{CH}) = 0.908 + 0.126R(\mathrm{CC}) \qquad (1)$$

This equation is based on R(CH, C_2H_2) = 1.06 Å.,[3] R(CC, C_2H_2) = 1.207 Å. and R(CH, C_2H_6) = 1.102 Å., R(CC, C_2H_6) = 1.543 Å. If it is used for ethylene with R(CC, C_2H_4) = 1.344 Å.[4] then R(CH, C_2H_4) = 1.077 Å. and if R(CC, C_2H_4) = 1.353 Å.,[8a,b] then R(CH, C_2H_4) = 1.078 Å. The relation between R(CH) and R(CC) is sufficiently accurate for present purposes. Its range of application is between R(CC) = 1.2 to 1.7 Å. at 25°.

3. Carbon–hydrogen bond energies (B(CH)) and carbon–hydrogen bond lengths (R(CH)) are connected by the expression

$$B(\mathrm{CH}) = 232.22 - 121.43R(\mathrm{CH}) \qquad (2)$$

It is based on R(CH, C_2H_2) = 1.06 Å. and B(CH, C_2H_2) = 103.5 kcal.[2] and R(CH,C_2H_6) = 1.102 Å. and B(CH,C_2H_6) = 98.4 kcal.[2] The range of valiidty is 1.05 to 1.13 Å. at 25°.

4. Oxygen–hydrogen bond energies (B(OH)) and oxygen–hydrogen bond lengths (R(OH)) in the range R(OH) = 0.95 to 1.0 Å. are described at 25° by

$$B(\mathrm{OH}) = 231.27 - 126.09R(\mathrm{OH}) \qquad (3)$$

which is based on B(OH, H_2O) = 110.6 kcal.[9] at R(OH, H_2O) = 0.957 Å. and B(OH, radical) = 107.7 kcal. at 0.98 Å.[10]

Carbon Monoxide.—Q(f) = 27.2 kcal.,[9] Q(a, th) = 257.3 kcal. and R(CO) = 1.131 Å.[11] The bond in carbon monoxide has the highest carbon–oxygen bond energy (257.3 kcal.), which strongly indicates that the atoms are trivalent[12,13] as in the isoelectronic nitrogen molecule. It is possible that the two π-bonds and the σ-bond further hybridize[14] and form the three equivalent bonds of a triple bond. The other four electrons exist as two non-bonding pairs. While there are arguments in favor of a double bonded structure,[15] the triple bond seems to be the better representation.

Carbon Dioxide.—Q(f) = 94.1 kcal.[9] and Q(a, th) = 384.1 kcal. with R(C=O) = 1.162 Å.[3] Hence the average bond energy is 192.1 kcal.

Ketene.—Q(f) = 14.6 kcal.[3] and Q(a, th) = 521.4 kcal. The microwave spectrum yields[16] R(CH) = 1.075 ± 0.01, R(C=C) = 1.315 ± 0.103 and R(C=O) = 1.16 ± 0.10 Å. In order to determine the bond energy system, the values for the carbon–hydrogen bond and the carbon–carbon double bond were taken from ethylene and the bond energy for the carbon–oxygen bond was determined by difference. The corresponding distances are within the limits as given by the microwave results. Hence B(C=O, 1.172Å.) = 184.8, B(C=C, 1.344Å.) = 134.0 and B(CH, 1.078Å.) = 101.3 kcal. Arendale and Fletcher[17] discuss several sets of possible bond distances. When the latter are used to calculate the corresponding Q(a, m) values, it is found that they are larger than the Q(a, th) by 20–60 kcal. It is believed that the present assumption that the carbon–carbon bond and the carbon–hydrogen bonds are ethylene-like is satisfactory because it yields resonable results in other molecules, for example butadiene.

Formaldehyde.—Q(f) = 27.7 kcal.[9] and Q(a, th) = 362.7 kcal. From the ultraviolet spectrum[18] the moments of inertia were determined to be: $I_x = 2.976$, $I_y = 21.64$ and $I_z = 24.61 \times 10^{-40}$ g.cm.^{2}, if the presently accepted values of the uni-

(8) (a) W. S. Gallaway and E. F. Barker, *ibid.*, **10**, 88 (1942); (b) G. Herzberg and B. P. Stoicheff, *Nature*, **175**, 79 (1955).

(9) F. D. Rossini, *et al.*, "Selected Values of Chemical Thermodynamic Properties," Cir. 500, Nat. Bur. Standards (U. S. Government Printing Office. Washington, D. C., 1952).

(10) G. A. Hornbeck, "Fifth Symposium on Combustion," Reinhold Publ. Corp., New York, N. Y., 1955.

(11) W. Gordy, *et al.*, "Microwave Spectroscopy," John Wiley and Sons, Inc., New York, N. Y., 1953.

(12) G. Herzberg, "Molecular Spectra and Molecular Structure. I. Spectra of Diatomic Molecules," Second Edition, D. Van Nostrand Co., Inc., New York, N. Y., 1950.

(13) A. C. Coulson, "Valence," The Clarendon Press, Oxford, England, 1952.

(14) G. G. Hall and J. Lennard-Jones, *Proc. Roy. Soc.* (*London*), **205A**, 357 (1951).

(15) L. H. Long and A. D. Walsh, *Trans. Faraday Soc.*, **43**, 342 (1947).

(16) H. R. Johnson and M. W. P. Strandberg, *J. Chem. Phys.*, **20**, 687 (1952).

(17) W. F. Arendale and W. H. Fletcher, *ibid.*, **21**, 1898 (1953).

(18) G. H. Dieke and G. B. Kistiakowsky, *Phys. Rev.*, **45**, 4 (1934).

versal constants are used.[19] The molecule lies in the x,y-plane. The microwave spectrum[20,21] yields $I_x = 2.974$, $I_y = 21.603$ and $I_z = 24.668 \times 10^{-40}$ g.cm.,^{2} in remarkable agreement with the ultraviolet results. Formaldehyde is not a rigid rotator and $I_x + I_y \neq I_z$. From these moments of inertia and results on C^{13}-formaldehyde and applying an appropriate correction for the effect of zero point vibration, the following distances result: R(CH) = 1.12 ± 0.01 and R(C=O) = 1.21 ± 0.01 Å. These values must be used since the moments of inertia are known so accurately. From eq. 2, B(CH, 1.12 Å.) = 92.6 kcal. so that by difference B(C=O, 1.21Å.) = Q(a, th) − 2B(CH) = 170.0 kcal. At 0°K., the similar calculation yields B(C=O) = 169.8 kcal. However, when this point is placed on the graph of Fig. 1a, it does not fit into a smooth curve (CO, CO_2 $H_2C{=}C{=}O$, $H_2C{=}O$, ROH). Since past experience[22] indicates that these bond energy–bond distance relations are represented by smooth curves, it is to be expected that a similar situation holds in this case also. Hence B(C=O, H_2CO) = 160.0 kcal. is taken at R(C=O, H_2CO) = 1.21 Å. (Fig. 1a). The difference of 10 kcal. is ascribed to the presence of polarizing hydrogen atoms or some other kind of an electrostatic interaction between the strongly negative oxygen atom and the hydrogen atoms of the molecule. The same situation is to be found in other aldehydes and the carboxylic acids.

Rather than invent an electrostatic interaction, it might be better to take B(C=O, H_2CO) = 160.0 kcal. from the curve of Fig. 1a at 1.21 Å. and then calculate by difference B(CH, H_2CO) = 1/2(362.4 − 160.0) = 101.2 kcal. at R(CH, H_2CO) = 1.077 Å. However, the latter distance is incompatible with the well-known moments of inertia of formaldehyde.

From these considerations the following bond energies are derived: B(CH, 1.12 Å.) = 96.2, B(C=O, 1.21 Å.) = 160.0 and B(O··H, 2.0 Å.) = 5.0 kcal. The latter bonding will be described in more detail later (discussion).

It is of interest that electron diffraction results[23] are in fair agreement with the findings of microwave spectroscopy, R(C=O) = 1.21 ± 0.01 and R(CH) = 1.09 ± 0.01 Å. The formaldehyde structure problem also has been studied by Davidson, Stoicheff and Bernstein.[24] They considered five possible cases of ground state parameters. Thompson and Linnett[25] applied Badger's rule[26] to the carbon–oxygen frequency in aldehydes and found R(C=O) = 1.21 Å. The bond energies B(C=O, CHO) and B(CH, CHO) are assumed to be constants of the aldehyde group, since no detailed geometric information is available for most aldehydes.

Acetaldehyde.—Q(f) = 39.8[9] and Q(a, th) = 651.1 kcal. The internuclear distances from the microwave spectrum are[27] R(CO) = 1.226, R(CH$_3$CHO) = 1.108, R(CC) = 1.493 and R(CH$_3$CH$_3$) = 1.10 Å. (assumed). It should be noted that distances derived from microwave studies are accurate only ± 0.01 Å. because of the effect of zero point vibration. Hence the following parameters are arbitrarily chosen: from formaldehyde B(C=O, 1.21 Å.) = 160.0 and B(CH, 1.12 Å.) = 96.2 kcal.; from acetone B(CC, 1.52 Å.) = 90.5 and B(CH, 1.10 Å.) = 98.7 kcal., leaving B(O..H) = 8.3 kcal. Other aldehydes (propyl-, isobutyl-, valeric- and heptaldehyde show similar behavior.

Glyoxal.—Q(f) = 73.4[9] and Q(a, th) = 639.3 kcal. The internuclear distances from electron diffraction[28] are R(CC) = 1.47 ± 0.02, R(C=O) = 1.20 ± 0.02 Å, with R(CH) = 1.09 Å. assumed. These parameters are in consonance with the following set of bond energies chosen: B(C–C, 1.44 Å.) = 110.0 kcal., B(CH, 1.09 Å.) = 100.0 kcal. and B(C=O, 1.21 Å.) = 160.0 kcal. leaving 10.0 kcal. for secondary ionic interaction. The molecule contains a conjugated system. It is seen that the central carbon–carbon bond is much stronger than the similar bond in ethane (B(CC, C_2H_6) = 86.0 kcal. at R(CC, C_2H_6) = 1.543 Å.).

Acetone.—Q(f) = 52.2[29] and Q(a, th) = 939.4 kcal. The structural features obtained from electron diffraction are[30] R(C=O) = 1.22 ± 0.02 Å. and R(CC) = 1.55 ± 0.02 Å. The bond picture is obtained on the assumption that B(C=O) = 160.0 kcal. at R(C=O) = 1.21 Å. and that there is minimal electrostatic interaction (2B(O··H) = 6.2 kcal.) between the oxygen atom of the carbonyl group and the nearest hydrogen atom of the two methyl groups. Then by difference B(CC, 1.52 Å.) = 90.5 and B(CH, 1.10 Å.) = 98.7 kcal. Other ketones (methyl ethyl, diethyl, methyl n-butyl and dipropyl) have a similar set of bond energies with the exception of B(O··H) which is 8.9, 10.2, 6.0 and 8.8 kcal., respectively.

Formic Acid.—A careful study[31] shows that Q(f) = 90.0 kcal. for the monomer (as an ideal gas without contamination by the dimer), whence Q(a, th) = 484.2 kcal. From the infrared spectrum[32] the three principal moments of inertia are $I_x = 75.8$, $I_y = 10.6$ and $I_z = 86.4 \times 10^{-40}$ g. cm.^{2} Several authors have studied the microwave spectrum. Rogers and Williams[33] obtained $I_x = 70.0$ and $I_z = 80.0 \times 10^{-40}$ g.cm.^{2}. Erlandsson[34] gives tentatively the following distances: R(CH) = 1.10, R(C=O) = 1.20 and R(C–O) = 1.34 and

(19) J. W. M. Dumond and E. R. Cohen, *Rev. Mod. Phys.*, **20**, 82 (1948).

(20) R. B. Lawrence and M. W. P. Strandberg, *Phys. Rev.*, **83**, 363 (1951).

(21) G. Erlandsson, *J. Chem. Phys.*, **25**, 579 (1956).

(22) G. Glockler, *J. Chem. Phys.*, **19**, 124 (1951).

(23) D. P. Stevenson J. H. LuValle and V. Schomaker, *J. Am. Chem. Soc.*, **61**, 2508 (1939).

(24) D. W. Davidson, B. P. Stoicheff and H. J. Bernstein, *J. Chem. Phys.*, **22**, 289 (1954).

(25) H. W. Thompson and J. W. Linnett, *J. Chem. Soc.*, 1391 (1937).

(26) R. M. Badger, *J. Chem. Phys.*, **2**, 128 (1934); **3**, 710 (1935).

(27) C. C. Lin and R. W. Kilb, *ibid.*, **24**, 631 (1956).

(28) J. E. LuValle and V. Schomaker, *J. Am. Chem. Soc.*, **61**, 3520 (1939).

(29) "International Critical Tables," Vol. V, McGraw-Hill Book Co., New York, N. Y., pp. 137, 167.

(30) P. W. Allen, H. J. Bowen, L. E. Sutton and O. Bastiansen, *Trans. Faraday Soc.*, **48**, 991 (1952).

(31) W. Waring, *Chem. Revs.* **51**, 171 (1952).

(32) V. Z. Williams, *J. Chem. Phys.*, **15**, 232 (1947).

(33) J. D. Rogers and D. Williams, *Phys. Rev.*, **83**, 210 (1951).

(34) G. Erlandsson, *Arkiv. Fysik*, **6**, 491 (1953).

R(OH) = 0.96 Å. Trambarulo and co-workers[35] reported $I_x = I_B = 69.590$, $I_y = I_A = 10.823$ and $I_z = I_C = 80.539 \times 10^{-40}$ g.cm.^{2} The molecule lies in the x,y-plane. The CH-bond direction is very closely parallel to the x-coördinate. The dimensions are R(C=O) = 1.22, R(C–O) = 1.34, R(OH) = 0.97 and R(CH) = 1.09 Å. In another microwave investigation[36] the same moments of inertia were found, but the dimensions reported are somewhat different: R(C=O) = 1.245, R(C–O) = 1.312, R(OH) = 0.95 and R(CH) = 1.085 Å. Since distances obtained from microwave spectra are only accurate to ± 0.01 Å., the bond energies adopted are

B(C=O) = 160.0 kcal. at R(C=O) = 1.21 Å. as in formaldehyde
B(C–O) = 106.0 kcal. at R(C–O) = 1.34 Å. (Fig. 1)
B(OH) = 109.0 kcal. at R(OH) = 0.97 Å. (eq. 3)
B(CH) = 99.9 kcal. at R(CH) = 1.09 Å. (eq. 2)

The difference between Q(a,th) and the sum of these bond energies (9.0 kcal.) is ascribed to the postulated intramolecular hydrogen bonding. The hydrogen atom attached to the central carbon atom is 1.9 Å. from the double bonded oxygen and the hydrogen atom of the hydroxyl group is 2.04 Å. from the same oxygen atom.

Formic Acid Dimer.—Q(f, dimer) = 194.2 kcal. and Q(a, th) = 982.6 kcal. Twice the sum of the bond energies of the monomer and the heat of dimerization (14.1 kcal. or two regular hydrogen bridges) and two second-order electrostatic interactions (18.0 kcal.) check Q(a, th, dimer). Hence the monomer bonds transfer to the dimer without change. Electron diffraction[37] gives distances for the monomer in good agreement with the set used above: R(C=O) = 1.21 ± 0.01 Å., R(C–O) = 1.36 ± 0.01, R(OH) = 0.97 ± 0.05, R(O–O) = 2.27 ± 0.005 Å. and R(CH) = 1.09 Å. was assumed.

Acetic Acid.—Q(f) = 103.6 kcal.[9,38,39] and Q(a, th) = 773.7 kcal.

The following set of bond energies B(C=O, 1.21 Å.) = 160.0, B(C–O, 1.34 Å.) = 106.0, B(OH, 0.970 Å.) = 109.0, B(CC, 1.508 Å.) = 93.0 and B(CH, 1.098 Å.) = 98.9 kcal. represent the usual bonds of the molecule, leaving 9.0 kcal. for B(O..H). These values will be adopted for the carboxyl group in general. It is the simplest assumption to make, since the dimensions of most carboxylic acids have not yet been studied. From electron diffraction[40] R(CC) = 1.54 ± 0.04, R(C–O) = 1.43 ± 0.03 and R(C=O) = 1.24 ± 0.03 Å. From the microwave spectrum[41] R(CC) = 1.497 Å., having assumed R(C=O) = 1.245, R(C–O) = 1.312, R(CH) = 1.08 and R(OH) = 0.95 Å. Using the present method, it is found that this set of values gives Q(a, m) = 769.3 as compared with Q(a, th) = 773.7 kcal. While this comparison may be considered a numerical check, there are features in these assumed distances which will have to be considered in more detail. For example R(CH) = 1.08 Å. is also the carbon–hydrogen distance in ethylene. It is difficult to believe that the carbon–hydrogen distance in the methyl group of acetic acid has this short length. Moreover if the bond energies are determined as usual from Figs. 1 and 2 and eq. 1, 2 and 3, using Taber's values for the four assumed and the one determined distance (R(CC)), it is found that Q(a, m) differs from Q(a, th) by −3.0% to +4.4% over the series of fatty acids. It appears that the assumed distances are not satisfactory.

Aliphatic Acids.—The heats of combustion or of formation and the heats of evaporation were taken from the usual sources.[9,27,37,38] The following acids were studied: formic, acetic, propionic, n-butyric, n-valeric, caproic, heptylic, pelargonic, n-capric, undecylic, lauric, myristic, palmitic and stearic acids. The bonds common to these molecules are the ones mentioned for acetic acid and B(CC, 1.543 Å.) = 86.0 and B(CH, 1.102 Å.) = 98.4 kcal. Q(a, bond) values agree with Q(a, comb) to within ± 0.1% for the series of acids studied. The Q(a, bond) values can be obtained from the equation

$$Q(\text{a, bond}) = 208.6 + 282.8n;\ n > 1 \qquad (4)$$

where n = number of carbon atoms of the acid.

Oxalic Acid.– Q(f) = 175.9 and Q(a, th) = 860.1 kcal. X-Ray studies[40] then yield these distances: R(CC) = 1.529 ± 0.02, R(C–O) = 1.285 ± 0.012 and R(C=O) = 1.187 ± 0.022 Å. These distances are for the crystalline dihydrate and this set of bond distances may not necessarily apply. However, the bonds used were the similar ones: B(C=O) = 160.0 kcal. at 1.21 Å., B(C–O) = 106.0 kcal. at 1.34 Å., B(OH) = 109.0 at 0.97 Å. and B(O··H) = 10.0 kcal. at ~2.0 Å. By difference B(CC) = 102.1 kcal. at 1.468 Å. The carbon–carbon bond is much stronger than in ethane since the molecule is a conjugated system.

Methyl Alcohol.—Q(f) = 48.1 kcal.[9] and Q(a, th) = 487.3 kcal. From the microwave spectrum,[42] these several internuclear distances are deduced: R(OH) = 0.937 and R(C–O) = 1.434 Å. R(CH) = 1.093 Å. is assumed. Hence B(OH) = 113.0, B(C–O) = 80.0 and B(CH) = 99.5 kcal., whence Q(a, m) = 491.5 kcal. or 3.2 kcal. larger than Q(a, th). In two other microwave studies[43,44] all geometric features were determined: R(OH) = 0.967, R(CO) = 1.428 and R(CH) = 1.098 Å., with the angles HCH = 109°6′ and COH = 107°16′. The barrier height is 1110 ± 60 cal. Hence B(OH) = 109.4 and B(CH) = 98.9 kcal. and by difference B(C–O) = 81.2 kcal. This latter value, with R(C–O) = 1.428 Å., is used to establish one point on the B(CO): R(CO) curve (Fig. 1). It is interesting to compare these accurate internuclear distances with the earlier work on electron diffraction and X-ray analysis. The former yielded

(35) R. Trambarulo and P. M. Moser, *J. Chem. Phys.*, **22**, 1622 (1954); R. Trambarulo, A. Clark and C. Hearns, Contract No. AF(600)-449, September 30, 1957.

(36) R. G. Lerner, J. P. Friend and B. P. Dailey, *J. Chem. Phys.*, **23**, 210 (1955).

(37) I. L. Karle and J. Karle, *ibid.*, **22**, 43 (1954).

(38) M. S. Kharasch, *Bur. Stand. J. Res.*, **2**, 359 (1929).

(39) F. R. Bichowsky and F. D. Rossini, "The Thermochemistry of the Chemical Substances," Reinhold Publishing Co., New York, N. Y., 1936.

(40) G. W. Wheland, "Resonance in Organic Chemistry," John Wiley and Sons, Inc., New York, N. Y., 1955.

(41) W. J. Taber, *J. Chem. Phys.*, **27**, 974 (1957).

(42) E. V. Ivash and D. M. Dennison, *ibid.*, **21**, 1804 (1953).

(43) P. Venkateswarlu and W. Gordy, *ibid.*, **23**, 1200 (1955).

(44) J. D. Swalen, *ibid.*, **23**, 1739 (1955).

R(C–O) = 1.44 ± 0.01 Å.[45] while the latter method[46,47] gave the following values: R(C–O) = 1.421, R(CH) = 1.10 and R(OH) = 0.96 Å. An earlier investigation[48] of the microwave spectrum indicated that R(C–O) = 1.428 Å. From the infrared spectrum it appeared that R(C–O) = 1.421 Å. on the assumption that R(OH) = 0.958 Å. as in water and R(CH) = 1.093 Å. as in methane.[49]

No ionic interaction is postulated between the oxygen and hydrogen atoms of the methyl group. It might be imagined to exist since the distance between the oxygen and the hydrogen atoms is only 2.1 Å. However, univalent oxygen is quite different from the carbonyl oxygen atom.

Ethyl Alcohol.—Q(f) = 56.2 kcal.[9] and Q(a, th) = 771.3 kcal. The internuclear distances obtained by electron diffraction[45] are R(CC) = 1.55 ± 0.02 and R(C–O) = 1.43 ± 0.02 Å. The bond energies of ethanol are estimated on the assumption that the methyl group maintains its character as in ethane, because it is expected that the influence of the oxygen-hydrogen bond on the remainder of the molecule is relatively small. The methylene group, next to the hydroxyl group is assumed to be as in methyl alcohol. Hence B(CC) = 86.0 kcal. at R(CC) = 1.543 Å., B(CH, CH_3–) = 98.4 kcal. at R(CH, CH_3–) = 1.102 Å., B(CH, CH_3OH) = 98.9 kcal. at R(CH, CH_3OH) = 1.098 Å. and B(OH, CH_3OH) = 109.4 kcal. at R(OH, CH_3OH) = 0.967 Å. Then by difference B(C–O, C_2H_5OH) = 82.9 kcal. at 1.420 Å.

***n*-Propyl Alcohol.**—Q(comb, liq) = 482.0 and Q(ev) = 11.5 kcal.[28] giving Q(f) = 62.0 and Q(a, th) = 1053.1 kcal. Adopting the same treatment as used in ethyl alcohol results in B(C–O) = 81.9 kcal., at R(CO) = 1.424 Å.

***n*-Butyl Alcohol.**—Q(comb, liq) = 639.0 and Q(ev) = 11.5 kcal.,[28] whence Q(f) = 78.8 and Q(a, th) = 1335.3 kcal. B(C–O) = 81.3 kcal. at R(CO) = 1.427 Å.

***n*-Amyl Alcohol.**—Q(comb, liq) = 787.0 and Q(ev) = 10.6 kcal.,[28] so that Q(f) = 82.9 and Q(a, th) = 1625.1 kcal. The same treatment yields B(CO) = 88.3 kcal. at R(CO) = 1.412 Å. It is however questionable that the material was pure *n*-amyl alcohol.[28]

Similarly *n*-heptyl and *n*-octyl alcohol have B(C–O) = 80.2 and 73.7 kcal. The average B(C–O) = 81.5 ± 0.7 kcal. at R(C–O) = 1.427 Å. for the six normal alcohols, eliminating *n*-amyl and *n*-octyl alcohols which are evidently out of line. No electrostatic interaction exists in these alcohols.

Ethylene Glycol.—Q(f) = 95.0[9] and Q(a, th) = 869.4 kcal. Electron diffraction experiments[45] give the following distances: R(CC) = 1.52 ± 0.02, R(CH) = 1.08, R(OH) = 0.97 and R(C–O) = 1.43 Å. R(OH) = 0.97 Å. was assumed. The following bond energies were taken: B(CC) = 91.0 at R(CC) = 1.52, B(CH) = 98.6 at R(CH) = 1.10, B(OH) = 109.4 at R(OH) = 0.967 and B(C–O) = 82.6 at R(C–O) = 1.422, kcal. and Å., respectively. No electrostatic interaction between hydrogen and oxygen atoms is present in this molecule.

Glycerol.—Q(f, liq) = 159.8 kcal.[50] and Q(ev) is estimated to be 22.1 kcal. from an extrapolation of vapor pressure measurements between 55 and 195° by Stedman.[51] Hence Q(a, th) = 1247.2 kcal. Using the estimated bond energies from ethylene glycol leaves B(C–O) = 81.3 kcal. Electron diffraction yields the following dimensions:[45] R(CC) = 1.54, R(CH) = 1.08 and R(CO) = 1.43 Å.

Dimethyl Ether.—Q(f) = 44.3 kcal.[9] and Q(a, th) = 759.4 kcal. B(CH) near the oxygen atom is taken from methyl aclohol, otherwise from ethane as also is B(CC). Then B(C–O) = 83.0 kcal. at R(C–O) = 1.422 Å. (Fig. 1.) Electron diffraction yields[52,53] 1.44 ± 0.03 and 1.42 ± 0.03 Å., respectively.

Diethyl Ether.—Q(f) = 57.5 kcal.[28] and Q(a, th) = 1324.4 kcal. Taking the bond structure as in $(CH_3)_2O$, there remains B(C–O) = 83.0 kcal. by difference. Then R(C–O) = 1.422 Å. From electron diffraction[45] R(CC) = 1.50 ± 0.02 and R(C–O) = 1.43 ± 0.02 Å.

Methyl Ethyl Ether.—Q(f) = 52.0 kcal.[28] and Q(a, th) = 1043.0 kcal. Taking the structure from $(CH_3)_2O$ and $(C_2H_5)_2O$, there results B(C–O) = 83.7 kcal.

Diamyl Ether.—Q(f) = 99.8 kcal.[37] and Q(a, th) = 3022.0 kcal. The usual treatment results in B(C–O) = 84.0 kcal. at 1.428 Å.

The average B(C–O, ether) = 83.4 ± 0.4 kcal. which is definitely different from B(CO, alcohol) = 81.5 ± 0.7 kcal.

Methyl Formate.—Q(f) = 83.6 kcal.[9] and Q(a, th) = 753.7 kcal. From electron diffraction[54] R(C=O) = 1.22 ± 0.03, R(C–O) = 1.37 ± 0.04 and R(C–O) = 1.47 ± 0.04 Å. The following bonds are taken from formic acid: B(C=O) = 160.0 kcal. at R(C=O) = 1.21 Å., B(C–O) = 106.0 kcal. at R(C–O) = 1.34 Å., B(CH) = 99.9 kcal. at R(CH) = 1.09 Å. and B(O . . H) = 9.3 kcal. at R(O · · H) = 2.0 Å. From methyl alcohol comes B(CH) = 98.9 kcal. at R(CH) = 1.098 Å. The difference between Q(a, th) and the sum of these bond energies is ascribed to the link between the acid and alcohol B(C–O) = 81.8 kcal. at 1.424 Å. In the original methyl alcohol, this bond is 81.2 kcal.

Methyl Acetate.—Q(f) = 89.5 kcal.[28] and Q(a, th) = 1035.5 kcal. Transferring appropriate bond energies from acetic acid and methyl alcohol yields B(C–O) = 82.4 kcal. at 1.44 Å.

Ethyl Acetate.—Q(f) = 95.0 kcal.[28] and Q(a, th) = 1316.8 kcal. The same treatment gives B(C–O) = 81.5 kcal.

Ethylene Oxide.—Q(f) = 12.2 kcal.[9] and Q(a, th) = 623.1 kcal. The microwave spectrum[55] yields

(45) P. W. Allen and L. E. Sutton, *Acta Cryst.*, **3**, 46 (1950).
(46) K. J. Tauer and W. N. Lipscomb, *ibid.*, **5**, 606 (1952).
(47) B. Dreyfus-Allain and R. Viallard, *Compt. rend.*, **234**, 536 (1952).
(48) H. D. Edwards, O. R. Gilliam and W. Gordy, *Phys. Rev.*, **76**, 196 (1949).
(49) D. G. Burkhard and D. M. Dennison, *Phys. Rev.*, **84**, 408 (1951).
(50) G. S. Parks, *et al.*, *J. Am. Chem. Soc.*, **68**, 2524 (1946).
(51) D. F. Stedman, *Trans. Faraday Soc.*, **24**, 289 (1928).
(52) L. E. Sutton and L. O. Brockway, *J. Am. Chem. Soc.*, **57**, 473 (1935).
(53) L. Pauling and L. O. Brockway, *ibid.*, **57**, 2684 (1935).
(54) J. M. O'Gorman, W. Shand, Jr., and V. Schomaker, *ibid.*, **72**, 4222 (1950).
(55) G. L. Cunningham, *et al.*, *J. Chem. Phys.*, **19**, 676 (1951).

the following accurate dimensions: $R(CC)$ = 1.472, $R(CO)$ = 1.436 and $R(CH)$ = 1.082 Å. and angles HCH = 116°41′, H_2C–C = 159°25′ and COC = 61°24′. The molecule is considered to have a structure like cyclopropane, which has "bent" carbon–carbon bonds. The carbon orbitals have their greatest overlap in a direction other than the carbon–carbon internuclear distances.[56] The simplest way to discuss this structure is to consider the carbon–carbon internuclear distance to be the chord of an arc, where the latter represents the bond distance. Hence $R(CC) = 1.472 \times 60°$ or 1.472 (radians) = 1.542 Å. The corresponding bond energy is $B(CC)$ = 85.0 kcal. The length of the carbon–hydrogen bond is 1.082 Å. and $B(CH)$ = 100.8 kcal. The carbon–oxygen bond energy is found from the difference: $1/2\ (Q(a, th) - 85.0 - 4 \times 100.8)$ or $B(CO)$ = 67.45 kcal. at $R(CO)$ = 1.486 Å. It is the arc for the carbon–oxygen bond. The total bond picture is

$B(CC, C_2H_4O)$ = 85 kcal. at $R(CC, C_2H_4O)$ = 1.542 Å. $B(CH, C_2H_4O)$ = 100.8 kcal. at $R(CH, C_2H_4O)$ = 1.082 Å.; $B(CO, C_2H_4O)$ = 67.5 kcal. at $R(CO, C_2H_4O)$ = 1.486 Å.

Discussion

It is seen that strong carbon–oxygen bonds have short distances and *vice versa* as is the case with other bonds studied so far. The behavior of molecules having hydrogen atoms adjacent to a carbonyl group is found to be unusual and is explained by an interaction like intramolecular hydrogen bonding. It is presumed that the two "lone pairs"[57,58] of electrons of the oxygen atoms, occupying either tetrahedral or trigonal orbitals, can interact with protons as described for the case of the usual hydrogen bonding.[59] Similar considerations indicate that for the present case either an ion–dipole interaction between a partially shielded proton and a lone-pair of electrons is operative to form a stable bonding ($B(O \cdot\cdot H)$) or a dipole–dipole interaction exists between the carbon–hydrogen dipole ($\mu(CH) = 0.57\ D$)[60,61] and the lone-pair dipole ($\mu = 2.8\ D$). If the geometry of the formaldehyde molecule mentioned above is used and if it is assumed that the proton charge is located at the mass-point of the hydrogen atom and that the lone-pair orbital dipole is in the plane of the molecule, with the negative end at the centroid of the trigonal orbital, then the energy of attraction between the ion and the dipole is −20.0 kcal. Since $B(O \cdot\cdot H) \doteq$ 5.0 kcal. it is seen that the proton must be heavily screened by its electron cloud and still be able to enter directly into bonding relations with the lone-pair dipole. The effective charge of the proton need only be $(4.8 \times 0.25) \times 10^{-10}$ e.s.u. to give an interaction energy of 5 kcal.

A dipole–dipole interaction can be described in the following manner. The carbon–hydrogen dipole ($\mu(CH) = 0.57\ D$) is considered to be the resultant of two dipoles, derived from the relations

$$R(C) + R(H) = 1.12 \text{ Å}. \qquad (5)$$

and

$$\mu(C) - \mu(H) = 0.57\ D \qquad (6)$$

or

$$R(C) - R(H) = 0.57/4.8 \text{ Å}. = 0.12 \text{ Å}. \qquad (7)$$

whence $\mu(C) = 2.97$ and $\mu(H) = 2.40\ D$. These dipoles are so positioned along $R(CH)$ that the hydrogen atom is positive or the resultant is $\mu(C–H^+)$. The electrostatic interaction between the CH-dipole and the lone-pair-dipole results in an attractive potential energy of −18.0 kcal. Again the electrical charges involved can be reduced by screening since only 5.0 kcal. are needed for interaction. It is assumed that the two CH-dipoles show little repulsion because of screening by the electron clouds between the protons.

It is of course clear that these simple electrostatic models cannot give an accurate picture of the real situation. Single charges and dipoles can only approximately represent electron clouds. However, the hydrogen bonding ($B(O \cdot\cdot H$,2.0 Å.)) is considered to be a real effect. It is not a resonance energy based on some arbitrary standard of reference devoid of physical meaning.

Another point of great interest is to consider the proton chemical shift in magnetic resonance.[62] These shifts have large positive values in aldehydes: $\delta(X\text{-}CHO) = 0.31$ and $\delta(C–CHO = 0.47)$ and also in carboxyl groups: $\delta(COOH = 0.64)$. They are the kind of molecule in which the electrostatic interaction between proton and carbonyl–oxygen operates. On the other hand molecules which have small positive or negative δ-shifts are: alcohols ($\delta(R–OH) = 0.01$), methyl groups with $\delta(H_3C–C\lessgtr) = -0.41$ or $\delta\ (H_3C\ C\lessgtr) = -0.33$ and methylene groups with $\delta(C–CH_2–X) = -0.17$. On this basis a mode of behavior different in degree is to be expected from the two classes of protons.

Even though there exists this distinction in the carbonyl groups, it is remarkable that so many bonds maintain their characteristic energies and their internuclear distances in a large variety of substances.

It is a pleasure to thank Dr. J. W. Dawson, Director of the Chemical Sciences Division, Office of Ordance Research, U. S. Army, for his interest in these calculations.

(56) A. C. Coulson and W. E. Moffitt, *ibid.*, **15**, 151 (1957); and *Phil. Mag.* **40**, 1 (1949).

(57) J. Lennard-Jones and J. A. Pople, *Proc. Roy. Soc.* (*London*), **202A**, 166 (1950); **205A**, 155 (1951).

(58) J. A. Pople, *ibid.*, **202A**, 323 (1950); **205A**, 163 (1951).

(59) W. G. Schneider, *J. Chem. Phys.*, **23**, 26 (1955).

(60) A. R. H. Cole and H. W. Thompson, *Trans. Faraday Soc.*, **46**, 103 (1950).

(61) I. C. Hisatsune and D. F. Eggers, Jr., *J. Chem. Phys.*, **23**, 487 (1955).

(62) L. H. Meyer, A. Saika and H. S. Gutowsky, *J. Am. Chem. Soc.*, **75**, 4567 (1953).

THE DECOMPOSITION OF HYDROGEN PEROXIDE ON ANTIMONY AND BISMUTH ALLOYS

BY P. P. CLOPP AND G. PARRAVANO[1]

The Franklin Institute Laboratories for Research and Development, Philadelphia, Pa.

Received March 3, 1958

The rate of the decomposition of hydrogen peroxide on Sb and Bi alloys has been determined. Kinetic parameters have been correlated with changes in the electronic structure of Bi and Sb brought about by the alloying process. In particular, the electronic electrochemical potential of Sb compounds can be qualitatively related to the activation energy of the catalytic reaction. These relationships are discussed in terms of present concepts on the catalytic activity of conducting surfaces.

The elucidation of the role played by the electronic structure of solid semi-conductors on their catalytic properties has been the subject of several recent investigations. These studies have been largely confined to metal oxides and related systems, while elemental semi-conductors and semi-metals have received less attention. The catalytic properties of germanium, tin, antimony and arsenic toward hydrogen and ammonia have been the subject of a thorough study.[2] The activity of germanium, silicon and III-V group compounds for the hydrogenation of formic acid also has been discussed,[3] while the chemisorption of several gases has been studied on semi-metals (As, Sb, Bi) and semi-conductors (Se, Te).[4] From these studies correlations between the nature of the solid and catalytic activity have been deduced and a number of behavior patterns have emerged. It is, therefore, of interest to explore additional systems in view of a critical evaluation of present concepts on the catalytic action of conducting surfaces. We have investigated the reaction kinetics of the decomposition of hydrogen peroxide on bismuth and antimony alloys, because the general form of the electronic structure of these compounds is known and they occupy a bridge position between metals and metallic oxides.

Experimental

Materials.—Bi alloys were made from pure components (McKay), with nominal composition of 0.1 atom % of alloying element, which, in all cases studied, is known to be completely soluble in Bi within the above composition range. GaSb and InSb were formed by direct combination of zone refined elements,[5] in approximately stoichiometric proportions, in a zone refining apparatus filled with dry hydrogen.[6] Samples produced in this fashion exhibited p-type conductivity; n-type materials were formed by doping with 1% Te alloy. Conductivity and d.c. Hall coefficient of InSb and GaSb were measured on samples with dimensions of approximately 1.0 cm. by 0.1 cm. by 0.3 cm. Catalytic activity of both Bi and Sb alloys was measured on samples prepared by grinding the original material in a diamond mortar (Bi alloys) or an agate mortar (Sb alloys). The ground material was fractionated by means of a series of standard sieves. The fraction collected was found to have a BET surface area of about 0.02 m.^{2}/g. for all Bi alloys and 0.04 m.^{2}/g. for all Sb alloys. Hydrogen peroxide (Merck, Superoxol) was diluted with triple distilled water, allowed to stand a week before use and handled in steam-cleaned vessels. Potassium permanganate solutions were prepared following the usual procedure and standardized with National Bureau of Standards sodium oxalate. Standardization was checked every two weeks.

Procedure.—The decomposition reaction was followed in a Pyrex glass, stirred vessel, kept at constant temperature (±1°). At different time intervals, samples were withdrawn from the reactor and the extent of decomposition determined by titration of the remaining hydrogen peroxide with $KMnO_4$ solution. Titrations were performed in a flask containing 5 ml. of 10% H_2SO_4 and 20 ml. of freshly distilled water, and carried out in the usual manner to an end-point at which the color remained for 30 sec. Experimental conditions were carefully chosen as to eliminate diffusion effects as controlling factors of the reaction rate. No homogeneous catalyst was present. This fact was checked by stopping an experiment, removing the catalyst and testing for decomposition over an extended period of time.

Measurements of conductivity and Hall effect of Sb compounds were made with a conventional d.c. method.[7] The electromagnetic field for Hall constant determination was electronically controlled to an accuracy of ±0.02% and could be varied from zero to 5000 oersteds. Potential measurements were made with a Wenner thermo-free potentiometer. Stainless steel whiskers were used as potential probes and lightly welded to the specimens by a high voltage discharge from a Tesla coil. Current contacts were made with large area stainless steel springs. Samples were cut from grown crystals with a diamond saw, and etched with a dilute HNO_3–HCl etch. The reported measurements of conductivity and Hall constant were obtained at 300°K.

Results

It was found that the decomposition of hydrogen peroxide on all samples tested could be expressed by a first-order rate equation, which has frequently been found in the past to describe accurately the course of the reaction

$$-\frac{d[H_2O_2]}{dt} = k[H_2O_2] \qquad (1)$$

An Arrhenius plot for all Bi alloys is presented in Fig. 1. From this plot, values for the activation energy E and preexponential factor A were computed and are summarized in Table I.

All data on Sb alloys could be fitted into an Arrhenius plot. The computed values of E and A together with those of the electrical conductivity σ, Hall constant R and electron or hole mobility μ, are collected in Table II. Electron and hole mobilities were obtained by means of the equation

(1) Department of Chemical Engineering, University of Notre Dame, Notre Dame, Indiana.

(2) K. Tamaru, THIS JOURNAL, **59**, 777 (1955); K. Tamaru, M. Boudart and H. Taylor, *ibid.*, **59**, 801 (1955); P. J. Fensham, K. Tamaru, M. Boudart and H. Taylor, *ibid.*, **59**, 806 (1955); H. Taylor, *Can. J. Chem.*, **33**, 838 (1955); K. Tamaru, *ibid.*, **33**, 1054, 60, 610, 612 (1950); K. Tamaru and M. Boudart, in "Advances in Catalysis," Vol. IX, Academic Press, Inc., New York, N. Y., 1957.

(3) R. H. Kingston (editor), "Semiconductor Surface Physics," University of Pennsylvania Press, 1957, article by G. M. Schwab.

(4) R. Suhrman and H. G. Wuttke, *Z. Elektrochem.*, **59**, 379 (1955); R. Suhrman, in "Symposium on Chemisorption," Keels, 1956; E. Greenhalgh and B. M. W. Trapnell, in "Advances in Catalysis," Vol. IX, Academic Press, Inc., New York, N. Y., 1957.

(5) D. P. Detwiler and W. M. Fox, *J. Metals*, *I*, 205 (1955).

(6) D. P. Detwiler, *Phys. Rev.*, **97**, 1575 (1955).

(7) We are grateful to Dr. D. P. Detwiler and Mr. W. M. Fox for making these measurements.

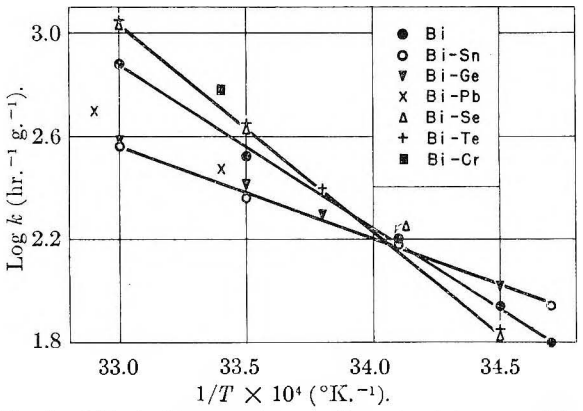

Fig. 1.—Effect of temperature on the rate of decomposition of H_2O_2 on Bi and Bi alloys.

TABLE I

ACTIVATION ENERGY E AND PRE-EXPONENTIAL FACTOR A FOR HYDROGEN PEROXIDE DECOMPOSITION ON Bi ALLOYS

Alloy	$\log A$ (hr.$^{-1}$ × g.$^{-1}$)	E, (kcal. × mole^{-1})
Bi + Sn Bi + Ge Bi + Pb	10.22	16.0
Bi	19.87	29.0
Bi + Cr Bi + Se Bi + Te	25.53	37.0

$\mu = 0.85R\sigma$(cm.^{2}, volt^{-1}, sec.$^{-1}$)

Discussion

The over-all decomposition reaction may be visualized to occur through the sequence[8]

$$Me + H_2O_2 \longrightarrow Me - O + H_2O \quad (2)$$
$$Me - O \rightleftharpoons Me + {}^1/_2O_2 \quad (3)$$

TABLE II

ELECTRICAL CONDUCTIVITY σ, HALL CONSTANT R, ELECTRON OR HOLE MOBILITY, μ, AT 300°K., PRE-EXPONENTIAL FACTOR A AND ACTIVATION ENERGY E FOR HYDROGEN PEROXIDE DECOMPOSITION ON GaSb AND InSb

Sample	σ (Ω^{-1} × cm.$^{-1}$)	R (cm.^{3} × coul.$^{-1}$)	μ (cm.^{2} × volt^{-1} × sec.$^{-1}$)	A (hr.$^{-1}$ × gr.$^{-1}$)	E (kcal. × mole^{-1})
GaSb-1	30.4	+15.2	394	0.85	5.7
GaSb-2	12.8	+56.7	619	0.2	4.8
GaSb-3	840.0	+ 0.5	356	1.8	7.3
GaSb-4	230.0	−10.3	2000	2.9	8.9
InSb-1	980.0	−19.2	1600	9	16.6
InSb-2	34.4	+664	19500	8.3	15.8
InSb-3	124	+ 2.32	290	7.0	14.3
InSb-4	182.4	∼+ 0.5	77.5	3.4	9.5

where Me–O is an oxygen atom adsorbed on the metal surface. If the rate of reaction 2 is slower than that of (3), then

$$-\frac{d[H_2O_2]}{dt} = k[1 - \theta][H_2O_2] \quad (4)$$

where θ is the fraction of the metal surface covered with adsorbed oxygen. At low θ's equation 4 can be simplified to

$$-\frac{d[H_2O_2]}{dt} \cong k[H_2O_2]$$

which is similar to equation 1. There is also the possibility of the scheme

$$Me + H_2O_2 \rightleftharpoons Me - O + H_2O \quad (2)$$
$$Me - O + H_2O_2 \longrightarrow H_2O + O_2 + Me \quad (5)$$

As a limiting condition it can be assumed that the rate of reaction 5 is slower than that of (2) and that the surface is almost wholly covered with adsorbed oxygen. Then, for the over-all reaction

$$\frac{-d[H_2O_2]}{dt} = k\theta[H_2O_2] \cong k[H_2O_2]$$

which is again similar to equation 1.

There are additional kinetic schemes, which may produce, under proper conditions, a rate equation similar to (1). These mechanisms are based on the interaction between adsorbed species as the kinetically determining step. Thus, adsorbed OH groups may be thought to be formed during the decomposition reaction by means of the sequence[9]

$$H_2O_2 + 2Me \rightleftharpoons 2Me\text{–}OH \quad (6)$$
$$2Me\text{–}OH \longrightarrow H_2O + Me\text{–}O + Me \quad (7)$$

which is operative in the gas phase reaction.[10] If the slow process involves reaction 7, the rate of the

$$v = k_7\theta'^2 \quad (8)$$

latter is (8) where θ' is fraction of surface covered with OH groups. From reaction 6, when $k'_6 << k''_6$

$$\theta' \cong (k'_6/k''_6)[H_2O_2]^{1/2}$$

where k'_6, k''_6 are the forward and backward rate constants for reaction 6, and, therefore, equation 8 becomes

$$v \cong k''[H_2O_2]$$

It is evident that additional information on the nature of the chemisorbed species formed during the catalytic decomposition is needed to arrive at definite conclusions on the catalytic mechanism of the decomposition reaction. Despite this shortcoming, however, it is still permissible to discuss in a general fashion the possibility of a correlation between the electrical properties of the surfaces involved and their catalytic activity.

Bismuth Alloys.—An inspection of Table I shows that a qualitative relationship can be established between the activation energy of the decomposition reaction and nature of the alloying element. Sn, Ge and Pb, which are group IV elements, decrease the activation energy, while Cr, Se, Te, which are group VI elements, increase it. Metallic Bi has a Brillouin zone containing nearly five electrons per atom. Since the number of valence electrons in Bi is five, the Brillouin zone will be almost completely filled. This situation determines the fact that the electrical and magnetic properties of Bi are very sensitive to small changes in the number of free electrons in the metal. Therefore, by additions of impurities like Pb, Sn, Ge, which have one less valence electron than Bi, the number of free electrons in Bi will decrease; while additions of Te, Se, with one more valence electron than Bi, will increase it. Confirmation of these effects was obtained by means of measurements of electrical conductivity on Bi and Bi alloys.[11]

(8) W. C. Bray and M. H. Gorin, *J. Am. Chem. Soc.*, **54**, 2124 (1932).

(9) J. Weiss, *Trans. Faraday Soc.*, **31**, 1547 (1935).

(10) Bonhoeffer and Pearson, *Z. physik. Chem.*, **14B**, 1 (1931).

(11) N. Thompson, *Proc. Roy. Soc. (London)*, **155**, 111 (1936).

Furthermore, Bi thin films have semi-conductor properties. Te acts as a donor by increasing the electron concentration and decreasing the electrical resistance of Bi.[12] We may conclude, then, that the present data provide support for a relation between the activation energy of the decomposition reaction and the electronic characteristics of the solid surface as typified by the electronic work function. A great deal of effort has been devoted in the past to provide a sound, theoretical justification for such a relationship. However, all treatments are based on particular assumptions on the behavior of the energy surface of the chemical reaction. At present, therefore, we must regard the above correlation as semi-empirical. This fact considerably limits the possibility of using the present results to predict the catalytic behavior of other, electronically similar, systems.

Previous observations on the relation between work function of catalytic metals and rate of hydrogen peroxide decomposition have shown that the latter increases when the former decreases and *vice versa*.[13] This is consistent with our conclusions, since metals like Pb, Sn, Ge, which upon alloying with Bi, increase the work function of the latter, were found to decrease the rate of decomposition, relatively to pure Bi, at temperatures above ~20°. Possibly such a relationship points to the formation of OH^- or similar anions as reaction intermediates.[14] Below 20°, however, the effect of additions on the rate of the decomposition reaction is inverted. Naively, this could be ascribed to a change in the reaction mechanism, with a larger kinetic contribution from positive ions, or to the presence of two different kinds of active centers on the catalytic surface. The inversion is very much reminiscent of concepts, often discussed in the past, on the dual character of additions to catalysts.[15] Finally, it is interesting to draw attention to the similarity between the present results and those obtained in a study of the electro-chemical reaction[16]

$$Fe(CN)_6^{-3} + e^- \longrightarrow Fe(CN)_6^{-4}$$

In this work, it was found that the overvoltage required for a given current density at a surface of pure Bi had a value lying between the values corresponding to Bi + Se, and Bi + Pb or Bi + Sn.

Antimony Alloys.—The density of states in the conduction and valence bands, N_c and N_v, of the prepared samples of InSb and GaSb at 300°K. is taken as: $N_c = 2.0 \times 10^{17}$, $N_v = 1.2 \times 10^{18}$ (cm.$^{-3}$) for InSb, $N_c = 1.2 \times 10^{18}$, $N_v = 2.0 \times 10^{18}$ (cm^{-3}) for GaSb.[17] Similarly, the width of the forbidden gap at 300°K., $E_c - E_v$, was computed at 0.18 and 0.67 e.v. for InSb and GaSb respectively.[17] Since

$$R = \frac{-3\pi}{8ne} \text{ (cm.}^3 \times \text{coul.}^{-1}\text{)}$$

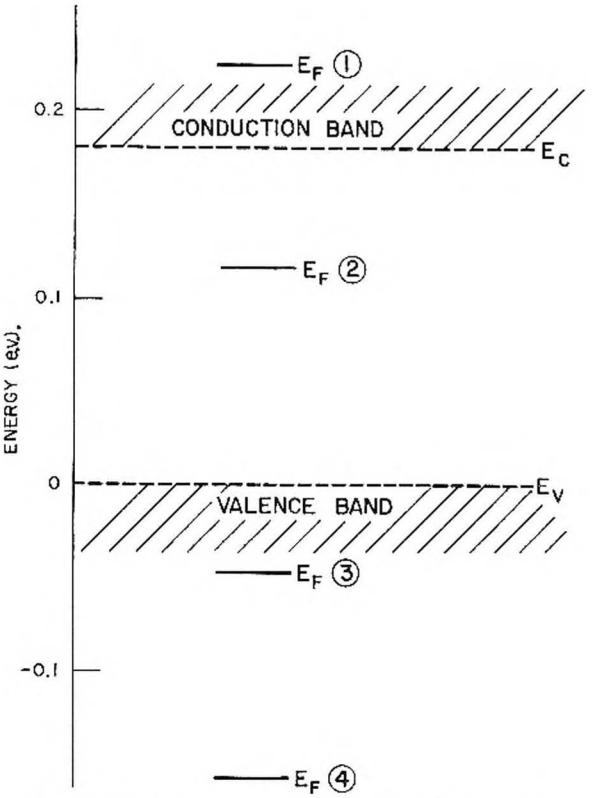

Fig. 2.—Electronic energy diagram for InSb samples.

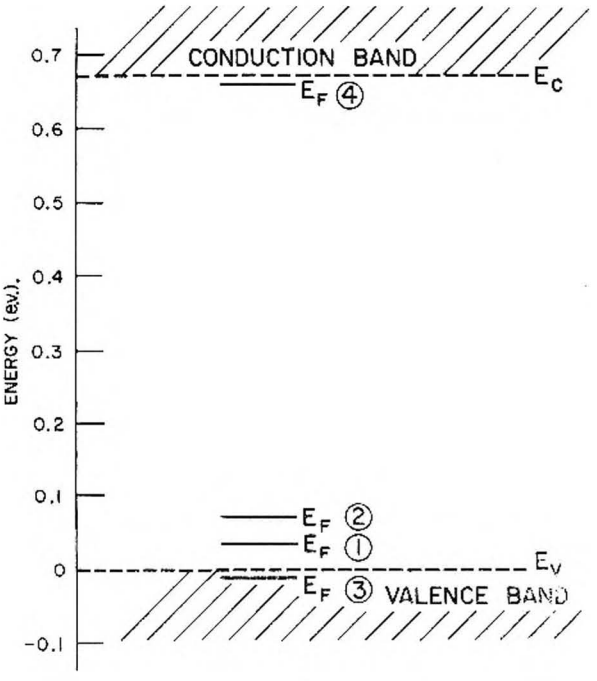

Fig. 3.—Electronic energy diagram for GaSb samples.

the carrier density is

$$n, p = \frac{7.37 \times 10^{18}}{|R|} \text{ (cm.}^{-3}\text{)}$$

Then

$$n = \frac{2}{\sqrt{\pi}} N_c F_{1/2}(\eta^*)$$

(12) R. Suhrman and H. G. Wuttke, *Z. Elektrochem.*, **59**, 379 (1955).
(13) J. Weiss, *Trans. Faraday Soc.*, **31**, 1547 (1935).
(14) J. H. de Boer, *Disc. Faraday Soc.*, **8**, 209 (1950).
(15) Th. Volkenstein, *J. Phys. Chem. (USSR)*, **23**, 917 (1949); E. Cremer, in "Advances in Catalysis," Vol. III, Academic Press, Inc., New York, N. Y., 1956.
(16) M. J. Brabers and W. G. Burgess, *Proc. Kon. Ned. Akad. v. Wet. Amsterdam*, **B56**, 439 (1953).
(17) R. G. Breckenridge, R. F. Blunt, W. R. Hosler, H. P. R. Frederikse, J. H. Becker and W. Oshinsky, *Phys. Rev.*, **96**, 571, 576 (1954).

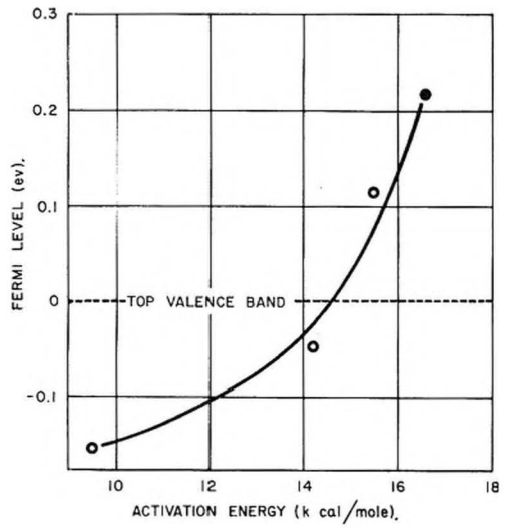

Fig. 4. Fermi level *versus* activation energy for H_2O_2 decomposition of InSb samples: ○, p-type; ●, n-type.

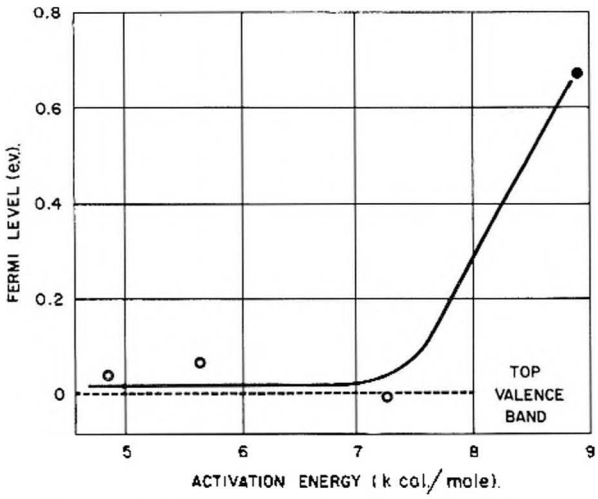

Fig. 5.—Fermi level *versus* activation energy for H_2O_2 decomposition on GaSb samples: ○, p-type; ●, n-type.

$$p = \frac{2}{\sqrt{\pi}} N_v F_{1/2}(\eta^{**})$$

Where $F_{1/2}(\eta^*)$ and $F_{1/2}(\eta^{**})$ are the so-called Fermi–Dirac integrals

$$F_j(\eta^*) = \int_0^\infty \frac{\eta_j d\eta}{1 + \exp(\eta - \eta^*)}$$

where $\eta = E_F/kT$ and E_F is the Fermi level.[18] Accurate values of $F_j(\eta^*)$ and E_F have been computed and can be found in tables.[19] At 300°K., for n-type materials $(E_F - E_c) = \eta^{*+} \times 0.025$ (e.v.) and for p-type $(E_v - E_F) = \eta^{**}$ 0.025 (e.v.). Values of E_F computed in this way for all samples are collected in Figs. 2 and 3.

In Fig. 4 and 5, these data are correlated with the computed activation energy E for the decomposition reaction. These plots indicate that, for both InSb and GaSb, it is possible to discuss a relationship between the position of the Fermi level of the catalyst before use and E or A, since there is a linear relationship between log A and E. Both the extent and direction of the change in E_F following the establishment of a surface oxidation–reduction steady-state during the catalytic reaction is not known, because it depends on the chemical nature and concentration of intermediates formed, and on the strength of their bonding with the surface. Unfortunately, as discussed previously, the kinetic data are insufficient to supply information on these points. However, it is plausible to assume that the Fermi level under steady-state condition is relatively displaced in an almost similar manner for all samples tested. Then, it is still possible to discuss the relative behavior of all Sb alloys tested. It is interesting to point out that the electronic type of the bulk solid has produced no significant change in kinetic behavior. Thus, n-type samples can be correlated along with p-type ones. This may be due to an inherent feature of the catalytic process, but it may also result from a local surface change from n- to p-type, due to the prevailing oxidizing conditions during the reaction. Whichever of these two possibilities is closer to physical reality, it is safe to conclude that, in the present case, the type of electron conduction of the *bulk* has no effect on the catalytic activity of the surface. Previous results obtained on catalytic systems different from the present one, have indicated that the activity is dependent on the nature of the majority carriers.[20] The present results are, however, at variance with the suggestion that changes in the type of semi-conductivity of the same material should, as a consequence, bring about basic changes in catalytic behavior.[21] Essentially, the relationship between E_F and E can be resolved, as discussed previously in the case of Bi alloys, in a correlation between the work function of the alloy and E. Since the work function strongly influences the binding energy of the adsorbate in both cases of a heteropolar and homopolar surface bond,[22] we are led to correlate the heat of adsorption with the activation energy of the reaction.[23] A relationship between these two parameters has been found to hold in many systems including electrochemical processes.[24] Furthermore, the heat of adsorption is a function of the position of the Fermi level of the catalytic surface,[25] and our results require that an increase in E_F should produce an increase in the activation energy, necessary for reaching the adsorbed state. Some possibilities have been suggested for this occurrence,[26] but they rule out anionic species as kinetically important intermediates.

Conclusions

The data reported are in qualitative agreement with some of the present views on the catalytic activity of semi-conductors, while they disagree with some others. The present results, which were

(18) J. S. Blakemore, *Electrical Communications*, June, 131 (1952).

(19) J. McDougall and E. C. Stover, *Phil. Trans. Roy. Soc. (London)*, **A237**, 67 (1938).

(20) F. S. Stone, *Trans. Faraday Soc.*, **49**, 201 (1953).

(21) R. H. Kingston (editor), "Semiconductor Surface Physics" Univ of Pennsylvania Press, 1957, p. 292, article by G. M. Schwab.

(22) J. J. Broeder, W. M. H. Sachtler, G. C. A. Schnit and L. L. van Reijn, *Z. Elektrochem.*, **60**, 838 (1956).

(23) R. A. Ogg and M. Polanyi, *Trans. Faraday Soc.*, **31**, 1375 (1935).

(24) Ruetochi and Delay, *J. Chem. Phys.*, **23**, 195 (1955).

(25) M. Boudart, *J. Am. Chem. Soc.*, **74**, 1531 (1952).

(26) D. D. Eley, "Reilly Lectures," Vol. VII, University of Notre Dame Press, Notre Dame, Ind., 1954.

obtained on relatively simple systems, indicate quite clearly that a qualitative theory, explaining all of the available experimental facts in this field, cannot yet be established. It is, therefore, futile to generalize results, gathered on few systems, in order to construct a general theory of catalytic action at conducting surfaces. In a general way, the results of this investigation support the idea that the "availability" of electrons for bond formation between the adsorbate and the conducting surface is affected and, therefore, dependent on the electronic characteristics of the latter. This conclusion applies whether the chemisorbed bond is covalent, ionic or intermediate in nature. This "availability" may be considered both in terms of energy and entropy, since in all of our samples a linear correlation between the activation energy and the pre-exponential factor obtains.

Acknowledgment. Financial support for this work was provided by the generous contribution of the Atlantic Refining Company and Esso Research and Engineering Company. The authors wish to express their thanks and appreciation for this help.

THE NAPHTHALENE–TETRALIN–HYDROGEN EQUILIBRIUM AT ELEVATED TEMPERATURE AND PRESSURE

BY THOMAS P. WILSON, EDWARD G. CAFLISCH AND GEORGE F. HURLEY

Contribution from the Research Department, Union Carbide Olefins Company, A Division of Union Carbide Corporation, South Charleston, West Virginia

Received March 20, 1958

The position of the naphthalene–tetralin–hydrogen equilibrium has been determined experimentally at temperatures between 360 and 475° and pressures up to 60 atmospheres. A method of correcting the equilibrium constants for deviations from the ideal gas laws has been devised. The corrected values of K_p for the hydrogenation of naphthalene can be represented by the relation $\log K_p = -13.13 + 7000/T$. The calculated heat of hydrogenation of naphthalene at 400° is −32.0 ± 1.2 kcal./gram mole.

Knowledge of the thermodynamics of the reactions involved in the hydrogen treatment of polycyclic hydrocarbons is very limited. Accurate chemical thermodynamic properties calculated from spectroscopic and third law data are available only for naphthalene[1] and decalins.[2] A semi-empirical calculation of the thermodynamic properties of tetralin also has appeared recently[3] and the results have been used to predict the naphthalene–tetralin equilibrium constant.[4] The naphthalene–tetralin equilibrium was studied experimentally[5] some years ago at low temperatures and pressures, but the results obtained were not of sufficient accuracy to provide a useful check on the calculations. The now reported measurements of the naphthalene–tetralin equilibrium provide an experimental check on the semi-empirical calculations[4] in a region of temperature and pressure of current technical interest. A method of calculating the activity coefficients necessary to convert the experimental results to the ideal gas basis has been devised, and checked with the data obtained.

Experimental

The equilibrium measurements were made in an apparatus typical of those employed in the study of catalytic hydrogen treatments of volatile liquid hydrocarbons. The catalyst charge was 150 ml. (0.96 inch i.d. tube) of $^1/_8$-inch pellets of Harshaw molybdena or cobalt molybdate on alumina—either Mo-0201-T or what was thought to be Co-Mo-0401-T. No significant differences between the catalysts were noted. Hydrogen flows varied from 35 to 150 liters per hour and hydrocarbon liquid feed rates from 30 to 300 ml. per hour. Establishment of equilibrium was demonstrated at the higher temperatures by showing the product composition to be independent of the feed rate of tetralin. At the lower temperatures, where minimum feed rates were necessary, establishment of equilibrium was demonstrated by feeding a tetralin–naphthalene mixture of very nearly the equilibrium composition and showing that this composition changed very little, although considerable naphthalene could be formed when tetralin alone was fed.

Liquid products were analyzed on a Perkin–Elmer Vapor Fractometer, Model 154-B. The chromatographic column was packed with 26% Apiezon "N" on "Chromosorb" and operated at 180° with helium as the carrier gas. Calibration with mixtures of the compounds of interest indicated the relative sensitivities[6] (area to weight ratios) to be: naphthalene, 1.00; tetralin 0.945; *cis*-decalin, 1.09; *trans*-decalin, 0.995.

In most cases analyses were based on areas of peaks identified only by their retention times. In two experiments at 475°, where side reactions became important, peaks from the chromatographic column were collected and examined by infrared. For this purpose a $^3/_4$ inch o.d. column 2.2 meters long was employed, and the sample size increased to about 2 ml. Separations made with this larger diameter column appeared to be at least as good as those obtained with the standard $^1/_4$ inch column.

The principal constituent present in a peak appearing at a retention time 76% of that of *trans*-decalin was shown to be *n*-butylbenzene. This peak was found in samples from runs at all temperatures investigated. The "*trans*-decalin" peak isolated from samples obtained in runs at 475° was found to contain four or five times as much methylindane as *trans*-decalin.

Results and Discussion

The experimentally determined values of the naphthalene–tetralin equilibrium constants are collected in Table I, with the conditions under which they were measured. These conditions are such that quite substantial deviations from ideal gas behavior are to be expected. The largest deviations should be exhibited by naphthalene and tetra-

(1) A. L. McLellan and G. C. Pimentel, *J. Chem. Phys.*, **23**, 245 (1955).

(2) T. Miyazawa and K. S. Pitzer, *J. Am. Chem. Soc.*, **80**, 60 (1958).

(3) A. Székely, *Acta Chim. Hung.*, **5**, 317 (1955).

(4) G. Rabo and A. Székely, *ibid.*, **5**, 453 (1955).

(5) A. Maillard, *Ann. combustibles liquides*, **10**, 95 (1935).

(6) These differ slightly from those reported by R. M. Soemantri and H. I. Waterman, *J. Inst. Petroleum*, **43**, 94 (1957).

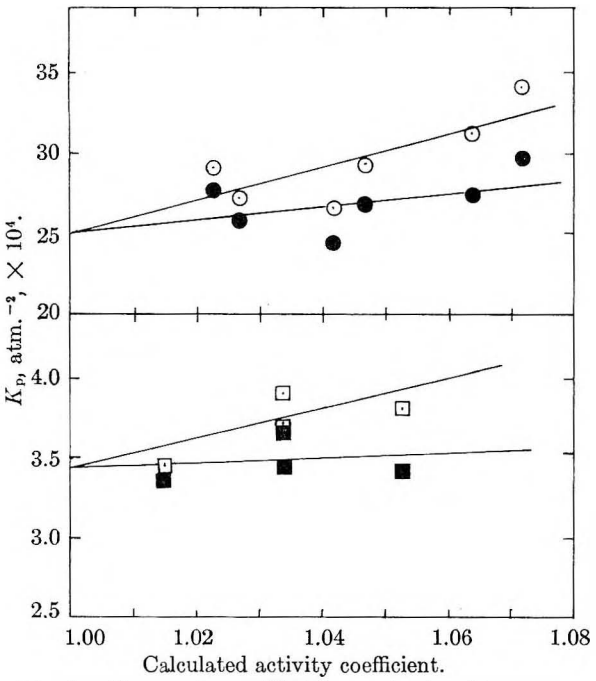

Fig. 1.—Changes in equilibrium constants with pressure: ⊙, 390° uncor.; ●, 390° cor., ⊡, 450° uncor.; ■, 450° cor.

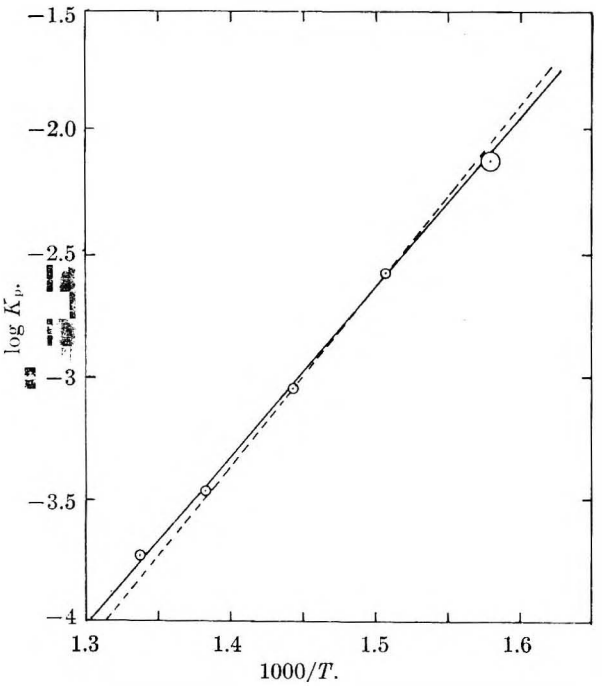

Fig. 2.—Naphthalene–tetralin–hydrogen equilibrium constants as a function of temperature. Solid line is best empirical representation of data. Dashed line represents calculations of Rabo and Székely.[4]

lin, but only the ratio of these fugacities appears in the equilibrium constant. The activity coefficients of these compounds in the mixture should be very nearly equal, according to the Lewis and Randall rule[7] for the fugacity of mixtures, since their critical temperatures and pressures are very nearly equal. Hence deviations of these two compounds from ideality would cancel out in K_p. The presence of the hydrocarbons would, however, be expected to change the behavior of the hydrogen, which otherwise could almost be treated as ideal. The hydrocarbon molecules occupy a portion of the gas phase, and when the finite sizes of hydrogen and hydrocarbon are considered the volume from which the centers of the hydrogen molecules are excluded becomes quite appreciable under the conditions employed.

TABLE I

EXPERIMENTAL DETERMINATIONS OF NAPHTHALENE–TETRALIN–HYDROGEN EQUILIBRIUM

Run no.	Temp., °C.	Pressure, atm. Total	Hydrocarbon	Measured[a] $K_p \times 10^4$, atm.$^{-2}$	Calcd. activity coefficient, hydrogen	Cor.[a] $K_p \times 10^4$ atm.$^{-2}$
99-6	360	14.6	3.54	89.3[b]	1.027	84.5[b]
106-4	360	21.4	5.38	74.6[b]	1.042	68.4[b]
137-7	390	21.4	3.15	29.0	1.023	27.6
102-4,5	390	35.0	8.5	31.1	1.064	27.3
103-5,6	390	35.0	10.1	34.0[b]	1.072	29.6[b]
139-5	390	35.0	5.28	26.4	1.042	24.3
141-4	390	35.0	2.83	27.1	1.027	25.7
143-3	390	62.2	4.88	29.2	1.047	26.7
104-6, 123-5	420	48.6	6.4	10.00[b]	1.048	9.10[b]
105-3, 125-9	420	48.6	5.4	9.82	1.043	9.00
110-5,6	450	21.4	2.2	3.45	1.015	3.35
111-3,4	450	41.8	4.3	3.68	1.034	3.44
112-8	450	41.8	4.3	3.90	1.034	3.65
108-4,6,10	450	62.2	7.3	3.80	1.053	3.41
135-4,10	475	35.0	3.4	2.06	1.024	1.96
113-6	475	62.2	7.68	1.94	1.056	1.74
114-5,6,7	475	62.2	6.9	2.10	1.053	1.89
145-5	475	62.2	3.6	2.01	1.033	1.88

[a] $K_p = (N_{C_{10}H_{12}}/N_{C_{10}H_8}\ N^2_{H_2}) \times 1/P^2$, where N_i = mole fraction of component i in the gas, P = the total pressure in atmospheres. K_p (corrected) = $K_p/\gamma^2_{H_2}$. [b] Feed contained 35% naphthalene, 65% tetralin by weight.

The excluded volume can be calculated in a manner similar to that employed[8] to evaluate the b term in the van der Waals equation for a single gas. It is only necessary to consider that all the hydrocarbon is present as isolated molecules when the hydrogen is added. If the diameter of a hydrogen molecule is taken to be 2.8 Å., and the hydrocarbon molecules are assumed to be discs 3 Å. thick and 9 Å. in diameter, the excluded volume is calculated to be about three times the actual volume of the hydrocarbon—assuming the hydrocarbon to have a density of 1.145 (naphthalene). This quantity was added to the b, 0.015 liter per mole, found empirically for hydrogen alone in the appropriate temperature range. The a term in the van der Waals equation of state for hydrogen was presumed to remain negligible in comparison to b. Values of the activity coefficient calculated in the above manner are shown in Table I.

Measurements of K_p were made over a range of total pressures and hydrocarbon partial pressures. These provide material with which to test the validity of the arguments presented concerning fugacities. It will be assumed that the calculated activity coefficients provide the best available measure

(7) G. N. Lewis and M. Randall, "Thermodynamics," McGraw-Hill Book Co., Inc., New York, N. Y., 1923, pp. 225–227.

(8) S. Glasstone, "Textbook of Physical Chemistry," Second Edition, D. Van Nostrand Co., Inc., New York, N. Y., 1954, p. 294.

of the relative tendencies of particular reaction conditions to produce deviations from ideal gas behavior. If, then, the observed values of K_p are plotted against the calculated activity coefficients, the points should fall on a line whose deviation from the horizontal provides a measure of the deviation of the system from ideality. The data obtained at 390 and 450° are plotted in this manner in Fig. 1. The corrected values of K_p are shown in the same figure for comparison. Within the rather large uncertainty in the experimental data, the calculated corrections can be said to be of the right magnitude. The corrected values therefore will be employed to characterize the equilibria.

The corrected K_p's for the naphthalene–tetralin equilibrium shown in Table I were fitted by least squares to an Arrhenius-type equation. The result is

$$\log K_p = -13.13 + \frac{7000}{T} \qquad (1)$$

where K_p is in (atmospheres)$^{-2}$ and T in degrees Kelvin. The standard deviation of individua points from this line is ±15%, the worst offender being the lowest temperature point where attainment of equilibrium was relatively uncertain. From the constants given, $\Delta H^0_{400} = -32.0 \pm 1.2$ kcal./g. mole and $\Delta S^0_{400} = -60.1$ cal./deg. mole. The uncertainty given for ΔH^0_{400} represents the 0.95 confidence limit calculated statistically from the experimental data. If a value of ΔH^0_{400} were determined accurately by some other means, the measurements of K_{0p} would serve to define ΔS^0_{400} to ±0.2 cal./deg. mole.

The equation given can be compared with that of Rabo and Székely[4]

$$\log K_p = -13.65 + \frac{7350}{T} \qquad (2)$$

Between 390 and 450° the differences in the two constants compensate and both equations fit the experimental data very well. This is shown in Fig. 2. The difference in the slopes of the two lines, while not very great, is still outside the calculated 0.95 confidence limits. At 475° the average of seven individual experimental determinations of the equilibrium constant would have to be too high by more than 20% if Rabo and Székely's calculations are correct. Until the purity of the materials separating into chromatographic peaks was determined it appeared possible that side reactions at the high temperature might lead to products which would interfere in the chromatographic analysis. Both the naphthalene and tetralin peaks proved, however, to be more than 95% the expected material, with the principal contamination of the tetralin being naphthalene—the nearest major constituent of the mixture. It, seems probable therefore, that equation 1 represents a significant improvement over equation 2 as a representation of the effect of temperature on the value of the naphthalene–tetralin–hydrogen equilibrium constant at temperatures between 350 and 500°.

Acknowledgment.—The authors are grateful to Mr. A. H. DuVall for the spectroscopic examinations of the products.

THE SOLUBILITY OF *CIS*- AND *TRANS*-DINITROTETRAMMINE-COBALT-(III) IODATE AND *CIS*- AND *TRANS*-DINITROTETRAMMINE-COBALT(III) *dl*-DINITROÖXALATODIAMMINE COBALTATE IN DIOXANE–WATER, ETHANOL–WATER AND ACETONE–WATER MIXED SOLVENTS AT 15 AND 25°

By H. LAWRENCE CLEVER AND FRANK H. VERHOEK

Contribution from the McPherson Chemical Laboratory of The Ohio State University, Columbus, Ohio

Received April 8, 1958

The solubilities of the iodate and the *dl*-dinitroöxalatodiammine cobaltate of the two cations *cis*- and *trans*-dinitrotetrammine-cobalt(III) have been determined in dioxane–water, ethanol–water and acetone–water mixtures at 15 and 25°. Values of ΔH^0, ΔF^0 and ΔS^0 for the solution process have been calculated.

This paper reports the results of a study of the change of solubility of the iodates and *dl*-dinitrooxalatodiammine cobaltates of *cis*- and *trans*-dinitrotetrammine-cobalt(III) with change in the dielectric constant of the solvent. The dielectric constant was changed by adding dioxane, ethanol or acetone to water. These salts were chosen because they are relatively insoluble, yet their concentrations can be determined accurately by analysis for ammonia. The comparison of the solubility of the *cis–trans* pair may help to determine which forces are important in the solution process.

Experimental

The cobaltammine complex ions were prepared by methods previously described.[1] The cobaltammine anion was obtained as ammonium *dl-cis*-dinitroöxalato-*cis*-diammine cobaltate by careful recrystallization.[2] The salts for solubility studies were formed by precipitation and purified by shaking with successive portions of water until a con-

(1) (a) S. M. Jorgensen, *Z. anorg. Chem.*, **2**, 279 (1892); **11**, 416 (1896); **17**, 455 (1898); (b) S. A. Mayper, H. L. Clever and F. H. Verhoek, THIS JOURNAL, **58**, 90 (1954).

(2) W. Thomas, *J. Chem. Soc.*, **123**, 618 (1923).

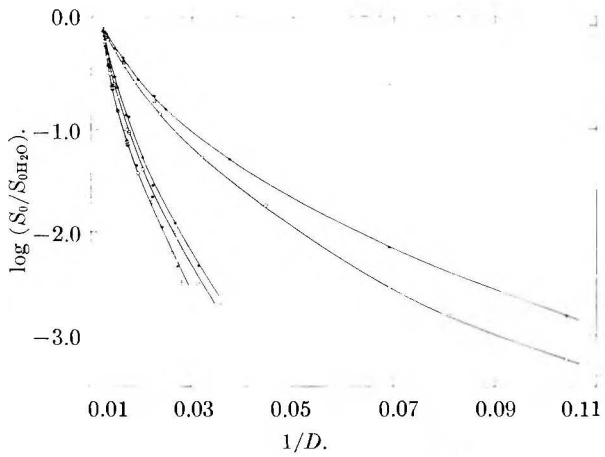

Fig. 1.—Solubility of dinitrotetrammine-cobalt(III) iodates in mixed solvents at 15°: curves 1, dioxane–water; curves 2, acetone–water; curves 3, ethanol–water; dots, *cis*-cation; circles, *trans*-cation.

Table I gives the solubilities in water. Three or four determinations were made, except for the iodates at 25°, and the average deviations are given.

Solubilities for one of the temperatures in the solvent mixtures are shown in Figs. 1 and 2 as plots[3] of the logarithm of the ratio of the solubility at zero ionic strength in the mixed solvent to the solubility at zero ionic strength in water as a function of the reciprocal of the dielectric constant.[4] The corrections to zero ionic strength were made using the Debye–Hückel limiting law throughout the whole dielectric constant range. As an approximate check on the applicability of the limiting law to these salts in these solvents in the region of higher dielectric constant, solubilities, for both iodates at 15° and both *dl*-dinitroöxalatodiammines at 25°, were determined in the presence of added potassium chloride in concentrations between 0.002 and 0.050 mole/l., in water and solvent mixtures for each solvent and salt, ranging down to a dielectric constant

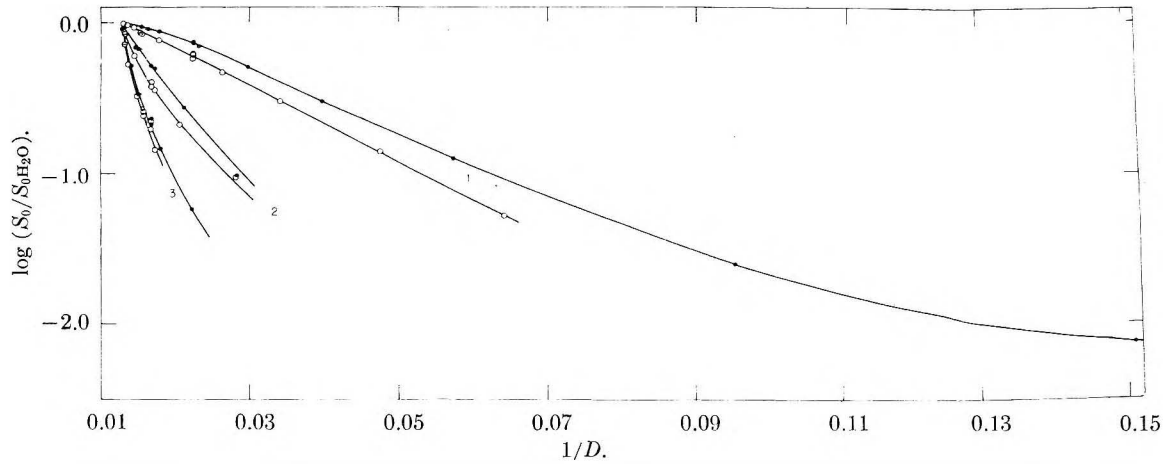

Fig. 2.—Solubility of dinitrotetrammine-cobalt(III) dinitroöxalatodiammine cobaltates(III) in mixed solvents at 25°: curves 1, dioxane–water; curves 2, acetone–water; curves 3, ethanol–water; dots, *cis*; circles, *trans*.

stant solubility was reached. Analysis gave the following results

	Found, % Co	Found, % NH_3	Theory, % Co	Theory, % NH_3
trans-Dinitrotetrammine-cobalt(III) iodate	14.84 ± 0.14	17.40	14.96	17.29
cis-Dinitrotetrammine-cobalt(III) iodate	15.16 ± 0.10	17.42		
trans-Dinitrotetrammine-cobalt(III) *dl*-dinitroöxalatodiammine cobaltate	24.51 ± 0.05		23.95	
cis-Dinitrotetrammine-cobalt(III) *dl*-dinitroöxalatodiammine cobaltate	24.18 ± 0 01			

The experimental procedure and analytical methods were similar to those previously described.[1b] Measurements were made at 15 and 25°. Careful experiments were made to ensure that equilibrium was established during the time the solid and solution were in contact, and in representative cases equilibrium was approached from "oversaturation"—by cooling to the equilibrium temperature a solution prepared at a higher temperature.

of 44. Plots of the negative logarithm of the solubility against the square root of the ionic strength gave straight lines and the extrapolated values at zero ionic strength are included on the figures. The slopes of these lines showed no astonishing deviations from the theoretical slope, though the slope was greater than the theoretical for all three measurements on the *cis* salts in ethanol-water.

The available theory[5] predicts that the curves in the figures should be straight lines. Only the *trans-dl*-dinitroöxalatodiammine cobaltate in dioxane–water mixtures at 25° approximates a straight line, and there is some indication that this is actually concave downward, as for the *cis*-cobaltate. At 15° the *trans*-cobaltate in dioxane–water shows a curvature like that of the other salts, but the "hump" for the *cis*-cobaltate persists at the

(3) The original data have been deposited as Document No. 5560 with the ADI Auxiliary Publications Project, Photoduplication Service, Library of Congress, Washington, D.C., U.S.A. A copy may be secured by citing the document number and by remitting $1.25 for photoprints, or $1.25 for 35 mm. microfilm, in advance by check or money order, payable to Chief, Photoduplication Service, Library of Congress.

(4) G. Akerlof, *J. Am. Chem. Soc.*, **54**, 4125 (1932); G. Akerlof and O. A. Short, *ibid.*, **58**, 1241 (1936); F. E. Critchfield, J. A. Gibson and J. L. Hall, *ibid.*, **75**, 1991 (1953).

(5) M. Born, *Z. Physik*, **1**, 45 (1920).

TABLE I

SOLUBILITIES OF *cis*- AND *trans*-DINITROTETRAMMINE-COBALT(III) IODATES AND *dl*-DINITROÖXALATODIAMMINE COBALTATES IN WATER AT 15 AND 25°

Iodate (mole/l. × 10^2)				*dl*-Dinitroöxalatodiammine cobaltate (mole/l. × 10^3)			
cis		*trans*		*cis*		*trans*	
15°	25°	15°	25°	15°	25°	15°	25°
3.99	5.97	2.02	2.86	1.25	2.12	0.346	0.553
±0.010		±0.003		±0.003	±0.000	±0.0017	±0.0035

TABLE II

HEAT, FREE ENERGY AND ENTROPY OF SOLUTION FOR *cis*- AND *trans*-DINITROTETRAMMINE-COBALT(III) IODATES IN SOLVENT MIXTURES WITH WATER

Wt. %	Dioxane						Ethanol						Acetone					
	cis			*trans*			*cis*			*trans*			*cis*			*trans*		
	ΔH^0	ΔF^0	ΔS^0	ΔH^0	ΔF^0	ΔS^0	ΔH^0	ΔF^0	ΔS^0	ΔH^0	ΔF^0	ΔS^0	ΔH^0	ΔF^0	ΔS^0	ΔH^0	ΔF^0	ΔS^0
0	11.1	3.7	25	10.7	4.5	21	11.1	3.7	25	10.7	4.5	21	11.1	3.7	25	10.7	4.5	21
10	11.4	3.8	26	9.9	4.9	17	16.1	4.4	39	10.9	5.3	19	13.5	4.2	31	11.4	5.1	21
20	10.8	4.5	21	9.4	5.4	14	15.7	5.2	35	15.4	6.0	32	14.2	4.8	32	13.4	5.7	26
30	10.8	5.0	19	10.2	5.9	14	17.8	5.9	40	14.3	6.7	26	15.0	5.3	32	14.3	6.3	27
40	10.0	5.5	15	9.5	6.6	10	19.9	6.6	45	16.7	7.4	31	14.1	6.0	27	12.7	7.2	18
50	9.0	6.3	9	7.7	7.4	1	15.1	7.3	26	18.5	8.2	35	13.8	6.8	23	12.0	7.9	14
60	4.7	7.4	−9	6.8	8.5	−6	14.9	8.1	23	17.2	9.0	28	..	..	..	..	..	..

TABLE III

HEAT, FREE ENERGY AND ENTROPY OF SOLUTION FOR *cis*- AND *trans*-DINITROTETRAMMINE-COBALT(III) *dl*-DINITROÖXALATODIAMMINE-COBALTATES IN SOLVENT MIXTURES WITH WATER

Wt. %	Dioxane			Ethanol			Acetone		
	ΔH^0	ΔF^0	ΔS^0	ΔH^0	ΔF^0	ΔS^0	ΔH^0	ΔF^0	ΔS^0
				cis					
0	17.6	7.4	34	17.6	7.4	34	17.6	7.4	34
10	16.7	7.4	31	21.3	8.0	45	19.2	7.6	39
20	15.7	7.5	28	20.1	8.6	39	18.9	7.8	37
30	14.3	7.6	23	21.9	9.2	43	16.1	8.1	27
40	12.8	7.8	17	..	..	..	15.4	8.4	23
50	9.9	8.1	6	..	..	..	14.0	8.8	17
60	8.3	8.7	−1	..	..	..	13.4	9.4	13
70	8.4	9.7	−5	..	..	..	11.9	10.1	6
				trans					
0	15.9	8.9	23	15.9	8.9	23	15.9	8.9	23
10	16.7	9.0	26	21.3	9.7	39	17.9	9.3	29
20	17.1	9.2	27	..	..	..	20.0	9.7	35
30	16.7	9.3	25	..	..	..	22.1	10.0	41

lower temperature. In every case the solubility as a function of $1/D$ changes least in dioxane–water and most in ethanol–water. This is the same order as found previously for the sulfates of these cations.[6] For all except the iodates in ethanol–water the solubility of the *cis*-salt changes less with $1/D$ than that of the corresponding *trans*-salt. On the basis of the Born equation this would be interpreted as a larger effective radius for the former. The radii are evidently not constant, however, and, except for dioxane–water mixtures, have unreasonably small values less than one ångström unit. The data do not distinguish different curves for the *cis*- and *trans*-iodates in ethanol–water mixtures at either temperature, and only a single curve has been drawn in Fig. 1.

If plots are made of log (solubility) against log (dielectric constant), only the curves for the iodates in dioxane–water approach the predicted slope[7] 3. Curves in the other solvents show greater slopes and those for the *dl*-dinitroöxalatodiammine cobaltates are not linear in dioxane–water and acetone–water mixtures.

Using the data at the two temperatures, values of the solubility at zero ionic strength were interpolated for even 10 wt. % intervals of organic solvent, and the heat, free energy and entropy of solution calculated. The results are recorded in Tables II and III. ΔH^0 and ΔS^0 are positive, and for these salts as for the sulfates,[1b,6] ΔS^0 is smaller for the *trans*- than for the *cis*-cation, while ΔH^0 is about the same for both. The usual tendency is for both ΔH^0 and ΔS^0 to increase with addition of the organic component, with some indication of a maximum in both functions. The behavior in dioxane–water is exceptional, since here ΔH^0 and ΔS^0 decrease with decreasing dielectric constant; this behavior is opposite also to that of the sulfates in dioxane–water mixtures.[1b]

It is confirmed by calculation[8] that the water concentration in a dioxane–water mixture is greater in the neighborhood of an ion than in the bulk of the solution. The ion thus exists in a

(6) H. L. Clever and F. H. Verhoek, THIS JOURNAL, **62**, 358 (1958).
(7) J. E. Ricci and T. W. Davis, *J. Am. Chem. Soc.*, **62**, 407 (1940).
(8) J. E. Ricci and G. J. Nesse, *ibid.*, **64**, 2305 (1942).

solvent of higher dielectric constant than corresponds to the measured value for the solvent mixture, and the points on curves such as those shown in the figures are to the right of their "proper" place. Calculations similar to those of Ricci and Nesse show[9] that the "sorting" effect is much less for ethanol–water, and the points for this solvent mixture are closer to their "proper" place. If solvation parallels the solvent sorting effect, then solvation energies would contribute more to the solution process in dioxane–water mixtures, and the heat of solution would decrease. Such a decrease is observed for the 1–1 electrolytes in this solvent pair.

(9) R. M. Hall, Ph.D. Dissertation, The Ohio State University, 1956.

The increase in heat of solution in the other solvents requires a heat-absorbing process to overcome the heat of solvation. This could be found in breakdown of aggregates in the solvent by the introduction of ions, as suggested by Frank and Evans.[10] If the heat required for this "melting" process is greater than the energy gained in solvation, a net increase in heat of solution results; if on further addition of organic component the relative magnitudes of the two energies change, a maximum in ΔH^0 can be explained. This interpretation still leaves the behavior of the sulfates in dioxane–water anomalous as compared to the 1–1 electrolytes in this solvent pair.

(10) H. S. Frank and M. W. Evans, *J. Chem. Phys.*, **13**, 507 (1945).

KINETICS OF THE OXIDATION AND NITRIDATION OF SILICON AT HIGH TEMPERATURES

BY J. W. EVANS[1] AND S. K. CHATTERJI

Department of Metallurgy, University of Manchester, Manchester, England

Received April 8, 1958

The kinetic behavior of silicon in oxygen, carbon dioxide, nitrogen and argon containing 0.2% by volume of nitrogen has been determined at 1200–1400° by means of a thermobalance. In oxygen and CO_2, the rate laws were shown to be parabolic. Erratic behavior was observed in pure nitrogen with the formation of a volatile silicon nitride but at a low partial pressure of nitrogen in argon, volatilization was absent and a logarithmic rate law was shown to hold.

Introduction

It is well known that the incorporation of small amounts of silicon into other metals can lead to a substantial improvement in the oxidation resistance of the alloy. Unfortunately silicon has a marked embrittling effect on other metals and is itself a hard and brittle material. However, its high intrinsic oxidation resistance in air has led recently to its suggested use in "cermets" (metal-refractories) in which pure silicon is the metallic constituent.

Comparatively little fundamental work has been carried out on the rate of reaction of silicon with oxygen and virtually none on the reaction with nitrogen. The latter reaction is of further importance since the product of the reaction, principally silicon nitride, Si_3N_4, is a promising high temperature special refractory.

Geil and McAdams[2] using an optical interferometric method found that silicon oxidized according to a parabolic rate law in the temperature range 500–950°. Brodsky and Cubicciotti,[3] using a volumetric absorption apparatus, measured the rate between 950–1160° and deduced a logarithmic rate law between these temperatures. However, their data at the extreme ends of this temperature range fitted a parabolic rate law equally well. Law[4] investigated the oxidation of silicon between 1000–1300°K. at pressures of oxygen in the region 10^{-2}–10^{-3} mm. His results demonstrated a parabolic rate law which was markedly pressure dependent.

No accurate work on the nitridation of silicon is known to the authors but it has been reported[5] that only silicon particles less than 0.1 mm. diameter can be nitrided completely in a reasonable time. Other workers[6] state that silicon powder reacts rapidly with nitrogen at 1350–1400° forming mainly Si_3N_4.

For the production of silicon nitride commercially, iron and alkaline earth fluorides are said to be valuable catalysts in promoting the silicon–nitrogen reaction. Nitrides other than Si_3N_4 are said to exist but data for these are lacking.

This present work describes the kinetic behavior of silicon in oxygen and CO_2 and in nitrogen and argon containing a trace of nitrogen at temperatures between about 1200–1400°.

Experimental

(i) **Materials.**—Silicon of purity 99.95% was obtained from the Morgan Crucible Co. The silicon was melted *in vacuo* in a thoria-lined alumina crucible, cast and roughly machined to size. Final polishing was carried out with metallurgical emery paper, ultimately with 4-0 grade to give a mirror finish. The final specimens were small rectangular blocks weighing approximately 1–2 g.

Oxygen, oxygen-free argon and oxygen-free nitrogen were obtained in cylinders from the British Oxygen Co. Pure carbon dioxide was obtained from the Carbon Dioxide Co.

Apparatus.—The reaction of silicon with the various gases was determined by means of a thermobalance. A platinum-wound resistance furnace was used with an impervious mullite reaction tube mounted vertically. Temperature control was maintained to ±5° over a three inch central zone by means of a mechanical controller operated by a Pt/Rh thermocouple. Connections to the mullite tube were made in

(1) Culcheth Laboratories, U.K.A.E.A., Warrington, England.

(2) G. W. Geil and D. J. McAdams, *J. Research Natl. Bur. Standards*, **28**, 593 (1942).

(3) M. B. Brodsky and D. Cubicciotti, *J. Am. Chem. Soc.*, **73**, 3497 (1951).

(4) J. T. Law, THIS JOURNAL, **61**, 1200 (1957).

(5) J. F. Collins and R. W. Gerby, *J. Metals*, **7**, 612 (1955).

(6) A. G. Nasini and A. Cavallini, *IX Cong. Intern. Quim. Pura Aplicada*, **3**, 280 (1934).

Pyrex glass with Araldite cement and these joints were water cooled.

The balance consisted simply of a precision glass spring (obtained from Still and Cameron, London) suspended from the inside of a ground glass joint above the furnace. The sensitivity of the spring was approximately 43 mg./cm. extension under a load of one g.; Hooke's law was obeyed over extensions of several cm. The entire spring was virtually maintained at room temperature and the specimens were suspended in the hot zone of the furnace by a fine silica rod; a small silica stirrup was used to support the silicon sample. The weight changes were obtained by measuring the changes in spring extension with a travelling microscope focused on a fine datum mark on the spring. Weight changes of better than 0.1 mg. could be observed without difficulty.

The usual arrangements were made for evacuating the furnace tube and for flowing dry gases through the system.

The procedure for making a measurement was as follows: The furnace was brought to temperature and the ground glass joint removed. The spring with its silica rod and silicon sample suspended from it was carefully attached to the hook. Whilst a rapid stream of argon was flowing through the furnace tube, the joint and spring assembly were lowered into position. This could be done in a few seconds and the furnace was then evacuated.

The travelling microscope was focused on the mark on the spring to obtain the initial reading. The appropriate gas was admitted and the weight gains followed by adjusting the microscope at suitable intervals to coincide with the datum mark; initially, readings were taken every minute and for longer intervals after the first hour. Many runs were extended over 24 hours.

Results

(i) **Oxygen.**—The rate of reaction of silicon with pure dry oxygen at one atmosphere and temperatures of 1201, 1255, 1303, 1360° was determined over periods of 24 hours; the results fit a parabolic law, *viz.*, $(\Delta m)^2 = kt+c$ satisfactorily as shown in Fig. 1. At all temperatures the initial rate of reaction was somewhat higher than the over-all parabolic rate curve which explains why the linear plots do not pass through the origin. The reaction product was invariably transparent cristobalite as shown by X-ray analysis. The stable silica phase in this region is tridymite but this particular variety appears to be difficult to form. It seems likely that part of the silica may be vitreous but this is not detected easily.

The activation energy for this process is calculated from the Arrhenius equation, *viz.*

$$\frac{\mathrm{d} \ln k}{\mathrm{d}T} = \frac{\Delta E^*}{RT^2}$$

where k is the parabolic rate constant and ΔE^* the activation energy.

The graph of log k against $1/T$ is shown in line a of Fig. 2. From the slope of this line the activation energy is 43 kcal.

(ii) **Carbon Dioxide.**—The reaction with dry carbon dioxide at one atmosphere was determined at 1212, 1301 and 1372°; as with oxygen the results fit a parabolic law. This graph is shown in Fig. 3. The initial rate is again faster than the over-all rate. The reaction product was translucent and rather deeply blue tinted but appeared by X-ray to be principally silica, although some carbon or silicon carbide may have been present.

From the graph of log k against $1/T$ for this reaction (line b in Fig. 2), the activation energy is 32 kcal.

(iii) **Nitrogen.**—Several runs were made in pure nitrogen at one atmosphere between 1200 and 1410°. The weight gains were erratic (Fig. 4)

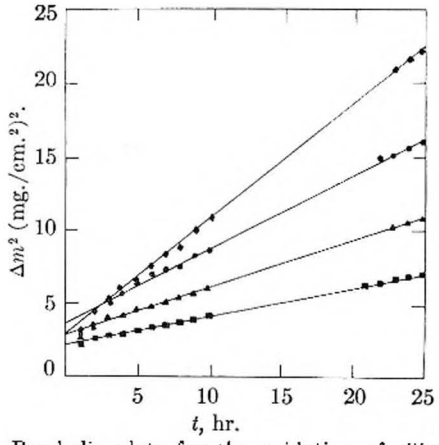

Fig. 1.—Parabolic plots for the oxidation of silicon: ◆, 1360°; ●, 1303°; ▲, 1255°; ■, 1201°.

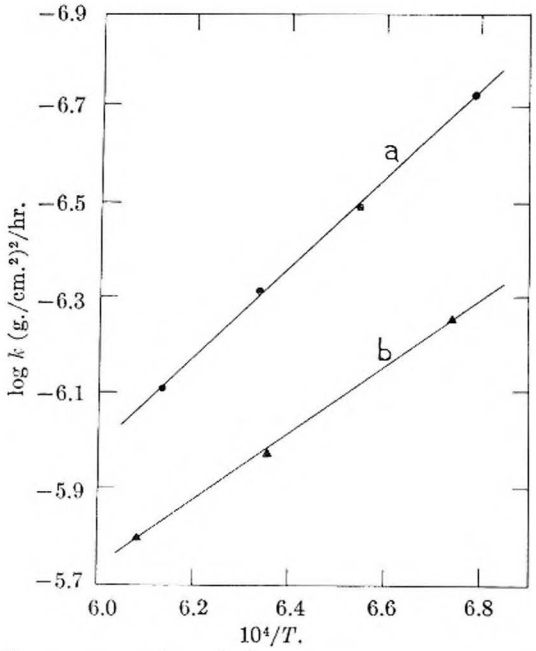

Fig. 2.—Logarithm of the rate *versus* inverse absolute temperature plots for the reaction of silicon with: ●, oxygen; ▲, carbon dioxide.

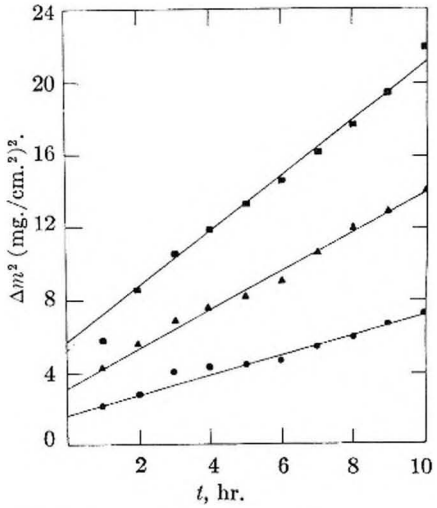

Fig. 3.—Parabolic plots for the reaction of silicon with carbon dioxide: ■, 1372°; ▲, 1301°; ●, 1212°.

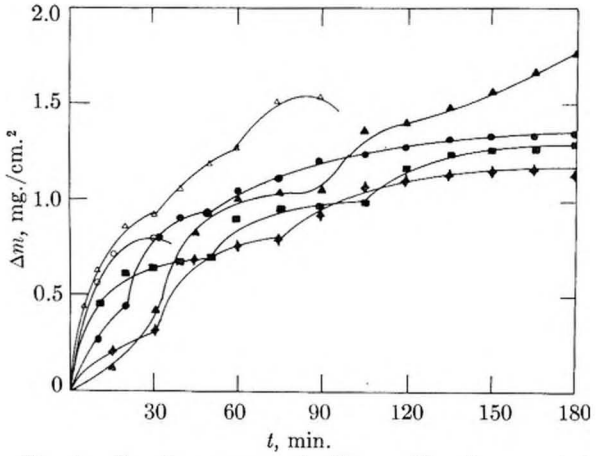

Fig. 4.—Reaction curves of silicon with nitrogen at 1 atm. pressure: ○, 1410°; ▲, 1354°; ■, 1251°, △, 1402°, ◐, 1308°, ◆, 1200°.

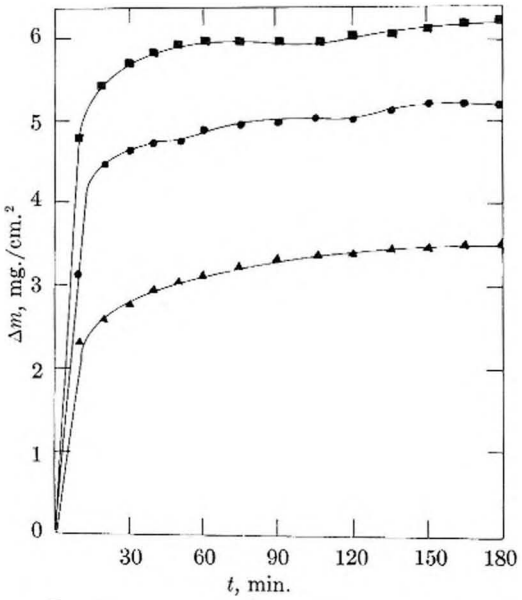

Fig. 5.—Reaction curves of silicon with argon gas containing nitrogen: ■, 1372°; ●, 1308°; ▲, 1208°.

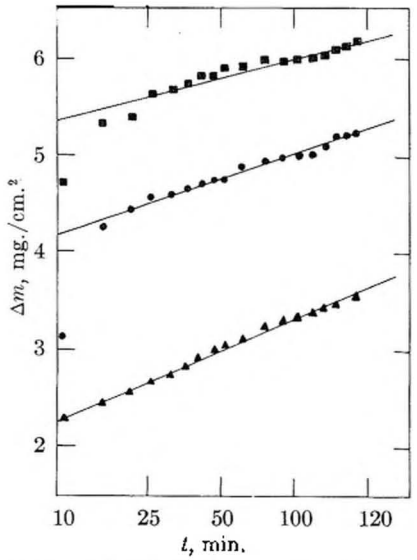

Fig. 6.—Δm *versus* log $(1 + t)$ curves for silicon with argon gas containing nitrogen: ■, 1372°; ●, 1308°; ▲, 1208°.

and at the higher temperatures the silicon appeared to gain and lose weight successively.

The product was the fibrous white nitride Si_3N_4 (as determined by X-ray); there was evidence of some volatilization since fine whiskers were found on the supporting silica rod, about a centimeter away from the specimen. The temperature coefficient of the nitridation could not, of course, be determined but an inspection of the results as plotted graphically suggests that the effect of temperature on the rate is relatively small.

(iv) **Argon Containing 0.2% Nitrogen.**—The effect of nitriding at a low partial pressure of nitrogen was studied by using argon which normally contains about 0.2% by volume of nitrogen. At the three temperatures studied, *viz.*, 1208, 1308 and 1372°, the reaction proceeded quite smoothly and regular weight gains were found (Fig. 5). The results also have been plotted according to the logarithmic rate law, *viz.*

$$\Delta m = k \log (1 + t)$$

and these are shown in Fig. 6. The reaction product was a dense white adherent scale of Si_3N_4. There was no evidence of the volatilization which had occurred in pure nitrogen.

The temperature coefficient, as with nitrogen, appears to be small.

Discussion

(i) **Oxidation in O_2 and CO_2.**—Apart from the faster initial rate due to atomic surface roughness the parabolic oxidation behavior in pure oxygen suggests that the oxide film grows by the diffusion of some species through it, the most probable being the inward diffusion of oxygen which could be molecular, atomic or ionic. The diffusion of molecular oxygen through the lattice is unlikely, whilst diffusion through "micro-cracks" would tend to lead to a logarithmic rate law rather than a parabolic one. The electrical properties of silica are ambiguous; recently Cohen[7] has determined the electrical conductivity of fused quartz at these high temperatures. One sample showed electronic behavior with values of the order of 10^{-4} mho/cm. for the conductivity in the temperature range 1000–1400° and, moreover, relatively insensitive to temperature. Another sample showed anomalous electrical behavior with essentially ionic conduction. Cohen attributed these marked differences to the presence of traces of metallic oxide impurities. Since our silicon samples contained trace impurities film growth by diffusion of oxygen ions is clearly possible. Equally, of course, a slight solubility of dissolved oxygen (in the silica lattice) could account for film growth by diffusion of neutral oxygen atoms inwards; this process would probably be pressure dependent.

The results generally confirm the observed parabolic behavior of Geil and McAdams[2] and Law[4] working under different conditions of temperature and pressure. The results of Cubicciotti and Brodsky[3] indicated that a parabolic rate law applied at the two extreme temperatures of 950 and 1160° but not in between; from these extreme values an apparent activation energy of 45 kcal.

(7) J. Cohen, *J. Appl. Phys.*, **28**, 795 (1957).

is obtained which is in reasonable agreement with the presently determined value of 43 kcal.

Law obtained an activation energy of 36 kcal. for the growth of silica formed at 1000–1300°K. with low gas pressures. His films were in the so called "thin film" region of 100–1000 Å. where the mechanism is almost certainly different from the present work on relatively thick films of the order of 100,000 Å.

The results for silicon in CO_2 show that whilst the rates are similar to those for oxygen, the absolute values are significantly faster with a lower activation energy of 32 kcal. Whilst the principal product of the reaction is silica given by the equation $Si + 2CO_2 = SiO_2 + 2CO$, small amounts of free carbon or silicon carbide may be formed by such reactions as $Si + CO_2 = SiO_2 + C$, and $2Si + CO_2 = SiO_2 + SiC$.

Presumably traces of these other products could be incorporated in the silica lattice and thus modify the diffusion behavior.

(ii) **Nitridation in N_2 and Argon with a Trace of N_2.**—The growth of nitride films on silicon is by a mechanism distinctly different from that of silica films. In pure nitrogen, the rate law could not be determined since volatilization of nitride was occurring simultaneously. The smooth nitriding reaction in argon with a trace of nitrogen was not accompanied by volatilization. Since the only important difference is that of nitrogen partial pressure, it is possible that traces of another more volatile nitride than Si_3N_4 was being formed in pure nitrogen, *e.g.*, Si_2N_3. The results would then imply that the dissociation pressure of this higher nitride was greater than about one mm. but less than 760 mm. in this temperature range for a hypothetical reaction

$$6Si_2N_3\,(\text{volatile}) = 4Si_3N_4 + N_2$$

This explanation is very tentative since no other nitride than Si_3N_4 was detected and the properties of other nitrides are virtually unknown. Si_3N_4 is, of course, appreciably volatile itself but only at substantially higher temperatures.

The logarithmic growth of the nitride film in argon containing a trace of nitrogen can be interpreted by assuming that nitrogen diffuses through minute cracks or faults in the growing film. As the film thickens the path for the nitrogen gas becomes increasingly tortuous and eventually becomes almost completely blocked. It is assumed that no ionic or atomic diffusion occurs within the lattice proper of the nitride. There is some support for this in that the temperature coefficient of the reaction rate is small or zero. It seems reasonable to suppose at these temperatures that the surface reaction between silicon and nitrogen is extremely rapid and that the over-all rate of reaction would be governed by the supply of nitrogen. The very low temperature coefficient would suggest that gaseous diffusion through microcracks in the nitride was the controlling step, rather than a diffusion process in the lattice itself.

The logarithmic growth clearly shows why complete nitriding of silicon powder would depend critically on the particle size, since once an initial film of nitride had formed rapidly, subsequent growth would be extremely slow. Collins and Gerby[5] state that in the production of commercial silicon nitride only particles less than 0.1 mm. in diameter can be nitrided completely in a reasonable time. A simple calculation from the present results confirms this value. A variety of catalysts have been described for this reaction, *e.g.*, iron. A simple explanation is that during nitriding the iron in the ferrosilicon is unaffected but becomes incorporated as an intimate mixture in the nitride film; differences in thermal expansion alone would give a less perfect film and hence facilitate nitrogen permeation.

Conclusions

At temperatures between about 1200–1400° silicon oxidizes in oxygen and CO_2 at one atmosphere according to a parabolic rate law.

In pure nitrogen, at similar temperatures, the nitridation is irregular and volatilization of, presumably, a silicon nitride occurs.

In nitrogen at a partial pressure of about 1.5 mm. the reaction follows a well-defined logarithmic rate law.

Acknowledgments.—Thanks are due to the Morgan Crucible Co. Ltd., London, for financial support of this work and for X-ray determinations. The authors are grateful to Dr. O. Kubaschewski for useful discussion.

PRECIPITATION KINETICS OF IONIC SALTS FROM SOLUTION

BY R. H. DOREMUS

General Electric Research Laboratory, Schenectady, N. Y.

Received April 4, 1958

Mechanisms for ionic crystal growth from solution are discussed and compared to experimental measurements of salt precipitation rates. In the systems considered the crystal growth rate is shown to be controlled by an interface process, rather than by bulk diffusion of solute. An adsorbed surface layer on the growing salt particles is proposed as the first stage in crystal growth from solution, and this proposal is shown to be consistent with the experimental results. It is concluded that in the systems considered nucleation occurs rapidly and the number of salt particles is constant during the measured growth period, and that factors as well as solute supersaturation influence the nucleation process.

Introduction

The growth of salt crystals from solution is a fascinating process. To learn something of its nature one can use a variety of techniques. The rate of crystal growth can be measured by following the disappearance of salt from a supersaturated solution, and some information about the crystal growth process can be deduced from such kinetic studies. In this paper mechanisms for the precipitation of ionic salts from solution will be discussed and compared to certain existing experimental measurements on crystal-growth rates.

The crystallization of salts from solution will be treated as a nucleation and growth process. Nucleation of discrete particles throughout the solution occurs when the solute supersaturation exceeds a critical value, and these nuclei then grow by transport of ions through the solution to the particles. In this paper isothermal growth of relatively insoluble salts from dilute aqueous solutions will be considered, and nucleation on the vessel walls will be neglected. It will be assumed that the particles are spherical and that the nuclei form in a very short initial period and consume a negligible amount of solute. After this short period the number of precipitate particles remains constant, so the depletion of solute that is measured experimentally occurs entirely by growth of the particles. These assumptions will be justified by subsequent consideration of experimental data.

Diffusion or Interface Control.—The growth of salt particles may be controlled by diffusion of ions through the solution, by a process at the particle–solution interface, or both of these mechanisms may be important. Turnbull[1] and Humphreys-Owen[2] derived the growth equation for a single particle growing in a solution of infinite extent when both diffusion and an interface reaction are important, and Frisch and Collins treated this case when a number of particles compete for solute.[3] For the present discussion the result of the latter authors for particles of negligible initial radius can be expressed in the form

$$\frac{(C_m - C_0)t}{R_f\rho} = \left(\frac{1}{b} + \frac{R_f}{D}\right)\frac{1}{6}\ln\frac{W^{1/3} + W^{1/3} + 1}{(1 - W^{1/3})^2} + \left(\frac{1}{b} - \frac{R_f}{D}\right)\frac{1}{\sqrt{3}}\tan^{-1}\frac{\sqrt{3}W^{1/3}}{2 + W^{1/3}} \quad (1)$$

In this expression C_m and C_0 are the initial and equilibrium molar solute concentrations, respectively, ρ is the salt density in concentration units, t is the time after nucleation, D is the solute diffusion coefficient, b is an interface growth coefficient, W is the fraction of total precipitation and R_f is the particle radius when precipitation is complete ($W = 1$). In terms of the average radius R of N particles per unit volume, W is given by

$$W = \frac{4\pi NR^3\rho}{3(C_m - C_0)} \quad (2)$$

In the derivation of eq. 1 the solute flux J per unit area of particle surface associated with the interface process was assumed to be equal to $b(C_r - C_0)$, where C_r is the molar solute concentration in the solution at the particle surface. In general J will be a more complicated function of $(C_r - C_0)$, but for this discussion of diffusion or interface control the simple form will suffice.

From eq. 1 the growth is controlled by an interface reaction when $D/R_f >> b$; in this case $C_r = (C_m - C_0)(1 - W) + C_0$, which is the average solute concentration throughout the solution. If $D/R_f << b$ the growth is diffusion-controlled except for the very earliest stages, and eq. 1 is the same as the result of Wert and Zener for the diffusion-controlled growth of spherical particles.[4–6]

The discussion of the experimental results will now be anticipated to determine whether a generalization regarding growth mechanism can be made. In aqueous solution at room temperature the diffusion coefficient for salt ions is usually about 10^{-5} cm.^{2}/sec. The experimental results considered below gave R_f values of about 10^{-5} cm. and b values from 0.002 to 0.03 cm./sec. Therefore $D/R_f >> b$, and one can conclude that the rate of crystallization for these results is entirely controlled by an interface reaction. Furthermore the solution is often stirred during crystal growth experiments, so in this case the transport of ions in the solution is even more rapid than for an unstirred solution. Thus for these conditions the solute concentration in the solution at the particle surface is always $(C_m - C_0)(1 - W) + C_0$, and in the following discussion we need to treat only the interface reaction to describe fully the crystallization kinetics.

Large individual crystals growing from concentrated solution have been studied under the microscope; the solute concentration around the crystal was determined from interference fringes due to refractive index differences.[7–9] In these experi-

(1) D. Turnbull, *Acta Met.*, **1**, 764 (1953).

(2) S. P. F. Humphreys-Owen, *Proc. Roy. Soc. (London)*, **A197**, 218 (1949).

(3) H. L. Frisch and F. C. Collins, *J. Chem. Phys.*, **21**, 2158 (1953).

(4) C. Zener, *J. Appl. Phys.*, **20**, 950 (1949).

(5) C. Wert and C. Zener, *ibid.*, **21**, 5 (1950).

(6) H. Markowitz, *ibid.*, **21**, 1198 (1950).

(7) W. F. Berg, *Proc. Roy. Soc. (London)*, **A164**, 79 (1938).

(8) C. W. Bunn, *Disc. Faraday Soc.*, **5**, 132 (1949).

ments the crystals were so large that the term bR was appreciable. Thus solute diffusion in the solution was important in the crystal-growth process, and the solute concentration at the particle surface was less than that at a distance from the particle. Indeed the two latter results were found in these studies and the authors correctly concluded that both diffusion in the solution and an interface reaction were contributing to the crystal-growth kinetics. In this present study these experiments will not be considered further, and attention will be focused on the growth of smaller crystals for which the interface process is controlling.

Equation 1 has been compared to experimental results on the growth of barium sulfate from solution by Collins and Leineweber[10]; their factor γ is equal to D/b in the present notation. In comparing the equation to their results, Collins and Leineweber assumed that

$$b = \frac{1}{6}\alpha\nu\bar{s} \qquad (3)$$

where α is an adsorption probability, ν is the diffusional displacement frequency and $\bar{s}$ is the mean diffusional displacement. Then

$$\frac{D}{b} = \frac{1}{6}\nu\bar{s}^2/\frac{1}{6}\alpha\nu\bar{s} \sim \frac{\bar{s}}{\alpha} \qquad (4)$$

This result implies that D enters into eq. 1 even for an interface-controlled process, since s is a constant. Thus the difference between a diffusion or interface-controlled process will appear only in the value of α($\alpha = 1$ and $\alpha < 1$, respectively). It will be shown below that the interface process is quite complex, so that eq. 3 describes b artificially, with all its functional variation coming in α. There is no reason to associate the frequency and displacement involved in bulk diffusion with the interface process; therefore it is misleading to describe b by eq. 3, and the form of eq. 1 is preferable to show the separation of the diffusion and interface processes.

Derivation of Growth Equations

The functional dependence between J and $C_r - C_0$ will now be derived from specific models for the interface-controlled growth process. These models are presented as plausible rationalizations of the kinetics of precipitation found experimentally, and certain aspects of them will doubtless need modification as more experimental data become available.

We will assume that the first step in conveying an ion from solution into a growing crystal lattice is adsorption onto the crystal surface. An adsorbed surface layer has often been invoked to explain crystal-growth results and many experiments have shown that such a layer is credible.[11-14] When an ion is adsorbed into this layer from aqueous solution it may be partially or completely dehydrated. For a one–one electrolyte solution containing only the precipitating ions the concentrations of anions and cations in the layer should be virtually equal, although the concentrations can differ very slightly due to preferential adsorption. We will assume that the number of ions available for reaction in the adsorbed layer is proportional to the number striking the surface less the number leaving it. Then the effective solute concentration in the surface layer is $k_a(C_r - C_0)$ for both ions, where k_a is a surface adsorption coefficient which is independent of ionic concentration. If the electrolyte is two–one, such as A_2B, the surface layer concentration of A is $2k_a(C_r - C_0)$ and that of B is $k_a(C_r - C_0)$.

There is general agreement that crystal growth proceeds by incorporation of molecules at kinks in a growth step on the crystal surface.[15] In the growth of ionic salts from solution the ions of opposite charge must combine stoichiometrically at some stage in the process to maintain electrical neutrality in the crystal lattice. Two ways this ion grouping can occur are: (A) on the particle surface to form salt "molecules" which then diffuse to growth steps; (B) by alternate incorporation of oppositely charged ions directly from the adsorbed layer at a kink in a growth step. Therefore two possible models for the interface process consist of the following stages. Model A: (1) Adsorption of individual ions from solution into a surface layer; (2) combination of these ions into a single uncharged salt "molecule" on the crystal surface; (3) incorporation of this molecule into the crystal lattice. Model B: (1) adsorption into a surface layer as for A; (2) alternate incorporation of oppositely charged ions into the crystal lattice. A discussion and derivation of growth equations for these two models follows. At first a solution with only the precipitating ions present, such as is formed by mixing equivalent amounts of barium hydroxide and sulfuric acid to produce a barium sulfate precipitate, will be considered, and then the case of non-stoichiometric ion concentrations will be treated.

Model A.—In this model the adsorbed ions combine in the surface layer to form neutral salt "molecules" that can fit into the crystal lattice. This step may involve further dehydration of the ions if they have retained any water of hydration in the surface layer. A variety of kinetic laws might apply for this model, depending upon the relative rates of the reaction to form molecules, the decomposition of the molecules back to ions, and the incorporation of the molecules into the crystal. In certain of the experiments to be discussed the flux J was found to be proportional to $(C_r - C_0)^3$ for one–one electrolytes and $(C_r - C_0)^4$ for two–one electrolytes. To explain these results it is necessary to postulate a rather unusual process. The only justification put forward for this postulation is that it is consistent with the experimental data.

When ions combine in the gas phase a third particle takes part in the reaction to stabilize the resulting molecule.[16] We will assume that an

(9) G. C. Kroeger and C. W. Miller, *J. Chem. Phys.*, **21**, 2018 (1953).

(10) F. C. Collins and J. P. Leineweber, THIS JOURNAL, **60**, 689 (1956).

(11) R. Marc, *Z. physik. Chem.*, **79**, 71 (1912).

(12) R. M. Barrer, "Diffusion in and through Solids," Cambridge Univ. Press 1941, pp. 337–381.

(13) C. W. Davies and A. L. Jones, *Trans. Faraday Soc.*, **51**, 812 (55).

(1914) G. W. Sears, *Acta Met.*, **3**, 361 (1955).

(15) W. K. Burton, N. Cabrera and F. C. Frank, *Phil. Trans. Roy. Soc.*, **243**, 299 (1951).

(16) E. A. Moelwyn-Hughes "Kinetics of Reactions in Solution," 2nd ed., Oxford Press, New York, N. Y., 1947, p. 19.

additional adsorbed ion also takes part in the surface combination process to form a salt molecule. Possibly this additional ion stabilizes the molecule by removing any excess water of hydration from the combining ions. Then the rate of formation of the surface molecules will be proportional to $k_a^3(C_r - C_0)^3$ for a one–one electrolyte and $k_a^4(C_r - C_0)^4$ for a two–one electrolyte. Furthermore we will assume that the rate of incorporation of surface molecules at the growth steps is a relatively rapid process, so the over-all flux of ions into the crystal is controlled by the rate at which surface molecules are formed. Then for one–one electrolytes

$$\frac{dC_r}{dt} = -NAk_m k_a^3(C_r - C_0)^3 \qquad (5)$$

in which N is the number of molecules per unit volume with average surface area A, and k_m is the rate coefficient for the combination process. Thus

$$J = -\frac{1}{NA}\frac{dC_r}{dt} = b(C_r - C_0)^3 \qquad (6)$$

where $b = k_m k_a^3$. For two–one electrolytes in a similar way

$$J = b(C_r - C_0)^4 \qquad (7)$$

where $b = 4k_m k_a^4$; in both these equations b is independent of ionic concentration.

Model B.—In this model the adsorbed ions collide directly with a kink in a growth step and are separately incorporated into the crystal lattice. Thus the rate of consumption of solute is proportional to the product of surface concentrations of the ions, or

$$\frac{dC_r}{dt} = -NAk_s k_a^2(C_r - C_0)^2$$

for a one–one electrolyte and

$$\frac{dC_r}{dt} = -4NAk_s k_a^3(C_r - C_0)^3$$

for a two–one electrolyte, where k_s is a rate coefficient which is constant with ionic concentration. This coefficient includes such factors as the frequency of collision of adsorbed ions with the kink and the probability of incorporation as a result of such a collision. When the equations for Model B are combined the results are

$$J = b(C_r - C_0)^2 \qquad (8)$$

for one–one electrolytes and

$$J = b(C_r - C_0)^3 \qquad (9)$$

for two–one electrolytes, with b equal to $k_s k_a^2$ and $4k_s k_a^3$, respectively.

For both models the differential equation of growth is

$$\frac{J}{\rho} = \frac{dR}{dt} = \frac{b(C_r - C_0)^m}{\rho} = b\frac{(C_m - C_0)^m(1 - W)^m}{\rho} \qquad (10)$$

where b and $(C_m - C_0)^m$ are time-independent and $m = 1, 2, 3$ or 4 depending upon which equation for J applies. The integrated result for $m = 1$ is eq. 1 above with $R_i/D = 0$, and for $m = 2$ a closed solution is possible. When $m = 3$ or 4 analytical integration of eq. 10 is difficult, but the result can be evaluated numerically. From eq. 10 one can see that in the initial stages of growth when W is small dR/dt is constant and W is proportional to t^3 for all values of m. An equation similar to eq. 10 with m equal to three or four has previously been compared to data on ionic crystal growth.[17,18]

In the above treatment the effective growth area was implicitly assumed to be proportional to the surface area of the growing particles. It is possible that after some stage of growth the effective growth area remains constant, rather than increasing with particle surface area. Then the particle surface area A must be replaced by an equivalent surface area A' which is constant with time. The growth equation can be expressed as

$$\frac{dW}{dt} = NA'b(C_m - C_0)^{m-1}(1 - W)^m \qquad (11)$$

which integrates to

$$\frac{1}{(1 - W)^{m-1}} - \frac{1}{(1 - W')^{m-1}} = (m - 1)NA'b(C_m - C_0)^{m-1}(t - t') \qquad (12)$$

where t' and W' are the time and fraction of reaction, respectively, when the effective growth area becomes constant.

Often in studies of ionic precipitation from solution seed crystals are added to a slightly supersaturated solution. In this case crystal growth takes place on the seed crystals and nucleation of salt particles is unnecessary. If the seed crystals are large enough their surface area will remain nearly constant throughout the deposition process, and eq. 11 will be valid with NA' the total surface area of the seed crystals per unit volume of solution. The integrated result is then

$$\frac{1}{(1 - W)^{m-1}} = (m - 1)NA'b(C_m - C_0)^{m-1}t \qquad (13)$$

Crystal growth experiments frequently involve mixing two soluble salts, such as barium nitrate and sodium sulfate, to give a precipitate. In this instance the above analysis is correct only if the initial concentrations of the precipitating ions are in the proper stoichiometric ratio, such as one-to-one for one–one electrolytes and two-to-one for two–one electrolytes. If the ratio is nonstoichiometric the analysis must be altered. In the following discussion we will assume that the nonprecipitating ions in solution do not form insoluble salts with the precipitating ions, so that the latter will be the only ions adsorbed in the surface layer. If the concentration ratio of precipitating ions in solution is not greatly different from the stoichiometric one the ratio of concentrations in the adsorbed layer will be stoichiometric. Thus for a one–one electrolyte one needs only to let C_m and C_r in the above analysis be the concentrations of the deficient ion in solution initially and at time t, respectively. This means that both ions are still effective in the growth process and that their concentrations in the adsorbed layer are equal because the particle remains essentially uncharged. The factor $C_r - C_0$ is also equal to the concentration of either ion yet to be precipitated before equilibrium is reached. The appropriate C_0 value is now the equilibrium concentration of deficient ion, which for a one–one electrolyte can be calculated from the relation

(17) R. A. Johnson and J. D. O'Rourke, *J. Am. Chem. Soc.*, **76**, 2124 (1954).

(18) A. E. Nielsen, *J. Colloid Sci.*, **10**, 576 (1955).

$$(C_e - C_d + C_0)C_0 = S$$

where C_e and C_d are the initial concentrations of excess and deficient ion, respectively, and S is the solubility product coefficient. For a two–one electrolyte the ionic ratio in the surface layer is the stoichiometric one, so again we need only substitute for C_m and C_r the appropriate molar salt concentrations corresponding to the deficient ion concentration in the solution. With these substitutions the above growth equations should apply to this case of non-stoichiometric concentration ratio.

If one ion is adsorbed more strongly to the precipitate particle than the other the particle retains an electrical charge and an electrical "double layer" is set up around the particle by the ions neutralizing this charge. This situation is familiar in Colloid Chemistry.[19] The particle charge tends to minimize selective adsorption, since the particle attracts the more weakly adsorbed ions of the opposite charge. Thus for ionic concentration ratios in solution equal or close to the stoichiometric one selective adsorption should be negligible, as assumed in the preceding paragraph. However if one precipitating ion is present in solution in great excess, it may be adsorbed to a much larger extent than the deficient ion, in spite of the resultant charge. In this case the crystal growth is controlled by the concentration of deficient ion only, since the surface concentration of the excess ion remains essentially constant. Then for both models the flux equations become $J = b(C_r - C_0)$ for one–one electrolytes, where C_r and C_0 are the concentration of deficient ion in solution and at equilibrium, respectively. For a two–one electrolyte A_2B, $J = b(C_r - C_0)$ if ion A is in large excess, and $J = b(C_r - C_0)^2$ if the ion B is in large excess. In all these equations b should be constant with time and with deficient ion concentration, but it may depend upon the initial concentration of excess ion in solution, so it cannot be compared directly with b values from the previous equations.

In all of the above discussion the reaction and adsorption coefficients were assumed to be invariant with concentration, although this is strictly true only if activities are used instead of concentrations. Some authors have calculated activities for interpretation of crystal-growth results from the Debye-Hückel equations, but these equations are valid only in dilute solutions, whereas the growth processes considered here all occur on the particle surface. A correct calculation of surface ionic activities is very difficult at present, because sufficient information about the state of ions adsorbed on a crystal surface is not available. Thus only concentrations will be used in the following comparisons of experimental results with the growth equations, and the assumption of concentration-independent coefficients will be justified from the comparisons.

Unfortunately we will be unable to calculate the growth coefficient b from most of the experimental results, since such a calculation requires knowledge of the number density of particles (or their final size). This can be seen from eq. 1; the experimental results give a W against t relation, and the required concentrations are known, but N and R_f are not, since few workers have measured either of these quantities independently. The change of N with initial supersaturation can be found by assuming that b is constant for a given system at one temperature, but its absolute value requires a separate measurement.

(19) E. J. W. Verwey and J. Th. G. Overbeek, "Theory of the Stability of Lyophobic Colloids," Elsevier, Amsterdam, 1948.

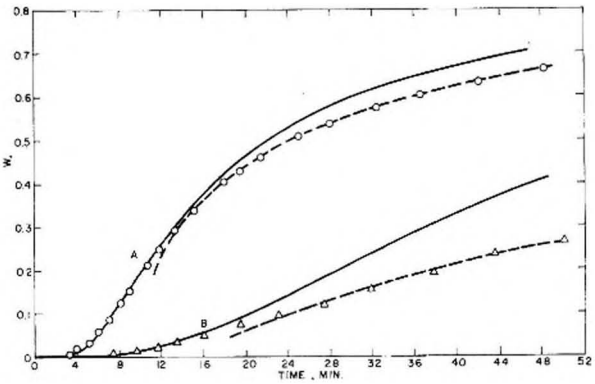

Fig. 1.—Turnbull's results for the precipitation of barium sulfate; equal initial ionic concentrations of 19.1×10^{-5} moles/l. Solid lines drawn from eq. 8, dashed lines from eq. 12; $m = 3$.

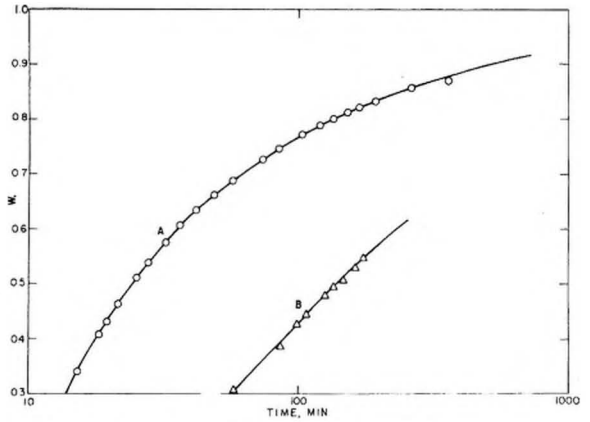

Fig. 2.—Turnbull's results for the precipitation of barium sulfate; equal initial ionic concentrations of 19.1×10^{-5} moles/l. Lines drawn from eq. 12, $m = 3$.

Comparison with Experimental Data

The equations already given above will now be compared to experimental data on the crystallization of salts from solution. Most of the experimental results were obtained by following the concentration of salt in solution by measuring the solution conductance. The value of W is then taken to be $(C_m - C_r)/(C_m - C_0)$ where C_r is the solute concentration in solution at time t, C_m is the initial solute concentration and C_0 is the equilibrium solute concentration calculated from the solubility product. The experiments discussed here were done at 25° unless otherwise noted. The results for different salts will be discussed separately.

Barium sulfate has been used frequently for crystallization studies because it precipitates slowly, is very insoluble, and is important in analytical chemistry. In this discussion a value of 1.2×10^{-16} mole^2/cm.^{3} will be used for the solubility product of barium sulfate. Turnbull measured the

precipitation of barium sulfate by mixing equivalent amounts of barium hydroxide and sulfuric acid, so that only the precipitating ions were present in solution.[1] His precise measurements during the early stages of growth showed that W was proportional to t^3 up to about 5% reaction, which is the result required by eq. 8. Therefore the crystal growth was controlled by an interface process, and the number of growth nuclei was constant, as assumed in the derivations of the growth equations in this discussion. If the precipitation were controlled by bulk solute diffusion the time exponent would be 3/2, and if nucleation continued after the initial period the exponent would be greater than 3. Turnbull's results for the precipitation of barium sulfate with an initial salt concentration of 19.1×10^{-5} mole per liter are shown in Figs. 1 and 2.[20] The initial concentrations were the same for the two runs shown, but the methods of mixing the solution were different. In Fig. 1 the solid lines were drawn from a numerical integration of eq. 10 with $m = 3$, and the dotted lines were drawn from eq. 12 with $m = 3$. In Fig. 2 the lines were drawn from eq. 12 with $m = 3$. Since $m = 3$ throughout both runs one can conclude that the same growth mechanism prevailed during both of them, although at a certain stage of precipitation the effective growth area became constant, rather than increasing as the particle surface area increased. The growth mechanism is that described by eq. 4, which corresponds to Model A.

The number density of particles in different solutions can be compared if their b values are the same. If τ is defined as the ratio of t to $\int_0^W [dz/z^{2/3}(1-z)^3]$, then τ is constant with W as long as eq. 10 with $m = 3$ is obeyed and is given by

$$\tau = \frac{(\rho/3)^{2/3}}{(4\pi N)^{1/3} b (C_m - C_0)^{5/3}} \qquad (14)$$

For two solutions 1 and 2 with the same b value

$$\frac{N_1}{N_2} = \left(\frac{\tau_2}{\tau_1}\right)^3 \left[\frac{(C_m - C_0)_2}{(C_m - C_0)_1}\right]^5 \qquad (15)$$

From this equation the number density of particles for solution A shown in Fig. 1 was about 22 times greater than N for solution B, although the initial concentrations were the same for the two solutions. In another experiment Turnbull measured the precipitation in a solution (C) mixed in the same way as solution B in Fig. 1, but having an initial salt concentration of 23.7×10^{-5} mole/l. The result of this run was a curve almost identical with that for solution A in Fig. 1. Thus from eq. 15 solution C had 3.5 times the number of particles that solution B had. Turnbull tabulated the results of several different precipitations at the same initial concentrations (see Table II, ref. 1) and showed that their τ values (particle density) depended upon the method of mixing, the solutions used and unknown factors.

In the later stages of precipitation when eq. 13 is obeyed a plot of $1/(1-W)^2$ against time is linear. The slope p of such a line equals $2NA'b(C_m - C_0)^2$, if A' is computed from W'

(20) The data for solution A, and for solution B in Fig. 2, have not been published previously, and the author is grateful to Dr. Turnbull for supplying them to him.

TABLE I

CALCULATION OF W'

Salt and soln.	C_m, moles/l.	p, min.$^{-1}$	τ, min.	W'
$BaSO_4$, A	19.1×10^{-5}	0.192	4.9	0.32
$BaSO_4$, B	19.1×10^{-5}	.024	13.6	.06
$SrSO_4$, E	7.5×10^{-3}	.119	9.0	.39
$SrSO_4$, F	5×10^{-3}	.058	14.4	.27

$$p = 2(4\pi N)^{1/3} b (C_m - C_0)^{8/3} (3W')^{2/3}/\rho^{2/3} \qquad (16)$$

Therefore from data for the early and late stages of precipitation some idea of the value of W (denoted as W'), which corresponds to the onset of constant effective growth area can be found, since from eq. 14 and 16

$$p\tau = 2(W')^{2/3} \qquad (17)$$

The slopes p and W' values for solutions A and B are shown in Table I; the W' values are about what one would expect from Fig. 1.

Collins and Leineweber measured the precipitation of barium sulfate by generating sulfate ion homogeneously in a solution of barium nitrate.[11] Nucleation therefore was not affected by local concentration excesses, which probably initiated it in the direct-mixing experiments. In Collins and Leineweber's solutions barium ion was present in considerable excess, from ratios of about 10 to 150 to one. Their results fitted eq. 1 with $R_f/D = 0$ (or eq. 10 with $m = 1$) throughout the precipitation process. The result of $m = 1$ is consistent with the equations found in the discussion of the effect of a large excess of one ion.

Collins and Leineweber measured the size of their precipitate particles from the dissymmetry of scattered light, so it is possible to calculate absolute values of b from their results. They chose to express their results in terms of an adsorption probability, as discussed above in connection with the question of diffusion or interface control. This discussion showed that such use of an adsorption probability was improper; in fact, their result of the same adsorption probability for different solvents would be surprising. The value of b can be computed from their α value as follows. From their relation for γ, $\gamma = s/\alpha = D/b$ or $b = 10^8 D\alpha$. Therefore their result of a nearly constant value of α for precipitation in water at a constant temperature (constant D) shows that b is constant with ionic concentration in solution, as assumed in the derivation of the present equations. In this case the average value of b was about 0.024 cm./sec., which means that the initial rate of growth of the particle radius was about 8 Å. per second from eq. 10. Variations in the α values reported for the same solvent doubtless reflect the experimental uncertainty in determining the particle radius from the dissymmetry of scattered light. The values of N calculated from these results range from about 1.5×10^8 to 1.5×10^9 particles per cm.^{3}. There is no correlation between the supersaturation, as calculated from the product of the ionic concentrations at the start of precipitation, and the number density, although the number of particles roughly increases as the initial sulfate concentration increases. Small impurity particles probably were the major nucleating agents; the authors concluded

that impurities affected the crystallization process from studies of precipitation with materials purified by different procedures.

Assuming that the solute molecules behave as a perfect gas we can compute an adsorption probability from kinetic theory. The flux of molecules striking one square cm. of surface per second is given by $C\sqrt{RT/2\pi M}$ where C is the concentration and M is the molecular weight of the molecules, R is the gas constant and T is the temperature. Thus the fraction of molecules adsorbed f is given by

$$f = \frac{Cb}{C\sqrt{\frac{Rt}{2\pi M}}} \approx 4 \times 10^{-6}$$

for sulfate molecules. Actually, of course, the flux of molecules striking the surface probably is smaller than that given by the kinetic theory expression.

Collins and Leineweber also measured the effect of solvent viscosity upon precipitation rate by crystallizing barium sulfate from various glycerol–water mixtures. Again the results should be interpreted in terms of the effect on growth coefficient rather than upon solute diffusion coefficient, since the solute diffusion in solution is not controlling the precipitation. The results showed that the product of b and the solvent viscosity was roughly constant; that is, that b was inversely proportional to solvent viscosity. This result is not surprising, since surface diffusion should be a factor in the coefficient b, and the diffusion coefficient for surface mobility is probably proportional to solvent viscosity.

Johnson and O'Rourke measured the precipitation of barium sulfate from mixtures of barium chloride and sodium sulfate with different ratios of the precipitating ions.[17] They attempted to analyze their results in terms of two processes, nucleation and growth, but the results of the above two studies show that in barium sulfate precipitation nucleation is completed before the experimental measurements are taken, and the entire process observed is one of growth. Johnson and O'Rourke's results for an initial sulfate-to-barium ion ratio of two-to-one are plotted in Fig. 3, using the deficient ion concentration to measure the extent of reaction. The line is drawn from an integration of eq. 10 with $m = 3$. The fit is good throughout the measured reaction time, showing that for this period the precipitation process proceeds by the same mechanism as for Turnbull's experiments in the initial stages of reaction.

Oden measured the precipitation of strontium sulfate at 20° when strontium hydroxide and sulfuric acid were mixed in equivalent amounts.[21,22] His results for three different initial concentrations are shown in Figs. 4 and 5. Oden used a C_0 value of 8×10^{-4} mole/l., and Kohlrausch[23] found 6.2×10^{-4} mole/l. as the solubility of $SrSO_4$; a value of 7.5×10^{-4} fits the data best, however, so it was used to make the plots in Figs. 4 and 5. The solid lines in these figures were drawn from eq. 8 with $m = 3$, whereas the dashed lines were drawn from eq. 12 with $m = 3$. For the solution with the highest initial concentration eq. 10 was followed throughout the period of precipitation, but for lower initial concentrations the effective growth area on a particle apparently became fixed at a certain stage of growth. The relative number densities of particles for the three solutions can be computed with eq. 15. From this calculation solution E had 1.4 times the number of particles in solution D, and solution F had 14 times the number of particles in solution D. These results are surprising, since the number density decreases with initial super-

(21) S. Oden, *Arkiv Kemi, Min., Geol.*, **9**, No. 23 (1926).
(22) S. Oden and D. Werner, *ibid.*, **9**, No. 32 (1926).
(23) F. Kohlrausch, *Z. physik. Chem.*, **64**, 121 (1908).

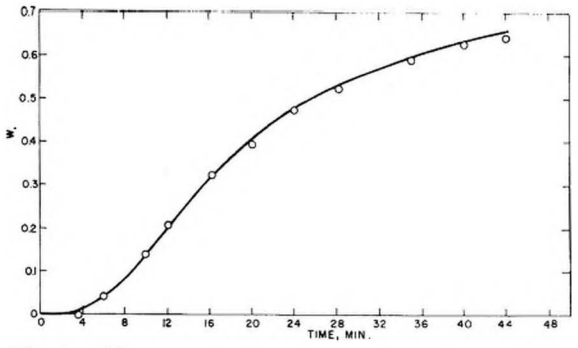

Fig. 3.—Johnson and O'Rourke's results for the precipitation of barium sulfate; initial concentrations: barium 12×10^{-6} mole/l., sulfate 24×10^{-6} mole/l. Line drawn from eq. 8, $m = 3$.

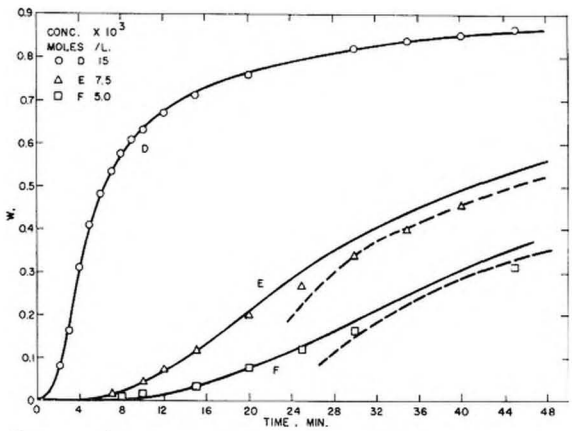

Fig. 4.—Oden's results for the precipitation of strontium sulfate; equal initial ionic concentrations. Solid lines drawn from eq. 8, dashed lines from eq. 12; $m = 3$.

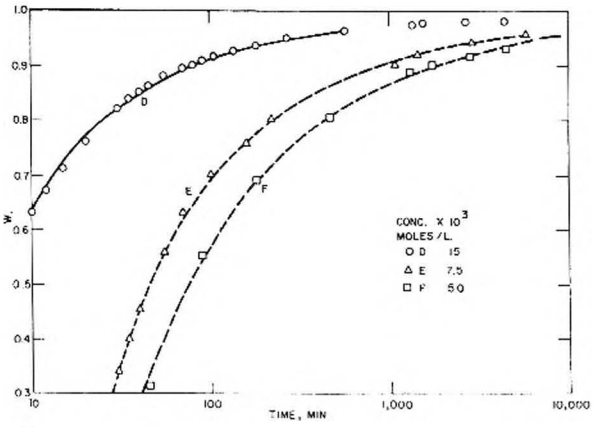

Fig. 5.—Oden's results for the precipitation of strontium sulfate; equal initial ionic concentrations. Solid line drawn from eq. 18, dashed lines from eq. 12; $m = 3$.

saturation increase. It is possible that the method of mixing was not the same in each case, or that more nucleating impurities were introduced into the solutions of lower supersaturation. For the later stages of precipitation the value of W' corresponding to the constant area A' can be calculated from eq. 17 as described above. These W' values are shown in Table I, and as for the barium sulfate solutions the calculated W' values are about what would be expected from Fig. 4.

Van Hook followed the precipitation of silver chromate by measuring the silver ion concentration with an electrical cell.[24] His data for three different initial silver chromate concentrations, taken from Fig. 4, ref. 24, are shown in Fig. 6. The plots of $1/(1 - W)^3$ against time are linear, so eq. 12 for a two–one electrolyte ($m = 4$) applies. Apparently the silver chromate crystallized by the same mechanism as barium and strontium sulfate, and the effective growth area on the crystal surface became constant early in the precipitation.

Howard and Nancollas measured conductimetrically the crystallization of silver chromate from slightly supersaturated solutions after seed crystals were added.[25] The supersaturation was so low that no nucleation of precipitate particles occurred; thus all crystallization took place on the surfaces of the seed crystals. The solutions were well stirred, so the interface reaction was controlling, although the seed crystals were larger than the particles in the experiments without added seeds. The surface area of the seed crystals changed by a negligible amount during the precipitation. The results fitted eq. 13 with $m = 3$, so Model B is applicable rather than Model A as found for Van Hook's experiments. The reason for this dissimilarity could be the different bulk supersaturations in the two sets of experiments. For Model A the rate of precipitation is proportional to the fourth power of the solute concentration, whereas for Model B the rate is proportional to the third power of this concentration. Thus for high concentrations Model A should apply, and at lower concentrations Model B should be controlling; since the solute concentrations in Van Hook's experiments were considerably higher than in Howard and Nancollas', this contention is consistent with the experimental results. Howard and Nancollas found that b was the same for different initial ionic ratios if the deficient ion concentration was used for C_r as described in the equations section.

Davies and his co-workers have measured the precipitation of silver chloride when seed crystals were added to slightly supersaturated solutions.[15,26] In these experiments the seed crystals were so large (3–5 μ in diameter) that their surface area did not change appreciably during the precipitation; however, the solutions were stirred vigorously, so the interface reaction was controlling. The results fitted eq. 13 with $m = 2$ and NA' equal to the total surface area of seed crystals per cm.^{3} of solution, and the growth coefficient b was the same for several different initial solute concentrations. If the initial ionic ratio was not one eq. 13 with $m = 2$ was still obeyed if the deficient ion concentration was used for C_r; the same value of b was found for all ionic ratios studied. Again Model B applied, apparently because the solute supersaturations were quite low. The total surface area of seed crystals NA' was known, so b could be calculated to be about 1.5×10^4 cm.^{4}/mole. sec.

(24) A. Van Hook, THIS JOURNAL, 44, 751 (1940).

(25) J. R. Howard and G. H. Nancollas, *Trans. Faraday Soc.*, 53, 1449 (1957).

(26) C. W. Davies and G. H. Nancollas, *ibid.*, 51, 818 (1955).

Discussion

Let us now consider certain aspects of the growth models proposed. It would be difficult to explain the kinetic results without invoking an adsorbed surface layer of ions. If the ions were incorporated at the growth sites directly from solution one would expect that the rate of crystal growth would be proportional to $C_r^m - C_0^m$ rather than $(C_r - C_0)^m$ as was found experimentally. In the experiments in which the ionic ratios in solution were not stoichiometric the growth rates were proportional to some power of the deficient ion concentration. Thus if more of the ion in excess was added (at least in moderate amounts) the rate of precipitation was unchanged. This result could not occur if the ions were incorporated directly from solution, since then the precipitation rate should be proportional to the product of the total concentrations of both ions in solution. Therefore the experimental measurements of the kinetics of ionic crystal growth from solution are best explained if an adsorbed surface layer of ions is postulated.

Fitting a solute unit directly into the crystal lattice from solution should be difficult. Even for uncharged molecules a collision at a kink in a growth step with just the right orientation to fit into the crystal lattice would be an improbable event. For ionic solutes the difficulties are even greater, because simultaneous or at least alternate collisions of oppositely charged ions with a kink would be even more improbable events. Furthermore many ions are solvated in solution, and desolvation would have to occur at the same time as the ion fits into the lattice. Thus the concept of an adsorbed layer, which permits desolvation and partial orientation before incorporation into the lattice, seems reasonable.

In certain of the crystallization experiments in which seed crystals were not added it was found that the effective growth area of the particle became constant at a certain stage in the precipitation. From Figs. 1 and 4 for barium and strontium sulfates we see that this phenomenon appeared at roughly the same time after the initial mixing in several different experiments. This result suggests that impurity adsorption influenced the formation of growth steps. The desorption of surface impurities could hinder formation of new growth steps; alternatively, impurity ions adsorbed from the solution could poison new growth steps as they are formed.

Some information on the nucleation process can be obtained from the results in which seed crystals were not added. The crystallization kinetics of barium and strontium sulfates are accurately described by a growth process only, so the assumption of a constant number of growing particles for these systems is justified. Thus the numerous

interpretations of the initial growth period in salt precipitation as an "induction period" or "time lag" for nucleation must be viewed with suspicion. In fact, nucleation during a measurable time occurs only under special conditions, such as in the experiments of Dunning and Notley on crystallization of cyclonite[27] and those of Schlichtkrull on insulin.[28] Usually nucleation of crystals in solution is completed in a very short time, and nucleation rates for such a system have not yet been measured experimentally. The above interpretations show that the differences in lengths of initial periods of growth are due to differences in both the number of nuclei present and the growth rate. The growth rate is strongly affected by the initial supersaturation, shown by the factor $(C_m - C_0)^m$ in eq. 10, and this effect is the one generally attributed to different nucleation rates by authors who theorize about the "induction period."

The influence of initial supersaturation upon the number of nuclei in the crystallizing salt solutions discussed above was less than generally supposed. Turnbull's results on barium sulfate showed that the method of mixing the solution could change the number density of particles by a greater factor than substantial variations in supersaturation changed it. Davis and Jones' experiments on silver chloride also showed a large variation in growth rate when solutions of the same initial solute concentrations were mixed in different ways.[29] The experiments of Collins and Leineweber on barium sulfate precipitation showed no consistent effect of initial supersaturation on particle number density, even though the nucleation process occurred uniformly throughout the solution, while Oden's results on strontium sulfate showed a decrease of particle density with increase of supersaturation, contrary to the expected increase. Thus the number of nuclei in these salt solutions was not entirely dependent upon solute supersaturation. The nucleation was doubtless heterogeneous, and the probable nucleating agents were minute colloidal impurity particles. The particle number density in Collins and Leineweber's experiments varied from 1.5 to 15×10^8 particles/cm.^{3}, which is within the range of possible impurity particle density. A spectrum of nucleating probabilities and different concentrations for the impurity particles could account for the variations in the density of precipitate particles with method of mixing, supersaturation and other unknown factors.

In conclusion the main results of this discussion are as follows. 1. For the systems considered the crystal growth was controlled by a process at the particle surface, rather than bulk diffusion of solute. 2. If no seed crystals were added nucleation occurred very rapidly when the initial solutions were mixed, and the number of salt particles remained constant throughout the measured growth period. 3. Surface adsorption of ions was found to be a necessary step in the growth process. 4. Functional relations between growth rate and solute concentration were established for barium and strontium sulfates. 5. These relations and those for other salts were rationalized in terms of two models for the incorporation of solute into the crystal lattice. 6. Factors such as the density of impurity particles and the method of mixing solutions were as important in the nucleation process as solute supersaturation.

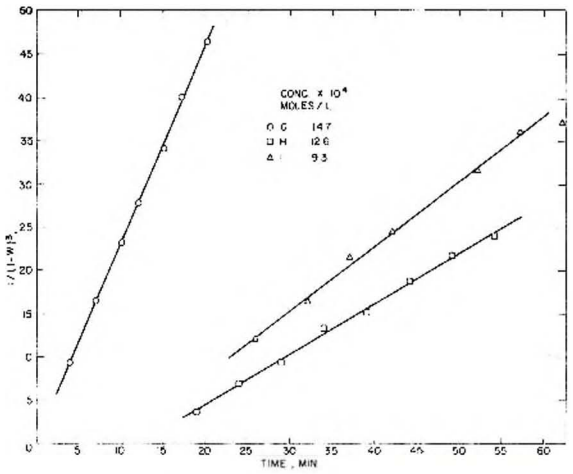

Fig. 6.—Van Hook's results for the precipitation of silver chromate; equal initial ionic concentrations. Ordinate scale must be divided by ten for solution I.

Acknowledgments.—The author wishes to thank D. Turnbull for introducing him to this subject and for making suggestions on the manuscript. He is also indebted to G. W. Sears, D. A. Vermilyea, F. S. Ham and H. W. Cahn for stimulating discussions.

Appendix

Simplified Derivation of Eq. 1.—From Fick's first law of diffusion $J = DG$ in which J is the flux of diffusing species per unit area and G is the concentration gradient of diffusing species. For three-dimensional growth of an isolated spherical particle from dilute solution Zener[4] finds that $G = (C_\infty - C_r)/R$ at the particle surface, where C_∞ is the solute concentration a long distance from the particle. To account for competing particles in a dilute solution C_∞ can be replaced by $(C_m - C_0)(1 - W) + C_0$. When these relations are combined with that for the flux $J = b(C_r - C_0)$ in the interface reaction and solved for C_r the result is

$$C_r = \frac{D(C_m - C_0)(1 - W)}{D + bR} + C_0$$

Since the deposition of solute on the particle surface is assumed to be uniform

$$J = \rho \frac{dR}{dt} = \frac{Db(C_m - C_0)(1 - W)}{D + bR}$$

The solution of this equation for particles of negligible initial radius is eq. 1.

(27) W. J. Dunning and N. T. Notley, *Z. Elekt.*, **61**, 55 (1957).

(28) J. Schlichtkrull, *Acta Chem. Scand.*, **11**, 439 (1957).

(29) C. W. Davies and A. L. Jones, *Disc. Faraday Soc.*, **5**, 103 (1949).

ABSORPTION MEASUREMENT WITH A LENS-CUVETTE IN SATURATED SOLUTIONS OF A METACHROMATIC DYE

BY JOHN W. KELLY[1] AND GUNNAR SVENSSON

Institute for Cell Research, Medical Nobel Institute, Karolinska Institutet, Stockholm

Received April 4, 1958

A lens-cuvette was used in a scanning and recording microspectrophotometer (Caspersson) to measure the absorbance of saturated aqueous solutions of toluidine blue. The cuvette is a plane-convex spherical lens resting convex face down on an optical flat plate, presenting layer thicknesses of 0.004 cm. to less than 0.0001 cm. The absorption spectrum of toluidine blue at the highest concentrations ($0.82–1.04 \times 10^{-1}$ *M*) resembles closely the well-known metachromatic spectra of dilute solutions of the dye in the presence of certain anionic polyelectrolytes or of the dye bound at selected sites in cells and tissues. This finding supports the theory of Schubert and Levine on metachromasy in solution. It suggests that application of this theory to metachromatically-stained solid substrates may be realized as the limited spectral analyses of these substrates are extended.

Special technical difficulties arise in securing thin layers of known dimensions for absorption measurement in highly concentrated solutions. Down to about 0.01 cm. thickness, cells are calibrated against solutions in standard cells by the Bouguer–Lambert law,[2] but "below say 0.005 cm. it becomes almost impossible to calibrate the thickness of an absorption cell precisely."[3] For certain infrared spectral analyses, where cells of the order of 0.001 cm. thickness are required, authors sometimes explicitly state that accurate cell dimensions cannot be quoted.[4] The well designed variable cell of Adams and Katz[5] illustrates problems typical of a multi-component assembly. Such cells are difficult to fill, empty and clean without disassembly so that it is not always possible to calibrate them by the Bouguer–Lambert law. Calibration may sometimes be effected by counting fringes, requiring special polishing for flat and parallel windows.

A lens-cuvette devised by Svensson[6] permits absorption measurements in layers of any thickness from a fraction of a micron to about 40 μ. The "cuvette" consists of a plane-convex spherical lens of quartz or glass resting convex face down on a plane-parallel plate of the same material. A drop of solution is drawn by capillarity between lens and plate and sealed with a drop of immiscible liquid. Layer thickness is determined by the distance of the measuring spot from the lens center. Main features of the lens-cuvette are: (1) elimination of all filling and cleaning difficulties; (2) easy manipulation of 0.1 μl. solution volumes; (3) measurement of solutions with absorbances of 0.1–5 per μ; (4) over-all measurement error of $\pm 1\%$.

In addition to general analytical uses for the lens-cuvette, the device bears a close dimensional relation to certain problems in the microspectrophotometry of biological objects. In such objects, the absorbing layer (tissue section or cell) is rarely thicker than 10 μ and the concentration of absorbing material may be well above the range accessible to standard solution measurement. Model systems of naturally-occurring compounds with selective absorption, such as nucleic acids, proteins or pigments, may be studied at high concentrations in the lens-cuvette. Applied chromogens, particularly dyes, may also be examined at concentration levels approaching or equalling those obtaining in solid, stained substrates.

A special study of the thiazine dye, toluidine blue, was made in the lens-cuvette. This dye is the most widely used of metachromatic dyes for the histochemical detection of strongly acidic polyelectrolytes, such as heparin or chondroitin sulfate. General features of metachromatic reactions are reviewed elsewhere.[7] The useful quality of metachromatic dyes is their marked susceptibility to color changes under the influence of appropriate substrates, called *chromotropes*. This quality is at least circumstantially related to the extreme deviations from Beer's law displayed by these dyes in the absence of any chromotrope. Setting forth a new theory of metachromasy in solution, Schubert and Levine[8] question the prevailing view that seems to require actual binding of dye to a substrate. Important evidence was found by these authors suggesting that the spectral changes of a metachromatic dye as it becomes highly concentrated are similar to the changes occurring when a chromotrope is added to a dilute solution of the dye. This evidence came from a study of dyes at the highest concentrations at which measurement could be made, limited only by the absorption cells.

The main object of this investigation was to obtain information for a comparison between the spectrum of toluidine blue in solution at maximum concentration and the spectra measured in the microspectrophotometer when the dye is bound in selected tissue or cellular sites. For a solution in the lens-cuvette, the limiting factor is the solubility of the absorbing compound.

Experimental and Results

Dyes.—Two samples of *toluidine blue O*, C. I. 925, were used. Sample 1 was obtained from the Hartman–Leddon Company, Philadelphia, and sample 2 was obtained from

(1) John Simon Guggenheim Fellow, 1957–1958. Permanent address: Medical College of Virginia, Richmond, Va.

(2) L. F. Epstein, F. Karush and E. Rabinowitch, *J. Opt. Soc. Am.*, **31**, 77 (1941).

(3) L. Michaelis, *Cold Spring Harbor Symp. Quant. Biol.*, **12**, 131 (1947).

(4) E. K. Plyler, *Disc. Faraday Soc.*, **9**, 100 (1950). See also papers of Brown and Sheppard and of Gore for discussion and references to other absorption cells.

(5) R. M. Adams and J. J. Katz, *J. Opt. Soc. Am.*, **46**, 895 (1956).

(6) G. Svensson, *Exp. Cell Research*, **9**, 428 (1955); *Mikrochim. Acta*, **1 6**, 645 (1956).

(7) J. W. Kelly, in "Protoplasmatologia," ed. by L. V. Heilbrunn and F. Weber, Springer-Verlag, Vienna, 1956, pp. 1–98; M. Schubert and D. Hamerman, *J. Histochem. and Cytochem.*, **4**, 159 (1956).

(8) M. Schubert and A. Levine, *J. Am. Chem. Soc.*, **77**, 4197 (1955).

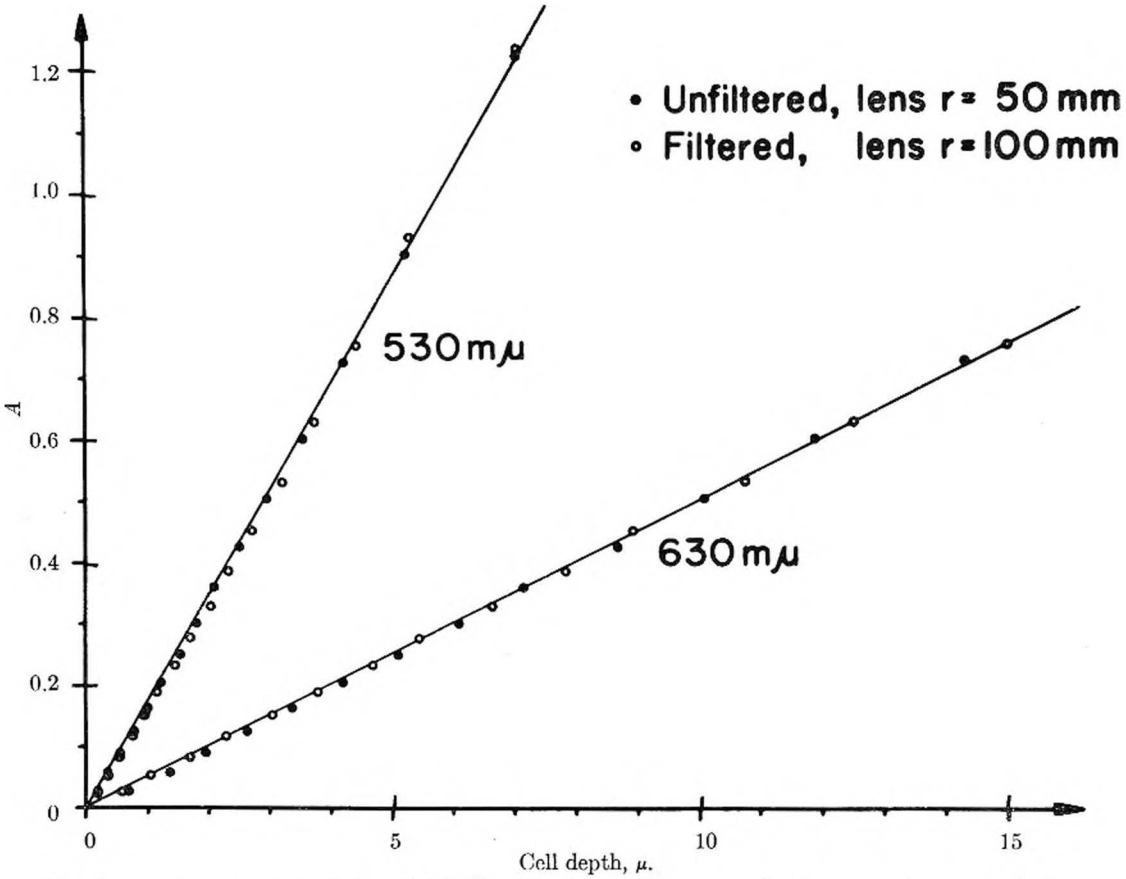

Fig. 1.—Absorbance of a saturated solution of toluidine blue (sample 2) measured at two wave lengths in the lens-cuvette. The slope of a line, or mean value of A/t, is used to calculate molar absorbance, ϵ_λ.

Apoteket Morianen, Stockholm. Dye contents of these samples were 72 and 50%, respectively, and molar concentrations were based on these values. It was not feasible to purify these particular samples further. Saturated solutions of each dye sample were read in the lens-cuvette before and after filtering through a sintered-glass filter. Concentrations of the filtered solutions were determined by drying aliquots and weighing residues. Further dilutions of the filtered solutions were made for reading in the lens-cuvette. Aliquots of all solutions were diluted to a suitable range for checking concentrations in a standard spectrophotometer. All measurements on these solutions were conducted at room temperature, about 24°.

Spectrophotometry.—The lens-cuvette can be used with any microspectrophotometer in which accurate measurement of the distance between lens center and measuring spot (microscope optical axis) can be made. The automatic scanning and recording ultramicrospectrograph of Caspersson[9] was used in the present study. In this instrument, an object is driven across the stage synchronously with the paper of an XY recorder. A signal of light intensity from the moving object is traced in the y-axis of the paper. For an absorbing solution in the lens-cuvette, the permanent record resembles a probability curve with peak transmission representing the center of the lens (see Svensson[6] for curve tracings).

A Zeiss PMQ-II spectrophotometer and 1.0 cm. quartz cells were used to measure absorbance of all dilute solutions. Absorption terms used in this paper are: *absorbance*, $A = \log I_0/I = kcd$, where k is absorptivity or specific absorbance c is concentration in grams per liter and d is cell depth in centimeters; *molar absorbance*, $\epsilon_\lambda = kM$, where M is molecular weight in grams.

The Lens-cuvette.—Quartz spherical lenses and optically flat plates comprised the cuvettes. Various solution concentrations were accommodated by a set of lenses of different radii: 21.4, 50, 100 and 200 mm. Paraffin oil was used to seal the dye solutions in the cuvette. The main principles of measuring in the cuvette are reviewed here; full details with descriptive figures are presented elsewhere.[6] The perpendicular distance from a plane tangent to a spherical surface is $t = x^2/2r$ (for $t << r$), where x is the distance in the plane from the point of tangency and r is the lens radius. For the lens-cuvette, t is the thickness of the liquid layer and x is the horizontal distance between measuring spot and lens center. As the lens is scanned, the changing thickness of an absorbing liquid layer is reflected in the bell-shaped curve of intensity recorded, with a peak corresponding to the lens center. The distance, a', between the arms of the curve, measured in the paper x-axis, for any value of intensity I measured in the y-axis, is directly related by a motion constant to $a = 2x$ in the lens-cuvette. The motion constant is obtained on the same paper by scanning a few millimeters of a stage micrometer and recording the sharp spikes of its 0.1 mm. divisions. Calculations are then made from the paper, according to the form $t = a^2/8r$. For a given wave length and solution concentration, a series of values, I_0 (near the peak of the intensity curve), $I_1, \ldots I_n$ and a corresponding series, $a_0, a_1, \ldots a_n$, are measured, in order to obtain the mean value of absorbance per unit thickness. The actual thickness for any value of I is $t - t_0$, since an arbitrary I_0 was chosen *not* at the center of the lens.

Figure 1 shows the results of typical measurements of absorbance in saturated toluidine blue solutions. It is seen that the lenses may be interchanged. The major consideration in matching of lens and solution is that recorded curves shall not be too flat or too narrow for accurate measurement. When the saturated solutions were measured before filtering, the presence of suspended particles appeared as numerous downward spikes in the intensity curves. These aberrations did not alter the fundamental shapes of the original curves nor interfere with calculations made from them, as Fig. 1 shows. It was usual to obtain eight to fifteen points at each wave length for a mean value of A/t, in order to plot one point in the absorption spectra of concentrated dye solutions (Fig. 2). This figure does

(9) T. Caspersson, *Cold Spring Harbor Symp. Quant. Biol.*, **21**, 1 (1956); T. Caspersson, G. Lomakka, G. Svensson and R. Säfström, *Exp. Cell Research*, **3**, 40 (1955); G. Lomakka, *ibid.*, **9**, 434 (1955).

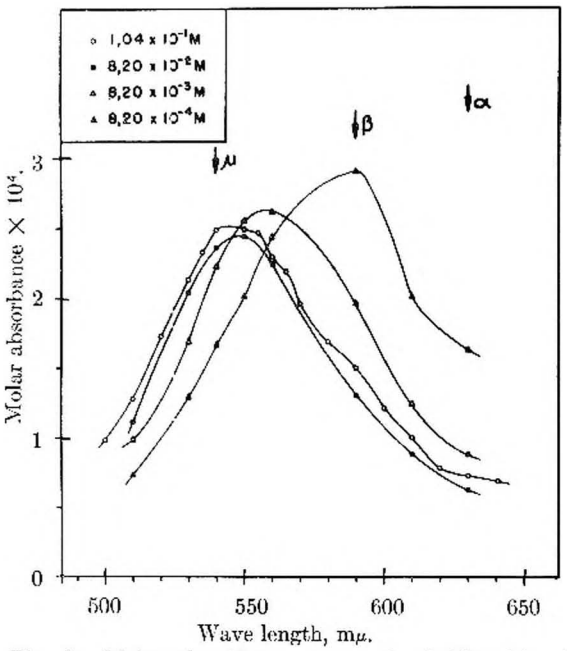

Fig. 2.—Molar absorbance curves of toluidine blue in highly concentrated solutions. The circles represent saturated solutions of sample 1 (*open-faced symbols*) and sample 2 (*solid symbols*). Other symbols represent lower concentrations of sample 2. The position of the nominal μ-band represents a range of peaks at 530–555 mμ that arise when various chromotropes (*e.g.*, heparin, chondroitin sulfate) are added to dilute solutions of toluidine blue. Other band regions are described in the text.

not include the well-known spectra of dilute solutions of toluidine blue. Samples 1 and 2, at concentrations of $0.82\text{–}1.01 \times 10^{-5}$ *M*, gave molar absorbances of 47,900–49,000 for the main absorption maxima (α-bands) at 630 mμ. In terms of a *metachromatic ratio*,[10] $A_{\mu\text{-band}}/A_{\alpha\text{-band}}$, values of about 0.25 are obtained for these non-metachromatic solutions. At 10^{-1} *M*, the new absorption maxima (μ-bands) are at 545–550 mμ and molar absorbances are about 25,000. Here the metachromatic ratio is 3.4–3.9.

Discussion

From numerous past investigations of metachromatic dyes in solution, some general spectral patterns have been established. In dilute aqueous solutions (10^{-7} to 10^{-6} *M*), only the α-band of a metachromatic dye is observed or a shoulder may be present in the absorption curve some 40–50 mμ toward lower wave lengths. As the dye is concentrated, this shoulder becomes the β-band at the progressive expense of the α-band. With further concentration, a succession of α-bands at still lower wave lengths and of lower absorbances are recorded. The extreme μ-band of the dye has been thought to arise only when an appropriate chromotrope is added to dye solutions. Positions of the characteristic bands for toluidine blue are shown in Fig. 2.

Earlier studies of methylene blue, thionine and toluidine blue in moderately concentrated solutions (to 2.5×10^{-3} *M*) gave little evidence of μ-bands.[3,11] Schubert and Levine[8] examined methylene blue at concentrations up to 5.33×10^{-3} *M*, where it is seen clearly that the spectrum of the dye is approaching the metachromatic state induced by a chromotrope. Similar indications were found for crystal violet and methyl green. An absorption cell depth of 0.01 cm. imposed a technical limit upon this investigation. With the lens-cuvette, the present study was limited by dye solubilities rather than depth of absorbing layer. *Saturated solutions of toluidine blue* (to 1.04×10^{-1} *M*) *display absorption spectra typical of those measured in dilute solutions of the dye in the presence of a chromotrope.* This observation supports the theory of Schubert and Levine, which is strictly limited to metachromasy in solution and does not apply to metachromatic staining.

Few spectral analyses are found on metachromasy in solid substrates, such as tissue sections, isolated cells, gels or smears. Flax and Himes[12] examined metachromasy in known sites of DNA, RNA or sulfuric acid esters and Carnes and Forker[13] studied cartilage and amyloid. Metachromatic spectra in mucus and egg-jelly, as well as cartilage, are also available.[7,14] These studies illustrate the types of spectra which must be considered in comparing stained substrates to model systems in solution. For example, cartilage and its product, chondroitin sulfate, usually yield comparable metachromatic spectra in tissue sections and solutions, respectively, but Carnes and Forker found an interesting difference between the two situations. Maximum metachromatic ratios of about 2 were obtained for toluidine blue and chondroitin sulfate; cartilage was more metachromatic with values of about 4. This difference may lie, as Carnes and Forker suggest, in the (unknown) higher concentrations of chromotrope and dye in stained materials. Alternatively, it must be remembered that the spectrum of a dye in solution with a chromotrope is the sum of the bound and unbound forms while the spectrum of a dye in tissue sections is that of the bound dye alone.[13] This would always have the effect of increasing the metachromatic ratios in tissue sections over those of comparable model systems in solution. In agreement with Carnes and Forker, metachromatic ratios of toluidine blue rarely exceed 2–2.5 for dye-chromotrope solutions and values of 4 or higher are not uncommon in some cellular or tissue regions. Now it is seen that metachromatic ratios close to 4 are obtained also in saturated solutions of toluidine blue.

It is to be expected that the spectra of metachromatic dyes especially will be more complex in histological objects than in the usual solutions investigated. The main requirement for applying solution information to the interpretation of these spectra lies in extending the limited microspectrophotometric analyses of metachromasy. Secondarily, it seems possible to conduct some experiments on solutions under conditions more closely approximating those existing in histological or cytological objects. It is conceivable, for example, that the lens-cuvette would be a useful adjunct to the microspectrophotometer in the critical problem of determining concentrations of chromotropes,

(10) J. M. Wiame, *J. Am. Chem. Soc.*, **69**, 3146 (1947); J. W. Kelly, *Arch. Biochem. Biophysics*, **55**, 130 (1955).

(11) E. Rabinowitch and L. F. Epstein, *ibid.*, **63**, 69 (1941).

(12) M. H. Flax and M. H. Himes, *Physiol. Zool.*, **25**, 297 (1952).

(13) W. H. Carnes and B. R. Forker, *Lab. Invest.*, **5**, 21 (1956).

(14) J. W. Kelly, Fifth Symposium on Histochemistry, Kiel, Germany, Oct. 24–27, 1957 (to be published).

as well as of dyes, in microscopic objects.

Acknowledgments.—The authors wish to express their appreciation to Ing. J. Kudynowsky for his excellent technical assistance. J. K. welcomes this opportunity to thank Prof. T. Caspersson for extending the facilities of this Institute to a guest.

APPLICABILITY OF THE KNUDSEN EFFUSION METHOD TO THE STUDY OF DECOMPOSITION REACTIONS. THE DECOMPOSITION OF MAGNESIUM HYDROXIDE

BY ERIC KAY AND N. W. GREGORY

Contribution from the Department of Chemistry at the University of Washington, Seattle, Washington

Received April 7, 1958

Expected equilibrium water pressures over $Mg(OH)_2$ and MgO and a condensation coefficient of unity are observed in effusion experiments at 28° only in the initial stages of the decomposition. As the reaction progresses pressures within the cell drop to immeasurably low values. At higher temperatures a constant steady state effusion pressure has been observed between 5 and 55% decomposition when the cell is kept continuously *in vacuo*. Under these conditions the system shows a pseudo-equilibrium behavior; P_S shows a systematic variation with cell orifice area; however, extrapolation to zero orifice area gives an apparent equilibrium pressure only a ten-thousandth that of the expected value, a condensation coefficient of 10^{-3}, and an apparent ΔH 58% larger than the thermodynamic value. A possible kinetic explanation is discussed. It is concluded that the effusion method can give very misleading results when applied to the determination of equilibrium characteristics of decomposition reactions involving substances of very low volatility.

With increasing interest in and need for characterization of chemical systems at high temperatures, the applicability of the Knudsen effusion method[1] to the study of decomposition equilibria has become of considerable importance. Because of the experimental simplicity of the method, it appears ideally suited for the study of reactions of the general type, solid (I) = solid (II) + gas, commonly encountered in the decomposition of halides, hydroxides, carbonates, etc. Recently a number of authors have pointed out that serious differences between steady-state pressures and true equilibrium pressures may result (even for simple vaporization processes) if the condensation coefficient is very small.[2-6] This coefficient may be defined as the fraction of the molecules colliding with the surface which actually condense. Its magnitude may be estimated by observing the dependence of steady-state effusion pressures on cell geometry and their relation to the true equilibrium pressure.[6]

We have made a study of the effusion method as a means of determining the equilibrium characteristics of the reaction

$$Mg(OH)_2(s) = MgO(s) + H_2O(g) \qquad (1)$$

This system was chosen primarily because thermodyamic properties of the substances involved are well-known.[7,8] Giauque and Archibald have carefully determined equilibrium vapor pressures of water in this sytem by a static manometric method in the vicinity of 200°. X-Ray diffraction work[9] has shown that only the two simple solid phases, $Mg(OH)_2$ and MgO, exist in the system. Furthermore $Mg(OH)_2$ occurs in nature in a high state of purity as brucite. Use of this material in initial work avoided much of the difficulty resulting from inability to prepare comparable samples of starting material.[7,10-12] Kinetic studies have shown rates of decomposition to be slow and a hysteresis loop was observed on comparing hydration and dehydration parts of the cycle.[13] Hence it was concluded that this system should provide a good test of the applicability of the effusion method.

Experimental

Samples of $Mg(OH)_2$ were placed in various carefully calibrated effusion cells and the rate of effusion of water vapor measured under molecular flow conditions.[14] Cells were placed in a glass tube immersed in a thermostat or, at higher temperatures, an electric furnace. Once a run was initiated the sample was maintained under high vacuum and water vapor removed continuously. The effusing water vapor was collected in a liquid air-cooled trap for measured intervals of time. To stop a run a stopcock connecting the collector to the sample was closed but evacuation continued by switching to an alternate pumping route. All the water vapor removed was collected so as to follow the extent of decomposition of the original sample as measurements progressed.

The effusate was transferred from the collecting trap to a small calibrated, thermostated volume in which its pressure was determined manometrically. As little as 10^{-7} mole of water could be measured. It has been shown that the ideal gas equation is adequate to determine the number of moles of water vapor as long as its pressure does not

(1) M. Knudsen, *Ann. Physik*, **28**, 1002 (1909).

(2) C. I. Whitman, *J. Chem. Phys.*, **20**, 161 (1952).

(3) S. Dushman, "Vacuum Technique," Chapter 2, John Wiley and Sons, Inc., New York, N. Y., 1949.

(4) K. Motzfeld, THIS JOURNAL, **59**, 139 (1955).

(5) R. Speiser and H. L. Johnston, *Trans. Am. Soc. Metals*, **42**, 283 (1950).

(6) J. H. Stern and N. W. Gregory, THIS JOURNAL, **61**, 1226 (1957).

(7) W. F. Giauque and R. C. Archibald, *J. Am. Chem. Soc.*, **59**, 561 (1937).

(8) W. F. Giauque, *ibid.*, **71**, 3192 (1949).

(9) R. Fricke, *et al.*, *Z. anorg. Chem.*, **166**, 244 (1927); G. F. Huttig and W. Frankestein, *ibid.*, **185**, 403 (1929); W. Bussem and F. Koberich, *Z. physik. Chem.*, **B17**, 310 (1932).

(10) D. R. Torgeson and T. C. Sahama, *J. Am. Chem. Soc.*, **70**, 2156 (1948).

(11) C. H. Shomate and E. H. Huffman, *ibid.* **65**, 1625 (1943).

(12) K. Taylor and L. S. Wells, *Bur. Standards J. Res.*, **21**, 133 (1938).

(13) R. I. Razouk and R. Sh. Mikhail, THIS JOURNAL, **59**, 636 (1955).

(14) Considerable care was taken in the design of effusion cells and the trapping system to keep Clausing factors as large as possible in accordance with well-established principles of effusion work.[2,6] Details may be found in the Doctoral Thesis of Eric Kay: "The Applicability of the Knudsen Effusion Technique to the Study of Decomposition Reactions. The $Mg(OH)_2$–MgO H_2O and NaOH–Na_2O–H_2O Systems," University of Washington, 1958.

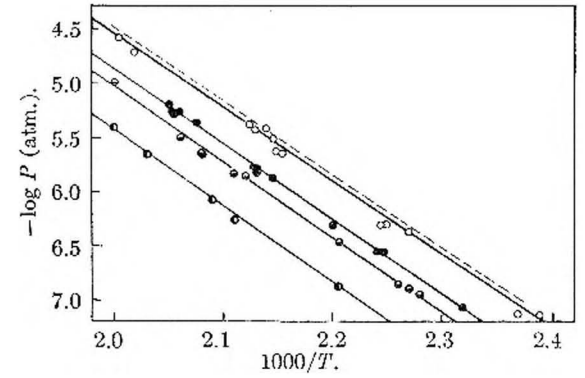

Fig. 1.—Steady-state effusion pressures above ground samples of brucite; 5–55% decomposition, 140–230°: ○, $f = 5.35 \times 10^{-4}$; ●, $f = 2.93 \times 10^{-3}$; ⊖, $f = 3.91 \times 10^{-3}$; ◐, $f = 2.02 \times 10^{-2}$; – – – –, apparent equilibrium pressure.

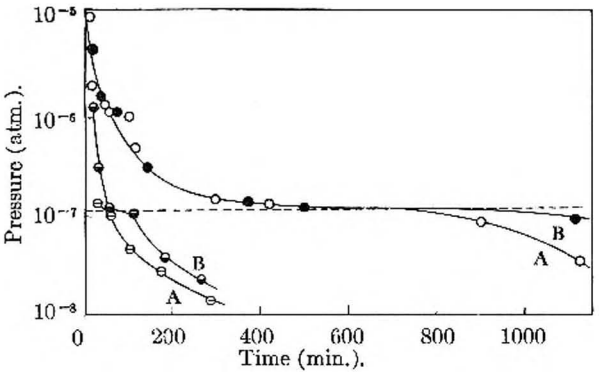

Fig. 2.—Steady-state effusion pressures in the initial stages of the decomposition (28°); A curves, 1 g. of large sheets of brucite; B curves, 1 g. (−20 + 60 mesh) of ground brucite: ⊖, ⊖, effusion (decomposition) rate $4.36 \times 10^{-3} P$ moles/second; ○, ●, effusion (decomposition) rate $4.63 \times 10^{-4} P$ moles/second; – – – –, equilibrium pressure according to Giauque and Archibald.

exceed *ca.* 0.7 that of the saturation value.[15,16] The quantity collected was related to the pressure in the effusion cell by the usual Knudsen equation.

Results

According to characteristics determined by Giauque and Archibald, the equilibrium vapor pressure of water above $Mg(OH)_2$ and MgO is *ca.* 10^{-6} atmosphere at room temperature. Initial effusion experiments (at 28°) gave pressures of this magnitude (values were higher until absorbed water was removed) for a very limited time only; pressures then fell off to immeasurably low values even though less than 0.1% of the sample had been decomposed. To bring the pressure back into a measurable range it was necessary to increase the temperature of the sample by *ca.* 150°. At these higher temperatures effusion steady-state pressures were finally established (after *ca.* 5% decomposition) which did not change on further continuous decomposition of the sample but which were many orders of magnitude lower than expected equilibrium values. Figure 1 shows the dependence of these steady-state pressures on temperature and on effusion cell geometry. The straight lines shown were obtained by varying the temperature randomly over the range plotted. The marked dependence of P_s on f (the ratio of orifice areas A_0 to cell cross-section areas A_s; the latter (from 2–4 cm.^{2}) is taken as an approximation to the effective vaporizing and condensing areas of the sample[6]) suggests a small condensation coefficient. Assuming the equation

$$P_e/P_s = 1 + f/\alpha \qquad (2)$$

derived from steady-state conditions,[5,6] the apparent equilibrium pressure P_e and the condensation coefficient α may be calculated. Alternately, P_e may be estimated by plotting the observed steady-state pressure as a function of A_0 (keeping the cell cross-section constant) and extrapolating to zero orifice area. Both methods give reasonably good extrapolations and essentially the same result; $\alpha = 1.8 \times 10^{-3}$ and $P_e = 2.5 \times 10^{-6}$ atmosphere at 463°K. No variation of α with temperature is indicated. The slopes of the lines in Fig. 1 are essentially the same and give an apparent heat of reaction of 31.2 kcal. The temperature dependence of P_e (apparent), dotted line Fig. 1, may be represented by the equation

$$\log P = \frac{-6820}{T} + 9.118$$

Actually, at 463°K. $P_e = 2.62 \times 10^{-2}$ atmosphere and $\Delta H = 19.78$ kcal. as determined by Giauque and Archibald. Thus P_e (apparent), Fig. 1, is lower than the actual equilibrium value by a factor of 10^4. This surprising result will be discussed in more detail after presenting other observations.

Because of the very small net rate of decomposition in the effusion cell, it is possible to follow the change in steady-state pressure in the initial stages of the decomposition. Fig. 2 shows the dependence of pressures on time, *i.e.*, on degree of decomposition. Results shown are from two independent samples, one large sheets cleaved from native brucite crystals[17] and the other a ground sample of brucite of the indicated particle size. The two set of curves correspond to different effusion rates; one cell had an orifice *ca.* ten times that of the other. Zero time represents the beginning of the first measurement, initiated as soon as molecular flow conditions could be established (a matter of a few minutes). The first measurements gave pressures above the expected equilibrium value, shown by the dotted line, which we attribute to desorption of water from the sample and/or walls of the cell. Of considerable interest is the brief leveling off (of pressures) at the equilibrium pressure of Giauque and Archibald. The extent of decomposition when the steady-state pressure falls below this equilibrium value is nearly the same in both cases. Grinding the sample increased this period slightly.

Figure 3 illustrates the effect of a more drastic change in particle size on the length of time equilibrium pressures were maintained; the rate of decomposition was the same as the larger value in Fig. 2. The behavior of a sample of Baker N.F.

(15) H. S. Frank, THIS JOURNAL, **33**, 970 (1929).

(16) I. R. McHaffie and S. Lehner, *J. Chem. Soc.*, **127**, 1559 (1925); THIS JOURNAL, **31**, 719 (1929).

(17) Brucite used was part of a piece of Texas Brucite obtained from Ward's Natural Science Establishment, Inc., 3000 Ridge Rd. E., Rochester 9, New York.

$Mg(OH)_2$ (chemically precipitated) and of rehydrated MgO (originally produced by decomposition of brucite) is shown and may be compared with those in Fig. 2. Even the rehydrated material, which is probably of colloidal dimensions, only maintains the equilibrum pressure until *ca.* 0.25% decomposed.

The condensation coefficient for the equilibrium portion of the decomposition must be very near unity. This is demonstrated by the independence of P_e (observed) on orifice area.

In Fig. 4 a comparison of steady-state pressures from the various samples of $Mg(OH)_2$ throughout the major part of their decomposition is shown. In identical cells, P_s values for the ground brucite particles are somewhat larger than pressures above the large sheets. On the other hand, the chemically precipitated $Mg(OH)_2$, which would be expected to have a still larger total surface area, gives the smallest steady-state pressure of the three shown. However, considering the magnitude of these pressures relative to true equilibrium values, these differences are small. Changing the quantity of a given kind of sample in the effusion cell (for example from 0.6 to 1.2 g. in a cell with largest f factor) did not cause a discernible change in the steady-state pressure.

By the time the constant low steady-state pressures were reached (at the higher temperatures) less than 5% of the brucite samples and 9% of the N. F. samples were decomposed. Figure 5 shows a typical approach to the constant steady-state pressure at 220°. This slow approach from lower pressures suggests a slow structural change. Once the upper value was reached, it remained unchanged throughout decomposition of the major part of the sample. In one experiment 55% of the sample was decomposed in a continuous series of measurements at various (randomly chosen) temperatures with reproducible variation of P_s along the lines shown in Fig. 1. In another the sample was further dehydrated by heating briefly to high temperatures and then cooled again to *ca.* 200°; essentially the same P_s value was observed with the sample about 80% decomposed. In the intermediate stages of the decomposition the build up of decomposition product, colloidal MgO, did not appear to cause appreciable lowering of the steady-state pressures; such an effect has been observed in the Mo_3Ge system.[18]

If evacuation of the sample were discontinued, water pressure within the cell increased slowly. On renewing effusion experiments, after a short interval, the first pressure measurement was high (approaching true equilibrium) but subsequent values dropped quickly to the same constant steady-state pressure observed before closing off the system. Water take-up by the dehydrated material is very slow at room temperature. An excess of water vapor (at its saturation (liquid) vapor pressure) was allowed to stand three weeks over a one-gram sample of $Mg(OH)_2$ 90% decomposed; at the end of this period the composition still corresponded to 70% MgO. Renewal of effusion experiments with this material showed the kind of behavior indicated for rehydrated MgO on Fig. 3.

Surface cooling does not appear important in the effusion experiments. Net rates of vaporization and hence energy demands are very small. No apparent change in the steady-state pressure in the equilibrium region was observed on changing the orifice area by a factor of ten. A change would surely be observed if surface cooling by evapora-

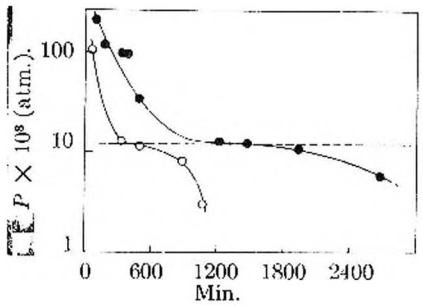

Fig. 3.—Duration of equilibrium pressures for finely divided magnesium hydroxide: ●, 1 g. of rehydrated MgO; ○, 1 g. of $Mg(OH)_2$ N. F. powder; – – – –, equilibrium pressure (Giauque and Archibald).

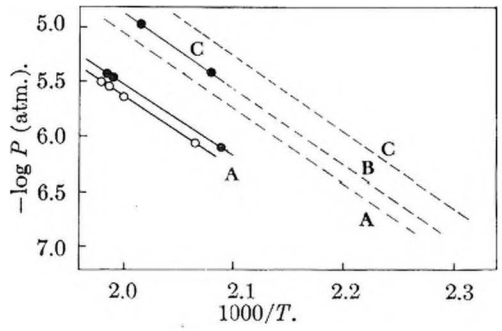

Fig. 4.—Steady-state pressures in various effusion cells for various samples of $Mg(OH)_2$: – – – –, data shown in Fig. 1; ●, 1 g. of large brucite sheets; ○, 1 g. of N. F. powder; A, $f = 3.91 \times 10^{-3}$; B, $f = 2.93 \times 10^{-3}$; C, $f = 5.35 \times 10^{-4}$.

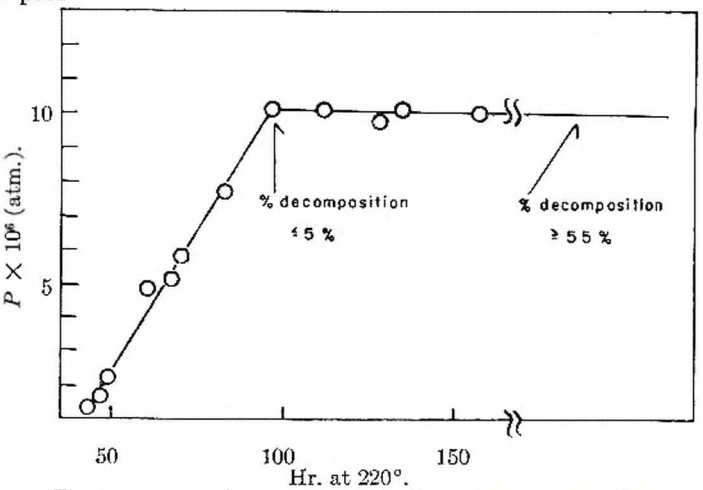

Fig. 5.—Approach to constant steady-state pressures after initial fall off at room temperature.

(18) R. J. Peavler and A. W. Searcy, *J. Am. Chem. Soc.*, **78**, 2076 (1956).

tion were an important effect. This same change in orifice area (and corresponding rate of decomposition) has a marked effect on the steady-state pressure in later stages of the decomposition as shown in Fig. 1. This comparison offers evidence that the fall-off in the latter case is associated with the low condensation coefficient rather than a manifestation of surface cooling.[19]

It should be pointed out that the estimate made of the condensation coefficient from equation 2 involves considerable uncertainty. The effect of α and A_s cannot be separated. The small value we have attributed to α might instead be characteristic of A_s; however this would require the effective vaporizing area to be exceedingly small relative to the total sample area; one would expect a more pronounced effect on grinding the sample than is observed. Some justification for assuming A_s to be the cell cross-sectional area has been found in a study of the vaporization of iodine.[6] While the two solid phase system of present concern is more complex, it has been demonstrated that the variation of P_s (in the 5–55% decomposition range) with the cell-cross sectional area A_s, A_0 held constant, is in reasonably good agreement with equation 2.

Discussion

Although a definite explanation of the effusion pressures in terms of the complex structural and diffusion effects involved on the reacting surfaces is not possible at this time, we suggest that the following features are of major importance. In the beginning stages of the decomposition only a small fraction of the magnesium hydroxide at the surface appears to be in sites most favorable for decomposition. In this part of the process the decomposition activation energy essentially corresponds to the thermodynamic heat of decomposition. Magnesium oxide formed appears to be in close contact with, perhaps essentially an integral part of, the magnesium hydroxide lattice since the recapture of water molecules with subsequent reformation of the hydroxide occurs readily. Here the condensation coefficient is very near unity. This is the first instance of which we are aware in which unit condensation coefficient has been clearly demonstrated for a decomposition reaction.

After the magnesium hydroxide in these favorable sites has been decomposed, both the rate of decomposition and the condensation coefficient decrease markedly, as concluded from P_s and its relationship to f. If only the rate of decomposition were to change, no dependence of the new steady-state pressure on orifice area should be observed unless the vaporizing area continously changes. If A_s is changing continuously, it is difficult to see how constant steady-state pressures would be observed over such a large range of per cent. decomposition. In addition P_s was found relatively insensitive to the quantity of sample in the cell. If the rate of decomposition remains constant and the condensation coefficient alone decreases, steady-state pressures should increase rather than decrease.

It is somewhat surprising that pressures in Fig. 5, showing the slow approach to the new steady-state constant pressure, are rising rather than falling. This is not a thermal equilibration problem as the sample has been at constant temperature for nearly 100 hours before the pressure plateau is reached. Rather it appears indicative of formation of a new kind of "pseudo-equilibrium" surface, with different properties from that involved in the initial phases of the decomposition. This "state" of the system appears then to remain unchanged throughout the major part of the decomposition, at least as long as water pressures and temperatures are maintained in the range shown on Figs. 1 and 4. Temperatures can be varied at random in this range and reproducible steady-state pressures observed. On one occasion a cell was cooled briefly and removed from the vacuum system and a new lid (with different orifice area) substituted; on renewing effusion experiments the expected steady-state pressures at the new f were quickly re-established. For these reasons, as well as the correlation of P_s with f already discussed, the system in this state has been said to show a pseudo-equilibrium behavior. The apparent decomposition energy, perhaps more nearly an activation energy, is larger than the thermodynamic heat by 11.4 kcal.

It is suggested by the work of others[20,21] that the large cleavage surfaces, 0001, of brucite crystals do not participate in the initial stages of the decomposition. We have observed that even after nearly complete decomposition, the external form of the brucite crystal is preserved, though it crumbles when subjected to mechanical force and is shown by X-ray powder patterns to have the MgO structure. Electron micrographs of replicas of the 0001 surface (taken with a Siemen's Elmiskop I by Dr. J. H. Luft of the Department of Anatomy, School of Medicine, University of Washington) at various stages of decomposition up to *ca.* 5% failed to show development of any detail on this smooth surface with resolution down to ten ångströms. Hence decomposition appears to occur largely at the edges, corresponding to the probable mode of growth of the original crystal. The rate of decomposition does not appear to be controlled by diffusion of water vapor out of changing long pores or crevices between 0001 layers, however; if this were the case, one would expect the pressure to fall continuously as decomposing sites receded into the crystal, particularly in measurements with large sheets of brucite. Similarly, a large effect on the steady-state pressure would be expected on grinding the crystals.

The low value of the condensation coefficient and rate of vaporization is not surprising in view of these structural characteristics and, as stated earlier, was generally anticipated from previously reported kinetic data. However, it is most surprising that extrapolation of effusion steady-state pressures to zero orifice area leads to an apparent equilibrium pressure 10^{-4} too low, but which correlates the observed pressures from all cells satis-

(19) R. Littlewood and E. Rideal, *Trans. Faraday Soc.*, **52**, 1598 (1956).

(20) D. R. Garrido, *Ion*, **11**, 206, 453 (1952).

(21) S. J. Gregg and R. J. Razouk, *J. Chem. Soc.*, SI, 36 (1949).

factorily. This extrapolation must in fact be inaccurate; the steady-state effusion pressure must rise to the true equilibrium value in the limit of zero orifice (orifices materially smaller than those used in this work are not experimentally practical). For the true equilibrium pressures to be maintained in effusion cells, the decomposing crystal surfaces must be able to re-form sites kinetically favorable for decomposition. Since MgO and $Mg(OH)_2$ both have negligible vapor pressures at the temperatures of the effusion work, reorientation cannot occur by a vapor phase mechanism and does not appear to occur readily by solid state diffusion.

Similar difficulties may well be encountered in other decomposition reactions, particularly when the solid phases involved have very low vapor pressures. It is apparent that effusion results must be interpreted with caution in such cases and that the method is not well-suited for determination of equilibrium properties. Without the availability of the work of Giauque and Archibald in the present system, the brief leveling off at the true equilibrium pressure might well have been ignored. It also has been demonstrated that even though an apparently normal extrapolation of steady-state pressures to zero orifice can be made, it may not lead to the correct result. It may be noted, however, that the effusion method has been applied successfully in a study of the decomposition of lithium hydroxide.[22]

This work was done with financial support of the Office of Ordnance Research, U. S. Army.

(22) N. W. Gregory and R. H. Mohr, *J. Am. Chem. Soc.*, **77**, 2142 (1955).

THE CRITICAL MICELLE CONCENTRATION OF ETHER ALCOHOL SULFATES, $R(OC_2H_4)_iOSO_3Na$[1]

BY J. K. WEIL, R. G. BISTLINE, JR., AND A. J. STIRTON

Eastern Regional Research Laboratory,[2] *Philadelphia 18, Pennsylvania*

Received April 21, 1958

The critical micelle concentration (c.m.c.) of sodium hexadecyl and octadecyl ether alcohol sulfates ($R(OC_2H_4)_iOSO_3Na$, i = 1,2,3,4) was measured by surface tension, dye titration and conductance methods. In moles per liter × 10,000 the values were 2.1, 1.2, 0.7, 0.8 in the hexadecyl series and 1.9, 0.8, 0.5, 0.4 in the octadecyl series, respectively. Although solubility as measured by the Krafft point increased with the number of ethenoxy groups, the c.m.c. decreased; apparently as a result of the combined effects of increased hydrophilicity and greater chain length.

Sulfated ether alcohols are surface active agents of increasing importance for detergent and allied uses. In a previous report[3] we have shown that sodium salts of sulfated ethenoxylated tallow alcohols with low ethenoxy content are considerably more soluble than the corresponding alcohol sulfates and have similar surface active properties. It seems desirable therefore to study the effect of ethenoxylation on fundamental solution properties such as critical micelle concentration (c.m.c.) for this class of compounds.

The commercial method for preparing ether alcohols, *i.e.*, the reaction of ethylene oxide with an appropriate fatty alcohol, results in a mixture, $R(OC_2H_4)_nOH$, where n is known only as an average value. This study is concerned with chemical individuals where n becomes i, or a specific integer, prepared through the Williamson synthesis from known purified starting materials.

Experimental

Ether Alcohol Sulfates.—Ether alcohols of known composition were prepared from the alkyl bromide and a glycol by a method described to us by Wrigley.[4] The pure ether alcohols were sulfated in a manner similar to that described elsewhere.[5] A 15% excess of chlorosulfonic acid was added dropwise to a stirred solution of 0.1 mole of ether alcohol in 150 ml. of chloroform cooled in an ice-bath at 10–20°. When the addition was completed the reaction mixture was allowed to warm to room temperature and stirring was continued for an hour. After chilling again to 10°, 100 ml. of absolute methanol was added and the solution was neutralized with 18 *N* sodium hydroxide. The product was crystallized and filtered from the reaction mixture, redissolved in hot absolute ethanol, insoluble inorganic salt was filtered from the hot solution and the product was recrystallized from the filtrate at room temperature. In some instances a second recrystallization from absolute alcohol was required. Carbon, hydrogen, sulfur[6] and sodium analyses of the first three members of each series were found to be within 0.3% of the theoretical value. The compound containing four ethenoxy groups was somewhat more difficult to purify.

Surface Tension.—The duNoüy tensiometer was used to measure surface tension. Since little change was observed with temperature variation over a limited range, measurement was made at room temperature, 25 ± 1°. Appropriate corrections[7] were applied to the readings to obtain surface tension in dynes per centimeter. Figure 1 is a surface tension *versus* log C plot for the ether alcohol sulfates derived from hexadecanol and Fig. 2 is a similar plot for the ether alcohol sulfates derived from octadecanol. The solutions were allowed to age one hour prior to measurement and measurements were repeated until four identical values were obtained. Since Nutting and co-workers[8] have shown that most of the change of surface tension with time, for sodium alkyl sulfates, occurs within 2 to 60 minutes, the values reported may be considered to be very nearly true equilibrium values.

Dye Titration.—Pinacyanole chloride was used as described by Corrin, Klevens and Harkins.[9] Five ml. of a

(1) Presented at the Meeting in Miniature of the Central Pennsylvania Section, American Chemical Society, University Park, Pa., March 15, 1958.

(2) Eastern Utilization Research and Development Division, Agricultural Research Service, U. S. Department of Agriculture.

(3) R. G. Bistline, Jr., A. J. Stirton, J. K. Weil and E. W. Maurer, *J. Am. Oil Chemists' Soc.*, **34**, 516 (1957).

(4) A. N. Wrigley, Ph. D. Dissertation, Temple University, 1958.

(5) J. K. Weil, A. J. Stirton and E. W. Maurer, *J. Am. Oil Chemists' Soc.*, **32**, 148 (1955).

(6) Microanalysis for C, H and S performed by Miss Laverne Scroggins.

(7) W. D. Harkins and H. F. Jordan, *J. Am. Chem. Soc.*, **52**, 1751 (1930).

(8) G. C. Nutting, F. A. Long and W. D. Harkins, *J. Am. Chem. Soc.*, **62**, 1496 (1940).

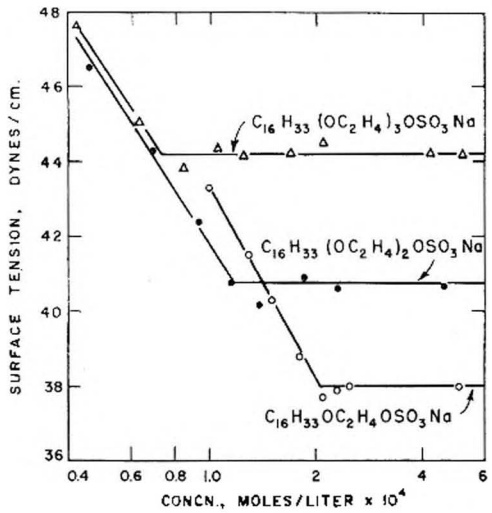

Fig. 1.—Surface tension *versus* logarithm of concentration in moles per liter for aqueous solutions of ether alcohol sulfates from hexadecanol.

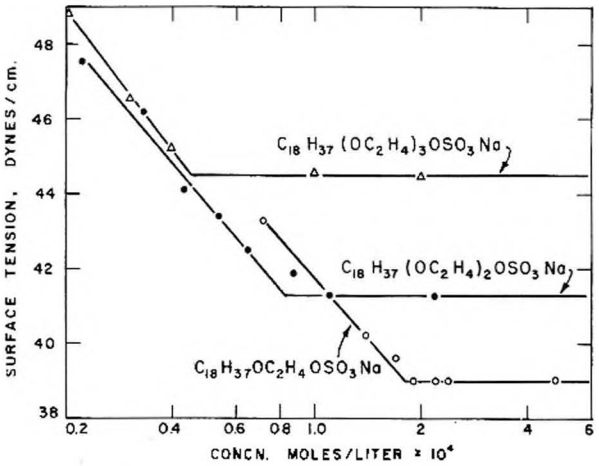

Fig. 2.—Surface tension *versus* logarithm of concentration in moles per liter for aqueous solutions of ether alcohol sulfates from octadecanol.

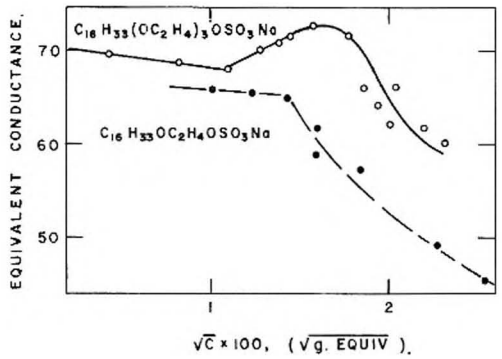

Fig. 3.—Variation of equivalent conductance with concentration of sodium hexadecyloxyethyl sulfate and sodium hexadecyloxyethoxyethoxyethyl sulfate at 25.00 ± 0.05°.

solution of 10^{-5} molar pinacyanole containing about twice the critical concentration of surface active agent was titrated with a solution containing only 10^{-5} molar pinacyanole. The c.m.c. was calculated from the titration required to obtain a visible color change from blue to purple.

Conductance.—A Leeds and Northrup conductivity bridge operating at 1,000 cycles was used to measure conductance at 25 ± 0.05°. A Jones cell, Leeds and Northrup type A,[10] having a cell constant of 0.050 ± 0.001 was used for all measurements. Surfactants were dissolved in water which had been passed through a column of Amberlite MB-1[10] to reduce specific conductance to $0.53-0.56 \times 10^{-6}$ mho, and values were corrected by subtracting the solvent conductance. Resistances above 10,000 ohms were determined by connecting a 10,000 resistance in parallel with the unknown. Figure 3 shows the conductance curve for sodium hexadecyloxyethyl sulfate [$C_{16}H_{33}OC_2H_4OSO_3Na$] and sodium hexadecyloxyethoxyethoxyethyl sulfate [$C_{16}H_{33}(OC_2H_4)_3OSO_3Na$].

Krafft Point.—The Krafft point, which is significant with respect to synthetic detergents as well as soaps, was used as a measure of the comparative solubility of the eight compounds. It was determined as the temperature at which a uniform 1% dispersion changed sharply to a clear solution on gradual heating.[11] The cloud point, or the temperature at which a clear 1% solution became turbid on gradual cooling, is less reproducible, but it is more important in defining the lowest temperature which may be used in the c.m.c. measurements.

Discussion of Results

Table I lists the c.m.c. for the ether alcohol sulfates at 25°, the Krafft points and cloud points and the c.m.c. for sodium hexadecyl sulfate at 30°. Since the Krafft points of sodium hexadecyl sulfate and sodium octadecyl sulfate are above room temperature we have no comparable c.m.c. for sodium octadecyl sulfate; and it was necessary to base the value for sodium hexadecyl sulfate on surface tension measurements at 30°. The agreement with Powney and Addison[12] may be regarded as acceptable when allowances are made for differences in temperature and for differences in the minimum observed. Generally good agreement is apparent in comparing the c.m.c. determined by dye titration, conductance and surface tension methods. The methods showed least agreement in the case of sodium octadecyloxyethyl sulfate, probably because the temperature of measurement was below the cloud point and the clarity of the detergent solution used for dye titration could not be assured.

The conductance curves of Fig. 3 show a considerable difference between the conventional shape for sodium hexadecyloxyethyl sulfate and that for sodium hexadecyloxyethoxyethoxyethyl sulfate. McDowell and Kraus[13] have shown increases above the c.m.c. for cationic surfactants with bulky groups at the hydrophilic end which are the same as that shown here by the compound with three ethenoxy groups. Thus we may determine the c.m.c. of the more highly ethenoxylated members of the series from the point where conductance increases rather than from the usual decrease. The conductance curve for sodium hexadecyloxyethoxyethyl sulfate, [$C_{16}H_{33}(OC_2H_4)_2OSO_3Na$] lies between the two curves shown on Fig. 3 and shows a smaller downward inflection at the c.m.c.

On first consideration it might be expected that ether alcohol sulfates with higher ethenoxy content would have higher c.m.c. values as a result of an

(9) M. L. Corrin, H. B. Klevens and W. D. Harkins, *J. Chem. Phys.*, **14**, 480 (1946).

(10) Reference to a manufactured product does not constitute recommendation by the U. S. Dept. of Agriculture over similar products not mentioned.

(11) M. Démarcq and D. Dervichian, *Bull. soc. chim.*, **12**, 939 (1945).

(12) J. Powney and C. C. Addison, *Trans. Faraday Soc.*, **33**, 1243 (1937).

(13) M. J. McDowell and C. A. Kraus, *J. Am. Chem. Soc.*, **73**, 2173 (1951).

TABLE I

SOLUTION PROPERTIES OF ETHER ALCOHOL SULFATES

Compound	C.m.c., moles/L., 25°, × 10,000 Conductance method	Surface tension method	Dye titration method	Krafft point 1% concn.	Cloud point, 1% concn.
$C_{16}H_{33}OSO_3Na$		4[a]		45°	30°
$C_{16}H_{33}OC_2H_4OSO_3Na$	2.34	2.1	2.2	36°	12°
$C_{16}H_{33}(OC_2H_4)_2OSO_3Na$	1.34	1.2	1.4	24°	8°
$C_{16}H_{33}(OC_2H_4)_3OSO_3Na$	1.23	0.7	1.0	19°	0°
$C_{16}H_{33}(OC_2H_4)_4OSO_3Na$		0.8	1.0		<0°
$C_{18}H_{37}OC_2H_4OSO_3Na$		1.9	1.1	46°	30°
$C_{18}H_{37}(OC_2H_4)_2OSO_3Na$		0.8	0.7	40°	19°
$C_{18}H_{37}(OC_2H_4)_3OSO_3Na$		0.5	0.5	32°	12°
$C_{18}H_{37}(OC_2H_4)_4OSO_3Na$		0.4	0.4	18°	12°

[a] Measurements at 30°.

increase in the hydrophilic nature of the compound. It was rather surprising then to find that as ethenoxylation was increased, the first three members of both ether alcohol sulfate series showed a small but definite decrease in c.m.c.

Klevens[14] has shown that the entire chain length rather than the length of the hydrophobic portion determines the c.m.c. of common anionic detergents; *e.g.*, "thus a C_{13} fatty acid, a C_{12} sulfonate, and a C_{11} sulfate all have c.m.c. values in the same range." Specifically the addition of a hydrophilic oxygen atom between a carbon atom and a sulfur atom of an alkyl sulfonate does not cause an increase but rather a decrease in c.m.c., similar to that produced by a methylene group in the same position. If this relationship would hold for the ether alcohol sulfates, however, a much greater decrease in c.m.c. with ethenoxylation would be shown, *i.e.*, a decrease by a factor of eight for each ethylene oxide unit.

It seems apparent that the end result in this case is a combination of two or more effects which result in slight decreases in critical micelle concentration with increased ethenoxy content. Since generally low values have been recorded for the c.m.c. of non-ionic type surfactants[15,16] this decrease may be explained by a decrease in anionic properties with a corresponding increase in non-ionic properties as ethenoxy content is increased. Further evidence for this transition toward non-ionic properties is found in the abnormal shape of the conductance curve of the more highly ethenoxylated materials above the c.m.c. which indicates an increase in bulk at the hydrophilic end.

The c.m.c. decreases with increase in the number of ethenoxy groups from 0 to 1 to 2 to 3, but the difference in c.m.c. between compounds with 3 and 4 groups is in doubt. Examination of higher members of the series would be required to establish the trend; however, purification difficulties increase with the number of ethenoxy groups.

It is interesting to observe, from Figs. 1 and 2, that surface tension values below the c.m.c. for either the hexadecyl or octadecyl series, fall on a common line for the series, within experimental error. In each case the c.m.c. is determined by the intersection of a common line with the horizontal line of surface tension values. Thus members of either series with higher surface tension at the higher concentration have lower c.m.c.

Preliminary observations by the dye titration method showed that sulfated ethenoxylated tallow alcohols $R(OC_2H_4)_nOSO_3Na$[3] with an average value of about $n = 2$ had nearly the same c.m.c. as that for the corresponding pure compound, $i = 2$.

Acknowledgment.—The authors are indebted to A. N. Wrigley for advice and assistance in preparing the ether alcohols.

(14) H. B. Klevens, *J. Am. Oil Chemists' Soc.*, **30**, 74 (1953).

(15) M. Cohen, *Mem. services. chim. état*, **36**, 93 (1951).

(16) L. Hsiao, H. N. Dunning and P. B. Lorenz, THIS JOURNAL, **60**, 657 (1956).

HYDROTHERMAL REACTIONS UNDER SUPERCRITICAL CONDITIONS. V. REACTIONS BETWEEN SILICA AND ALKALINE EARTH METAL SALTS

BY JAMES F. CORWIN

Contribution from the Department of Chemistry, Antioch College, Yellow Springs, Ohio

Received April 25, 1958

The reaction of dilute solutions of the salts of the alkali earth metals with silica has been investigated by using the devitrification of clear fused quartz as a measure of the rate of reaction, and X-ray, optical and chemical analysis as a measure of the structure of the crystallized material. By carrying out these reactions under controlled conditions using compounds of the alkaline earth metals it has been found that the crystalline structures resulting from the reactions of these solutions vary in a systematic way from α-cristobalite and several other modifications of the silica structure to silicate minerals. The rate of reaction and the formation of crystalline structures are correlated with the initial pH of the solution and the relative dimensions of the ions involved. On the basis of these correlations, the natural occurrence of α-quartz and talc is inferred since the concentration of these dilute solutions is quite similar to that of ground water.

Introduction

The investigation of the reactions of the alkaline earth metal oxides with silica glass[2] and a more complete evaluation of calcium and strontium hydroxide reactions[3,4] has shown that the presence of these materials in high temperature water contributes to the formation of β- and finally α-cristobalite from fused silica in those cases where the silicates formed are soluble enough to maintain, by hydrolysis, the necessary pH for this formation.[5] These results failed to explain why α-quartz which is the result of the reactions of the alkali metal compounds with silica under the same conditions was not formed in spite of the fact that α-quartz is found in nature surrounded by alkaline earth metal minerals. Another point left unexplained is the formation of β-cristobalite as an initial, stable, crystalline form when this form has been generally characterized as an unstable intermediate.

In order to try to find an answer to the first of these questions, a series of experiments involving other calcium compounds usually found in nature was planned, and to answer the second, a series using the fluorides of the alkaline earth metals which are in general less soluble than the oxides or hydroxides, so that the reactions would be slower and some insight into the nature of the initial phases of the reactions could be obtained.

Experimental

The equipment and methods used for reactions and for the analysis of reaction products were identical with those already described.[2,3] All chemicals used conformed to C.P.A.C.S. Standards of Purity.

Results and Discussion

Table I contains the results obtained when the alkaline earth fluorides were used.

BeF_2 which is very soluble in water at room temperature gave quite different results from those obtained from the remainder of the alkaline earth metal fluorides. When the runs were made at the same concentration, the BeF_2 reaction resulted in soluble compounds and only 4.0 mg. of solid was recovered. A second pair of runs then was made using 0.1 N BeF_2 and solid material was formed, but crystal analysis gave new materials that could not be identified by current X-ray files and optical constants.

The initial pH of all the solutions is low enough that little devitrification would be expected in the time used for the experiments; however, the hydrolysis of fluorides would make the solution alkaline enough to allow the devitrification reaction to proceed.[5]

Since the calcium salts are more prevalent in nature than the other members of the alkaline earth metal group, a number of calcium salts were used under the same conditions. A set of experiments designed to re-evaluate the reaction of MgO with water and silica was performed and these with the data obtained when calcium salts were used are contained in Table II.

The calcium phosphates showed little devitrification of the silica rod, and the X-ray data showed no silica in the solid material recovered from the reaction vessel. Chemical analysis confirmed these results since almost all the silica was found in the solution. Analysis of the solid showed 3.0% SiO_2 in the solids from $Ca(H_2PO_4)_2 \cdot H_2O$, 0.2% from $CaHPO_4 \cdot 2H_2O$ and 7.8% from $Ca_3(PO_4)_2$.

$CaSO_4$ and $CaCl_2$ gave very similar results to those obtained when $Ca(OH)_2$ is used[3]; however, the $CaCl_2$ reaction was accompanied by a considerable reaction with the vessel walls and the solid material was colored with iron and chromium compounds.

The reactions of silica with $CaCO_3$ resulted in a mixture of crystalline materials which gave X-ray patterns similar to, but definitely different from, crystalline materials obtained in the formation of synthetic Tobermorite ($XCaO \cdot SiO_2 \cdot YH_2O$ where $X \sim 1$ and $Y \sim 1$). This material could be of similar composition, but with variations in the amount of CaO, SiO_2, H_2O ratio. This would account for the X-ray patterns of the crystalline material.

The MgO experiments were conducted as a repetition of earlier work[2] where the reaction resulted in a coating on the silica rod that showed no

(1) This research was supported in part by the United States Air Force through the Air Force Office of Scientific Research of the Air Research and Development Command, under contract No. AF 18(600)1490. Additional support was received from the U. S. Army Signal Corps (Contract No. DA 36-039 SC-64605) through its Signal Corps Engineering Laboratories at Fort Monmouth, New Jersey. Reproduction in whole or in part is permitted for any purpose of the United States Government.

(2) J. F. Corwin, R. G. Yalman, J. W. Edwards and G. E. Owen, Paper No. 1, THIS JOURNAL, **61**, 939 (1957).

(3) J. F. Corwin, R. G. Yalman, J. W. Edwards and E. R. Shaw, Paper No. II, *ibid.*, **61**, 941 (1957).

(4) J. F. Corwin, R. G. Yalman, J. W. Edwards and E. R. Shaw, Paper No. IV, *ibid.*, **61**, 1437 (1957).

(5) R. G. Yalman and J. F. Corwin, Paper No. III, *ibid.*, **61**, 1432 (1957).

TABLE I

Fluoride concn. 0.025 *N*, 10 g. of silica glass rod, 400°, 125 ml. vol., 340 atm., 48 hr.

Fluoride	pH_i[a]	pH_f[b]	Wt. loss silica rod, %	Optical and X-ray data of solids and devitrified material
BeF_2 (1)	5.8	3.3	2.94	Reaction products soluble. Only 4 mg. solid recovered
BeF_2[c] (2)	5 8	2.5	5.25	40–50% irregular isotropic. n = 1.440–1.450 30–40% irregular birefringent. n = 1.510–1.520 X-ray gives pattern unidentified by A.S.T.M. file
MgF_2	5.7	3.2	1.64	70–80% birefringent. n = >1.400 MgF_2 X-ray mostly MgF_2. Small amount of talc, $3MgO{\cdot}4SiO_2{\cdot}H_2O$
CaF_2	4 5	4 0	5.26	X-Ray mostly CaF_2, 10% β-cristobalite
SrF_2	6.2	3.6	14 7	X-Ray β-cristobalite and SrF_2
BaF_2	5.8	3.2	14.6	X-Ray β-cristobalite and BaF_2

[a] Initial pH at room temperature. [b] Final pH at room temperature. [c] More concentrated 0.10 *N* solution used.

TABLE II

Salt concn. 0.025 *N*, 10 g. of silica glass rod, 400°, 125 ml. vol., 340 atm., 48 hr.

Salt	pH_i[a]	pH_f[b]	Wt. loss silica rod, %	Optical and X-ray data devitrified material
$Ca(H_2PO_4)_2H_2O$	3.2	2 5	1.27	50-60% crystalline. n = 1.630–1.640 X-Ray complicated, but $Ca_2P_2O_7$-I was identified
$CaHPO_4{\cdot}2H_2O$	6.8	5.6	1.45	n = 1.64 1.65. X-Ray hydroxy apatite structure, $Ca_3(PO_4)_2$ or $Ca_{10}(OH)_2(PO_4)_6$
$Ca_3(PO_4)_2$	6 9	5.9	1.45	Same as $CaHPO_4{\cdot}2H_2O$
$CaSO_4$	6.8	5.2	3.19	X-Ray β-cristobalite. Anhydrous $CaSO_4$
$CaCO_3$	9.6	6.3	4.60	Not identifiable by A.S.T.M. file
$CaCl_2$	5.8	5.2	9.26	X-Ray β-cristobalite
MgO	10.3	5.8	4.56	X-Ray very poorly crystallized. $3MgO4SiO_2{\cdot}H_2O$ (talc) amorphous material also
MgO	10.3	8.8	No silica used	X-Ray- small crystalline size $Mg(OH)_2$ (Brucite)

[a] Initial pH at room temperature. [b] Final pH at room temperature.

crystalline character. In this work the rod was scraped vigorously in order to obtain all of the devitrified material. This technique resulted in the identification of some crystalline material.

Conclusions

Due to solubility of the reactant and of the products when BeF_2 was used, the results definitely separate this reaction from that of the other alkaline earth metal compounds. Unlike the others, the hydrolysis of the salt cannot be used to explain the reaction since BeO[2] did not show any devitrification reaction under the same conditions. Before conclusions can be reached concerning the reactions of beryllium salts further investigation is indicated.

The remainder of the fluoride work shows that the alkaline earth metal fluorides react by two steps, first the hydrolysis of the fluoride to form HF and the corresponding metal hydroxide and the OH^- ion from the hydroxide causes the devitrification to proceed. This is the same reaction postulated for NaF.[5] Further proof that the reaction is the same is shown by the similarity in solid reaction products to those reported.[2-4] The difference in reaction is primarily one of rate since the fluorides are so insoluble even in hot water the reactions are slowed down by the reduction in concentration of the OH^- ion. The faster reactions of the hydroxides[2] in some cases caused coatings over the surface, and a subsequent reduction in devitrification which did not coincide with the basicity of the hydroxide. When the fluorides are used no such interference with the reaction is encountered, and the amount of devitrification coincides with the increase in basic quality of the alkaline earth metals.

The formation of talc (Table I) in the MgF_2 run is similar to the other alkaline earth metals since talc is an alternate layer structure of β-cristobalite and brucite, $Mg(OH)_2$.[6] MgO alone under the same conditions of temperature and pressure forms brucite (Table II). Talc is also formed when MgO is reacting with SiO_2, but much amorphous material also is formed due to the speed of reaction.

The formation of β-cristobalite is expected due to the low pH of the solution[5] in all of the alkaline earth metal reactions, but in the case of Ca, Sr and Ba salts the difference in structural dimensions of the hydroxides and the packing in their crystal forms, they will not fit between the layer structure which is the proposed form of the β-cristobalite.[7] Thus the two insoluble materials, β-cristobalite and the fluorides, are found separate in the solid phase.

Although crystalline α-quartz is found in nature along with alkaline earth metal minerals, none has been found in any of our experiments. If the quartz were formed at the same time as the other minerals from ground water reactions, it was probably due to the presence of soluble alkali metal salts that have since been leached from the mass, and not to reactions of any of the alkaline earth metal salts. Even when reaction times were

(6) L. Pauling, *Proc. Nat. Acad. Sci.*, **14**, 603 (1928).

(7) F. Laves and W. Nieuwendkamp, *Z. Kristallographie*, **90**, 273, 279, 377 (1935).

extended to thirty days under supercritical conditions, no α-quartz was formed.

Acknowledgments.—The author wishes to acknowledge the help of Mr. Joseph Strauch who performed the chemical analysis and optical work, and of Dr. Warren O. Groves and Mr. Ralph Ferguson of the Monsanto Chemical Company, Dayton, Ohio, for the X-ray patterns and their analysis.

TERNARY SYSTEM ISOAMYL ALCOHOL–ISOPROPYL ALCOHOL–WATER AT 10, 25 AND 40°

BY VERNON W. ARNOLD AND E. ROGER WASHBURN

Department of Chemistry and Chemical Engineering, University of Nebraska, Lincoln, Nebraska

Received April 28, 1958

Isopropyl alcohol is completely miscible with water and with isoamyl alcohol at ordinary temperatures while the latter two liquids have limited miscibility in each other. The ternary solubility curves and the distribution of isopropyl alcohol between the conjugate liquids have been determined at 10, 25 and 40°.

Introduction

The solubility curves were determined by an extension of Alexejeff's method[1] as used for ternary systems by Jones and Grigsby.[2] This method, in common use for binary solubilities, has the advantage that repeated observations may be made on the same sample. The temperatures, at which cloudiness indicated the appearance of a second liquid phase, were measured with a thermistor. The proportions of water in the less dense, or water poor, phases were determined by titration with Karl Fischer reagent as was done for some solutions by Purnell and Bowden.[3]

Experimental

Materials.—The isoamyl alcohol, 3-methyl-1-butanol, used in most of this work was prepared from isobutyl bromide by a method similar to that described by Timmermans and Hennaut-Roland.[4] Isobutylmagnesium bromide was allowed to react with paraformaldehyde. The resulting compound was hydrolyzed and the alcohol which was formed was purified until the constants recorded in Table I for sample A were obtained.

Some distribution measurements were made at 40° with isoamyl alcohol, 3-methyl-1-butanol, obtained from the Fisher Scientific Company. This material had the constants listed for sample B in Table I. The optical rotation indicated the presence of some of the optically active isomer 2-methyl-1-butanol.

The isopropyl alcohol was obtained from the Eastman Kodak Company. After intensive drying with active calcium oxide, the alcohol was distilled yielding material having the constants recorded in Table I.

TABLE I

	B.p. (cor.), °C.	d_4^{25}	n_D^{25}
Isoamyl alcohol A	131.9	0.8051	1.4048
Isoamyl alcohol B	...	.8073	1.4052
Isopropyl alcohol	82.2	.7809	1.3748

Solubility Curves.—The compositions of ternary solutions saturated with respect to isoamyl alcohol or water or both of these materials were determined in the following manner. Isoamyl alcohol and water, in a known ratio by weight, were placed in a specially prepared saturation cell. This cell was made from a 50-ml. volumetric flask by the addition of a second glass stoppered neck to the bulb of the flask. A thermistor, Type 14B from the Western Electric Company, fitted with a ground glass connector was incorporated in one of the necks of the cell and was used as a resistance thermometer to determine the temperature of the contents of the cell.

Measurements had been made of the resistances of the thermistor at temperatures determined with a platinum resistance thermometer the constants of which had been determined by the Bureau of Standards. An equation of the type

$$\log R = \frac{A}{t^0 + C} + B$$

was found to be suitable. The constant C, 323.5, was found by a selected point method. The constants A and B were then determined by the method of least squares to be 2091.2 and −2.7168, respectively. The final equation was used in the form

$$t^0 = \frac{2091.2}{\log R + 2.7168} - 323.5$$

The thermistor had a resistance of 3577 ohms at 10° and 1086.5 ohms at 40°.

The cell containing the heterogeneous mixture of isoamyl alcohol and water was heated in a variable temperature water-bath, to about 45°. Isopropyl alcohol was then added until homogeneity resulted, and the amount of alcohol added was determined by weight. The mixture was shaken mechanically in the bath while the temperature was lowered slowly until a uniform cloudiness throughout the mixture indicated the appearance of a second liquid phase. The temperature then was raised slowly until the cloudiness disappeared. This was repeated until temperatures corresponding to the appearance and disappearance of the second liquid phase showed satisfactory agreement. The amount of isopropyl alcohol in the mixture then was increased by a small addition. The described procedure was repeated to determine the new temperatures corresponding to the appearance and disappearance of the second liquid phase for the new concentrations. Five or more such pairs of concentration–temperature measurements were determined over the temperature range from 10 to 40° for each of fourteen different weight ratios of isoamyl alcohol to water.

A curve, mean solution temperature *vs.* weight per cent. of isopropyl alcohol, was then plotted for each of the fourteen ratios. In determining the mean solution temperature, the temperature corresponding to the appearance of a second liquid phase was weighted twice as heavily as that corresponding to its disappearance. The concentrations of isopropyl alcohol corresponding to 10, 25 and 40° were read from these curves. The concentrations of the other two components were calculated from their weight ratios and the concentration of isopropyl alcohol. These results are recorded in Table II.

The solubility of isoamyl alcohol in water was determined by Alexejeff's method[1] using sealed tubes. The solubility of water in isoamyl alcohol was determined by analyzing saturated solutions at each of the temperatures with Kar Fischer reagent.

(1) M. W. Alexejeff, *Bull. soc. chim.*, **38**, 145 (1882).

(2) H. E. Jones and W. E. Grigsby, *Ind. Eng. Chem.*, **44**, 378 (1952).

(3) J. H. Purnell and S. T. Bowden, *J. Chem. Soc.*, 539 (1954).

(4) J. Timmermans and E. Hennaut-Roland, *Anal. soc. espan. fis. Quim.*, **27**, 460 (1929).

TABLE II

SOLUBILITIES AT 10, 25 AND 40°

The plait points are indicated with asterisks.

Isoamyl alc., wt. %	Water, wt. %	Isopropyl alc., wt. %
	10°	
2.8	97.2	0.0
2.0	95.1	2.9
2.0	88.6	9.4
2.7	78.3	19.0
3.5	75.8	20.7
5.2	71.4	23.4
8.3	65.6	26.1
10.8	61.1	28.1
14.0	55.7	30.3
19.7	46.7	33.7
26.1	38.1	35.8
32.1	31.9	36.0
36.7	28.2	35.1
46.4	22.2	31.4
52.3	19.7	28.0
60.6	16.4	23.0
70.9	13.5	15.7
91.0	9.0	0.0
*14	*56	*30
	25°	
2.4	97.6	0.0
2.0	95.1	2.9
2.0	88.6	9.4
2.8	81.0	16.2
3.6	78.5	18.0
5.4	73.8	20.9
8.5	67.5	24.0
11.1	62.9	26.0
14.4	57.3	28.4
20.2	47.9	32.0
26.8	39.0	34.3
32.8	32.7	34.5
37.6	28.8	33.6
47.5	22.7	29.8
53.5	20.1	26.4
62.2	16.8	21.0
72.5	13.8	13.8
90.2	9.8	0.0
*14	*58	*28
	40°	
2.2	97.8	0.0
2.0	95.1	2.9
2.0	88.6	9.4
2.9	83.0	14.1
3.7	80.4	16.0
5.5	75.4	19.1
8.7	68.9	22.4
11.4	64.2	24.5
14.6	58.3	27.1
20.5	48.6	30.9
27.2	39.6	23.3
33.4	33.2	33.4
38.2	29.3	32.5
48.4	23.2	28.4
54.4	20.5	25.1
63.5	17.2	19.3
74.1	14.1	11.8
86.6	10.4	0.0
*12	*63	*25

The plait points were determined by means of large scale conjugation curves on triangular plots. The values agree with those obtained by the method of Treybal, Weber and Daley[5] within ±2.0%.

There is a region in the water-rich part of the phase diagram in which the compositions of the saturated ternary solutions do not vary a measurable amount with change in temperature from 10 to 40°. The solubility curves for the three temperatures are almost indistinguishable in this region. Compositions between which the three solubility curves must pass were determined. Isoamyl alcohol was added slowly, with shaking, to mixtures of isopropyl alcohol and water. When the time required for the solution of one drop of isoamyl alcohol became great, the temperature was varied from less than 10° to more than 40° without any noticeable change in the appearance of the clear solution. This composition was recorded. Two drops of isoamyl alcohol then were added causing a slight cloudiness which persisted throughout the same temperature range. This composition was recorded. The difference in composition was of the order of a tenth of one per cent. Two such pairs of determinations were made. The means of the results of each pair of these determinations are the identical compositions recorded in the second and third rows for each of the three temperatures in Table II.

Distribution.—Mixtures of the three components were prepared in such proportions by weight that two liquid layers were present at equilibrium. The mixtures were shaken in a constant temperature bath at the desired temperature until equilibrium was reached. The layers were then allowed to separate. Samples of the less dense, or water poor, layers were then removed and the proportions of water were determined by analysis with Karl Fischer reagent. The original gross compositions of the mixtures then were plotted on a large scale graph of the ternary solubility data. The water content of the less dense phase of each mixture was located on the solubility curve. Straight tie lines were then drawn through the corresponding gross compositions and solubilities of the phases of lower density. The proportions of the other components in the less dense layers and the compositions of the more dense conjugate layers were then read from the intersections of the tie lines with solubility curves. Because of the larger proportions of water in the more dense layers, analysis for water with the Karl Fischer Reagent was not as accurate as by the graphical method. The tie line or distribution data are recorded in Table III. "B" refers to Sample B of isoamyl alcohol listed in Table I. The analyses of the conjugate solutions containing isoamyl alcohol B were accomplished by the use of refractive index–composition curves.

Discussion

Ternary systems having the same pair of partly miscible liquids, isoamyl alcohol and water, but with methyl,[6] ethyl[6] and *n*-propyl[7] alcohols as the consolute liquid are represented with this system in Fig. 1. As would be expected, an increase in the length of the carbon chain of the consolute alcohol increases the proportion of the consolute alcohol in the less dense, or water poor, phase. The curve representing isopropyl alcohol lies between the curves for *n*-propyl and ethyl alcohols. The same order of increasing tendencies for these consolute alcohols to enter the less dense phase was noted in

(5) R. E. Treybal, L. D. Weber and J. F. Daley, *Ind. Eng. Chem.*, **38**, 817 (1946).

(6) F. Fontein, *Z. physik. Chem.*, **73**, 212 (1910).

(7) J. Coull and H. B. Hope, THIS JOURNAL, **39**, 967 (1935).

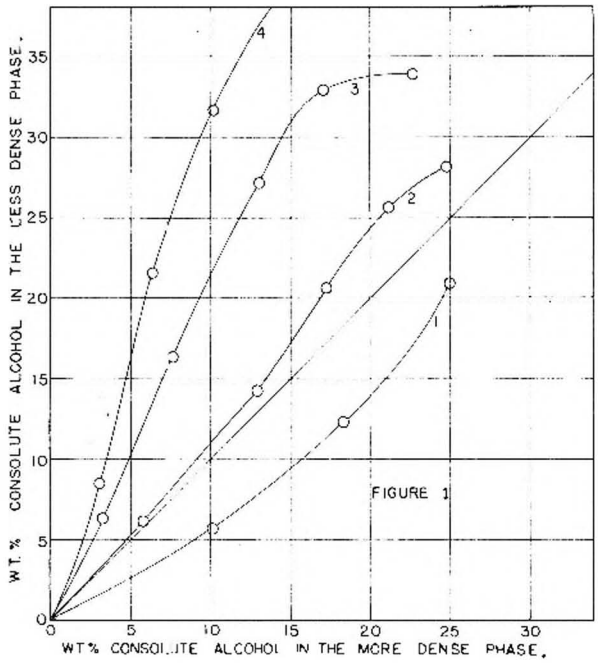

Fig. 1.—Distribution of several alcohols between isoamyl alcohol and water.

Curve	*Consolute alcohol*	*Temp., °C.*
1	Methyl	28
2	Ethyl	15.5
3	Isopropyl	25
4	*n*-Propyl	25

systems involving cyclohexane, in place of isoamyl alcohol, as the liquid partly miscible with water.[8] If the distribution of the consolute alcohols is determined by the relative tendencies for hydrogen bonding in the conjugate layers then isopropyl alcohol must have a greater tendency to combine with water by hydrogen bonding than does *n*-propyl alcohol. This is in line with the observation that the contraction in volume which occurs when isopropyl alcohol is dissolved in water is greater than the contraction observed for solutions of *n*-propyl alcohol in water but smaller than observed with aqueous solutions of methyl or ethyl alcohols.[9]

Isoamyl alcohol is more effective than cyclohexane in extracting each of the four lower alcohols from aqueous solutions. It is not obvious how relative tendencies for hydrogen bonding can account for *all* of these cases of competitive solubility.

If the assumptions are made that the association of isopropyl alcohol dissolved in isoamyl alcohol is chiefly to the dimeric form while the monomeric form is distributed between the isoamyl alcohol and water layers, the ideas of Moelwyn-Hughes[10] may be employed for the calculation of equilibrium constants and related quantities.

These ideas lead to the conclusion that a plot of the ratios of the concentrations of isopropyl alcohol in the isoamyl alcohol layers to the concentrations in the water layers as the ordinates *versus* the concentrations in the water layer as the abscissas should yield a straight line. The intercept of this line with the axis of ordinates is the equilibrium constant, K_1, for the distribution of the monomer. The slope is equal to $2K_1^2/K_2$ where K_2 is the dissociation constant for the dimeric form of the isopropyl alcohol.

Smooth curves rather than straight lines are obtained for this system. The initial slopes increase with increase in temperature and at 25 and 40° the slopes are so great that it is not possible to obtain a value for the intercept in which we can have confidence. The great increase in initial slope and the very pronounced maximum in the curves for 25 and 40° indicate large changes in the complex equilibria in these solutions in this range of temperature.

TABLE III

CONCENTRATIONS—CONJUGATE LIQUIDS AT 10, 25 AND 40°

Gross composition		Less dense liquid		More dense liquid	
Isoamyl alc., wt. %	Water, wt. %	Isoamyl alc., wt. %	Water, wt. %	Water, wt. %	Isopropyl alc., wt. %
		10°			
18.81	73.78	78.9	11.6	91.5	6.9
17.91	70.00	69.2	13.9	87.7	10.6
16.91	65.56	56.8	17.9	83.5	14.6
16.32	60.88	44.1	23.4	79.6	18.0
14.10	57.54	27.9	36.1	71.5	23.6
		25°			
32.41	63.04	82.1	11.5	94.6	3.5
17.40	72.99	69.0	14.6	90.5	7.5
19.69	75.40	52.2	20.6	85.0	12.7
19.95	70.46	39.5	27.6	80.6	16.4
11.24	63.81	25.5	40.6	72.0	22.0
		40°			
24.11	70.34	78.5	12.9	94.3	3.8
17.68	72.26	65.9	16.4	91.3	6.8
16.04	69.35	53.6	20.8	87.4	10.5
14.75	64.19	38.9	28.9	81.7	15.1
15.47	59.86	29.9	36.5	77.5	18.0
		B 86.2	11.4	95.9	1.6
		B 81.5	12.3	95.1	2.6
		B 79.3	12.7	94.6	3.1
		B 74.5	13.8	93.5	4.4
		B 63.5	16.8	90.4	7.7
		B 46.9	23.8	85.5	12.2
		B 42.8	26.2	84.1	13.2

(8) E. R. Washburn, C. E. Brockway, C. L. Graham and P. Deming, *J. Am. Chem. Soc.*, **64**, 1886 (1942).

(9) I. I. Zaslavskii, *J. Gen. Chem., U.S.S.R.*, **19**, 985 (1949).

(10) E. A. Moelwyn-Hughes *J. Chem. Soc.*, 850 (1940).

HEAT CAPACITY OF PHOSPHORIC ACID SOLUTIONS, 15 TO 80°

BY EDWARD P. EGAN, JR., BASIL B. LUFF AND ZACHARY T. WAKEFIELD

Division of Chemical Development, Tennessee Valley Authority, Wilson Dam, Alabama

Received May 3, 1958

The heat capacities of phosphoric acid solutions containing 5 to 85% H_3PO_4 were measured at 15, 25, 40, 60, 70 and 80°. Curves of heat capacity against temperature were inflected sharply above 60° for solutions containing more than 5% H_3PO_4. The calculated partial molal properties of the components are tabulated as functions of concentration and temperature.

As part of a broad study of the thermodynamic properties of phosphate systems, the specific heats of phosphoric acid solutions containing 5 to 85% H_3PO_4 were measured at temperatures of 15 to 80°. Partial molal heat capacities, heat contents, free energies and entropies of the solutions were calculated from the measured specific heats and known data[1,2] at 25°.

Earlier measurements of similar character seem to be limited to the specific heats at 21° and the average specific heats between 21° and the boiling points.[3] These specific heats averaged about 0.3% higher than the present measurements.

Phosphoric Acid Solutions.—Phosphoric acid hemihydrate, $2H_3PO_4 \cdot H_2O$, was twice crystallized from reagent grade phosphoric acid. The hemihydrate was mixed with the calculated amounts of distilled water to yield solutions with nominal concentrations of 5, 10, 15, 20, 30, 40, 50, 60, 70, 80 and 85% H_3PO_4 by weight. More dilute solutions involve relatively large inherent errors of measurement, whereas more concentrated solutions are so hygroscopic that they would require special apparatus.

The compositions of the solutions were determined from measurements of their densities[4] at 25°. The solutions stood 6 months before the first measurements of specific heat were made. At the start and near the end of the measurements, the densities of the 5, 40 and 85% solutions were redetermined; the greatest change in density was 0.04 mg. per ml.

Construction and Operation of Calorimeter.—The calorimeter was used as a solution calorimeter in other work,[5] and only the modifications to fit it for measurements of heat capacities of solutions are described here. The hollow stirrer shaft was plugged, and a snug-fitting neoprene washer was placed on the shaft below the bottom bearing in an attempt to seal the vapor space in the calorimeter from the atmosphere. The volume of the calorimeter vessel below the constricted neck was 850 ml.—of the vapor space in the neck, 160 ml.

For the measurements at 15 and 25°, and for part of the measurements at 40°, the copper–manganin thermometer and the heater were wound on a thin-walled copper tube, and the assembly was coated with Apiezon wax. The thermometer was calibrated frequently against an NBS-certified platinum resistance thermometer. The assembly proved satisfactory at 25°. When cooled to 15° or heated to 40°, however, the wax occasionally was cracked by thermal shock, with resultant exposure of electrical connections to the acid solutions.

Upon completion of about half the measurements at 40°, the heater was replaced with a 4-lead helical constantan heater that was mounted in a glass spiral and suspended from the calorimeter cover by 5-mm. glass tubes through which the leads were passed. The thermometer was replaced with a capsule-type platinum resistance thermometer which was immersed in oil in a small glass capsule suspended from a 3-mm. glass rod that extended through the hollow stirrer shaft. A small oil seal between the shaft and the rod separated the vapor space from the atmosphere. Several redeterminations of specific heats at 15, 25 and 40° showed that the measurements were unaffected by the radical changes in the heater and thermometer.

The calorimeter bath was operated about 1° above the nominal temperature so that the corrections would be in one direction. A water-bath was used at 15, 25 and 40°, and the calorimeter was sealed liquid-tight in the supporting frame with Apiezon wax. An oil-bath was used at 60, 70 and 80°, and the calorimeter was sealed with an epoxy resin (Carl H. Biggs, potting compound P-420). The Apiezon wax was soluble in oil, whereas the resin would not remain tight in water.

The charge of phosphoric acid solution, in a special 850-ml. volumetric flask, was adjusted to thermal equilibrium and to volume in the bath in which the measurement was to be made. The charge was introduced into the calorimeter at a slightly lower temperature, the weight of the charge being determined by differential weighing of the flask at room temperature, with buoyancy correction.

For measurements at 60° and above, the cover of the calorimeter was preheated 5 to 10° above the temperature of the bath to prevent condensation on the cover before the assembly was placed in the bath, a precaution unnecessary at the lower temperatures.

The calorimeter system, with the stirrer active, was allowed 30 minutes to approach equilibrium with the bath. Foreperiod temperature readings were taken for 15 minutes, and then measured energy was introduced to raise the temperature of the solution 0.5°. Temperatures were read for an intermediate period of 15 minutes, then measured energy was introduced to give a second temperature rise of 0.5°. Temperatures were read for a final period of 15 minutes. The initial temperature was so adjusted that the mid-point temperature of the first heating period was 0.25° below the nominal temperature, and that of the second heating period was 0.25° above the nominal temperature. Essentially duplicate determinations of the specific heat thus were obtained for each concentration of solution at each temperature.

The space above the solution in the calorimeter was assumed to be isolated from the atmosphere. The heat required for its saturation with vapor entailed corrections based upon vapor pressures and heats of vaporization.[3] It was assumed that only water was evaporated.

The correction for heat leak was made by the method of Dickinson,[6] an arbitrary value of 0.60 of the interval being used for the corrected temperature rise. In runs at the lower temperatures where the copper–manganin thermometer-heater assembly was used, the temperature and the energy input could not be read during a heating period because of the thermal conduction of the copper tube. The heat leak correction required for this assembly was used, for consistency, in runs made with the independent, glass-enclosed heater and thermometer.

The bridge unbalance on the copper–manganin thermometer was read to the nearest 0.1 μv. on a Wenner potentiometer (low range). The temperature readings were reproducible within ±0.0002°. The platinum resistance thermometer was read with a Mueller bridge, and temperature differences were read to four decimal places. The ice-point resistance of the thermometer was checked periodically, and the Mueller bridge was calibrated against an NBS-certified 10-ohm resistor.

The input energy was measured with a Wenner potentiometer (high range). The reference potential was six

(1) T. D. Farr, Tennessee Valley Authority, *Chem. Eng. Rept.*, No. 8 (1950).

(2) K. L. Elmore, C. M. Mason and J. H. Christensen, *J. Am. Chem. Soc.*, **68**, 2528 (1946).

(3) M. M. Popov, N. N. Feodos'ev and S. M. Skuratov, *Trans. Sci. Inst. Fertilizers (U. S. S. R.)*, **110**, 23 (1933).

(4) J. H. Christensen and R. B. Reed, *Ind. Eng. Chem.*, **47**, 1277 (1955); E. P. Egan, Jr., and B. B. Luff, *ibid.*, **47**, 1280 (1955).

(5) E. P. Egan, Jr., Z. T. Wakefield and K. L. Elmore, *J. Am. Chem. Soc.*, **78**, 1811 (1956).

(6) H. C. Dickinson, *Bull. Natl. Bur. Standards*, **11**, 257 (1914).

unsaturated standard calomel cells, certified by NBS and maintained at 25°. Time was measured with a 1000-second timer that was graduated to 0.1 second and driven through a 60-cycle frequency standard. One defined calorie was taken as 4.1840 absolute joules—the ice point as 273.16°K. The average precision of the specific heat determinations was ±0.0004 cal. deg.$^{-1}$ g.$^{-1}$ of solution.

Specific Heats.—Corrected specific heats for each concentration of phosphoric acid solution at the mid-point temperature of each heating period are listed in Table I. Equations for s, specific heat in cal. deg.$^{-1}$ g.$^{-1}$ of solution, in terms of t^2 where t is temperature in °C., were fitted to the data in Table I, and the specific heat was calculated for each concentration of acid at integral temperatures of 15, 25, 40 and 60°. With the exception of one anomalous but reproducible point for 50% H_3PO_4 at 40°, the specific heats were smooth functions of temperature between 15 and 60°.

TABLE I

OBSERVED SPECIFIC HEATS OF PHOSPHORIC ACID SOLUTION, CAL. DEG.$^{-1}$ G.$^{-1}$

4.46% H_3PO_4		9.35% H_3PO_4		14.89% H_3PO_4	
t, °C.	s	t, °C.	s	t, °C.	s
14.748	0.9623	14.735	0.9218	14.731	0.8800
15.301	.9625	15.291	.9223	15.252	.8804
24.704	.9631	24.704	.9256	24.753	.8851
25.273	.9628	25.273	.9258	25.285	.8848
39.517	.9650	39.745	.9298	39.746	.8897
40.270	.9647	40.270	.9293	40.290	.8908
59.762	.9686	59.587	.9329	59.736	.8953
60.293	.9680	60.128	.9328	60.269	.8948
69.740	.9692	69.810	.9377	69.735	.8989
70.269	.9710	70.329	.9373	70.259	.8986
79.714	.9698	79.730	.9392	79.735	.9031
80.269	.9712	80.262	.9382	80.285	.9022
19.21% H_3PO_4		29.33% H_3PO_4		39.87% H_3PO_4	
t, °C.	s	t, °C.	s	t, °C.	s
14.721	0.8472	14.739	0.7728	14.741	0.7027
15.298	.8476	15.302	.7727	15.267	.7036
24.723	.8525	24.742	.7788	24.740	.7092
25.295	.8522	25.311	.7790	25.311	.7098
39.740	.8590	39.745	.7883	39.728	.7207
40.264	.8592	40.269	.7881	40.248	.7199
59.747	.8670	59.745	.7989	59.767	.7312
60.283	.8679	60.282	.7995	60.318	.7314
69.752	.8709	69.738	.8003	69.741	.7347
70.291	.8702	70.264	.7998	70.264	.7354
79.736	.8699	79.738	.8010	79.722	.7403
80.284	.8693	80.290	.8010	80.266	.7406
49.36% H_3PO_4		59.54% H_3PO_4		70.10% H_3PO_4	
t, °C.	s	t, °C.	s	t, °C.	s
14.742	0.6321	14.674	0.5668	14.779	0.5097
15.333	.6329	15.259	.5658	15.428	.5099
24.731	.6394	24.739	.5754	24.730	.5158
25.311	.6397	25.326	.5756	25.326	.5152
39.738	.6517	39.679	.5870	39.698	.5260
40.341	.6527	40.210	.5860	40.154	.5248
59.783	.6625	59.723	.5997	59.711	.5366
60.372	.6617	60.261	.6000	60.223	.5377
69.745	.6688	69.850	.6044	69.748	.5438
70.253	.6696	70.376	.6053	70.279	.5435
79.728	.6714	79.725	.6073	79.725	.5460
80.264	.6718	80.286	.6072	80.272	.5476
79.97% H_3PO_4		84.81% H_3PO_4			
t, °C.	s	t, °C.	s		
14.760	0.4595	14.762	0.4391		
14.817	.4600	15.307	.4397		
24.724	.4671	24.708	.4440		
25.302	.4666	25.319	.4442		
39.736	.4746	39.872	.4517		
40.252	.4757	40.406	.4529		
59.753	.4862	59.749	.4624		
60.295	.4863	60.271	.4626		
69.751	.4918	69.736	.4671		
70.286	.4923	70.272	.4675		
79.726	.4937	79.737	.4696		
80.276	.4947	80.290	.4707		

Plots of s against temperature changed abruptly in slope between 60 and 70°. The temperature-specific heat relation for a given composition did not lend itself to convenient expression over the entire range 15 to 80°. Specific heats at integral temperatures of 70 and 80° were estimated by plotting s against t at each observed temperature, drawing a straight line between the points, and reading the value of s on the line at 70.0 or 80.0°. Where replicate determinations had been made, the average of the intersections of the lines with the 70 or 80° ordinate was taken as the most probable value of s. The series of measurements at all compositions at 70° and the nominal composition at 15% were included after a number of the measurements had been made to define more closely the behavior of the specific heats above 60°.

The rapid change in specific heat with elevation of the temperature above 60° may reflect a change in the property of water. Zwicky[7] showed that the compressibility of water changes markedly above 60°. He concluded that water in a solution under the influence of the internal electric field generated by the dissolved ions is affected in much the same way as water under pressure and that the specific heats should increase significantly above 60°. In a few measurements on potassium chloride solutions, Gucker[8] found the same effect as was observed in the present study; the specific heat of a potassium chloride solution was smaller at 80° than at 20°. The degree of hydration of the ions in phosphoric acid solutions is unknown but likely is affected considerably by changes in temperature. The specific heats of sulfuric acid and, to a less extent, of acetic acid show[9] abrupt changes in slope above 60°.

The specific heats of the solutions at each integral temperature were expressed as a cubic power series of the concentration w, in weight %, and a smooth curve was fitted to the deviations from each equation. Each equation then was solved for s at 1% intervals of w, the calculated values were corrected from the deviation curve, and the corrected values were extrapolated to 100% H_3PO_4. Although cubic equations often will not extrapolate smoothly, the present extrapolations were smooth. The results appear to be reasonable and perhaps will be acceptable until measured values are available. The smoothed specific heats at integral concentrations and temperatures are listed in Table II. The specific heats of water are from Osborne and co-workers.[10]

(7) F. Zwicky, *Physik. Z.*, **27**, 271 (1926).

(8) F. T. Gucker, Jr., *J. Am. Chem. Soc.*, **50**, 1005 (1928).

(9) Landolt-Börnstein, "Physikalisch-chemische Tabellen," Supplement 3, 5th ed., Julius Springer, Berlin, 1936, p. 2283.

As a check on the thermal corrections at the high temperatures, measurements were made of the specific heat at 80° of a solution with a composition corresponding to $KCl \cdot 25H_2O$. The results, 0.8418 and 0.8409 cal. deg.$^{-1}$ g.$^{-1}$, are to be compared with 0.8415 cal. deg.$^{-1}$ g.$^{-1}$ as calculated from a value reported by Gucker[8] for the ratio of the specific heat of the solution to that of water at 80° and Osborne's[10] value for the specific heat of water.

TABLE II

SMOOTHED SPECIFIC HEATS OF PHOSPHORIC ACID SOLUTIONS, CAL. DEG.$^{-1}$ G.$^{-1}$

Wt. % H_3PO_4	15°	25°	40°	60°	70°	80°
0	1.0004	0.9990	0.9987	1.0010	1.0013	1.0030
5	0.9576	.9591	.9613	0.9638	0.9654	0.9667
10	.9172	.9208	.9251	.9282	.9330	.9347
15	.8794	.8839	.8895	.8946	.8980	.9017
20	.8414	.8465	.8534	.8622	.8652	.8639
25	.8042	.8102	.8184	.8287	.8303	.8297
30	.7679	.7743	.7833	.7945	.7956	.7968
35	.7322	.7387	.7479	.7601	.7623	.7658
40	.6971	.7036	.7134	.7256	.7294	.7342
45	.6622	.6689	.6803	.6911	.6969	.7008
50	.6281	.6353	.6477	.6580	.6649	.6674
55	.5952	.6030	.6149	.6274	.6334	.6350
60	.5639	.5725	.5838	.5970	.6021	.6042
65	.5361	.5439	.5545	.5673	.5724	.5754
70	.5096	.5166	.5264	.5385	.5440	.5474
75	.4844	.4960	.4998	.5114	.5172	.5202
80	.4606	.4662	.4746	.4861	.4919	.4941
85	.4380	.4434	.4511	.4614	.4666	.4692
90[a]	.4174	.4228	.4294	.4389	.4429	.4454
95[a]	.3994	.4045	.4096	.4187	.4212	.4227
100[a]	.3839	.3889	.3918	.4008	.4013	.4010

[a] Extrapolated.

Derived Thermal Data.—The conventional expressions[11] for ϕc, $\bar{C}_{p_2}$ and $(\bar{C}_{p_1} - \bar{C}^0_{p_1})$ were modified for use with data on a basis of weight %

$$\phi c = \frac{[100s - (100 - w)s^0]M_2}{w}$$

$$\bar{C}_{p_2} = \phi c + \frac{w(100 - w)}{100} \frac{\partial \phi c}{\partial w}$$

$$(\bar{C}_{p_1} - \bar{C}^0_{p_1}) = -\frac{M_1}{M_2} \frac{w^2}{100} \frac{\partial \phi c}{\partial w} = -0.183839 \frac{w^2}{100} \frac{\partial \phi c}{\partial w}$$

where s and s^0 are the respective specific heats of solution and of water at the same temperature, w is weight % H_3PO_4, and the other terms have their usual significance.

The apparent molal heat capacity, ϕc, was calculated at 1% intervals of concentration. The slope, $\partial \phi c/\partial w$, was calculated with use of 7-point first-derivative coefficients.[12]

The partial molal heat capacity of H_3PO_4 in phosphoric acid solutions, $\bar{C}_{p_2}$, was calculated from ϕc and $\partial \phi c/\partial w$. Plots of $\bar{C}_{p_2}$ against w were not smooth curves; abrupt changes in slope occurred at concentrations corresponding to 0.1, 2.2, 4, 8 and 15 molal H_3PO_4. Similar abrupt changes at these concentrations have been observed in the density, conductivity, pH and activity of phosphoric acid solutions at 25°. The break at 2.2 m H_3PO_4 was the most pronounced, and a break at this concentration occurs in all the other properties. The breaks correspond perhaps to changes in the number of species present in the solution or to marked changes in the relative concentrations of the species. An elucidation of the structure of phosphoric acid solutions would aid materially in explaining the breaks. At concentrations above 15 m, the $\bar{C}_{p_2}$ curves were fairly smooth and almost parallel at all temperatures.

The value of $\bar{C}^0_{p_2}$, the partial molal heat capacity of H_3PO_4 at infinite dilution, must be determined if $\bar{C}_{p_2}$ is to be used in calculating the temperature coefficients of the thermodynamic properties of phosphoric acid solutions. The shape of the $\bar{C}_{p_2}$

TABLE III

PARTIAL MOLAL HEAT CAPACITY OF H_3PO_4 IN PHOSPHORIC ACID SOLUTIONS, $\bar{C}_{p_2}$

Wt. % H_3PO_4	15°	25°	40°	60°	70°	80°
5	16.23	21.90	26.51	26.97	32.70	33.68
10	23.95	24.84	27.20	30.09	30.24	34.48
15	22.86	23.73	27.13	34.96	32.85	30.39
20	23.30	25.05	28.02	32.64	30.60	29.05
25	24.78	26.25	28.64	30.76	30.18	31.88
30	25.94	26.80	28.02	30.77	32.18	35.43
35	26.71	27.41	28.67	30.59	32.57	35.18
40	26.92	27.62	30.45	30.58	33.00	34.69
45	27.70	28.68	31.26	30.56	33.50	32.27
50	28.46	29.87	31.32	33.29	33.99	33.14
55	29.97	31.40	32.04	34.60	34.41	34.17
60	32.06	33.10	33.70	34.93	35.10	36.35
65	33.96	34.11	34.63	35.49	36.17	36.86
70	34.85	34.94	35.52	36.27	37.09	37.40
75	35.43	35.70	36.28	37.42	37.91	37.93
80	36.07	36.46	36.97	37.74	38.26	38.41
85	36.45	37.03	37.56	38.27	38.45	38.82
90	37.13	37.61	38.01	38.84	38.97	39.09
95	37.50	37.98	38.28	39.17	39.24	39.24
100	37.63	38.11	38.39	39.28	39.33	39.33

TABLE IV

RELATIVE PARTIAL MOLAL HEAT CAPACITY OF WATER IN PHOSPHORIC ACID SOLUTIONS, $-(\bar{C}_{p_1} - \bar{C}^0_{p_1})$

Wt. % H_3PO_4	15°	25°	40°	60°	70°	80°
5	0.0214	0.0203	0.0196	0.0001	0.0481	0.0638
10	.1527	.0711	.0293	.0521	−0.0185	.0633
15	.1261	.0319	.0202	.1904	0.0717	−0.0569
20	.1451	.1258	.0611	.1008	−0.0368	−0.0511
25	.2241	.1428	.0878	−0.0029	−0.0564	0.0933
30	.3046	.1817	.0394	−0.0064	0.1007	.3532
35	.3741	.2365	.1005	−0.0216	.1348	.3268
40	.3897	.2538	.3021	−0.0235	.1823	.2750
45	.4974	.4006	.4114	−0.0247	.2499	−0.0320
50	.6223	.5984	.4136	0.4309	.3310	0.1140
55	.9298	.9103	.5734	.6768	.4138	.3234
60	1.4653	1.3402	.9921	.7604	.6007	.8789
65	2.0226	1.6466	1.2754	.9321	.9243	1.0377
70	2.3718	1.9602	1.6143	1.2395	1.2773	1.2395
75	2.6566	2.3350	1.9896	1.8024	1.6742	1.4994
80	3.0615	2.8133	2.4214	1.9814	1.8661	1.7990
85	3.3829	3.3125	2.9380	2.4691	2.0640	2.1543
90	4.2544	4.0608	3.5217	3.1911	2.7221	2.5047
95	5.1070	4.9046	4.1712	3.9555	3.3217	2.8522
100	6.0704	6.0061	5.0758	4.8534	3.9728	3.1271

(10) N. S. Osborne, H. F. Stimson and D. C. Ginnings, *J. Research Natl. Bur. Standards*, 23, 197 (1939).

(11) H. S. Harned and B. B. Owen, "The Physical Chemistry of Electrolytic Solutions," Reinhold Publ. Corp., New York, N. Y., 1943, p. 242.

(12) H. E. Salzer, "Tables of Coefficients for Obtaining the First Derivative Without Differences," Natl. Bur. Standards, Applied Math. Ser. 1948, 2.

TABLE V

RELATIVE PARTIAL MOLAL HEAT CONTENT OF PHOSPHORIC ACID IN PHOSPHORIC ACID SOLUTIONS, $(\bar{H}_2 - \bar{H}^0_2)$

Wt. % H_3PO_4	15°	25°	40°	60°	70°	80°
5	534	559	583	656	708	800
10	756	831	875	982	1029	1113
15	953	1017	1050	1191	1283	1360
20	1074	1147	1199	1337	1403	1462
25	1139	1227	1293	1422	1478	1545
30	1261	1359	1424	1539	1605	1699
35	1545	1648	1723	1847	1915	2010
40	1977	2081	2169	2320	2392	2489
45	2308	2422	2525	2686	2762	2852
50	2607	2731	2845	3024	3112	3209
55	2917	3057	3189	3387	3485	3587
60	3247	3405	3562	3764	3879	3994
65	3574	3747	3917	4146	4257	4381
70	3945	4126	4308	4554	4675	4808
75	4321	4509	4703	4969	5099	5237
80	4676	4871	5076	5352	5487	5629
85	5034	5234	5449	5735	5874	6019
90	5306	5512	5734	6030	6172	6320
95	5510	5720	5947	6249	6393	6544
100	5569	5780	6009	6313	6458	6610

must be integrated with respect to temperature. For lack of a satisfactory method of determining $\bar{C}^0_{p_2}$, $(\bar{H}_2 - \bar{H}^0_2)$ for 0.1 H_3PO_4 at 25° was taken as a reference point, so that

$$(\bar{H}_2 - \bar{H}^0_2)_m - (\bar{H}_2 - \bar{H}^0_2)_{0.1} = (\bar{H}_2 - \bar{H}^*_2)_m$$

The value of $\bar{C}_{p_2}$ then was taken at the same reference point, 0.1 molal H_3PO_4, and values of

$$(\bar{C}_{p_2})_m - (\bar{C}_{p_2})_{0.1} = (\bar{C}_{p_2} - \bar{C}^*_{p_2})_m$$

were calculated for all temperatures and concentrations of solution. On integration with respect to temperature of $(\bar{C}_{p_2} - \bar{C}^*_{p_2})$, there was obtained

$$(\bar{H}_2 - \bar{H}^*_2)_T = (\bar{H}_2 - \bar{H}^*_2)_{25} + \int_{25}^{T} (\bar{C}_{p_2} - \bar{C}^*_{p_2})\, dT$$

In the integration of $(\bar{C}_{p_2} - \bar{C}^*_{p_2})$ with respect to temperature, values for each concentration were plotted against temperature, and an arbitrary smooth curve was drawn through the points. Values of $(\bar{C}_{p_2} - \bar{C}^*_{p_2})$ were read from the curve at 0.5° intervals between 15 and 40° and at 1° intervals between 40 and 80°. The shorter intervals below 40° were necessary to obtain enough points for a satisfactory tabular integration. The integration was made with 5-point Lagrangian integration coefficients.[14]

TABLE VI

RELATIVE PARTIAL MOLAL HEAT CONTENT OF WATER IN PHOSPHORIC ACID SOLUTIONS, $-(\bar{H}_1 - \bar{H}^0_1)$

Wt. % H_3PO_4	15°	25°	40°	60°	70°	80°
5	1.942	2.150	2.448	2.700	2.936	3.511
10	5.051	6.141	4.616	5.447	5.678	5.938
15	10.16	10.82	11.14	13.42	14.90	14.82
20	13.84	15.22	16.63	18.34	18.36	17.90
25	17.74	19.56	21.19	22.27	21.94	22.28
30	26.83	29.21	30.84	30.66	31.04	33.18
35	52.32	55.23	57.73	58.15	58.70	60.96
40	100.1	103.2	107.4	110.7	111.4	113.8
45	144.6	149.1	155.2	159.9	161.4	162.8
50	194.4	200.6	208.2	216.6	220.6	222.8
55	257.8	267.0	278.5	291.2	296.6	300.1
60	340.1	354.2	371.9	389.4	396.1	403.4
65	441.1	459.4	481.2	502.8	512.0	521.5
70	580.6	602.1	628.8	657.1	669.7	682.3
75	766.0	790.9	823.1	860.9	878.3	894.2
80	993.6	1023	1062	1106	1125	1144
85	1294	1328	1375	1429	1452	1473
90	1661	1703	1760	1828	1857	1883
95	2128	2178	2247	2328	2364	2395

The value of $(\bar{H}_2 - \bar{H}^0_2)$ for 0.01 m phosphoric acid at 25°, as calculated from the heat of dilution data, was 41 cal. The value of $(\bar{C}_{p_2} - \bar{C}^*_{p_2})$ for 0.01 m acid at each temperature was calculated. Then, at each temperature

$$(\bar{H}_2 - \bar{H}^0_2) = (\bar{H}_2 - \bar{H}^*_2) + [(\bar{H}_2 - \bar{H}^*_2)_{0.1} - (\bar{H}_2 - \bar{H}^*_2)_{0.01}] + 41$$

This calculation entails the assumption that $(\bar{H}_2 - \bar{H}^0_2)_{0.01} - (\bar{H}_2 - \bar{H}^0_2)_0 = 41$ cal. at all temperatures.

Values of $(\bar{H}_2 - \bar{H}^0_2)_T$ were recalculated with $(\bar{H}_2 - \bar{H}^0_2)$ at 25° and $\bar{C}_{p_2}$ at T°, both values for

curves, however, precludes the use of conventional methods[11] for the extrapolation to infinite dilution. Gucker and Schminke[13] were skeptical about the extrapolation of $\bar{C}_{p_2}$ to $m = 0$ in any event.

The partial molal heat capacities of H_3PO_4, $\bar{C}_{p_2}$, are listed in Table III—the relative partial molal heat capacities of water in phosphoric acid solutions, $(\bar{C}_{p_1} - \bar{C}^0_{p_1})$, in Table IV.

Values of $(\bar{H}_2 - \bar{H}^0_2)$ for phosphoric acid solutions at 25° have been published.[1] For the present paper, however, $(\bar{H}_2 - \bar{H}^0_2)$ at 25° (Table V) was recalculated from unpublished heats of dilution, $(\phi_L - \phi^0_L)$, of phosphoric acid. For calculations of $(\bar{H}_2 - \bar{H}^0_2)$ at other temperatures, the relative partial molal heat capacity, $(\bar{C}_{p_2} - \bar{C}^0_{p_2})$,

(13) F. T. Gucker, Jr., and K. H. Schminke, *J. Am. Chem. Soc.*, **54**, 1358 (1932).

(14) Works Progress Administration, Mathematical Tables Project, "Tables of Lagrangian Interpolation Coefficients," Columbia University Press, New York, N. Y., 1944.

TABLE VII

RELATIVE PARTIAL MOLAL FREE ENERGY OF PHOSPHORIC ACID IN PHOSPHORIC ACID SOLUTIONS, $(\bar{F}_2 - \bar{F}^0_2)$

Wt. % H_3PO_4	15°	25°	40°	60°	70°	80°
5	−424.8	−458.5	−510.2	−582.2	−620.1	−659.9
10	89.22	64.67	24.86	−32.70	−63.86	−96.79
15	424.4	404.9	372.9	326.0	298.6	268.8
20	700.8	686.6	661.8	623.3	600.9	576.7
25	953.4	945.4	929.1	902.1	885.7	867.5
30	1203	1199	1189	1171	1159	1144
35	1464	1459	1447	1426	1412	1396
40	1746	1736	1716	1683	1663	1640
45	2044	2035	2012	1975	1952	1927
50	2347	2336	2313	2273	2250	2223
55	2674	2663	2640	2598	2573	2580
60	3030	3020	2996	2954	2928	2899
65	3402	3393	3371	3328	3302	3272
70	3789	3780	3758	3715	3688	3657
75	4181	4173	4151	4107	4079	4048
80	4565	4558	4537	4494	4466	4434
85	4939	4932	4911	4868	4840	4807
90	5269	5264	5246	5205	5178	5147
95	5594	5593	5581	5548	5524	5497
100	5708	5709	5699	5670	5649	5623

5.0 m acid, as the reference points. This calculation contributed nothing mathematically, but it did test the consistency of the $\bar{C}_{p_2}$ data. The two reference points gave values of $(\bar{H}_2 - \bar{H}^0_2)$ that differed by an average of 10 cal. The two sets of values were averaged, and the average values were used in subsequent calculations. The averaged values of $(\bar{H}_2 - \bar{H}^0_2)$ as a function of temperature are shown in Table V.

The calculation of $(\bar{H}_1 - \bar{H}^0_1)_T$ from $(\bar{H}_1 - \bar{H}^0_1)_{25}$ and $(\bar{C}_{p_1} - \bar{C}^0_{p_1})_T$ was straightforward. The values of $(\bar{H}_1 - \bar{H}^0_1)$ as a function of temperature are shown in Table VI.

Values of a_1 and a_2 for phosphoric acid solutions also have been published.[2] The results of unpublished work show that a_u, as used in reference 2, is the same as a_2. Values of a_i were calculated from $(\bar{H}_i - \bar{H}^0_i)$ at each temperature by the relation

$$\ln (a_i)_T - \ln (a_i)_{25} = -\frac{1}{R}\int_{25}^{T} \frac{(\bar{H}_i - \bar{H}^0_i)}{T^2}\, dT$$

The calculated values of a_1 and a_2 at each temperature were converted to partial molal free energies by the relation

$$(\bar{F}_i - \bar{F}^0_i) = RT \ln a_i$$

Values of $(\bar{F}_2 - \bar{F}^0_2)$ as functions of temperature are shown in Table VII, and values of $(\bar{F}_1 - \bar{F}^0_1)$ are shown in Table VIII. The published vapor pressure data[1] serve as an indirect check on the measured heat capacities. Values of a_1 are converted to vapor pressures by the relation

TABLE VIII

RELATIVE PARTIAL MOLAL FREE ENERGY OF WATER IN PHOSPHORIC ACID SOLUTIONS, $-(\bar{F}_1 - \bar{F}^0_1)$

Wt. % H_3PO_4	15°	25°	40°	60°	70°	80°
5	6.31	6.46	6.67	6.9[illegible]	7.05	7.17
10	13.52	13.79	14.20	14.78	15.06	15.33
15	22.25	22.66	23.24	23.96	24.25	24.52
20	32.98	33.62	34.51	35.60	36.11	36.64
25	46.48	47.44	48.80	50.52	51.37	52.23
30	63.90	65.14	66.90	69.20	70.35	71.47
35	87.06	88.21	89.80	91.82	92.83	93.80
40	118.2	118.8	119.5	120.4	120.8	121.0
45	158.4	158.8	159.1	159.2	159.2	159.1
50	208.9	209.3	209.5	209.4	209.1	208.7
55	275.2	275.6	275.7	275.2	274.6	273.9
60	364.6	365.2	365.3	364.3	363.4	332.4
65	477.8	478.7	479.1	478.3	477.4	476.3
70	627.3	628.5	629.2	628.2	627.2	625.8
75	818.0	819.4	820.0	818.6	817.1	815.0
80	1065	1067	1068	1067	1066	1064
85	1387	1390	1392	1391	1390	1388
90	1813	1818	1822	1824	1824	1822
95	2543	2557	2574	2592	2600	2607
100	...	3365	...	...	...	...

$$a_1 = p/p_0$$

The calculated vapor pressures agree with those in reference 1 within ±1%—the limit of accuracy of the vapor pressure data.

The 5% intervals of concentration in the tables are space-saving but are too broad to show adequately the trends of the data.

Partial molal entropies may be calculated from the relation

$$(\bar{S}_i - \bar{S}^0_i) = \frac{(\bar{H}_i - \bar{H}^0_i) - (\bar{F}_i - \bar{F}^0_i)}{T}$$

CHROMATOGRAPHIC SEPARATION OF A NON-IONIC POLYETHER SURFACTANT

BY JOSEPH KELLY AND HAROLD L. GREENWALD

Rohm and Haas Co., Bristol, Pa.

Received May 6, 1958

A mixed *p-t,t*-octylphenoxy-polyoxyethylene-ethanol, with 9.7 ethylene oxide units per phenol ($OPE_{9.7}$), was separated into its component compounds by chromatography. Silicic acid columns were used with mixed chloroform–acetone eluents. The shape of the elution curve suggests that the resolution was sufficient for the isolation of quite pure species. Agreement with the expected distribution of species from the ethylene oxide plus phenol condensation reaction is satisfactory.

Studies of the properties of non-ionic surface active agents, prepared by the addition of ethylene oxide to molecules containing an active hydrogen, have long been devilled by the fact that such preparations always result in mixtures. Flory[1] has suggested that the molecular weight distribution obtained corresponds to a Poisson distribution. Mayhew and Hyatt[2] obtained mixtures with a narrow range of molecular species by distillation in a centrifugal molecular still. They found differences, generally not very large, between the properties of the narrow cuts and the normal material in some uses. Several other workers[3] used short path distillation to get narrow range fractions. Gallo[4] investigated the paper chromatography of several polyether surfactants and obtained elongated spots in some instances. A British patent[5] discloses the fractionation of octylphenoxyundecaoxyethylene-ethanol into three parts by fractional precipitation from mixed solvents.

Probably the only previously reported samples of high purity were those synthesized by the Williamson ether syntheses from distilled hexaoxyethylene glycol.[6] This method, used in this case to give but one polyoxyethylene chain length, probably can be modified to give pure compounds with several other chain lengths. At high chain lengths difficulty in distilling the polyether may be expected.

The present work was started with the hope of obtaining a series of pure non-ionic surfactants with a common hydrophobe in sufficient quantity to study the solution properties of individual members. Fractionation of the readily available mixtures produced by the usual synthesis seemed feasible. For fractionations of this type there are several attractive features of column chromatography. It has been used to separate gram quantities of non-ionic materials with high resolution. The elution curve itself is a fair indication of the resolution achieved and thus of the purity of the products. Demonstration of the purity of a polyether non-ionic surfactant when the likely impurities differ by one ethylene oxide unit is difficult to do by most methods.

Materials.—The *p-t,t*-octylphenoxy-polyoxyethylene-ethanol (OPE_n) was made by adding ethylene oxide to *p-t,t*-octylphenol, in the mole ratio 9.7 to 1, in the presence of sodium hydroxide. Ethylene oxide with a quoted minimum purity of 99% was used. Commercial octylphenol was recrystallized three times from hexane before use. In work done on other samples in these laboratories it has been shown by freezing curves that this procedure produces *p-t,t*-octylphenol with about one mole per cent. of impurity (with the limitations of intepretation inherent in this method). The sodium hydroxide in the $OPE_{9.7}$ was neutralized with sulfuric acid, digested with a little added water, vacuum freed of water then filtered in the presence of Celite 545 (Johns Manville Corp.) to remove the sodium sulfate. The sulfate ash remaining in the sample was found to be 0.07%. Solvents used were

Chloroform—Mallinckrodt, U.S.P.

Acetone—Mallinckrodt or Baker, C.P.

Methanol—Mallinckrodt C.P.

Benzene—Mallinckrodt C.P.
These were pretreated by passing through columns of alumina—Merck, Reagent, suitable for chromatographic adsorption

Isooctane—Merck spectrophotometric reagent was used as supplied

Aluminum oxide—Woelm, non-alkaline (almost neutral) activity grade I, for chromatographic adsorption—was used as supplied

Silicic acid—Mallinckrodt A.R., 100 mesh powder, suitable for chromatographic analysis by the method of Ramsey and Patterson—was used as supplied.

Apparatus.—Several columns were used in this work. Ones measuring 30 cm. long by 3.5 or 2.5 cm. dia. for pilot work, and the others 120 cm. long by 6 cm. dia. and 80 cm. long by 5 cm. dia. for working up larger samples.

A Beckman D.U. Spectrophotometer was used for spectrophotometric measurements.

A Misco Interval Timer and Fraction Collector was used in collecting fractions from the longer columns. A clock motor fraction collector of our own design was used for collection of fractions from the smaller columns.

Procedure.—In general the method of Reichstein and Shoppee[7] was followed. The amount of material in each cut was determined by either of two methods: (1) evaporate the fraction to dryness in a stream of nitrogen and weigh the sample; (2) evaporate a 1-ml. aliquot of the fraction to dryness, dissolve in 10 ml. of chloroform and determine the optical density of the solution at 277 $m\mu$ in a 1 cm. quartz cell. Elution curves were constructed by graphing weight or number of moles (or optical density of the chloroform solution) against cumulative eluate volume.

Identification of the material present in the eluent was done after combining fractions in the neighborhood of the peaks of the elution curves. One method used was the determination of the cloud point of a 1% aqueous solution following the procedure of Cross.[8] The cloud point *vs.* polyether chain length (n) curve is established only for mixtures with n representing an average value. Thus it was useful in the preliminary work, but not after quite pure fractions were obtained and the order of elution known. A better determination of the number of ether groups in the molecule was obtained by determining the molecular weight

(1) P. J. Flory, *J. Am. Chem. Soc.*, **62**, 1561 (1940).

(2) R. L. Mayhew and R. C. Hyatt, *J. Am. Oil Chemists' Soc.*, **29**, 357 (1952).

(3) J. V. Karabinos and E. J. Quinn, *ibid.*, **33**, 223 (1956); L. M. Kushner, W. D. Hubbard and A. S. Doan, THIS JOURNAL, **61**, 371 (1957).

(4) U. Gallo, *Boll. chim. farm.*, **92**, 332 (1953).

(5) British Petroleum Co., Ltd., D. H. Desty and C. L. A. Harbourn, British Patent 756,334, Sept. 5, 1956.

(6) B. A. Gingras and C. H. Bayley, *Can. J. Chem.*, **35**, 599 (1957).

(7) T. Reichstein and C. W. Shoppee, *Disc. Faraday Soc.*, **7**, 305 (1949).

(8) J. M. Cross, Official Proceedings, 36th Mid-Year Meeting, Chemical Specialties Manufacturers Assoc., June 13, 1950.

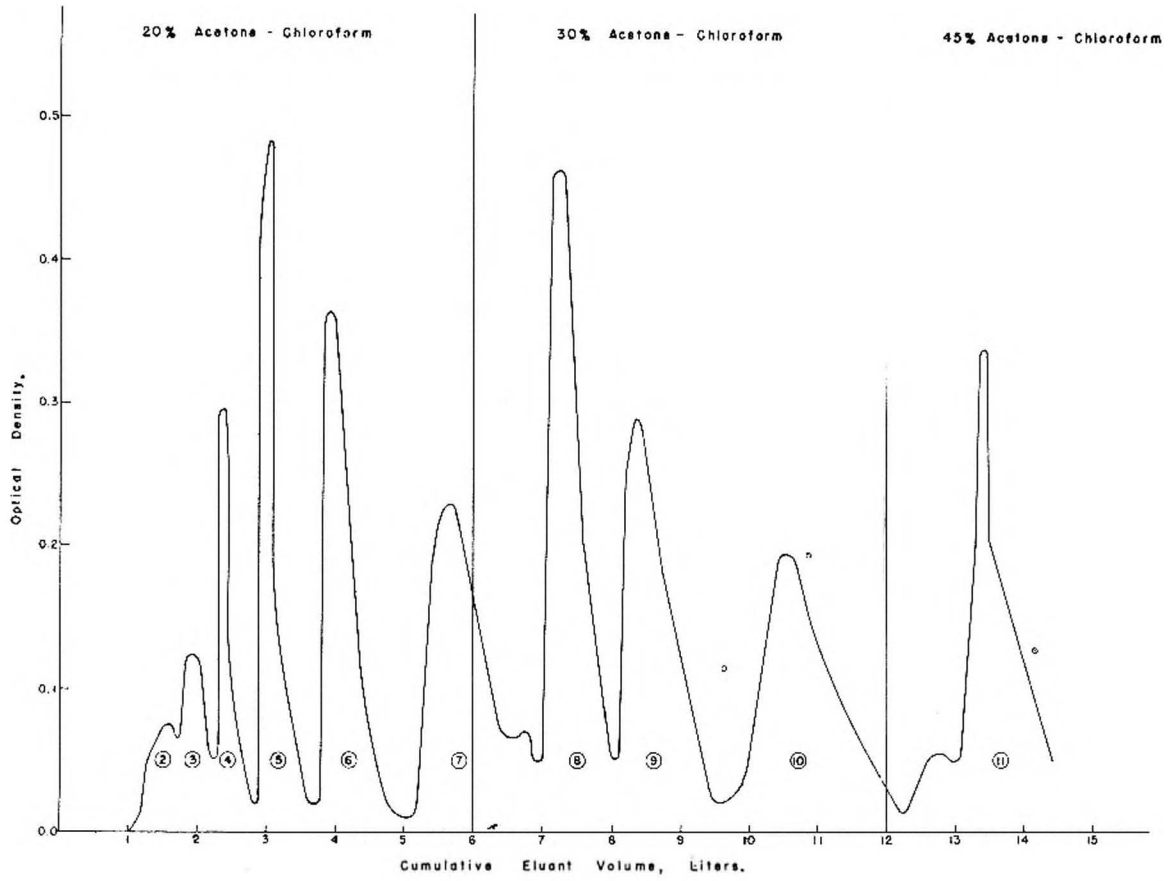

Fig. 1.

via ultraviolet absorption. The band in the neighborhood of 275 mμ presumably is due to the benzene ring in these molecules. Measurement of the molar extinction coefficient ϵ of commercial OPE_n samples, with n varying from 5 to 13, indicated no change of ϵ or λ with n. Optical constants were then determined on the starting material and used throughout the work. They are

in chloroform, $\lambda = 277.5$ mμ, $\epsilon = 1.53 \times 10^3$
in isooctane, $\lambda = 277.5$ mμ, $\epsilon = 1.63 \times 10^3$
in water, $\lambda = 275.5$ mμ, $\epsilon = 1.33 \times 10^3$

where λ is the wave length of maximum absorption in the band and ϵ is the optical density divided by the concentration in moles/liter and the path length in centimeters. In this procedure it was necessary to be careful to eliminate traces of acetone.

Preliminary experiments were carried out using the 30-g. columns of Woelm alumina in 2.5 cm. dia. glass tubes with one gram of $OPE_{9.7}$ as adsorbate. Solvent systems used for column development were: (1) chloroform, benzene, ethyl acetate, acetone, water; (2) various benzene–butanol solutions and (3) combinations of chloroform–benzene and chloroform–acetone solutions. Determinations of the ether chain length indicated that the chain length went through a minimum during elution in each case. Because of these failures, work with alumina as the adsorbent was discontinued.

A 30-g. charge of silicic acid was tried as the adsorbent in the 2.5 cm. tubes. Benzene, various benzene–chloroform solutions and chloroform failed to move any of the adsorbate out of the column. Chloroform–acetone solutions with acetone content increasing from 20 to 100% produced fractions containing OPE_n's with n increasing smoothly from less than 6.9 to greater than 14. The resolution was too low to indicate appreciable separation of compounds with adjacent n values. Increasing the weight of silicic acid to 45 g. gave some resolution with a 20/80 acetone/chloroform eluent. Repeating this procedure with silicic acid dried for 18 hours at 100° decreased the resolutions somewhat.

Upon going to larger columns with greater length to diameter ratios the columns adopted were 6 cm. dia. containing 830 g. of silicic acid slurried in 80/20 chloroform/acetone solution. A 10-g. charge of $OPE_{9.7}$ dissolved in the same solvent was placed on the column. The solvent schedule used was either

(1) 10 l. of 80/20 chloroform/acetone
5 l. of 50/50 chloroform/acetone
or (2) 5 l. of 80/20 chloroform/acetone
6 l. of 70/30 chloroform/acetone
5 l. of 55/45 chloroform/acetone

Results

The second schedule was the more successful and gave the elution curve plotted in Fig. 1. Small bumps appear at 6.7 and 12.7 l. and are probably the breakthrough positions of the new solvent. Readings of optical density were made at *ca.* 50 or 100 ml. intervals and the resulting curve smoothed slightly. Three points were, however, rather far from the line and are plotted separately at 9.7, 10.9 and 14.1 liters. These may be due to experimental errors—196 fractions were cut and optical densities determined in this run.

Numbers encircled in Fig. 1 are the "n" assignments for the given peak. Table I gives the calculated and measured, by ultraviolet spectroscopy, molecular weights for this experiment, run 6, and two others. It is obvious that just counting peaks gives the correct assignments.

Two values are given for $n = 9$, run 4 in Table I. Eluent fractions for this peak were combined into two groups. The first, fractions up through the peak, had a measured molecular weight of 623.

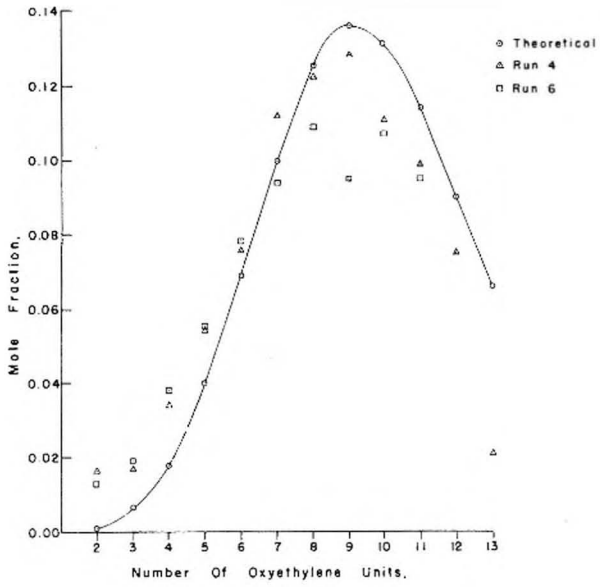

Fig. 2.

Fractions between the peak and the following trough when combined had the lower molecular weight, 605. It is probable that this difference is not significant and that our uncertainty in the molecular weight determination may be as high as 5%. Appreciable contamination of these fractions by the nearest neighbor compounds in the column would have led to the first group having a lower molecular weight.

Figure 2 is a plot of mole fraction *vs.* number of oxyethylene units given by the Poisson distribution (points connected by a line which, of course, has no significance). Points obtained in two runs are plotted on the same graph and are in fair agreement with the theoretical values. The agreement is probably good enough for this chromatographic procedure to be useful in analytical applications.

TABLE I

MOLECULAR WEIGHT OF COMBINED FRACTIONS

"n" value	Mol. wt.	Obsd. values Run 1	Run 4	Run 6
4	383	389		
5	426	420		
6	470	466		
7	514	526	520	494
8	558	556		
9	602	602	623–605	596
10	646		643	
11	690		679	700

In recovering the compounds from solution it was found that the product was straw colored if the solvents were distilled off (the starting material was water white). Evaporation of solvents at low temperature in a stream of nitrogen produced less color. Dissolving the higher n value samples in methanol showed that the samples contained a small amount of solid material, possibly silicic acid. This was removed by filtering the 5–10% solution through a fine glass frit and washing with two equal volumes of methanol.

We plan to study some of the surface and solution properties of the pure compounds.

We wish to thank Mr. W. Rinear and Dr. J. L. Rainey for the sample of pure $OPE_{9.7}$ and Drs. I. Rosenthal and A. R. Weiss for instruction in the techniques of chromatography.

THERMAL DECOMPOSITION OF METAL ACETYLACETONATES MASS SPECTROMETER STUDIES

BY JOAN VON HOENE, ROBERT G. CHARLES[1] AND WILLIAM M. HICKAM

Westinghouse Research Laboratories, Pittsburgh 35, Pennsylvania

Received May 9, 1958

The heat stabilities of nine metal acetylacetonates, in the absence of oxygen, have been examined as a function of temperature. Those products from the decomposition which were gaseous at room temperature were identified, and their quantities determined, by means of a mass spectrometer. Acetone and carbon dioxide were found to be major decomposition products for all the acetylacetonates studied. For some of the chelates, acetylacetone and methane were also among the principal decomposition products. A number of other gases were found to be present also in smaller quantities. The order of decreasing heat stability for the acetylacetonates, based on the evolution of gaseous products, was found to be Na(I) > Cr(III) > Al(III) > Ni(II) > Cu(II) > Fe(III) > Co(II) > Co(III) > Mn(III).

An earlier paper described the relative heat stabilities of a series of metal acetylacetonates at 191° in the absence of oxygen.[2] In the present work the decomposition of some of these compounds (formula I) has been examined in greater detail as a function of temperature. Those decomposition products, which are gaseous at room temperature, have been identified and their quantities determined by means of a mass spectrometer.

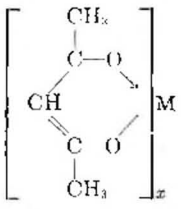

$x = 1, 2, \text{ or } 3$ (I)

Experimental Procedure

The metal acetylacetonates used in this investigation were prepared, purified and dried as described previously.[2] Fifty-mg. samples of the compounds were sealed, at a pressure of less than 10^{-2} mm., into 10-cc. Pyrex glass containers

(1) Inquiries regarding this work should be addressed to this author.

(2) R. G. Charles and M. A. Pawlikowski, THIS JOURNAL, 62, 440 (1958).

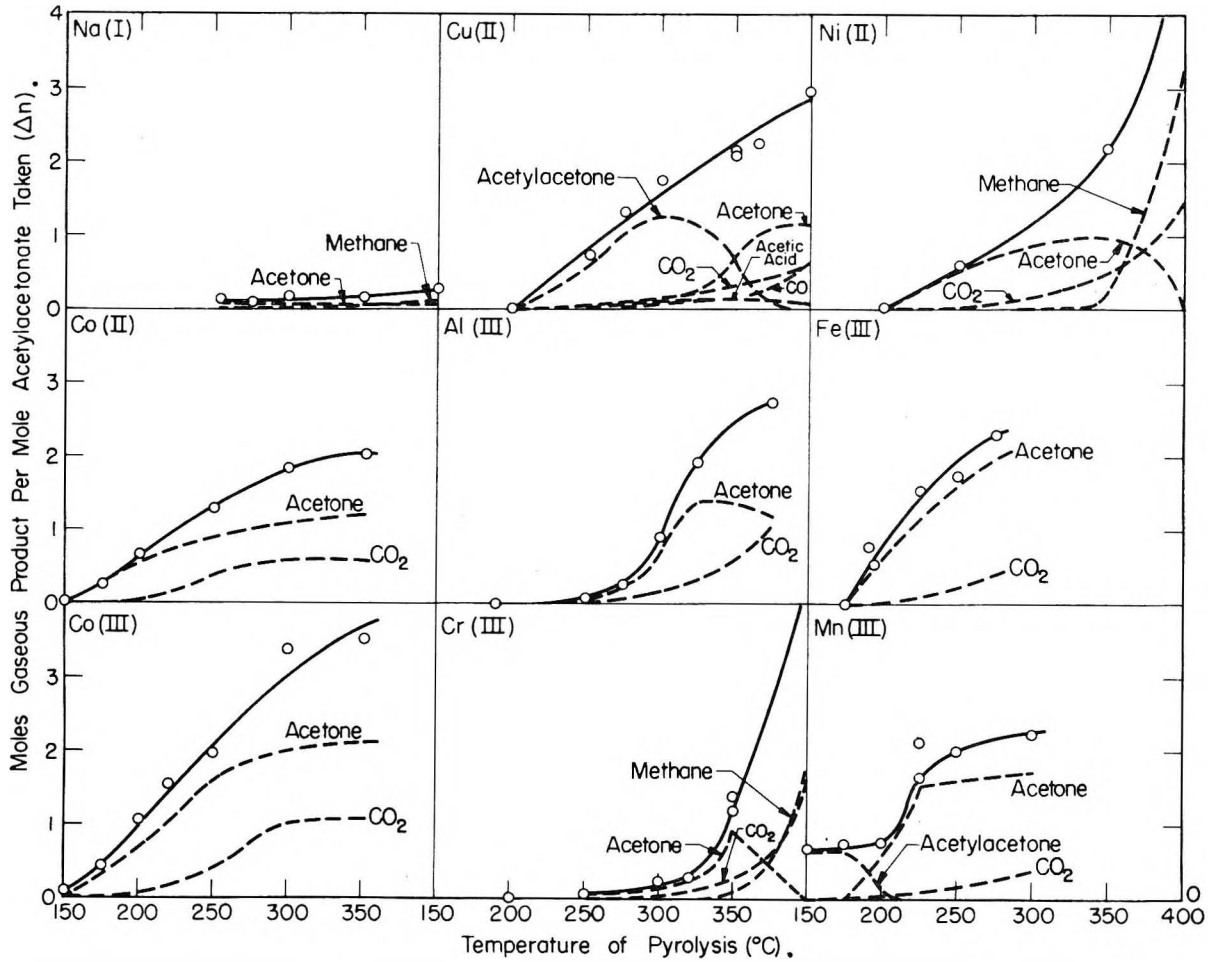

Fig. 1.—Gaseous decomposition products from pyrolysis of metal acetylacetonates as a function of pyrolysis temperature: solid lines, total products; dashed lines, principal components; measurements at room temperature, duration of pyrolysis, 4 hr. (For clarity experimental points are given only for the total gas results.)

closed at one end by a glass break-off tip. Final sealing of a sample under vacuum was accomplished by slowly collapsing the glass at the seal point during pumping. The sample remained at room temperature during the pumping and sealing operations. The design of the sample containers used assured no sublimation of the acetylacetonates out of the hot zone during the degradations. Similar sample containers constructed of Vycor glass were used for the degradations above 400°.

Each degradation run was carried out by placing the entire sample container into a preheated tube furnace, maintained at constant temperature by means of an automatic controller utilizing a thermocouple sensing element. Although initially under vacuum, the samples at the furnace temperatures were subjected to the pressures of the gaseous decomposition products. The pressures within some of the tubes, at the higher temperatures, were 2 to 3 atmospheres. After the desired period of heating (usually four hours) the tube was removed and cooled rapidly to room temperature.

Direct sealing of the sample container to the mass spectrometer vacuum system then permitted re-entry to the degradation products without contamination. This was accomplished by the dropping of a glass enclosed iron slug magnetically held above the break-off tip. The gaseous degradation products were, in this way, expanded into a known calibrated volume (usually 1000 ml.). The pressure of the expanded gas was determined by means of either a mercury manometer or the micromanometer associated with the Consolidated mass spectrometer, depending on the pressure. Considerable care was exercised to ensure proper mixing of the gases in order to obtain a representative sample. Empty sample containers processed in an identical manner to the true samples yielded a background of the order of only 0.1% of that obtained from any significant degradation of the metal acetylacetonates. The analyses of all samples were carried out with the combined use of the Consolidated No. 21-103 mass spectrometer and the Datatron No. 205 electronic computer.

Measurement of the pressure and volume of the expanded gas at room temperature and the determination of the molecular composition of the gas mass spectrometrically, permitted the calculation of the total weight of each gaseous constituent. In the final analyses the results are expressed in terms of moles of gas evolved per mole of initial acetylacetonate taken.

Results and Discussion

In Fig. 1, Δn (the ratio of moles of gaseous decomposition product to moles of chelate taken) for the four-hour runs is plotted as a function of temperature for the principal decomposition products, and also for the total quantity of gas formed in each case.[3]

From Fig. 1 it will be noted that all the acetylacetonates studied decompose to some extent within the temperature range of 150 to 400°. As a group, therefore, the acetylacetonates are less stable to heat than some other metal chelates that have been studied, for example, some of the phthalocyanines.[4] The acetylacetonates are more similar in stability to the Schiff base chelates reported by Marvel, Aspey and Dudley.[5] It is interesting that

(3) Each point in Figs. 1 and 2 represents a separate experiment.

(4) C. E. Dent and R. P. Linstead, *J. Chem. Soc.*, 1027 (1934).

(5) C. S. Marvel, S. A. Asprey and E. A. Dudley, *J. Am. Chem. Soc.*, **78**, 4905 (1956).

Cr(III) acetylacetonate has been reported to distil unchanged at 340°.[6] It is apparent from Fig. 1 that considerable decomposition will occur unless the distillation is done quickly.

The temperature at which gas evolution first becomes appreciable for the acetylacetonates is dependent on the metal present (Fig. 1). It is possible to arrange these compounds in the approximate order of decreasing heat stability based on the temperature required to produce significant amounts of gaseous decomposition products. The order obtained is Na(I) > Cr(III) > Al(III) > Ni(II) > Cu(II) > Fe(III) > Co(II) > Co(III) > Mn(III).[7,8] The heat stability order obtained here is in general agreement with the results of the earlier study[2] where the relative heat stabilities of a series of acetylacetonates were compared at 191° in a nitrogen atmosphere.

Also in agreement with the results obtained in the earlier study,[2] no general correlation was observed here between the above heat stability series and other properties of the metal acetylacetonates or with properties of the parent metal ions. Since the rate of decomposition for the acetylacetonates might reasonably be expected to change on going from the solid to the liquid phase, it was of interest to compare the results plotted in Fig. 1 with the reported melting points of these compounds (Table I). The temperature at which decomposition for the Fe(III) acetylacetonate first becomes appreciable was found to nearly coincide with the melting point for this compound. This was not found to be the case for the other acetylacetonates studied, however, nor was any break in the curves of Fig. 1 noted at the melting point for any of the compounds.

The principal gaseous decomposition products for many of the acetylacetonates are acetone and carbon dioxide (Fig. 1). For the Co(II), Co(III), Al(III) and Fe(III) acetylacetonates, these are the only products formed, in large amount, throughout the temperature range studied. In the case of Ni(II) and Cr(III) acetylacetonates, large amounts of methane are found, in addition, at the higher temperatures.[9]

The Cu(II) and Mn(III) acetylacetonates differ from the other compounds studied in that acetylacetone is the principal decomposition product observed for the lower temperatures. This fact suggests that the mechanism for the decomposition of these chelates may be different from that for the decomposition of the other acetylacetonates mentioned. Significant amounts of carbon monoxide and acetic acid also were found for the Cu(II) acetylacetonate at the higher temperatures.

A detailed discussion of the mechanism of the decompositions studied probably is not justified. It is not known whether the gaseous products shown in Fig. 1 are the products initially formed in the degradations. It is interesting, however, that two of the major observed products, acetone and acetylacetone, involve very little rearrangement of the atoms from the manner in which they occur in the acetylacetonate molecules. It may be significant that the production of methane at the higher temperatures, for the Ni(II) and Cr(III) acetylacetonates (Fig. 1) is accompanied by a decrease in the acetone content of the gas mixture. Methane has been identified[10] as one of the thermal decomposition products of acetone, although at higher temperatures than those used here. An inverse relationship also exists between the acetylacetone and acetone concentrations in the gas evolved by the Cu(II) and Mn(III) chelates. This suggests that acetylacetone is formed initially but then decomposes at the higher temperatures to form acetone. It is possible that acetylacetone may be an intermediate in the production of acetone for some of the other acetylacetonates also. Acetylacetone was, in fact, found (although only in small quantities) for most of the other acetylacetonates studied.

It may be significant that two of the major decomposition products found here, acetone and carbon dioxide, are formed also by the pyrolysis of some metal acetates.[11,12] The latter compounds have the same atomic grouping II found in the metal acetylacetonates.

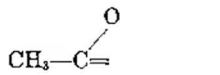

(II)

For two of the acetylacetonates, Fe(III) and Al(III), a brief study was made of the heat decomposition as a function of time, at constant temperature. Temperatures were chosen at which the decomposition was appreciable in four hours. In the case of Fe(III) acetylacetonate, both the total amount of gas and the individual components were calculated in the same manner as for the four-hour runs. For the Al(III) chelate only the total amount of gas was determined. Results are given in Fig. 2.

For the Fe(III) chelate in Fig. 2, Δn for the total gas appears to approach a limit with time. The curve obtained is very similar to that found at 191° by a different method.[2] The principal products observed for the Fe(III) acetylacetonate decomposition were acetone and carbon dioxide over the period 0 to 20 hours (Fig. 2).

The value of Δn for total gas in Fig. 2 for Al(III) acetylacetonate increases with time but does not appear to approach a limit within 20 hours. The gaseous products of the decomposition were in this case not analyzed.

(6) G. Urbain and A. Debierne, *Compt. rend.*, 129, 302 (1899).

(7) In determining this order, the relative positions of those compounds which begin to decompose at about the same temperature were established by comparing the Δn values at temperatures above the initial decomposition temperature.

(8) It is recognized that the order given might be somewhat different if the amount of undecomposed acetylacetonate were chosen as the criterion of stability.

(9) In addition to the gases indicated in Figs. 1 and 2, a number of other gaseous decomposition products were found to be present in smaller amounts. These include mesityl oxide, methyl acetate, butene-1, propylene, propane, hydrogen, mesitylene and water. Numerical tables of the quantities of these gases (together with the data plotted in Figs. 1 and 2) have been deposited as Document 5719 with the A.D.I. Auxiliary Publication Project, Photoduplication Service, Library of Congress, Washington, D. C. A copy may be secured by citing the Document number and by remitting $1.25 for photoprints, or $1.25 for 35 mm microfilm in advance by check or money order payable to: Chief Photoduplication Service, Library of Congress.

(10) C. D. Hurd, "The Pyrolysis of Carbon Compounds," A.C.S Monograph No. 50, (Chemical Catalog Co.) Reinhold Publishing Corp., New York, N. Y., 1929, p. 248.

(11) W. Kronig, *Z. Angew. Chem.*, 37, 667 (1924).

(12) Ref. 10, p. 481.

TABLE I

APPEARANCE OF METAL ACETYLACETONATES HEATED 4 HOURS *in Vacuo*

Acetyl acetonate	M.p., °C. lit.	Appearance of solid Before heating	After heating
$NaC_5H_7O_2$	218	White crystalline powder	Yellow-brown 250–275°; red-brown 300°; brown 350°; black 400°
$Cu(C_5H_7O_2)_2$	>230	Dark blue crystalline powder	Brown and black crystals 251°; metallic Cu and brown residue 275–400°
$Ni(C_5H_7O_2)_2$		Light green crystalline powder	Unchanged 150–200°; amber 250°; charred 349–399°
$Co(C_5H_7O_2)_2$		Dark purple crystalline powder	Amber 175–208°; charred, some green material 250–352°
$Co(C_5H_7O_2)_3$	213	Dark green crystalline powder	Charred, some pink material 175–220°; charred black mixed with green 250–351°
$Al(C_5H_7O_2)_3$	194	Orange[a] crystals	Unchanged 190°; amber 250–325°; brown 375°
$Fe(C_5H_7O_2)_3$	184	Dark red crystals	Unchanged 175°; amber and black 190–275°
$Cr(C_5H_7O_2)_3$	216	Maroon crystalline powder	Unchanged 200°; maroon and charred 250–350°, dark green liquid when hot; completely charred 399°
$Mn(C_5H_7O_2)_3$	184	Dark green powder	Light brown 150–175°; dark brown, charred, 200–300°

[a] The color indicates a trace of iron(III) acetylacetonate.

In Table I the appearances of the solid residues from decomposition are summarized. In general, the visual extent of decomposition parallels the amount of gas produced (Fig. 1), decomposition usually being accompanied by a darkening of the solid phase. For the Na(I) acetylacetonate, however, the appearance of the residues indicates that some decomposition has occurred in the temperature range 250–285° and to a greater extent at higher temperatures despite the fact that little gas is produced.[13] This would seem to indicate that the principal products of decomposition are in this case non-volatile.

No attempt was made in the present studies to identify the components of the solid residues formed. What appeared to be metallic copper was visible from the decomposition of the Cu(II) acetylacetonate. Metallic deposits of this type were not observed for the other compounds studied.

Interesting color changes were observed for some of the residues. Cr(III) acetylacetonate (or its decomposition products) was observed to give a green liquid at 250 to 350° which set to a maroon solid on cooling. The change was reversible at 250°.

Decomposition of the Co(II) compound gave rise to some green material, perhaps indicating oxidation to Co(III). Conversely, decomposition of the Co(III) acetylacetonate gave some pink material, possibly indicating some reduction to Co(II). It is planned to study the residues obtained in more detail.

(13) Significant amounts of methane were, however, produced at 494°.[2]

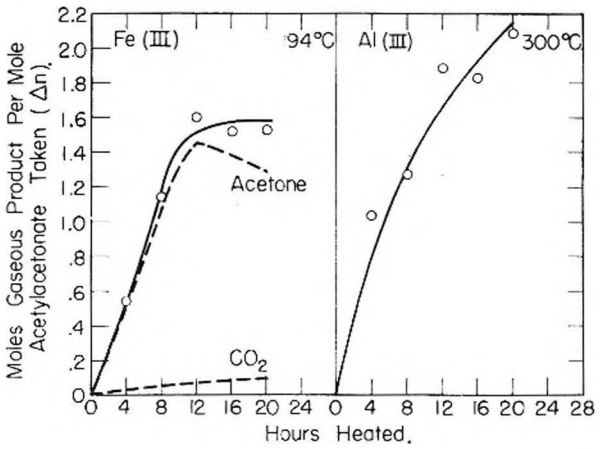

Fig. 2.—Gaseous decomposition products from pyrolysis of metal acetylacetonates at constant temperature: solid lines, total products; dashed lines, principal components; measurements at room temperature.

Acknowledgments.—The writers are grateful to Mr. J. F. Zamaria, Miss I. Laminack, and Mrs. M. H. Loeffler, all of whom assisted in the experimental portion of this work.

DIFFUSION IN PARAFFIN HYDROCARBONS

BY DEAN C. DOUGLASS AND DAVID W. MCCALL

Bell Telephone Laboratories, Inc., Murray Hill, New Jersey

Received May 10, 1958

The Carr–Purcell spin-echo method has been used to measure the self-diffusion coefficients of the normal paraffins C_5H_{12}, C_6H_{14}, C_7H_{16}, C_8H_{18}, C_9H_{20}, $C_{10}H_{22}$, $C_{18}H_{38}$ and $C_{32}H_{66}$. The measurements were made over a temperature range in order to obtain activation energies. Within experimental error the plots of log D *vs.* $1/T$ are linear. As expected the diffusion coefficients decrease with increasing molecular weight. The activation energies increase with increasing molecular weight. It is proposed that the elementary diffusion process involves the translation of an extended molecule parallel to its chain axis. A reduced temperature plot of the diffusion coefficient clusters the data in an interesting manner and the diffusion coefficients for all the hydrocarbons extrapolated to their respective critical points are approximately equal.

I. Introduction

A satisfactory molecular theory of transport properties for liquids has not yet been developed. This is due, in part, to the inherently complicated nature of the liquid state but it is also important that experimental investigations of transport properties, other than viscosity, have been carried out in too few systems. For example, Johnson and Babb[1] were able to report experimental values for self-diffusion coefficients in only ten non-electrolytes and to our knowledge only two liquids[2] have been added to this list since their review. The present paper is a comparative study of self-diffusion in several paraffin hydrocarbons.

The discovery of nuclear magnetic resonance spin-echoes by Hahn[3] and the ensuing theoretical analysis[4,5] of the experiment led to a new technique for measuring self-diffusion coefficients which does not require the presence of unusual isotopes. Spin-echo measurements may be used to measure self-diffusion coefficients rapidly and under a variety of experimental conditions. This method is employed in the present study using the proton magnetic resonance.

Probably the only theory of liquid diffusion that has established contact with the experimentalists is the Eyring theory of rate processes.[6–8] This is because the theory provides simple equations which have been quite successful in correlating experimental data and the parameters of the equations are interpreted in terms of a simple model for the diffusion process. According to Eyring's theory[6]

$$D = \lambda^2(kT/h)\exp(-\Delta F^*/R) \qquad (1)$$

where ΔF^* is the free energy of activation and λ^2 is the mean square jump length. This equation will form the basis for the discussion of the data reported herein.

II. Analysis of the Experiment

The essentials of the spin-echo experiment have been clearly described by Hahn.[9] The basic experiment for a "90-180°" pulse sequence may be qualitatively described as follows. The specimen being studied is contained in a coil whose axis is perpendicular to an externally applied magnetic field. At equilibrium the nuclear magnetic moments tend to be aligned parallel with the external field, forming a macroscopic magnetization. A short, intense burst of radiofrequency energy at the resonant frequency is applied to the specimen through the coil and the magnetization is rotated 90° relative to H_0. After the pulse the magnetization vector undergoes free precession about the field direction at a frequency proportional to the magnetic field strength. This precessing magnetization induces a voltage in the coil. However, because the field is never strictly uniform over the sample, the total magnetization vector of the sample must be thought of as the resultant of many partial magnetization vectors, each precessing at a frequency slightly different from the others. That is to say, since there is a distribution in field over the sample there is also a distribution in frequency. Immediately after the 90°-pulse all of the partial magnetization vectors are in phase. However, because of their different precession frequencies, they rapidly dephase and the voltage induced in the coil decreases to zero.

At a later time, τ, the component of each partial magnetization vector which is perpendicular to the coil axis is rotated 180° by a 180°-pulse. This is equivalent to a reflection of the partial magnetization vectors in the plane determined by the coil axis and the field direction. If two partial magnetization vectors have their *relative* phase angle increasing before the 180°-pulse it will be decreasing after the 180°-pulse and *vice versa*. Provided we assume that the rate of precession of each partial magnetization vector remains constant over the period 2τ, the 180°-pulse will bring all the partial magnetization vectors into phase at time 2τ (where τ is the time between the 90°- and 180°-pulses). During the time the magnetization vectors are in phase a voltage, called a "spin-echo," is induced in the coil.

If the sample is in a non-uniform magnetic field and diffusion occurs, then the average magnetic field seen by a given nucleus between times 0 and τ is not necessarily the same as the average magnetic field seen by this nucleus between times τ and 2τ. Thus the phase gain between 0 and τ is not, in general, the same as the phase loss between τ and 2τ and the number of nuclei brought back into phase at 2τ is reduced. Thus the effect of

(1) P. A. Johnson and A. L. Babb, *Chem. Revs.* **56**, 387 (1956).
(2) E. Fishman, THIS JOURNAL, **59**, 469 (1955).
(3) E. L. Hahn, *Phys. Rev.*, **80**, 580 (1950).
(4) H. Y. Carr and E. M. Purcell, *ibid.*, **94**, 630 (1954).
(5) T. P. Das and A. K. Saha, *ibid.*, **93**, 749 (1954).
(6) S. Glasstone, K. J. Laidler and H. Eyring, "The Theory of Rate Processes," McGraw Hill Book Co., Inc., New York, N. Y., 1941.
(7) J. O. Hirschfelder, D. Stevenson and H. Eyring, *J. Chem. Phys.*, **5**, 896 (1937).
(8) J. F. Kincaid, H. Eyring and A. E. Stearn, *Chem. Revs.*, **28**, 301 (1941).
(9) E. L. Hahn, *Physics Today*, **6**, 4 (1953).

diffusion is to reduce the voltage induced in the coil by the "spin-echo."

By assuming a random walk model of diffusion and a uniform field gradient over the sample Carr and Purcell[4] were able to derive an expression equivalent to

$$V_{max} = A(2\tau) \exp(-2\gamma^2 G^2 D\tau^3/3) \quad (1)$$

where V_{max} is the maximum amplitude of the echo voltage and $A(2\tau)$ is assumed to be independent of the field gradient G, and the diffusion coefficient D. Thus $A(2\tau)$ may be measured with $G = 0$ and D is then determined from the slope of a plot of $\ln(V_{max}/A)$ *vs.* τ^3 when $G \neq 0$.

The result of Carr and Purcell may be obtained without reference to a random walk model of diffusion in the following manner. The phase accumulated by a precessing magnetic moment at time $t > \tau$ where τ is the time at which the 180°-pulse is introduced is given by

$$\Phi = \gamma \left\{ \int_0^\tau H(t)\, dt - \int_\tau^t H(t)\, dt \right\}$$

If the sample resides in a uniform magnetic field gradient

$$H(t) = H_0 + Gx(t)$$

where $x(t)$ gives the position of the moment then

$$\Phi = \gamma \left\{ G \int_0^\tau x(t)\, dt - G \int_\tau^t x(t)\, dt + H_0(2\tau - t) \right\}$$

$$\Phi = \Phi_0 + G\gamma \left\{ \int_0^\tau x(t)\, dt - \int_\tau^t x(t)\, dt \right\}$$

or

$$\Phi = \gamma G \left\{ \int_0^\tau x(t)\, dt - \int_\tau^t x(t)\, dt \right\} \quad (2)$$

where Φ is now the phase of the precessing magnetic moment relative to the phase of a moment in the uniform static field, *i.e.*, relative to a magnetic moment located by $x(t) = 0$ for all t. The signal induced in the spectrometer coil is proportional to the resultant magnetic moment which is rotating in the plane perpendicular to the applied magnetic field. The resultant moment is[4]

$$M_\tau = M_0 \int_{-\infty}^{\infty} p(\Phi) \cos \Phi\, d\Phi \quad (3)$$

where $p(\Phi)$ is the probability density of moments having relative phase Φ. $p(\Phi)$ can be computed directly from equation 2 by first making the substitution $Y(t) = x(t) - x_0$ where x_0 is the initial position of the precessing moment being followed. Then

$$\Phi = \gamma G \left\{ \int_0^\tau Y(t)\, dt - \int_\tau^t Y(t)\, dt \right\} + \gamma G x_0 (2\tau - t)$$

$$\Phi = \Phi_1 + \gamma G(2\tau - t)x_0 \quad (4)$$

Φ_1 and x_0 are independent variables and therefore

$$p(\Phi) = g(\Phi_1)\, h(x_0) \quad (5)$$

$Y(t)$ is simply the position of a diffusing particle which starts at $Y = 0$ at time $t = 0$. Therefore, the probability density for $Y(t)$ is a solution of the usual diffusion equation

$$\frac{\partial c}{\partial t} = D \frac{\partial^2 c}{\partial Y^2}$$

If the size of the sample is large compared to the distance a precessing moment moves during the time of the experiment (2τ), then

$$c = (2\pi tD)^{-1/2} \exp(-Y^2/4Dt) \quad (6)$$

The probability density for the integral of a variable which has a gaussian probability density is gaussian.[10] Therefore

$$g(\Phi_1) = (2\pi \langle \Phi_1^2 \rangle_{av})^{-1/2} \exp(-\Phi_1^2/2\langle \Phi_1^2 \rangle_{av}) \quad (7)$$

where

$$\langle \Phi_1^2 \rangle_{av} = \gamma^2 G^2 \left\langle \left\{ \int_0^\tau Y(t)\, dt - \int_\tau^t Y(t)\, dt \right\}^2 \right\rangle_{av} \quad (8)$$

$$\langle \Phi_1^2 \rangle_{av} = \gamma^2 G^2 \left\{ \int_0^\tau \int_0^\tau \langle Y(t)Y(s) \rangle_{av}\, dt\, ds - 2 \int_0^\tau \int_\tau^t \langle Y(t)Y(s) \rangle_{av}\, dt\, ds + \int_\tau^t \int_\tau^t \langle Y(t)Y(s) \rangle_{av}\, dt\, ds \right\}$$

$$\langle Y(t)Y(s) \rangle_{av} = \langle Y^2(t) \rangle_{av} \text{ if } t < s$$
$$\langle Y(t)Y(s) \rangle_{av} = \langle Y^2(s) \rangle_{av} \text{ if } t > s \quad (9)$$

From equation 6

$$\langle Y^2(t) \rangle_{av} = 2Dt$$

Substitution of equation 9 into equation 8 and integration gives

$$\langle \Phi_1^2 \rangle_{av} = 4\gamma^2 G^2 D(\tau^3 - \tau^2 t + t^3/6) \quad (10)$$

For a cylindrical sample with the field gradient perpendicular to the cylinder axis

$$h(x_0) = (2/\pi a^2)(a^2 - x_0^2)^{1/2} \text{ when } |x_0| \leq a$$
and
$$h(x_0) = 0 \text{ when } |x_0| > a \quad (11)$$

where a is the radius of the cylinder.

Making use of equations 7 and 10 one may integrate equation 3 with the result

$$M_\tau = M_0 \exp(-\langle \Phi_1^2 \rangle_{av}/2)\, J_1[\gamma G a(2\tau - t)]/\gamma G a(2\tau - t) \quad (12)$$

Setting $t = 2\tau$ and using equation 9

$$M_\tau = M_0 \exp(-2\gamma^2 G^2 D\tau^3/3) \quad (13)$$

Inclusion of the conventional T_1 and T_2 effects gives an equation of the form

$$M_\tau = A(2\tau) \exp(-2\gamma^2 G^2 D\tau^3/3) \quad (14)$$

in agreement with the result of Carr and Purcell.[4]

III. Experimental Arrangement and Procedure

The spin-echo spectrometer has been described in detail by Schwartz[11] and will not be gone into here. A Varian Associates 12" magnet system was used. The samples were contained in thin-walled glass tubes and insulation was provided by either Styrofoam or asbestos. The coil, sample and insulation were enclosed in a phenol-fiber box. A Pyrex glass tube outside the work coil separates the sample chamber and the insulation. The temperature was controlled by passing heated or cooled nitrogen gas through the sample chamber. A copper–constantan thermocouple was used to measure the temperature.

The magnetic field gradient coils consisted of 34 turns (17 on each side of the sample) of number 20 copper wire. Power was supplied by three heavy-duty 6-volt storage batteries connected in series. Return wires for the coils were placed as far from the sample as possible. The current was measured by means of a Weston ammeter. Under normal operating conditions a current of 4.00 amperes was used. This corresponds to a gradient of 1.39 gauss/cm. in our apparatus.

(10) M. E. Munroe, "Theory of Probability," McGraw–Hill Book Co., Inc., New York, N. Y., 1951, p. 92.

(11) J. Schwartz, *Rev. Sci. Instr.*, **28**, 780 (1957).

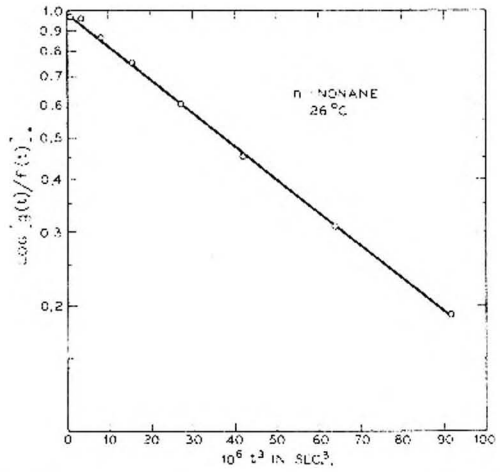

Fig. 1.—Typical experimental plot of $\log(V_{max}/A)$ *vs.* $(2\tau)^3$. The sample was *n*-nonane.

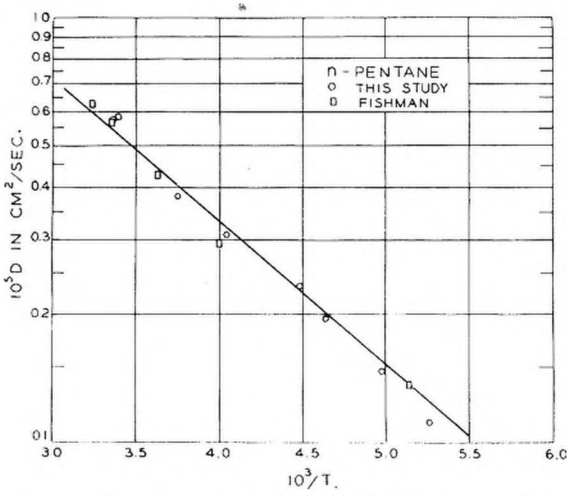

Fig. 2.—The logarithm of the self-diffusion coefficient for *n*-pentane *vs.* reciprocal temperature. The data of Fishman[2] are given for comparison.

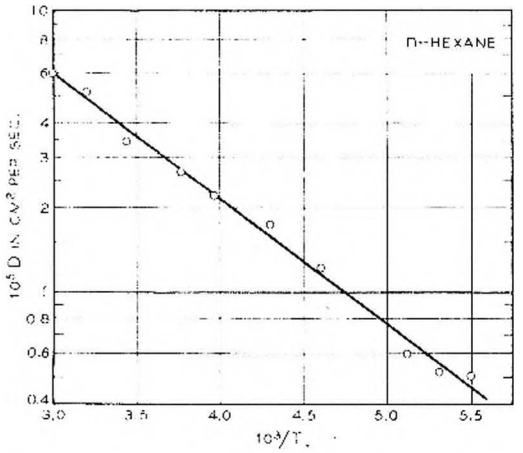

Fig. 3.—The logarithm of the self-diffusion coefficient for *n*-hexane *vs.* reciprocal temperature.

The field gradient was measured by means of a method suggested by Carr and Purcell.[4] If the specimen is contained in a cylindrical tube of diameter a and the field gradient is perpendicular to the cylinder axis, the shape of the echo is given by (equation 12)

$$J_1(\gamma Gta/2)/(\gamma Gta/2)$$

where J_1 is the first-order Bessel function. The observed shape agrees very well with the predicted form. It follows that $\gamma G = 7.664/a\Delta t$ where Δt is the separation in time between the first minima of the echo. The diameter of the sample tube was determined by weighing the amount of mercury contained in a known length. We believe that the accuracy of G determined in this way is better than the 5% figure estimated by Carr and Purcell.[4]

The adjustment of the apparatus has been described previously by Schwartz.[11] In determining the diffusion coefficient the following procedure was employed. The echo amplitude was measured as a function of the time between the 90°-pulse and the echo, with the field gradient current turned off. The decay observed is due to (1) the magnetic field inhomogeneity, which was quite small, and (2) the nuclear spin exchange interactions and chemical shifts which give rise to multiplet structure in n.m.r. high resolution spectra.[12,13] The latter interaction dominated the former in the liquids studied. This indicates the very homogeneous nature of the magnet employed in this work. Of course, in molecules in which there is only one structural type of proton and there are no other magnetic nuclei (*e.g.*, benzene) the decay is determined by the small inhomogeneities present in the applied magnetic field. We refer to the decay envelope with the gradient current turned off, $A(2\tau)$, as a "T_2-plot" even though the shape of the envelope may be quite complex. The decay function V_{max} is then determined with the field gradient current turned on. Thus a plot is made of the logarithm of the ratio of the two decay functions *vs.* (2τ),[3] the slope is $-(\gamma G)^2D/12$. A typical plot is shown in Fig. 1.

Because the T_2-decay in the paraffins in governed by chemical shift and exchange interactions one expects the function to be independent of temperature.[13] This has indeed been found to be the case. However, for each diffusion coefficient reported herein a T_2-plot was determined for the experimental conditions.

In the hydrocarbons studied the magnetic field gradient dominated the decay, *i.e.*, V_{max} decayed much faster than $A(2\tau)$, but in ethanol the opposite is true for values of G accessible to us. Even in this case, however, the diffusion coefficient was determined to be within reasonable agreement with values reported in the literature. Thus we believe our procedure for eliminating the T_2-decay to be valid even in extreme cases.

The experimental uncertainty in D is difficult to assess and undoubtedly varies with the noise level. Under ideal conditions the experimental error was probably less than 5%. In passing it may be mentioned that convection, if present, would be evident in non-linearity of the t^3 plot (Fig. 1.

The liquid specimens, except for *n*-$C_{18}H_{38}$ and *n*-$C_{32}H_{66}$, were obtained from the Phillips Petroleum Company. The samples were the "Pure Grade," 99 mole % minimum. The liquids were used without further purification. Many of the measurements on *n*-hexane were made on a 95 mole % specimen (Phillips Technical Grade) but no difference was observed between samples. The *n*-$C_{18}H_{38}$ was obtained from the Eastman Kodak Co. The *n*-$C_{32}H_{66}$ was synthesized by Dr. W. L. Hawkins of these laboratories.

IV. Experimental Results and Discussion

Figures 2 to 6 are log D *vs.* $1/T$ plots for the various liquids studied. The solid lines were fitted by means of the usual least squares procedure. Figures 2 and 4 also contain the data of Fishman,[2] determined by tracer techniques, for comparison. Our results and those of Fishman are in excellent agreement. The activation energies obtained from Figs. 2 to 6 are recorded in Table I. The errors were estimated in the usual least squares manner[14] and include only random errors. Table I also includes activation energies for viscosity determined from data taken from the literature. The parallelism in activation energies is striking

(12) E. L. Hahn and D. E. Maxwell, *Phys. Rev.*, **88**, 1070 (1952).

(13) H. S. Gutowsky, D. W. McCall and C. P. Slichter, *J. Chem. Phys.*, **21**, 279 (1953).

(14) W. J. Youden, "Statistical Methods for Chemists," John Wiley and Sons, Inc., New York, N. Y., 1951.

and tends to support the view that the molecular motions which make themselves evident in viscosity and diffusion are closely related.

The results may be summarized qualitatively as follows:

1. The coefficients of self-diffusion are logarithmic in reciprocal temperature within our experimental error.
2. The dependence of the coefficients of self-diffusion on temperature becomes more pronounced as the molecular weight is increased, *i.e.*, the activation energy increases.
3. The coefficients of self-diffusion decrease with increasing molecular weight other things equal.
4. A reduced temperature plot of all the data groups the curves in a single region. There is some indication that these curves tend to converge at the critical point.

TABLE I

Liquid	E_D, kcal./mole	$10^5 D$, cm.²/sec.	E_η, kcal./mole	$10^2\eta$, g.-cm./sec.
n-Pentane (25°)	1.54 ± 0.07[b]	5.45	1.8[a]	2.2
n-Hexane (25°)	2.07 ± .13	4.21	1.78	2.9
n-Heptane (25°)	2.19 ± .06[b]	3.12	1.98	3.8
n-Octane (25°)	2.42 ± .18	2.00	2.09	5.1
n-Nonane (25°)	3.08 ± .10	1.70	2.40	6.7
n-Decane (25°)	3.56 ± .09	1.31	2.51[c]	8.5
n-Octadecane (50°)	3.94 ± .18	0.46	3.85	23.4
n-Dicetyl (100°)	5.64 ± .27	0.30	4.79	53.6

[a] Ewell and Eyring[15] report 1.58 kcal./mole for *n*-pentane but we obtain 1.8 kcal./mole from the same data. [b] Fishman[2] reports values of 1.6 and 2.2 kcal./mole for *n*-pentane and *n*-heptane, respectively. [c] The viscosity data for *n*-decane show two regions; one with activation energy 2.51 kcal./mole and one with activation energy 3.3 kcal./mole. The lower value was chosen as the temperature range corresponded with that of the present study.

The difference between the two activation energies can be predicted on the basis of the Eyring theory. The Eyring equation for the coefficient of self-diffusion is

$$D = \lambda^2(kT/h)\exp(\Delta S^*/R)\exp(-\Delta H^*/RT) \quad (15)$$

and the Eyring equation for the coefficient of viscosity is

$$\eta = (\lambda_1 h/\lambda_2\lambda_3\lambda^2)\exp(-\Delta S^*/R)\exp(\Delta H^*/RT) \quad (16)$$

where λ_1 is the distance between two layers (in the viscosity model), λ_2 is the molecular length perpendicular to the direction of flow, and λ_3 is the molecular length parallel to the direction of flow. λ is the jump length. It is apparent that $\lambda_1\lambda_2\lambda_3 = V/N$ where V is the molar volume and N is the Avogadro number.

The activation energies are often defined as

$$E_\eta = R\ \mathrm{d}\ln\eta/\mathrm{d}(1/T)$$

and

$$E_D = -R\ \mathrm{d}\ln D/\mathrm{d}(1/T)$$

Combining these definitions with equations 15 and 16 it can be seen that

$$E_D - E_\eta = RT - R\ \mathrm{d}\ln(\lambda_1/\lambda_2\lambda_3)/\mathrm{d}(1/T)$$

or

$$E_D - E_\eta \cong RT(1 - T\alpha/3) \quad (17)$$

where α is the coefficient of thermal expansion.

(15) R. H. Ewell and H. Eyring, *J. Chem. Phys.*, **5**, 726 (1937).

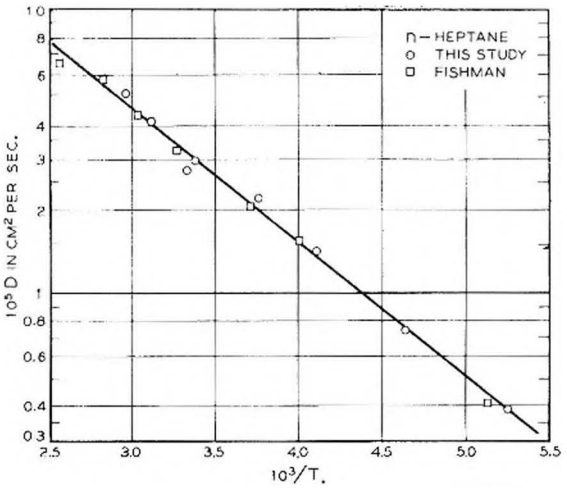

Fig. 4.—The logarithm of the self-diffusion coefficient for *n*-heptane *vs.* reciprocal temperature. The data of Fishman[2] are given for comparison.

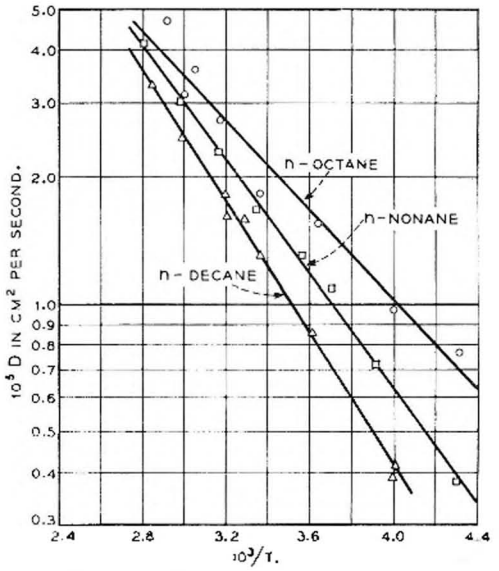

Fig. 5.—The logarithm of the self-diffusion coefficients for *n*-octane, *n*-nonane and *n*-decane *vs.* reciprocal temperature.

In obtaining the latter relation $(N/V)^{1/3}$ was substituted for $\lambda_1/\lambda_2\lambda_3$. In more energetic processes both terms would be negligible but examination of Table I shows that $E_D - E_\eta$ is appreciable. The differences (excepting *n*-pentane) are of the correct sign and order of magnitude. The Eyring theory is not unique in predicting the activation energy difference. For example, the Einstein–Stokes relation $(D\eta/kT) = (1/6\pi a)$ gives $E_D - E_\eta = RT$.

By combining equations 15 and 16 and making use of $\lambda_1\lambda_2\lambda_3 = (V/N)$ we may solve for λ_1 and $\lambda_2\lambda_3$ as

$$\lambda_1 = (D\eta V/NkT)^{1/2} \quad (18)$$

and

$$\lambda_2\lambda_3 = (VkT/D\eta N)^{1/2} \quad (19)$$

Table II contains values for λ_1 and $\lambda_2\lambda_3$ computed from the self-diffusion data of the present study and viscosity and density data taken from the

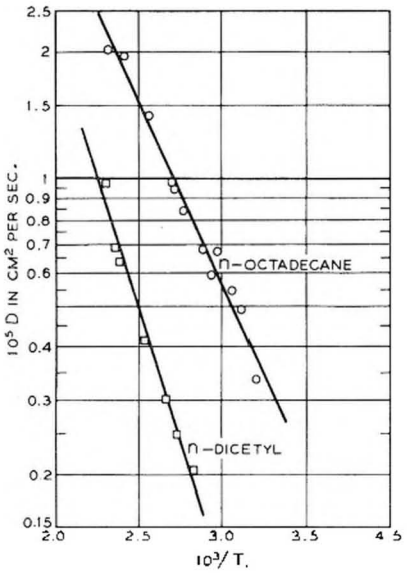

Fig. 6.—The logarithm of the self-diffusion coefficients for *n*-octadecane and *n*-dicetyl *vs.* reciprocal temperature.

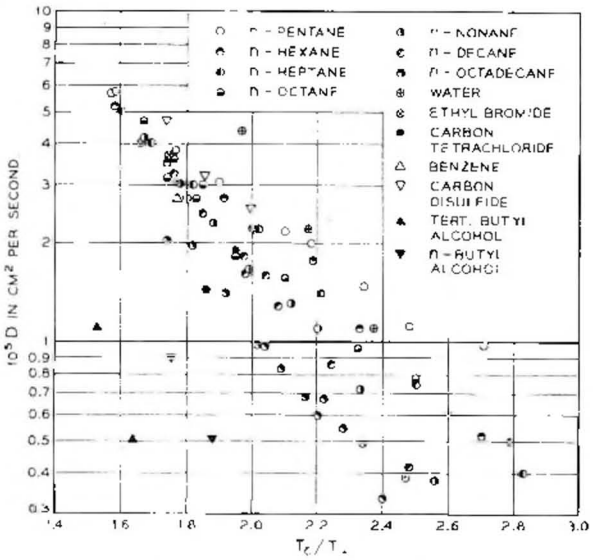

Fig. 7.—The logarithm of the self-diffusion coefficients for various liquids (this study and reference 1) *vs.* reciprocal reduced temperature.

literature.[16-18] The low values of λ_1 for the lower molecular weight materials suggests that the long axis of the molecules must be associated with λ_2 or λ_3. It is also of interest to note that λ_1 is very nearly independent of temperature, *i.e.*, $\lambda_2\lambda_3$ reflects the entire effect of thermal expansion.

Another relationship, readily obtained from equations 15 and 16, is

$$(kT/D\eta) = \lambda_2\lambda_3/\lambda_1$$

This is used frequently in conjunction with the assumption

$$\lambda_2\lambda_3/\lambda_1 = (V/N)^{1/3}$$

to yield

$$(kT/D\eta)(N/V)^{1/3} = 1$$

Table II also contains experimental values for this quantity and it is seen that these are substantially greater than unity. Li and Chang[19] have contended that the reason for this discrepancy, which is observed in other liquids as well as those studied here, lies in an error in the Eyring theory for the viscosity, *i.e.*, the relative velocity of adjacent layers is not properly considered. However, although the modifications of Li and Chang are capable of accounting for all the data (as long as there is complete freedom of choice of liquid structure), we feel that the difficulty may arise, at least in part, in assuming that $\lambda_2\lambda_3/\lambda_1 = (V/N)^{1/3}$. In fact, owing to the tendency of a shearing force to orient molecules such that their greater dimensions lie parallel to the direction of flow, one would expect $\lambda_2\lambda_3/\lambda_1$ to be always greater than $(V/N)^{1/3}$.

Figure 7 is a semi-log plot of the self-diffusion coefficients *vs.* T_c/T for all liquids for which the necessary data were available to us. T_c is the critical temperature.[17] It is seen that all the data lie in the same region of the graph and that the points show signs of converging at high temperatures, *i.e.*, at the critical point. In Table III we list the self-diffusion coefficients extrapolated to the critical point. We can, at present, offer no explanation for this behavior but Fig. 7 may be useful for estimating diffusion coefficients for liquids which have not been measured.

TABLE II

Liquid	λ_1(Å.)[a]	$(\lambda_2\lambda_3)^{1/2}$(Å.)[a]	$\frac{(kT/\eta D)}{(N/V)^{1/3}}$[a]
n-Pentane	2.4	9.0	6.1
n-Hexane	2.5	9.3	5.8
n-Heptane	2.7	9.7	5.5
n-Octane	2.7	10.0	5.6
n-Nonane	2.8	10.2	5.5
n-Decane	2.9	10.5	5.5
n-Octadecane	3.5	12.4	5.1
n-Dicetyl	5.7	12.9	3.0

[a] All data are for 25° except for *n*-octadecane, 50 and dicetyl, 100°.

TABLE III

Liquid	10^4 $D(Tc)$(cm.²/sec.)
n-Pentane	1.4 ± 0.1
n-Hexane	1.8 ± .2
n-Heptane	1.7 ± .1
n-Octane	1.6 ± .2
n-Nonane	2.3 ± .2
n-Decane	2.3 ± .3
n-Octadecane	1.5 ± .1

Let us now turn to the consideration of the mechanism of the diffusion process in the materials studied. Previous discussions have necessarily been based primarily upon viscosity–temperature studies but it is presumed that the molecular motions involved in the two phenomena are the same. Hirschfelder, Stevenson and Eyring[7] described a mechanism which views the passage of two molecular layers past one another by means of the instantaneous formation of a double molecule, one

(16) E. B. Giller and H. G. Drickamer, *Ind. Eng. Chem.*, **41**, 2067 (1949).

(17) Am. Petroleum Inst., Res. Proj. 44, Natl. Bur. Standards, Washington, D. C., 1945.

(18) J. Timmermans, "Physico-Chemical Constants of Pure Organic Compounds," Elsevier Publ., Inc., New York, N. Y., 1950.

(19) J. C. M. Li and P. Chang, *J. Chem. Phys.*, **23**, 518 (1955).

molecule taken from each layer, which rotates through an arc thus permitting the two molecules to pass one another with a minimum of excess volume, and hence energy. More recently Moore, Gibbs and Eyring[20] have modified this picture. These authors consider the elementary process of flow to involve the movement of a dislocation by one lattice position. This is a process which requires coöperation between at least two molecules; one gains energy as it moves out of a lattice position and one loses energy as it moves into a lattice position. The activation energy is considered a measure of the degree of coöperation and is small compared with the dislocation energy. Bondi[21] has also used the Eyring theory as a basis for the description of the flow process and concludes that the liquid structure plays only a minor role. Only the state of order is thought to be important.

Although we feel that there is still not enough experimental information available to establish any mechanism we wish to suggest a model which, in a qualitative way, can account for the observations which have been made. We shall concern ourselves only with the normal paraffins in the present discussion. It seems reasonable that a long molecule acted upon by a shearing force, as in a viscosity experiment, will tend to be aligned parallel to the direction of flow. Thus the direction of molecular flow is parallel to the long axis of the molecule. However, it seems unlikely that the jump length λ is as large as the molecular dimension λ_3 along the molecular axis. Instead we expect λ to be one or two segment lengths. Further, we expect λ, and hence the volume of activation ΔV^* to be independent of the length of molecule. The evidence bearing on this suggestion is meager but encouraging. In the diffusion of *n*-hexane, *n*-octane and *n*-decane through polyethylene it has been observed that ΔV^* is about 50 cm.^{3} for each liquid.[22] This suggests motion by jumps of two segment lengths. Also, ΔV^* derived from the pressure coefficients of viscosity[23] for *n*-pentane, *n*-hexane and *n*-decane are about 18 cm.^{3}. However, plots of log η *vs.* p show considerable curvature at low pressures and the ΔV^* of interest here is given by the limiting slope at atmospheric pressure. This should be larger than the value 18 cm.^{3} which is obtained from the average slope between one and 500 atmospheres.

The heat of activation for viscosity and self-diffusion contains a term $p_i\Delta V^*$ which has been denoted ΔH_h^*.[21] p_i is the internal pressure of the liquid and ΔH_h^* is the energy required to form a hole of volume ΔV^* in the liquid. If ΔV^* is constant, the observed increase in ΔH^* with increasing chain length can be explained in terms of the increase in internal pressure in the series C_5H_{12}, $\cdots$, $C_{10}H_{22}$. If the volumes of activation are computed on the assumption that $\Delta H^* = p_i\Delta V^*$, they are found to be about 30 cm.^{3}.

Much more experimental and theoretical work needs to be done before the mechanism of molecular motion in the paraffins is established. It is apparent that accurate pressure dependences of both η and D will be of value in understanding the mechanism of motion.

Acknowledgment. –We wish to acknowledge helpful discussions with H. G. Drickamer, University of Illinois, E. N. Gilbert, W. P. Slichter and P. W. Anderson, and also the able assistance of E. W. Anderson.

(20) R. J. Moore, P. Gibbs and H. Eyring, THIS JOURNAL, **57**, 172 (1953).

(21) A. Bondi, *J. Chem. Phys.*, **14**, 591 (1956).

(22) D. W. McCall and W. P. Slichter, *J. Am. Chem. Soc.*, **80**, 1861 (1958).

(23) P. W. Bridgman, "The Physics of High Pressure," G. Bell & Sons, London, 1952.

INTERACTIONS OF METALS WITH THEIR MOLTEN SALTS. I. THE NICKEL–NICKEL CHLORIDE SYSTEM*

BY J. W. JOHNSON, DANIEL CUBICCIOTTI AND C. M. KELLEY

Stanford Research Institute, Menlo Park, California

Received May 15, 1958

Nickel metal has been found to have appreciable solubility in molten nickel chloride. The depression of the freezing point of nickel chloride (1009.1°) by the dissolved metal was measured and a eutectic point found at 977.5° and 9 mole % Ni. The constitution of the solution is discussed in the light of the freezing point depression.

Introduction

The phenomenon of metals dissolving in their molten salts has received considerable attention in recent years.[1–3] These studies have been largely confined to the metals of Groups I and II of the periodic table, with some excursions into Groups III, IV, V and the rare earths. Existing hypotheses designed to explain the nature of metal-metal salt solutions have, in general, been specifically directed toward a given group or class of elements. Thus, they do not lend themselves to predictions or explanations of systems outside these groups or classes.

The present investigation of the nickel–nickel chloride system had its inception in a survey of other metal-metal halide systems for appreciable solubility of the metal. It is hoped that data on new systems will provide some elements of an

* This work was sponsored jointly by the Atomic Energy Commission and Stanford Research Institute.

(1) D. D. Cubicciotti and C. D. Thurmond, *J. Am. Chem. Soc.*, **71**, 2149, 4119 (1949); **74**, 1198 (1952).

(2) M. A. Bredig, J. W. Johnson and Wm. T. Smith, Jr., *ibid.*, **77**, 307 (1955); M. A. Bredig, H. R. Bronstein and Wm. T. Smith, Jr., *ibid.*, **77**, 1454 (1955).

(3) J. D. Corbett and S. von Winbush, *ibid.*, **77**, 3964 (1955); J. D. Corbett, S. von Winbush and F. C. Albers, *ibid.*, **79**, 3020 (1957); J. D. Corbett and R. K. McMullan, *ibid.*, **77**, 4217 (1955).

explanation and reveal useful applications of this effect.

Experimental

Materials.—Analytical reagent grade $NiCl_2 \cdot 6H_2O$ and high purity nickel metal fragments were used in this investigation.

The nickel chloride was dehydrated by heating in a Vycor tube through which a stream of dry HCl was passing. The temperature was raised gradually to 550° and held for several hours. After cooling to room temperature, the anhydrous salt containing absorbed HCl was stored in a desiccator for future use. The nickel metal fragments were immersed in a 50–50 mixture of concd. nitric acid and glacial acetic acid and gently heated for 15 minutes. This treatment resulted in a clean surface on the nickel fragments which were then rinsed in distilled water several times, dried under vacuum and stored in a desiccator.

Apparatus and Procedure.—Thermal analysis of samples of known composition was employed to determine the solubility limits of the Ni–$NiCl_2$ system in the salt-rich region. For this purpose, 20 mm. bore Vycor tubes 3 in. long were sealed at one end and a thermocouple well blown in to a distance of $^1/_2$ in. above the bottom. A 4 in. piece of 7 mm. bore Vycor tubing was sealed to the other end for use in loading, evacuation and subsequent sealing under vacuum. The use of Vycor as a container material was dictated by the reactivity of $NiCl_2$ with iron or steel. Nickel was obviously not suitable in this study. Sealed tubes were required because of the high vapor pressure of $NiCl_2$ which has a sublimation pressure of 1 atmosphere some 30° below the melting point.

A platinum–platinum 10% rhodium thermocouple (calibrated at the melting points of NBS standard samples of tin, lead, zinc, aluminum and copper metals) was used to determine the sample temperature. The maximum correction to be applied occurred at the melting point of copper, 1083.3° where the couple read 1081.5. The e.m.f. of the couple was measured with a Rubicon precision potentiometer.

Heating of the samples was accomplished with a 16 in. Marshall furnace having a 3 in. bore and equipped with external taps to which resistances could be attached to reduce temperature gradients.

The procedure employed was to load the Vycor tube with approximately 20 g. of anhydrous $NiCl_2$, containing adsorbed HCl gas, and then to attach the tube to the vacuum line. Pumping was continued at room temperature until the pressure was reduced to 5×10^{-5} mm. then a clam shell heater was placed around the sample and the temperature slowly raised to 550° maintaining the pressure at the above value. The sample was held for one hour at this temperature and pressure, and then allowed to cool to room temperature while still under vacuum. This treatment was judged adequate to remove the last traces of HCl from the $NiCl_2$. The tube was detached from the vacuum line, a weighed amount of nickel metal added corresponding to the composition desired, and the tube reattached to the vacuum line and the pressure again reduced to 5×10^{-5} mm. At this point, the portion of the tube containing the charge was sealed off under vacuum with a hand torch leaving a small hook at the top.

The sealed tube was weighed and hooked to the end of a heavy Chromel wire, the thermocouple was inserted in the well, and the whole assembly lowered into the furnace. The temperature was raised slowly to approximately 1050° and held for one hour to allow complete solution of the metal in the molten salt. At the end of the hour the furnace current was reduced to allow the sample to cool through the desired temperature range. Readings of the e.m.f. of the couple were recorded every minute to determine thermal inflections and halts corresponding to initial precipitation of $NiCl_2$ and solidification at the eutectic temperature and composition. At least two cooling curves were taken for each composition to ensure reproducibility of the thermal effects observed.

After the cooling curves were obtained on each sample, the tube was weighed, opened, and the $NiCl_2$ dissolved in distilled water. The nickel, which remained as a finely divided precipitate in the beaker, was dried and weighed. The weights of the Vycor, the finely divided nickel metal, and the sealed tube allowed the composition to be calculated. The absence of any traces of the original nickel fragments together with the absence of temperature gradients along the tube (thus eliminating the possibility of mass transfer) was taken as evidence that complete solution of the nickel metal had occurred.

Results and Discussion

The data obtained in this study are summarized in the first three columns of Table I. These solutions supercooled about 1° in some cases and it was necessary to obtain the temperature at which the break occurred by extrapolation. This introduces an uncertainty in the tabulated temperatures estimated at ± 0.3°.

TABLE I

MELTING POINT DEPRESSION OF $NiCl_2$ BY NICKEL

Comp., mole % Ni	Temp., °C. Initial break	Eutectic halt	Activity $NiCl_2$ (calcd.)	Calcd. for Ni° Mole fraction $NiCl_2$	Act. coefficient $NiCl_2$
0.00	1009.1	...	1.000	1.000	1.000
0.92	1006.1	...	0.983	0.9908	0.992
1.84	1002.2	...	.962	.9816	.980
4.25	994.3	976.0	.918	.9575	.959
6.10	988.1	977.4	.886	.9390	.944
7.42	983.5	977.6	.862	.9258	.929

The melting point of anhydrous $NiCl_2$ was found to be 1009.1 ± 0.3°, which is to be compared with 1001° obtained by Fischer and Gewehr,[4] 1007–1010° by Jones,[5] and 1030° derived by Coughlin[6] from heat content measurements. The value of 1030° is somewhat disconcerting in view of the high purity $NiCl_2$ used and the careful experimentation involved in its determination. However, alleviating factors exist in that: (1) the measurement of heat content is not a sensitive method for the determination of the melting point; (2) so-called "premelting effects" were observed in the temperature range of 1008 to 1013° which encompasses the values found by Jones[5] and the present work; and (3) impurities present in concentrations of at least 5 mole % would be required to lower the melting point from 1030 to 1009°. Our analysis showed impurities could not have been present in excess of 0.3 mole per cent.

The portion of the Ni–$NiCl_2$ system examined in the course of this work represents about the limit of information obtainable by the method since the solubility curve rises very steeply to the right of the eutectic point, which occurs at 9.1 mole % metal and at a temperature of 977.5 ± 0.3°.

The form of the metallic nickel recovered from the solidified melt by dissolving the $NiCl_2$ in water is of considerable interest. The metal was in the form of fibers 300–400μ long and having a diameter of 1 to 1.5 μ. Microscopic examination revealed most of the fibers to be made up of two or three straight sections attached to each other at sharp angles while some were straight throughout their entire length. The angularity may be a function of the cooling conditions or possibly of the anion of the salt since preliminary tests on $NiBr_2$ resulted in fibers with a high proportion of single straight sec-

(4) W. Fischer and R. Gewehr, *Z. anorg. allgem. Chem.*, **222**, 303 (1935).

(5) G. P. Jones, Royal School of Mines, London, private communication.

(6) J. P. Coughlin, *J. Am. Chem. Soc.*, **73**, 5314 (1951).

tions. The conspicuous absence of branched fibers in the samples examined may be significant. In addition to the fibers, a small portion of the metal was in the form of hexagonal platelets; however, these were not present in all of the melts.

The freezing point depressions of $NiCl_2$ and the experimental heat of fusion of the pure salt provide a basis for speculation concerning the constitution of the melt. The data can be interpreted in two ways and both of these are discussed below: (1) a standard cryoscopic calculation of the number of moles of particles formed per g. atom of nickel metal dissolved has been made; (2) the nickel metal was assumed to be monatomically dispersed in solution and the deviation of the activity of nickel chloride from Raoult's law was calculated.

For the calculation of the number of moles of particles formed per g. atom of nickel dissolved the usual assumptions were made: (a) Raoults' law is obeyed by $NiCl_2$; (b) no solid solution occurs; (c) the heat of fusion is constant over the range of interest. The latter assumption is valid to within 1% from Coughlin's heat content data on liquid and solid $NiCl_2$. The heat of fusion of $NiCl_2$ calculated from the concentration of dissolved nickel and attendant freezing point depressions results in a value of 9,150 cal./mole, while the experimental heat of fusion of $NiCl_2$ reported by Coughlin[6] is 18,450 cal./mole.

The calculated value of the heat of fusion of $NiCl_2$ being very nearly one-half that of the experimental value strongly suggests the existence of two particles in solution per atom of nickel dissolved. A reasonable inference is that univalent nickel ion is formed by the reaction

$$Ni^0 + Ni^{+2} \longrightarrow 2Ni^{+1} \qquad (1)$$

The chemistry of nickel indicates that univalent compounds are not unlikely and this probably foreshadows the transition to copper, which is commonly unipositive. At least one compound containing +1 nickel has been characterized.[7] The existence of the nickel in the metallic state in the solidified melt at room temperature requires that the +1 state be unstable with respect to Ni^0 and Ni^{+2} at some intermediate temperature. Such disproportionation could occur in the transition from liquid to solid.

Recalling the controversy engendered by some previous reports of subhalide formation in metal–metal salt systems, it is pertinent to examine the possibility of an interpretation on a physical basis. The activities and the activity coefficients of $NiCl_2$ consistent with the experimental data were calculated using the relation

$$\ln a_1 = \ln \gamma_1 x_1 = -\frac{\Delta H_f}{R}\frac{(T_m - T)}{T_M T} \qquad (2)$$

where the subscript 1 refers to $NiCl_2$, a_1 is activity, γ_1 activity coefficients and x_1 mole fraction. ΔH_f = 18,450 cal./mole, T is the experimentally determined freezing point and T_M = 1282.1°K., the melting point of $NiCl_2$. The results of these calculations appear in Table I.

As is to be expected from the experimental results, the activity coefficients of $NiCl_2$ are less than unity reflecting the negative deviation from Raoult's law. It must be emphasized that these activity coefficients, which are very nearly equal to the mole fraction of $NiCl_2$, are not referred to the same temperature but to the freezing point of the particular solution in question. The activity coefficients of $NiCl_2$ do not fall below 0.92 in the range examined. Thus, in the absence of information concerning activity coefficients in such systems, a physical interpretation cannot be ruled out.

Therefore despite a factor of 2 in the heat of fusion corresponding to an absolute difference of 9,000 cal./mole, obtained from the two assumptions, it seems the physical picture is not unduly strained to explain the data. It must be admitted that sub-halide formation is an appealing explanation and exhibits positive deviations at the higher concentrations, in accord with other metal–salt systems, but this cannot be considered confirmation.

In the opinion of the authors a decision cannot be made concerning the state of the dissolved nickel in nickel chloride with the available data. Extreme caution must be observed when using freezing point depression measurements to determine the nature of dissolved species in these systems.

(7) H. Remy, "Treatise on Inorganic Chemistry," translated by J. S. Anderson and edited by J. Kleinberg, Elsevier Publ. Co., 1956, Vol. II, p. 311.

A SPECTROPHOTOMETRIC METHOD FOR THE DETERMINATION OF OVERLAPPING IONIZATION CONSTANTS

BY KOK-PENG ANG

Chemistry Department, University of Malaya, Singapore

Received May 21, 1958

A new spectrophotometric method for the determination of overlapping ionization constants of dibasic acids is described. The method has been tested successfully on the data for isophthalic acid.

The ionization of a dibasic acid may be represented as

$$R_1 \rightleftarrows R_2 + H^+$$
$$R_2 \rightleftarrows R_3 + H^+$$

where R_1 can be a cation, *e.g.*, in glycine hydrochloride; a neutral molecule, succinic acid; or an anion, *e.g.*, dihydrogen citrate anion.

The thermodynamic and concentration ionization constants are

$$K_1 = \frac{[R_2]\gamma_2}{[R_1]\gamma_1} a = k_1 \frac{\gamma_2}{\gamma_1} \qquad (1)$$

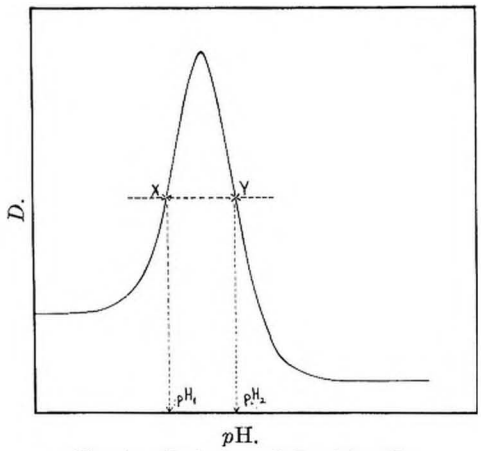

Fig. 1.—Variation of D with pH.

$$K_2 = \frac{[R_3]\gamma_3}{[R_2]\gamma_2} a = k_2 \frac{\gamma_3}{\gamma_2} \qquad (2)$$

where the brackets denote molar concentrations, γ_1, γ_2, γ_3, the activity coefficients of the species R_1, R_2, R_3, respectively, and "a" is the hydrogen ion activity.

If ϵ_1, ϵ_2 and ϵ_3 are the molar extinction coefficients of the species R_1, R_2, R_3, respectively, the optical density D of a solution containing a mixture of these species in a cell of 1 cm. length is given by

$$D = \epsilon_1[R_1] + \epsilon_2[R_2] + \epsilon_3[R_3] \qquad (3)$$

If C is the total acid concentration, then

$$C = [R_1] + [R_2] + [R_3] \qquad (4)$$

From equations 1, 2, 3 and 4 the following relationship is obtained, where ϵ is the molar extinction coefficient of a solution containing a mixture of the various species

$$a^2(\epsilon - \epsilon_1) + ak_1(\epsilon - \epsilon_2) + k_1k_2(\epsilon - \epsilon_3) = 0 \qquad (5)$$

In equation 5, ϵ and "a" are measured for each solution. Of the molar extinction coefficients of the three species, ϵ_1 and ϵ_3 may usually be obtained from strongly acid and alkaline solutions, respectively, but if the ionization constants are of the same order there is no direct way of measuring ϵ_2. If the measurements of ϵ are made at three pH values, three simultaneous equations of the type of (5) can be solved for k_1, $k_1\epsilon_2$ and k_1k_2; this has been done recently for p-aminobenzoic acid[1] but much reliance has to be put on the three experimental measurements. Thamer and Voigt[2] have devised a method applicable if, at a given wave length, the optical density *vs.* pH curve has a maximum or minimum. Their method demands an accurate knowledge of the D and pH values at this maximum (or minimum) which may not always be easy to measure, *e.g.*, in the case of vanillylamine hydrochloride.[3] The method now described utilizes points in the middle portions of the steep sections of the D *vs.* pH plot.

For a monobasic acid, equation 5 simplifies to

$$k_1 = \frac{\epsilon - \epsilon_1}{\epsilon_2 - \epsilon} a \qquad (6)$$

an equation similar to that of Stenström and Goldsmith[4] with hydrogen ion activity in the place of hydrogen ion concentration. If the ionization constants of a dibasic acid are well separated, *i.e.*, when $k_1/k_2 > 1000$, no great error is involved if the second step of ionization is assumed to operate only when the first is complete. If such an assumption is made, then, during the first stage of the neutralization of the acid, the third term of equation 5 is negligible in comparison with the first two terms and the equation reduces to that of a monobasic acid and equation 6 becomes applicable. In the second stage a^2 is small compared with ak_1 and k_1k_2 and equation 5 reduces to

$$k_2 = \frac{\epsilon - \epsilon_2}{\epsilon_3 - \epsilon} a \qquad (7)$$

an equation similar to that of Banks and Carlson[5] with hydrogen ion activity replacing their hydrogen ion concentration.

In the method now proposed, a plot of D at a fixed wave length is made against pH (Fig. 1). Let ϵ be the observed extinction coefficient at X and at Y where the hydrogen ion activities are a_1 and a_2, respectively. Then

$$a_1^2(\epsilon - \epsilon_1) + a_1k_1(\epsilon - \epsilon_2) + k_1k_2(\epsilon - \epsilon_3) = 0$$

and

$$a_2^2(\epsilon - \epsilon_1) + a_2k_1(\epsilon - \epsilon_2) + k_1k_2(\epsilon - \epsilon_3) = 0$$

from which

$$\epsilon = \epsilon_2 - k_2P \qquad (8)$$

where

$$P = \frac{(\epsilon - \epsilon_3)(a_1 + a_2)}{a_1a_2}$$

and

$$\epsilon = \epsilon_1 + k_1Q \qquad (9)$$

where

$$Q = \frac{(\epsilon_2 - \epsilon)}{(a_1 + a_2)}$$

All the quantities in P are directly measurable; ϵ_3 is calculated from the optical density of a sufficiently alkaline solution. k_2 thus may be readily obtained by plotting ϵ against P. The intercept of the plot gives ϵ_2 which together with the other measurable quantities is used to compute Q. The plot of ϵ against Q now gives k_1.

When the ionization constants are well separated, $a_1 >> a_2$ and equations 8 and 9 approximate to equations 7 and 6, respectively.

From equations 8 and 9 this relationship arises

$$k_1k_2 = \frac{(\epsilon - \epsilon_1)}{(\epsilon - \epsilon_3)} a_1a_2$$

At the maximum $a_1 = a_2 = a_0$ and $\epsilon = \epsilon_{max}$, whence

$$k_1k_2 = \frac{(\epsilon_{max} - \epsilon_1)}{(\epsilon_{max} - \epsilon_3)} a_0^2$$

an expression identical to that of Thamer and Voigt.[2]

The data of Thamer and Voigt on isophthalic acid have been treated by the present method with the results shown in Table I.

(1) R. A. Robinson and A. I. Biggs, *Australian J. Chem.*, **10**, 128 (1957).

(2) B. J. Thamer and A. F. Voigt, THIS JOURNAL, **56**, 225 (1952).

(3) R. A. Robinson and A. K. Kiang, *Trans. Faraday Soc.*, **52**, 327 1956).

(4) W. Stenström and N. Goldsmith, THIS JOURNAL, **30**, 1683 (1926).

(5) C. V. Banks and A. B. Carlson, *Anal. Chim. Acta*, **7**, 291 (1952).

TABLE I

FUNCTIONS P AND Q

pH_1[a]	pH_2[a]	ϵ[a]	$10^{-7}P$	$10^{-8}Q$
2.90	5.047	2600	1.571	5.17
3.00	4.89	2640	1.416	6.07
3.10	4.765	2678	1.296	7.11
3.20	4.66	2714	1.201	8.29
3.30	4.577	2750	1.153	9.57
3.40	4.497	2785	1.102	10.93
3.50	4.405	2823	1.037	12.15
3.60	4.295	2858	0.944	13.15
3.70	4.185	2885	0.864	13.97

[a] From the data of Thamer and Voigt.[2]

From plots of ϵ against P and Q values of $pk_1 = 3.51$ with standard deviation $= \pm 0.03$, and $pk_2 = 4.36 \pm 0.08$ were obtained; these can be compared with $pk_1 = 3.49 \pm 0.08$ and $pk_2 = 4.40 \pm 0.08$ given by Thamer and Voigt. However, some scatter of the points in the plots of ϵ against P and Q was observed. It was decided therefore to redetermine the D *vs.* pH curve paying particular attention to the middle portions of the steep sections on both sides of the maximum.

Experimental and Results

Isophthalic acid was purified by the method used by Thamer and Voigt. A stock solution of the sodium salt of concentration 3×10^{-3} M was prepared with freshly boiled distilled water by adding the requisite amount of sodium hydroxide to the acid. Aliquot portions were diluted to 1.6×10^{-4} M for optical density measurements. Acetate, formate and phosphate buffers were used in the pH range between 2.7 and 7.4. Below pH 2.7 hydrochloric acid solutions were used. Solutions with pH between 2.7 and 5.5 were maintained at constant ionic strength by the addition of sodium chloride.

Optical density measurements were made with a Beckman Model DU Spectrophotometer equipped with a water-jacketed cell compartment. In every case appropriate blanks were used and all measurements carried out with matched silica cells of 1 cm. length and at a temperature of 25°. The wave length drum was set at one value throughout the measurements.

The pH was measured with a Beckman Model G pH meter fitted with glass and calomel electrodes. The instrument was standardized at pH 4.00 with 0.05 M potassium hydrogen phthalate solution.

TABLE II

OPTICAL DENSITIES OF ISOPHTHALIC ACID

$\lambda = 248$ mμ, $C = 1.608 \times 10^{-4}$ M

Soln. no.	pH	D	Soln. no.	pH	D
1	0.30	0.354	20	3.89	0.410
2	1.19	.354	21	3.99	.414
3	2.09	.355	22	4.09	.413
4	2.73	.365	23	4.11	.410
5	2.77	.367	24	4.18	.409
6	2.93	.372	25	4.28	.405
7	2.98	.372	26	4.38	.401
8	3.05	.375	27	4.49	.397
9	3.095	.378	28	4.60	.390
10	3.17	.381	29	4.675	.383
11	3.21	.382	30	4.77	.379
12	3.31	.386	31	4.87	.373
13	3.405	.393	32	4.97	.367
14	3.47	.397	33	5.22	.355
15	3.49	.397	34	5.29	.350
16	3.58	.403	35	5.54	.348
17	3.68	.404	36	5.86	.343
18	3.69	.407	37	6.75	.337
19	3.79	.408	38	7.37	.337

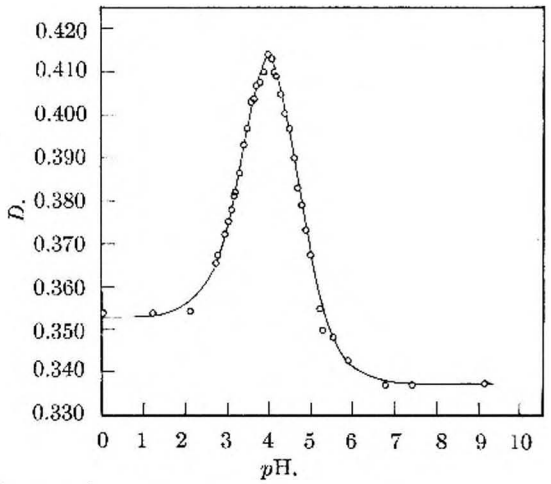

Fig. 2.—Plot of D against pH at $\lambda = 248$ mμ: circles, experimental points; solid line, calculated.

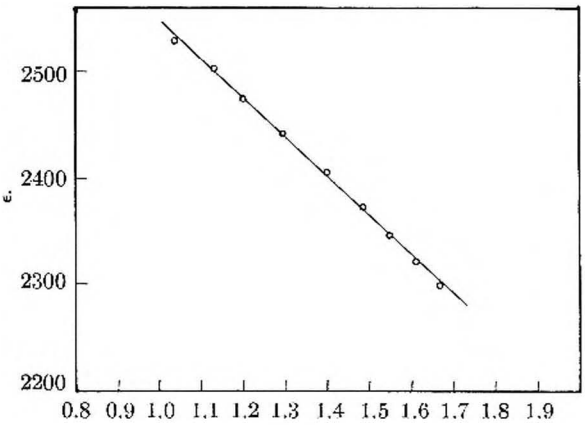

Fig. 3.—Plot of ϵ against function P.

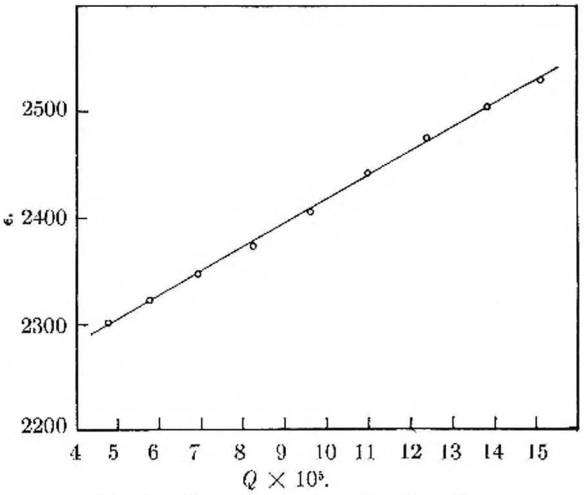

Fig. 4.—Plot of ϵ against function Q.

The results are shown in Table II and Table III and in Figs. 2, 3 and 4.

Solutions no. 4–35 were made up to a total ionic strength of 0.014 by the addition of the requisite amount of sodium chloride. Solutions no. 1–3 contained hydrochloric acid, solutions no. 4–23 formate buffer, solutions no. 24–35 acetate buffer and solutions no. 36–38 phosphate buffer

TABLE III

FUNCTIONS P AND Q

pH_1	pH_2	ϵ	$10^{-7}P$	$10^{-6}Q$
2.90	4.905	2302	1.671	4.79
3.00	4.845	2323	1.611	5.80
3.10	4.780	2348	1.550	6.94
3.20	4.715	2374	1.486	8.26
3.30	4.635	2406	1.400	9.63
3.40	4.543	2442	1.295	10.99
3.50	4.455	2475	1.200	12.41
3.60	4.375	2504	1.130	13.87
3.70	4.277	2529	1.036	15.14

The values of ϵ differ from those of Thamer and Voigt; in this region of the spectrum, however, ϵ changes rapidly with change in wave length and the difference may well be due to slight difference in the wave length drum of the instruments used. A difference of less than 1 mμ in the drum calibration would account for the discrepancy. What is of more interest to us is the difference between values of ϵ at different pH values rather than their absolute values. Figures 3 and 4 show less scatter of points than those obtained with the data of Thamer and Voigt, and yield the data

$$\epsilon_1 = 2193 \pm 3 \qquad pk_1\ 3.65 \pm 0.02$$
$$\epsilon_2 = 2911 \pm 3 \qquad pk_2\ 4.44 \pm 0.02$$

Measurements in alkaline solutions give $\epsilon_3 = 2096$. The value of ϵ_1 compares very well with the experimentally determined value of 2200. It sometimes happens that ϵ_1 cannot be measured directly, but it will be noted that a knowledge of the value of ϵ_1 is not required in the present method. The above five constants were used to calculate the solid line of Fig. 2 from equation 5 and the relationship $D = \epsilon C$. If the necessary activity coefficients are calculated by the equation

$$-\log \gamma = 0.5092Z^2\sqrt{I}/(1 + \sqrt{I})$$

then $pK_1 = 3.70 \pm 0.02$ and $pK_2 = 4.60 \pm 0.02$. These values compare well with the final values of $pK_1 = 3.62 \pm 0.06$ and $pK_2 = 4.60 \pm 0.08$ reported by Thamer and Voigt from measurements at two wave lengths.

Acknowledgment.—The author wishes to thank Professor R. A. Robinson for helpful discussions in the course of the work.

THE ADSORPTION OF KRYPTON ON GERMANIUM[1]

BY ARTHUR J. ROSENBERG

Lincoln Laboratory, Massachusetts Institute of Technology, Lexington, Massachusetts

Received May 26, 1958

The partial molal free energies ($\overline{\Delta\mu}$), heats ($\overline{\Delta h}$) and entropies ($\overline{\Delta s}$) of the adsorption of krypton on vacuum-crushed germanium crystals were derived from data obtained at 77.8°K. and at 82.3°K. in the pressure range of 10^{-4} to 4 mm., which corresponds to coverages of 0.15 to 2.0 monolayer equivalents. With the assumption that the bulk polarizability of germanium is preserved at the surface, a lower limit on the adsorption energy was calculated by lattice summations of atomic dispersion potentials and r^{-12} repulsion potentials. The calculated values are too large, and it is concluded that the nearly degenerate space-charge region associated with a germanium surface invalidates atomic polarizability as the source of adsorptive energy. At low surface coverages, the variations in $\overline{\Delta h}$ indicate an energetically heterogeneous surface. The transition from first- to second-layer adsorption is relatively abrupt; $|\overline{\Delta h}|$ drops sharply, and $\overline{\Delta s}$ exhibits a minimum. Oxygenation of the surface diminishes $|\overline{\Delta\mu}|$ for the adsorption of more than 0.5 monolayer of krypton. At lower krypton coverages, $|\overline{\Delta\mu}|$ first rises, then falls with increasing oxygen coverage. Oxygenation diminishes both $|\overline{\Delta h}|$ and $|\overline{\Delta s}|$. The over-all variation in both functions is similar to those on the bare surfaces, but the transition from first- to second-layer adsorption is not abrupt.

Introduction

Recent experimental studies have shown that an excess electron hole conductivity is associated with clean germanium surfaces.[2] This effect is presumed to originate in the extra energy states for electrons that arise quantum mechanically from the termination of a crystalline lattice at its surface.[3] Electrons entering these states attract an equal number of electron holes into the region under the surface plane. These holes, which are free to move parallel with the surface, enhance the normal surface conductivity. By making reasonable assumptions concerning the relation of the trap levels to the Fermi level and on the mobility of holes in the space-charge region, Handler[2] places the lower limit on the number of trapped electrons at 10^{12} per cm.^{2}, and sets the theoretical upper limit at *ca.* 10^{15} per cm.^{2}. Most of the corresponding holes circulate within a few interatomic spacings of the surface plane. Indeed, there is evidence that the accumulation of fixed negative charge on the surface atoms is sufficient to force the valence band to cross the Fermi level and create a thin region at the surface that is degenerate with respect to electron holes.[4] To this extent, the surface acts as a semi-metal,[5] such as bismuth. This behavior is observed even at 80°K.[4] at which the bulk effectively becomes an insulator.[6] This phenomenon should be reproduced to some extent in all crystalline semiconductors. Its importance in adsorption processes is evident. When electrons are transferred between a semiconductor and a foreign atom adsorbed upon its

(1) The research reported in this document was supported jointly by the Army, Navy and Air Force under contract with the Massachusetts Institute of Technology.

(2) P. Handler, "Semiconductor Surface Physics," Ed. R. H. Kingston, U. of Penn. Press, 1957, p. 23.

(3) I. Tamm, *Physik Z. Sowjetunion*, 1, 733 (1932).

(4) P. Handler, to be published.

(5) K. Lark-Horovitz, *et al.*, *Phys. Rev.*, 69, 250 (1946).

(6) F. Seitz, "Modern Theory of Solids," McGraw-Hill Book Co., New York, N. Y., 1940, p. 425.

surface, the trap structure and the associated space-charge region can undergo profound changes which can influence the course of chemisorption and other surface reactions.[7]

In true physical adsorption, on the other hand, the electrochemical properties of surfaces are, to a first approximation, unaffected by the adsorption process. Thus the adsorption of rare gases is generally attributed to the interaction of transient electrostatic multipoles in the gas atom and those in the adsorbent (dispersion energy), and to the polarization of the gas atom by any permanent electrostatic field associated with the surface (polarization energy).[8]

The dispersion energy is related to the polarizabilities of the adatom and of the adsorbent. The polarizability of an insulator resides in its atoms, while that of a metal resides principally in the conduction electrons. Both systems have been treated quantum-mechanically,[9] but only the former yields unambiguous results.[8] Comparing these results with experimental energies of adsorption provides some insight into the real polarizability of a surface. In principle, one may ascertain from studies of the adsorption of rare gases whether the adsorptive properties of a surface can be practically represented in terms of the atomic properties of the adsorbent.

In the present paper the results of a series of detailed measurements on the adsorption of krypton on germanium surfaces at 77.8 and 82.3°K. are summarized. The data permit calculation of partial molal thermodynamic quantities for the adsorption process, and the energy of adsorption thus derived is compared with the theoretical energies calculated with the assumption that the dispersion energy originates in the polarizability of individual germanium atoms. The variation of the adsorption energy with increasing surface coverage, and the corresponding variations in the entropy and in the free energy of adsorption are discussed qualitatively. The results for clean surfaces are compared with measurements on the same surfaces after deliberate exposure to oxygen which is strongly chemisorbed.

Experimental

Highly purified germanium (3 grams, 30 ohm-cm., p-type) was crushed under high vacuum in a closed system. The powder, with a surface area of 2600 cm.^{2}, was sealed off in a 1-cc. bulb and transferred through a breakseal to a gas-adsorption apparatus. The crushing and purification techniques and the adsorption apparatus have been described elsewhere.[10,11] The only revision in the latter,[11] which was originally designed for the precise measurement of small surface areas, consisted in the insertion of a 10-inch U-tube of 2-mm. capillary tubing between the sample chamber and the mercury cutoff. The system was outgassed by prolonged flaming. All mercury vapor was then removed from the sample chamber side by immersing the U-tube in liquid nitrogen. Thenceforth, to the completion of the subsequent experiments, the U-tube was continuously immersed in liquid nitrogen (between measurements) and trichloroethylene–Dry Ice (during measurements). The breakseal of the sample chamber was cracked, and the dead-space volume was calculated from krypton expansion into the sample chamber. The chamber was then immersed in a Dewar flask that contained liquid nitrogen for adsorption measurements at 77.8°K., and a mixture of liquid nitrogen and oxygen for measurements at 82.3°K. The temperature of the bath, monitored in each case by a nitrogen vapor-pressure thermometer, was maintained within ±0.03°. Light was rigorously excluded from the sample chamber in order to eliminate its thermal effect.[12] The technique for determining the adsorption isotherms has been given previously.[11] An extended correction had to be made for thermal transpiration and the appropriate data were obtained.[13]

In the isotherm measurements that will be described the capillary connection leading to the sample chamber consisted of sections of 2.145 mm. and 4.20 mm. tubing. The thermostat level was centered on the larger capillary when the buret pressure fell below 50 μ, and on the smaller capillary at higher pressures. As a check on the thermal-transpiration corrections,[13] the results at a given coverage were repeated frequently with both capillaries, and were found to be in agreement.

Great precision was needed because of the small temperature difference (4.5°K.) that was employed to derive the thermodynamic quantities. Since the temperatures and volumes of the apparatus were known precisely, only the pressure measurements were a significant source of random experimental error. As illustrated earlier,[11] the thermistor manometer can measure krypton pressures directly with a precision of 0.1% (or better) in the range 20–2,000 μ. In the present case isotherm measurements were extended with good precision to 5,000 μ by closing the sample chamber at equilibrium, expanding the gas remaining in the buret to a readable pressure and back-calculating. At pressures below 20 μ, the uncertainty in pressure measurements can be reduced to 0.003 μ so that, except for the very lowest readings, the error on this account did not exceed 1%. The most direct check on the experimental error was the reproducibility of a given point on an isotherm; except in the region of desorption hysteresis, a uniform precision of better than 0.5% was obtained for the equilibrium adsorption pressure at any given krypton coverage. This was confirmed repeatedly for the sample that has been discussed and for similar samples.

Suitable corrections were introduced for the almost negligible adsorption on the small area presented by the sample chamber walls.

Both the krypton and oxygen employed were of spectroscopic purity.

Results

Adsorption Isotherms.—Adsorption and desorption isotherms of krypton upon the crushed germanium were measured at three stages of oxidation.

Stage I: "essentially bare"; before the deliberate addition of oxygen; surface concentration of chemisorbed oxygen $\lesssim 0.2 \times 10^{14}$ atoms/cm.^{2}; krypton isotherms at 77.8 and 82.3°K.

Stage II: "partially oxygenated"; after the (instantaneous) adsorption of a single charge of 21,570 μcc. of O_2 at 20°; surface concentration of chemisorbed oxygen $\backsimeq 5.6 \times 10^{14}$ atoms/cm.^{2}; krypton isotherm at 77.8°K.

Stage III: "saturated"; after the logarithmic uptake of an additional 28,300 μcc. of O_2 in 720 minutes at 20°; surface concentration of oxygen $\backsimeq 12.5 \times 10^{14}$ atoms/cm.^{2}; krypton isotherms at 77.8 and 82.3°K.

It has been shown[14] that the uptake of oxygen by

(7) (a) K. Hauffe, *Advances in Catalysis*, **7**, 213 (1955); (b) P. Aigrain and C. Dugas, *Z. Elektrochem.*, **56**, 363 (1952).

(8) (a) S. Brunauer, "Adsorption of Gases and Vapors," Princeton Univ. Press, Princeton, N. J., 1943, p. 180; (b) J. H. deBoer, *Advances in Catalysis*, **8**, 17 (1956); (c) J. M. Honig, *Ann. N. Y. Acad. Sci.*, **58**, 741 (1954).

(9) (a) F. London, *Z. Physik*, **63**, 245 (1930); (b) H. Margenau and W. G. Pollard, *Phys. Rev.*, **60**, 128 (1941); F. J. R. Prosen and R. G. Sachs, *ibid.*, **61**, 65 (1942).

(10) A. J. Rosenberg, P. H. Robinson and H. C. Gatos, *J. App. Phys.*, **29**, 771 (1958).

(11) A. J. Rosenberg, *J. Am. Chem. Soc.*, **78**, 2929 (1956).

(12) A. J. Rosenberg and C. S. Martel, Jr., THIS JOURNAL, **61**, 512 (1957).

(13) A. J. Rosenberg and C. S. Martel, Jr., *ibid.*, **62**, 457 (1958).

(14) M. Green, J. A. Kafalas and P. H. Robinson, "Semiconductor Surface Physics," Ed. R. H. Kingston, U. of Penn. Press, 1957, p. 349.

TABLE I

ADSORPTION OF KRYPTON ON CRUSHED GERMANIUM

		Equilibrium pressure in μ				
$N \times 10^{-16}$	θ[b]	p_{I}(77.78°K.)	p_{I}(82.33°K.)	p_{II}(77.78°K.)	p_{III}(77.78°K.)	p_{III}(82.33°K.)
200.3	0.1533	0.426[a]	1.727	0.1415	0.141	0.572
267.0	.2030	0.862	3.311	0.359	0.383	1.469
333.8	.2539	1.497	5.550	0.757	0.868	3.210
400.6	.3047	2.358	8.55	1.419	1.758	6.32
467.3	.3554	3.474	12.41	2.452	3.296	11.58
532.5	.4042	4.820	17.01	3.924	5.729	19.62
596.4	.4536	6.502	22.73	6.067	9.38	31.46
669.2	.5089	8.997	30.95	9.552	15.60	50.55
734.7	.5580	11.91	40.15	14.29	23.34	73.4
804.6	.6119	16.11	53.0	21.58	35.24	107.3
862.1	.6556	20.47	65.9	29.84	47.44	142.8
923.7	.7025	26.30	83.1	43.16	63.8	189.1
989.8	.7527	34.12	108.6	62.38	85.5	251.6
1060.6	.8070	46.35	148.8	89.12	115.4	334.0
1136.4	.8642	66.9	211.2	127.4	155.3	442.3
1190.1	.9050	88.3	271.4	160.3	188.4	531.8
1275.1	.9696	136.5	408.1	216.3	249.5	698.0
1335.2	1.015	184.1	535.5	264.3	299.3	835
1398.1	1.063	244.9	693.0	317.8	356.4	992
1464.1	1.113	318.6	879	386.4	423.7	1172
1605.3	1.221	493.1	1317	543.2	589.0	1591
1720.1	1.308	631.0	1674	671.5	735	1966
1843.1	1.402	764	2017	803.6	887	2354
1975.9	1.502	881	2322	933.4	1040	2747
2116.2	1.609	991	2617	1069.0	1175	3110
2267.4	1.724	1099	2902	1202	1297	3442
2429.7	1.848	1205	3197	1306	1409	3747
Bulk condensation		1878	4935	1878	1878	4935

[a] The uncertainty in p for a given θ is <0.5%. [b] $\theta = N/(1.315 \times 10^{18})$.

crushed germanium corresponds to 12.8×10^{14} atoms/cm.^{2} (19.8 μcc. O_2/cm.^{2}) in 720 minutes at 20°, and increases thereafter at a rate of 12% per decade in time. The result was independent of conductivity type and was obtained both when the sample was crushed under an oxygen atmosphere and when it was crushed under vacuum, transferred through a breakseal to the adsorption apparatus and subsequently oxidized. In the present case the total measured uptake of oxygen was 49,870 μcc., compared with a predicted uptake of 50,400 μcc. based on a surface area of 2550 cm.^{2} (see below). The difference -500 μcc. or 0.2×10^{14} oxygen atoms/cm.^{2} is attributed to contamination of the sample by outgassed oxygen, and is divided, arbitrarily, between stage I and stage II in the proportion of elapsed experimental time in each stage, *viz.*, 10 days and 2 days, or 0.16 and 0.04×10^{14} oxygen atoms per cm.^{2}, respectively. It should be noted, however, that in the rechecks of the isotherm points in stage I, no systematic deviations were perceptible, and in similar experiments the isotherms (normalized to unit surface area) on unoxidized samples were identical.

More than 400 krypton isotherm points were determined and a summary based upon interpolations of each adsorption isotherm is given in Table I. For $\theta = N/(1.315 \times 10^{18}) \lesssim 0.5$, the data are well fitted by equations of the form

$$\log p = a + b \log N + cN \qquad (1)$$

Table II summarizes the parameters obtained by fitting the data to the B.E.T. equation[15]

$$\frac{P}{(P_0 - P)N} = \frac{1}{N_m C} + \frac{C-1}{N_m C} \times \frac{P}{P_0} \qquad (2)$$

where P_0 is the saturation pressure of bulk krypton at the temperature of the experiment. C is a constant which relates to the heat of adsorption. N_m is presumed to give the number of adatoms in a fully packed monolayer. Calculations were made both for values of P_0 corresponding to the vapor pressure of solid krypton (1878 μ at 77.8°K., 4935 μ at 82.3°K.) and to the vapor pressure of supercooled liquid krypton (2723 μ at 77.8°K., 6978 μ at 82.3°K.).[16] The equation gives an excellent fit of the data for the ranges of P/P_0 indicated in the table. The range of fit is better with P_0 (liquid). N_m is independent of temperature and, unlike the parameter, C, is not strongly affected by surface oxygenation. This matter will be discussed below. Earlier experiments on oxygenated germanium[11] have shown that 19.4 Å.^{2} is an appropriate factor

TABLE II

PARAMETERS OF THE B.E.T. EQUATION

Oxidation stage	Temp., °K.	p_0 = supercooled liquid $N_m \times 10^{-18}$	C	$<p/p_0<$	p_0 = solid $N_m \times 10^{-18}$	C	$<p/p_0<$
I	77.8	1.347	179	0.025–0.32	1.263	174	0.02–0.15
II		1.338	86	.04 – .3	1.217	98	.03 – .18
III		1.280	87	.04 – .3	1.188	80	.04– .25
I	82.3	1.338	154	.02 – .16	1.253	150	.02– .18
III		1.265	85	.05 – .3	1.181	70	.05– .25

(15) S. Brunauer, P. H. Emmett and E. Teller, *J. Am. Chem. Soc.*, **60**, 309 (1938).

(16) J. J. Meihuizin and C. A. Crommelin, *Physica*, **4**, 1 (1937).

for N_m obtained with P_0 (liquid) to obtain the surface area of the sample. The area so calculated is 2550 cm.^{2}.

Reversibility of Adsorption.—The reversibility of krypton adsorption below one monolayer was established by the identity of the adsorption and desorption isotherms. At higher coverages, however, desorption hysteresis[17] was observed. The position of the desorption curve fell higher, the higher the value of θ from which desorption commenced. The data for one such curve are given in Table III. Inasmuch as the surfaces were prepared by crystal fracture, desorption hysteresis cannot be attributed to surface porosity in the usual sense. It is likely that surface cracks or fissures are responsible.

TABLE III

DESORPTION HYSTERESIS

Stage I; 77.8°K.; desorption commencing at $\theta = 2.463$ ($p = 1573$ μ)

p, μ	$\theta_{Adsorption}$	$\theta_{Desorption}$	$\theta_{Desorption}/\theta_{Adsorption}$
1259	1.879	1.967	1.047
1014	1.607	1.659	1.032
939.2	1.535	1.583	1.031
791.0	1.403	1.448	1.032
510.0	1.211	1.238	1.022
459.1	1.181	1.205	1.020
371.4	1.128	1.148	1.018
233.8	1.039	1.054	1.014
179.9	0.9950	1.005	1.010
115.5	0.9305	0.9280	0.997
73.30	0.8650	0.8630	0.998
57.37	0.8280	0.8267	0.998
42.97	0.7817	0.7823	1.001
33.77	0.7398	0.7415	1.002

Thermodynamics of Adsorption.—Gas adsorption is governed at equilibrium by the condition that the partial molal free energy of the adsorbable species be the same in the condensed phase and in the ambient vapor. This condition, applied to the experimental isotherms, $N(p,T)$, provides the means by which the thermodynamic properties of the adsorbate can be derived from those of the vapor.

The definitions of the quantities[18] that will be discussed and their relation to isotherm data[19] are

Partial molal free energy of adsorption

$$\overline{\Delta\mu} \cong (\partial G/\partial N)_{T,A} - \mu_g^* = RT \ln (p/p^*) \quad (3)$$

Partial molal heat of adsorption

$$\overline{\Delta h} \cong (\partial H/\partial N)_{T,A} - h_g = R[T_2T_1/(T_2 - T_1)] \ln (p_2/p_1)_{N/A} \quad (4)$$

Partial molal entropy of adsorption

$$\overline{\Delta s} \cong (\partial S/\partial N)_{T,A} - s_g^* = \overline{\Delta h}/T + R \ln (p^*/p) \quad (5)$$

where N is the number of atoms adsorbed at a partial pressure p and at a temperature T (the pressures p_1 and p_2 correspond to different temperatures, T_1 and T_2) upon a sample with a surface area A, which yields an over-all condensed phase (adsorbent + adsorbate) characterized by Gibbs free energy, heat content and entropy represented by G, H and S; μ_g^* and s_g^* are the molar free energy and entropy of the adsorbed species in the gas phase at a standard pressure p^* (which will be taken as one atmosphere) and h_g is the molar heat content of the gas, which is independent of pressure. The usual assumptions are made that the gas phase is ideal, the molar volume of the gas phase greatly exceeds the partial molal volume of the condensed phase, and the partial molal properties of the condensed phase are insensitive to hydrostatic pressure.

There is another, and fundamental, premise underlying the definitions. The influence of the adsorbate upon the thermodynamic properties of the adsorbent must be confined to a depth that is small

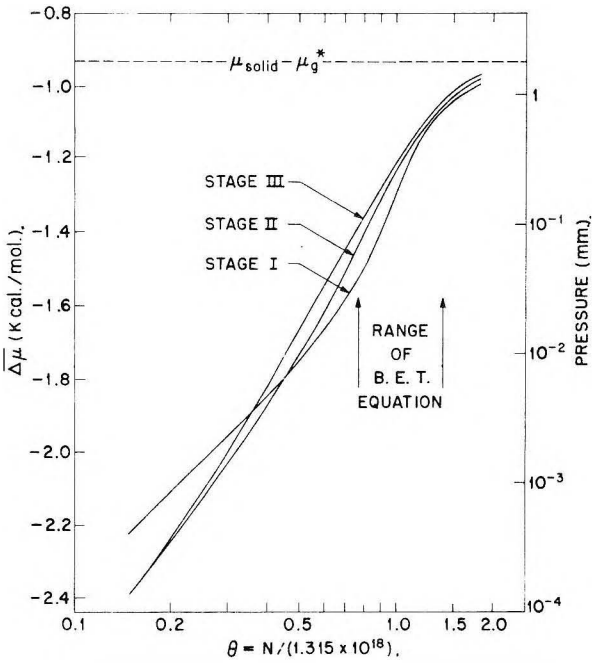

Fig. 1.—Partial molal free energy of adsorption; 77.8°K.; experimental uncertainty <2 cal./mole.

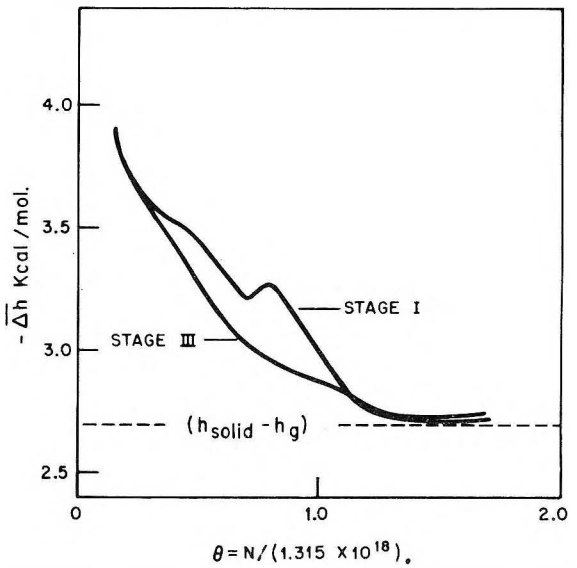

Fig. 2.—Partial molal heat of adsorption; 77.8–82.3°K.; experimental uncertainty <60 cal./mole.

(17) Ref. 8a, p. 394.

(18) We had hoped that the *integral* molar quantities might be derived by integration of the partial quantities or by Hill's[19] more accurate procedure which utilizes the integral $\int_0^p N \, d \ln p$. These calculations were precluded, however, by our inability to make a reliable extrapolation of the data to $N = 0$.

(19) T. L. Hill, *J. Chem. Phys.*, **17**, 520 (1949); *Advances in Catalysis*, **4**, 801 (1952).

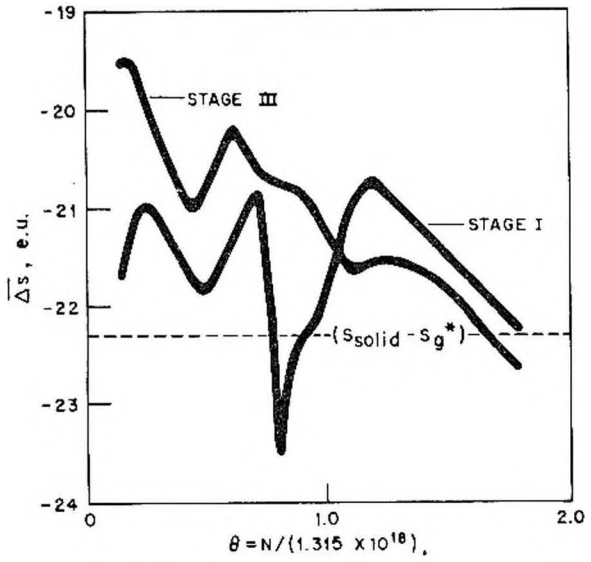

Fig. 3.—Partial molal entropy of adsorption; 77.8°K.; experimental uncertainty <0.7 e.u.

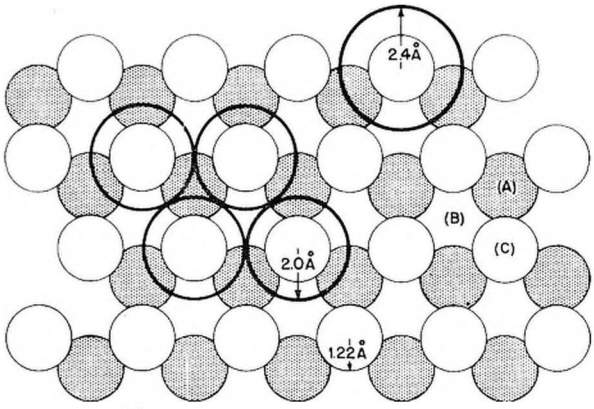

Fig. 4.—Adsorption sites on {111} germanium surface. While the distance of closest approach of atoms in bulk germanium is 2.44 Å., the internuclear separation of germanium atoms in any {111} plane is 4.0 Å. Coincidentally, this corresponds to the distance of closest approach between the atoms of solid krypton. A {111} germanium plane should, therefore, accommodate a close-packed krypton film, as is indicated. Comparison of the N_m values for the adsorption of Kr and N_2 on the same sample of germanium (and for many other materials) suggests, however, that the effective separation of krypton in a fully packed monolayer is 4.8 Å. The value 4.0 Å. was assumed for the calculation of Z_0 for the various adsorption sites, but use of the larger value does not alter the conclusions given in the text.

compared with the particle diameter. This permits the use of A and N/A as conditions of constraint in eq. 3–5, by lifting the restriction that the adsorbent be uniformly dispersed (*i.e.*, that the adsorbent be composed of particles of identical size and shape). This assumption is justified in the present study because the minimum particle diameter exceeds 10^4 Å. Under these conditions, it can be shown that the definitions apply even if the sample contains a mixture of crystal faces.

For conceptual purposes, it is useful to define $\theta' = N/N_m$, the monolayer equivalents of adsorbed gas. Although N is a proper thermodynamic variable, θ' is not, inasmuch as N_m is temperature dependent (see Table II). We therefore define $\theta = N/\bar{N}_m$, where $\bar{N}_m$ is the average value of N_m (*i.e.*, 1.315×10^{18} or 0.0492 cc. S.T.P.). Since θ is related to N/A by a fixed constant of proportionality, it can be used as a proper constraint in eq. 4, without sacrificing its conceptual use as a description of the number of layers of adsorbed krypton.

Partial Molal Free Energy of Adsorption.—$\overline{\Delta\mu}$ was calculated from the data taken at 77.8°K. for each of the three stages of oxygenation. The results are summarized in Fig. 1, in which the variations with log θ are given. Since $\overline{\Delta\mu}$ is proportional to log p (eq. 3), log p is an alternative ordinate in Fig. 1; the curves may, therefore, be viewed as logarithmic isotherms. In this connection, the tendency to linearity at low coverages (*i.e.*, to a Freundlich isotherm[20]) is evident. This tendency is implicit in eq. 1, the empirical relation utilized for interpolation. For orientation purposes, the range of θ over which the B.E.T. isotherm equation is applicable is also outlined. Within this range, the three isotherms bear a regular relationship to each other which, however, breaks down at lower θ.

The more negative the chemical potential, the more stable is the condensed phase at a given krypton coverage. Hence, we observe that oxygenation of the surface steadily attenuates the stability of subsequently adsorbed krypton when $\theta \gtrsim 0.5$. However, at $0.2 < \theta < 0.5$, the stability first increases, then decreases, as oxygenation is carried progressively to saturation.

Partial Molal Heat of Adsorption.—The variation of $\overline{\Delta h}$ with θ at stages I and III is shown in Fig. 2. $\overline{\Delta h}$ varies from -3900 cal./mole where $\theta = 0.15$ to -2700 cal./mole where $\theta \approx 1.5$. The differences are small, however, except when θ approaches unity, where $\overline{\Delta h}_I$ shows a major inflection. Minor inflections occur in both curves at $\theta = 0.4$.

Partial Molal Entropy of Adsorption.—The results for stages I and III are given in Fig. 3 where the entropy of condensation to solid krypton is shown for comparison. Below $\theta \sim 1$, the general effect of oxygenation is to reduce $|\overline{\Delta s}|$, that is, to increase the entropy of adsorbed krypton. This accounts for the enhanced stability of the adsorbate when $\theta < 0.5$. The variations of $\overline{\Delta s_I}$ and $\overline{\Delta s_{III}}$ with θ are similar at low θ, minima being indicated at $\theta = 0.45$. As θ approaches and passes through unity the curves depart with $\overline{\Delta s_I}$ showing a major minimum, and $\overline{\Delta s_{III}}$, a (more or less) gradual decline.

Calculation of Adsorption Energy Assuming a Dielectric Adsorbent.—We assume a germanium surface wherein the spatial relationship and polarizabilities of the atoms do not differ significantly from those of the atoms in the bulk, and neglect the minute bulk conductivity at 80°K.[5] The dispersion potential then arises from the interaction of transient atomic electrostatic multipoles and it can be obtained by a lattice summation of pair interactions between the gas atom and each atom in the adsorbent.[8] The energy of adsorption E is then given by

(20) G. Halsey, *Trans. Faraday Soc.*, **47**, 649 (1951).

$$E = \Phi_{22} + \Phi_{22+} + \Phi_R + \Phi_P \quad (6)$$

where Φ_{22} is the sum of the individual dipole–dipole potentials, and Φ_{22+} is the sum of all higher-pole potentials (dipole–quadrupole, quadrupole–quadrupole, and so on). Φ_P is the polarization energy associated with permanent fields at the surface. Φ_R, the only positive quantity in eq. 6, is the repulsion potential, due predominantly to electron cloud interpenetration. Φ_{22} is the dominant term. If Φ_{22+} and Φ_P are neglected, we obtain a lower limit on the magnitude of E; that is

$$|E_{\text{lower limit}} = \Phi_{22} + \Phi_R| \quad (7)$$

Φ_{22} is given[8] by

$$\Phi_{22} = -C \sum_r r^{-6} \quad (8)$$

where r is the internuclear separation of the adatom and an atom of the adsorbent.

The constant C has been formulated by Slater and Kirkwood[21] as

$$C_{S-K} = \frac{3\epsilon h}{4\pi m^{1/2}} \frac{\alpha_1\alpha_2}{(\alpha_1/n_1)^{1/2} + (\alpha_2/n_2)^{1/2}} = 1.72 \times 10^{-60} \text{ erg-cm.}^{-6} \quad (9)$$

and by Kirkwood and Muller[22] as

$$C_{K-M} = 6mc^2 \frac{\alpha_1\alpha_2}{\alpha_1/X_1 + \alpha_2/X_2} = 2.43 \times 10^{-58} \text{ erg-cm.}^{-6} \quad (10)$$

where m and ϵ are the electronic charge and mass, h is Planck's constant, and c is the speed of light; α_1, n_1 and X_1, and α_2, n_2 and X_2 are the polarizability, the number of electrons in the outer shell, and the magnetic susceptibility of an adsorbate atom and of an adsorbent atom, respectively. The values of C_{S-K} and C_{K-M} were obtained by taking $\alpha_{Kr} = 2.46 \times 10^{-24}$ cm.^{3},[23] $\alpha_{Ge} = 4.5 \times 10^{-24}$ cm.^{3} (from the index of refraction at 80°K. = 4.0),[24] $n_{Kr} = 8$, $n_{Ge} = 4$, $X_{Kr} = 4.65 \times 10^{-29}$ cm.^{3},[25] and $X_{Ge} = 2.63 \times 10^{-29}$ cm.^{3}.[26] We use the average of C_{S-K} and C_{K-M}, $\bar{C} = 2.1 \times 10^{-58}$ erg-cm.$^{-6}$.

The principal cleavage plane of germanium[27] is {111} and it is expected that {111} faces will predominate in the crushed sample. Young has calculated the sums of r^{-6} for points above a {111} plane of a face-centered cubic lattice.[28] Germanium has a diamond-cubic structure[29] and contains two interpenetrating face-centered sublattices of germanium atoms separated from each other by a ($^1/_4$, $^1/_4$, $^1/_4$) translation. Thus, Young's summations can be adapted for a calculation of Φ_{22} above a {111} germanium surface. This face presents a triangular array of atoms, as shown in Fig. 4. Φ_{22} has been calculated for lines normal to the surface above points A, B and C. The close-packed radius of krypton is 2.02 Å.,[30] and that of germanium is 1.22 Å.[29] If these dimensions are preserved in the surface region, the center of an adsorbed krypton atom will approach an equilibrium distance Z_0 which equals 2.44, 1.74 and 3.24 Å. over sites A, B and C, respectively. The corresponding values of Φ_{22} are given in Table IV. With the assumption that the repulsion potential between a krypton atom and a germanium atom varies as r^{-12}, it can be shown by a straightforward argument that, at Z_0

$$\Phi_R = \frac{C}{2} Z_0^6 \sum_r r^{-12} \quad (11)$$

Equation 11 need only be taken over the nearest 10–15 adsorbent atoms to obtain more than 95% of the contribution to Φ_R. This was done; the results are shown in the third column of Table IV. The last column gives the sum of Φ_{22} and Φ_R.

TABLE IV

CALCULATIONS OF DISPERSION AND REPULSION TERMS IN THE ADSORPTION POTENTIAL

Site[a]	Z_0, Å.	$\Phi_{22}(Z_0) = -C\Sigma r^{-6}$, kcal./mole	$\Phi_R(Z_0) = \frac{C}{2} Z_0^6 \Sigma r^{-12}$, kcal./mole	$\Phi_{22}(Z_0) + \Phi_R(Z_0)$ kcal./mole
A	2.44	−11.0	4.6	− 6.4
B	1.74	−22.4	6.8	−15.6
C	3.24	− 5.15	1.3	− 3.75

[a] See Fig. 4.

Values of E may be compared approximately with the experimental values of $\overline{\Delta h}$,[31] which, for the range of krypton coverages studied, varies from −3900 to −2700 cal./mole. It is seen that $|\overline{\Delta h}|$ is much smaller than the lower limit on $|E|$ for the two most probable adsorption sites (A and B) on a (111) germanium surface. The actual discrepancy must be still greater, since Φ_{22} and Φ_R cancel each other to a first approximation at the equilibrium distance, Z_0, for the adsorption of a rare gas atom on the surface of a dielectric,[8] and since the trapped charge on a germanium surface will necessarily make $\Phi_P < 0$.

It is of interest that $|\Phi_{22}|$ alone is usually smaller than $|\overline{\Delta h}|$, and the difference is frequently used to calculate the contribution of other factors.[32] In the present case there is no ambiguity. The theoretical values are much too large.

Discussion

Energy of Adsorption.—It is clear from the results that the energy of krypton adsorption cannot be accounted for in terms of the atomic properties of bulk germanium. Specifically, it appears that the polarizability in the space-charge region differs in kind from that in the bulk. It is significant that in the adsorption of rare gases on metal surfaces, $|\overline{\Delta h}|$ is also much smaller than $|\Phi_{22}|$. The present data appear consistent, therefore, with the proposition of Handler,[4] based on the experimental observation of excess surface conductivity, that a clean germanium surface is metalloid in character.

(21) J. C. Slater and J. G. Kirkwood, *Phys. Rev.*, **37**, 682 (1931).

(22) J. G. Kirkwood, *Physik. Z.*, **33**, 57 (1932).

(23) S. Brunauer, "Adsorption of Gases and Vapors," Princeton University Press, Princeton, N. J., 1943, p. 189.

(24) C. D. Salzburg and J. J. Villa, *J. Opt. Soc. Am.*, **47**, 244 (1957).

(25) Landolt-Börnstein, "Tabellen," 6th ed., Vol. I.1, p. 394.

(26) D. K. Stevens, J. W. Cleland, J. H. Crawford, Sr., and H. C. Schweinler, *Phys. Rev.*, **100**, 1084 (1955).

(27) G. A. Wolf, "Semiconductor Surface Physics," Ed. R. H. Kingston, University of Pennsylvania Press, Philadelphia, Pa., 1957, p. 377.

(28) D. M. Young, *Trans. Faraday Soc.*, **47**, 1228 (1951).

(29) R. W. G. Wyckoff, "Crystal Structure," Vol. I, Interscience Publishers, Inc., New York, N. Y., 1951.

(30) R. W. G. Wyckoff, *ibid.*

(31) In the classical limit of the Langmuir model, $\Delta h = \Delta h_\infty + E + {}^1/_2RT$. In real systems the difference between Δh and E may be as much as two to three times RT, but the conclusions of this section are not affected.

(32) Ref. 7b.

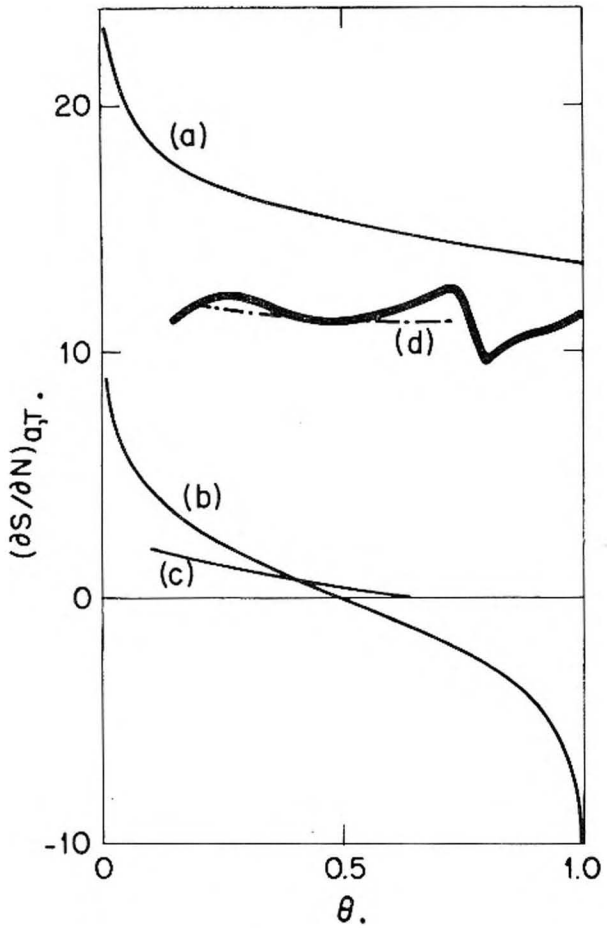

Fig. 5.—Partial molal entropies of adsorption according to elementary models of the adsorbate. See text for description.

Theories concerning the energy of rare-gas adsorption on metal surfaces should be adaptable, in principle, to the present problem. If we assume that the "polarizability" of a region containing electron holes could be properly defined, it would still be necessary to have good estimates of the charge distributions at a clean germanium surface and in the associated space-charge region. The present uncertainties in these quantities preclude a reliable test. For instance, the value of the polarization potential, Φ_p, attributable to the electrostatic field at the surface should be of the order of $10^{-25} N_T^2$ cal./mole, where N_T is the density of trapped electrons at the surface. Thus, within the currently accepted limits of 10^{12}/cm.^{2} and 3×10^{14}/cm.^{2} for N_T,[1] the value of Φ_p should be about -10^{-2} and -10^4 cal./mole. Within this uncertainty, the contribution of Φ_p may either dominate the over-all energy of adsorption or be quite insignificant.

It was assumed in the calculation of dispersion energy that the adsorbent is inert, that is, its electrochemical properties are unaffected by krypton. Recent studies[33,34] have shown, however, that the work function of metals can be altered by the adsorption of rare gases, suggesting[33] the formation of a quasi chemical bond[35,36] between adatom and substrate. It was emphasized earlier that $\overline{\Delta h}$ measures changes in the entire system, *i.e.*, simultaneous variations in both the energy of the adsorbate and of the adsorbent. A fall in $|\overline{\Delta h}|$ at low krypton coverages cannot reasonably be predicted for a perfect crystalline surface which is inert to the adsorbate. $|\overline{\Delta h}|$ will either remain constant or rise as $\theta \rightarrow 1$ because of lateral interaction between adatoms.[7b] Consequently, a decline in $|\overline{\Delta h}|$ at low coverages is generally attributed to surface heterogeneity.[37] If a quasi chemical bond is formed, however, the observed decline in $|\overline{\Delta h}|$ at low θ (Fig. 2) may be explained by the arguments adduced for the variation of heats of chemisorption with surface coverage.[38] Against this possibility we can cite Rhodin's observation[39] that a decay in $|\overline{\Delta h}|$ at low argon coverages of polycrystalline copper is not found when single copper crystals are used. This implies that surface heterogeneity, not an intrinsic perturbation of the adsorbent by the adsorbate, underlies the effect.[37]

From the similarities both in magnitude and shape of the $\overline{\Delta h}$ *vs.* θ curves, it appears that the mechanism of adsorption is similar for bare and oxygenated germanium surfaces. The chemical nature of the oxygenated surface is still a subject of controversy,[2,40,10] but it should be noted that the electrical properties of cleaned germanium surfaces are not greatly changed by the adsorption of oxygen. The work function changes by less than 0.3 volt[41] and the changes in the surface conductivity and field-effect mobility are also small.[2] Since related properties may well be critical in the adsorption of krypton on germanium, it is not surprising that the heats and their variation are similar for stages I and III.

Entropy of Adsorption.—In principle, the entropy of adsorption may be predicted from statistical considerations.[42–46] Theoretically the problem is complex since the components of the entropy—vibrational, configuration and translational—are not easily separable.[43,44] Recourse is generally made to simple models in which one factor is assumed to be dominant. Figure 5 compares such calculations with the observed values of $\overline{\Delta s}$. Figure 5a gives the values of $\overline{\Delta s}$ for a model of a perfect two-dimensional gas; 5b, for a model of immobilized adatoms on a perfect surface; 5c, for a model of immobilized adatoms on a heterogeneous surface; 5d is similar to 5c except that three degrees of vibrational freedom, with $\nu = 7.6 \times 10^{11}$ sec.$^{-1}$, are accorded to each adatom. The approximate agreement of 5d with the experimental curve is

(33) J. C. P. Mignolet, *J. Chem. Phys.*, **21**, 1298 (1953).
(34) R. Gomer, to be published.
(35) R. S. Mulliken, *J. Am. Chem. Soc.*, **72**, 600 (1950).
(36) R. S. Mulliken, THIS JOURNAL, **56**, 801 (1952).
(37) G. Halsey, *Adv. in Catalysis*, **4**, 259 (1952).
(38) Ref. 7b.
(39) T. N. Rhodin, Jr., *J. Am. Chem. Soc.*, **72**, 5692 (1950).
(40) M. Green, "Semiconductor Surface Physics," Ed. R. H. Kingston, University of Pennsylvania Press, Philadelphia, Pa., 1947, p. 362.
(41) J. A. Dillon, Jr., and H. E. Farnsworth, *J. App. Phys.*, **28**, 174 (1957).
(42) C. Kemball, *Adv. in Catalysis*, **2**, 233 (1952).
(43) F. C. Tompkins, *Trans. Faraday Soc.*, **46**, 569 (1950).
(44) D. H. Everett, *Proc. Chem. Soc.*, 38 (Feb, 1957).
(45) T. L. Hill, *J. Chem. Phys.*, **16**, 181 (1948); **17**, 520 (1949).
(46) J. H. de Boer, "Dynamical Character of Adsorption," Oxford, 1953.

forced, of course. It serves only to illustrate that the observed entropies are not inconsistent with independent theoretical estimates, that the permissible vibrational frequencies of physically adsorbed atoms lie between 10^{11} sec.$^{-1}$ and 10^{13} sec.$^{-1}$.[45,46]

More definitive is the minimum in $\overline{\Delta s}$ which occurs at $\theta = 0.8$. This is unquestionably associated with completion of the first layer and occupation of the second. An approximate integration of $\overline{\Delta s}$ was carried out using the ideal configurational entropy, $R \ln [(1 - \theta)/\theta]$,[44] to extrapolate $\overline{\Delta s}$ to $\theta = 0$. The integral entropy so obtained exhibits a minimum very close to $\theta = 1$. This gives a measure of statistical support[47] to the B.E.T. value of N_m, on which the coverage values are based. Of considerable interest is the fact that oxygenation of the surface, while eliminating the minimum in $\overline{\Delta s}$, (Fig. 3) does not substantially affect the value of N_m (Table II). This provides a notable demonstration of the empirical consistency of the B.E.T. equation.

(47) T. L. Hill, *Advances in Catalysis*, **4**, 250 (1952).

Free Energy of Adsorption.—It is of interest that for the adsorption of between 0.2 and 0.5 monolayer of krypton, $\overline{\Delta\mu}$ goes through a minimum as the surface is progressively oxygenated (Fig. 1). It is not possible, therefore, to construct $\Delta\mu$ for stage II for a given krypton coverage in this range by a linear combination of $\overline{\Delta\mu}$ for stage I and that for stage III. This demonstrates that oxygenation is a continuous process that occurs uniformly over the surface and not in patches. It indicates, furthermore, that the oxygenated layer changes in character as the oxygen coverage approaches that of a monolayer. This tends to confirm earlier proposals on surface rearrangement[2,40,10] that were based on the kinetics and heats of oxygenation,[14] the changes in electrical surface properties with progressive oxygenation,[3,41] and the thermal restoration of oxygenated germanium surfaces.[10]

Acknowledgment.—The author wishes to acknowledge most gratefully the skillful technical assistance of Mr. Charles S. Martel, Jr.

AGGREGATION OF SOME OF THE AMINE EXTRACTANT SPECIES IN BENZENE

BY KENNETH A. ALLEN

Oak Ridge National Laboratory, Oak Ridge, Tennessee[1]

Received June 2, 1958

In light scattering measurements at 546 mμ the normal sulfates of tri-*n*-octylamine, di-1-isobutyl-3,5-dimethylhexylamine, methyldi-*n*-octylamine, 1,3-ethylpentyl-4-ethyloctylamine and di-*n*-decylamine showed aggregation numbers of 1, 4, 9, 11 and 38, respectively, in benzene solution. Tri-*n*-octylamine bisulfate is dimeric. The linear dependences on concentration of the 90°/0° scattering ratios indicated that these solutes were monodisperse. The uranyl sulfate complexes of these amine sulfates were all monomeric except that of the primary amine, which appeared to be a dimer. The monomeric natures of tri-*n*-octylamine sulfate and of the di-*n*-decylamine sulfate–uranyl sulfate complex were confirmed by isopiestic and viscosimetric measurements.

Introduction

In previous papers an apparent constant amine sulfate activity in the extraction of sulfuric acid by benzene solutions of tri-*n*-octyl- and di-*n*-decylamines was interpreted as indicating aggregation of the amine salts.[2] Similar evidence for other amines has arisen during the extensive investigations on their use as extractants for uranium.[3] The present light scattering study (supported by isopiestic and viscosimetric measurements) was undertaken in order to establish reliable estimates of the actual particle sizes involved in these systems, with a view toward further elucidation of the associated two-phase equilibria. The results of this study have not, in general, substantiated the previous interpretation of the apparent activity constancy of these solutes. For example, tri-*n*-octylamine sulfate proved to be monomeric, and only one of the other amine sulfates (di-*n*-decyl) proved to be as large as had been considered reasonable for consistency with the equilibration behavior. Even in this case, one of the important extraction mechanisms based on aggregation has proven untenable (see footnote 10). Further work aimed at resolution of these apparently real discrepancies is in progress and will be described in future publications. The present paper reports weight average molecular weights for the sulfates and the uranyl sulfate complexes of tri-*n*-octyl-, di-1-isobutyl-3,5-dimethylhexyl-, methyldi-*n*-octyl-, 1,3-ethylpentyl-4-ethyloctyl- and di-*n*-decylamines.

Experimental

The particular amines studied were chosen on the basis of one or more of such considerations as purity, availability, previous theoretical interest and demonstrated process applicability. Characterizations of the amines, the sulfates and the uranyl sulfate complex forms are shown in Tables I and II. The compounds were prepared by equilibrating benzene solutions of the amines with aqueous phases containing calculated quantities of sulfuric acid and uranyl sulfate. The pertinent analytical methods have been described elsewhere.[3,4] The apparent monomeric molecular weights shown in Table II were computed from

(1) Operated for the U.S.A.E.C. by Union Carbide Nuclear Company.

(2) K. A. Allen, THIS JOURNAL, **60**, 239 (1956); **60**, 943 (1956).

(3) K. B. Brown, C. F. Coleman, D. J. Crouse and A. D. Ryon, "Progress Report on Raw Materials," ORNL-2268, April 26, 1957; K. B. Brown, C. F. Coleman, D. J. Crouse, J. O. Denis and J. C. Moore, "The Use of Amines as Extractants for Uranium from Acidic Sulfate Liquors—A Preliminary Report," AECD-4142, May 27, 1954; J. G. Moore, K. B. Brown and C. F. Coleman, "Further Studies of the Amines as Extractants for Uranium from Acid Sulfate Solutions," AECD-4145, June 24, 1955.

(4) K. A. Allen, *J. Am. Chem. Soc.*, **80**, 4133 (1958); *Anal. Chem.* **28**, 1144 (1956); A. S. Meyer, Jr., *ibid.*, (in press).

TABLE I

NAMES AND STRUCTURES OF THE AMINES

Amine	Abbreviation	Structure
Tri-*n*-octyl	TOA	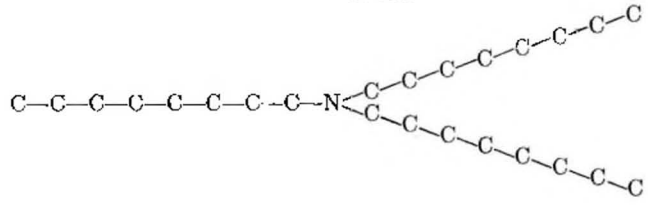
Di-1-isobutyl-3,5-dimethylhexyl	DBM	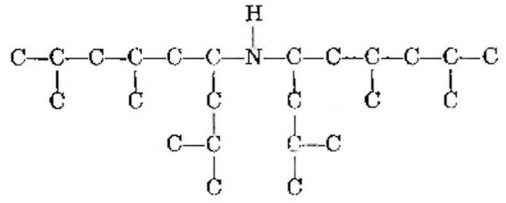
Methyldi-*n*-octyl	MDO	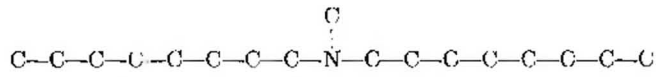
1,3-Ethylpentyl-4-ethyloctyl	EPO	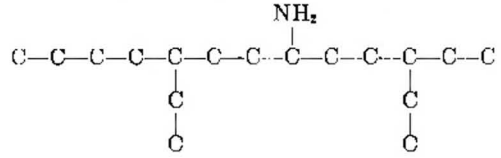
Di-*n*-decyl	DDA	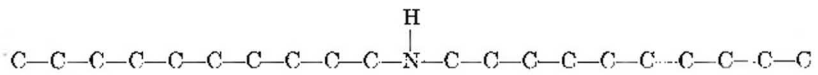

the weights of amine and water per mole of sulfuric acid for the sulfates, and the weights of amine, acid and water per mole of uranium for the complexes.

TABLE II

AMINE SOLUTE CHARACTERIZATIONS

A. Amines

	Neut. equiv. Found	Neut. equiv. Theor.	Composition, % Primary	Composition, % Secondary	Composition, % Tertiary
TOA	354	354	<0.5	<0.5	>99
DBM	370	354	1	98	1
MDO	270	255	2	1	97
EPO	255	255	>99	<0.5	<0.5
DDA	300	298	<0.5	98	2

B. Amine sulfates[a]

	$[\Sigma R]/[H_2SO_4]$	$[H_2O]/[H_2SO_4]$	Apparent monomeric mol. wt.
TOAS	1.97	4.0	877
TOAHS	1.09	1.0	505
DBMS	1.98	2.7	877
MDOS	2.02	10.4	826
EPOS	1.96	8.3	684
DDAS	1.98	2.0	730

C. Amine–uranium sulfates

	$[\Sigma R]/[U]$	$[H_2SO_4]/[U]$	$[H_2O]/[U]$	Apparent monomeric mol. wt.
TOASU	4.10	1.90	3.8	2060
DBMSU	4.46	2.00	5.0	2300
MDOSU	4.14	1.96	6.0	1830
EPOSU	6.00	2.65	7.0	2280
DDASU	4.80	2.00	2.0	2040

[a] Concentrations are in moles per liter of the benzene solutions; ΣR is the total titratable nitrogen and U is the organic uranium.

Brice—Phoenix equipment was used for the optical measurements.[5] These were run at 546 mμ in order to avoid fluorescence exhibited by some of the solutes at 436 mμ. Rayleigh ratios were calculated from the value 16×10^{-6} cm.$^{-1}$ for benzene, which was considered a judicious mean of those reported in the definitive paper by Carpenter and Krigbaum.[6] The viscosities were measured at 25.0 ± 0.002°, using an Ostwald viscometer calibrated with benzene and aqueous glycerol solutions.

For the scattering measurements the solutions were forced through ultrafine filters under 10–15 lb. pressure of dry nitrogen. One pass was usually sufficient for obtaining optical (45°/135°) symmetry; none of the data to be reported required dissymmetry corrections. After several dilutions had been made in the photometer, the solutions were refiltered and another series was run. Filtered benzene was run before and after each series.

Results and Discussions

Refractive index increments for the three tri-*n*-octylamine solutes are shown in Fig. 1. Similar linearity was exhibited by the other solutes. It is to be noted that the increments were negative in all cases; *i.e.*, the refractive indices of the solutes were lower than that of benzene. Since the partial, $\partial n/\partial c$, appears squared in the expression for K

$$K = \frac{2\pi^2 n_1^2}{N_0 \lambda^4} \left(\frac{\partial n}{\partial c}\right)^2$$

where c is in g./ml., n_1 is the refractive index of the solvent, N_0 is Avogadro's number and λ is the wave length, the negative values of $\partial n/\partial c$ do not affect the applicability of the usual theoretical relationships.

The scattering data are shown in Figs. 2-5. The

(5) B. A. Brice, M. Halwer and R. Speiser, *J. Optical Soc. Am.*, **40**, 768 (1950); B. A. Brice and M. Halwer, *ibid.*, **41**, 1033 (1951).

(6) D. K. Carpenter and W. R. Krigbaum, *J. Chem. Phys.*, **24**, 1041 (1956).

ordinates on these plots are the ratios between the 90° and 0° scale readings on the recorder, using the same neutral filter combination for the incident light intensity as was used for benzene. The relative scattering, and the calculated Rayleigh ratios, were thus independent of the neutral filter transmittancies. Also, since the refractive index differences were small, and identical geometry held for all the measurements, no refractive index corrections were necessary. However, a few of the solutes showed anomalously high depolarizations; these will be discussed below.

It is to be noted that the scattering ratios were linear functions of the concentrations for all the solutes, within the observed experimental deviations. Thus, denoting the scale reading ratios as r_{90}, the Rayleigh ratio increments, R_{90}/c, are given as

$$\left(\frac{R_{90}}{c}\right)_0 = \frac{(R_{90})_{C_6H_6}}{(r_{90})_{C_6H_6}} \frac{\Delta r_{90}}{\Delta c}$$

where the subscript zero denotes the limiting (constant) values of R_{90}/c indicated by the slopes.

It is apparent from the data that the intercepts were not necessarily the same as $(r_{90})C_6H_6$. The latter ratio was firmly established for the equipment used, and it was thought at first that the differences were due to de-aggregation of the solutes at the c.m.c. (critical micelle concentration), which could thus be estimated from the point where the r_{90} *vs.* c line crossed the $(r_{90})C_6H_6$ value. Some of the solution intercepts were higher than $(r_{90})C_6H_6$, however; in addition, the trioctylamine results could not possibly involve a c.m.c. Whatever the causes, it is inconceivable that the steady, linear decreases in the observed ratios could have resulted from chance fluctuations as large as the differences between the $(r_{90})_0$ and $(r_{90})C_6H_6$ values. The Rayleigh ratio increments, therefore, which depend only on the slopes, are considered reliable.

The molecular weights shown in Tables III and IV were computed from the limiting relation

$$\left(\frac{Kc}{R_{90}}\right)_0 = \frac{1}{M}\left(\frac{6 - 7\rho}{6 + 6\rho}\right)$$

where ρ is the observed depolarization ratio, i_H/i_V, measured with unpolarized incident light. The aggregation numbers N were obtained by dividing these M values by the respective apparent monomeric weights of Table II.

TABLE III

OPTICAL DATA AND MOLECULAR WEIGHTS OF THE AMINE SULFATES

Solute	$-\frac{\partial n}{\partial c}$	$K \times 10^5$	$\left(\frac{R_{90}}{c}\right)_0 \times 10^6$	ρ	M	N
TOAS	0.0594	0.0292	45.8	~0.25	890	1
TOAHS	.0444	.0164	56.4	~0.5	960	2
DBMS	.0580	.0279	100	0	3,600	4
MDOS	.0728	.0440	330	0	7,500	9
EPOS	.0600	.0299	234	0	7,800	11
DDAS	.0470	.0183	586	0.068	28,000	38

It is apparent from Table III that the amine sulfates exhibited a wide range of particle sizes. Similar solutes, such as various quaternary ammonium salts in benzene, and primary *n*-alkylamine carboxylates in benzene and cyclohexane, have been found to show aggregation numbers of from 3 to *ca.* 40.[7] Since it is unlikely that deviations

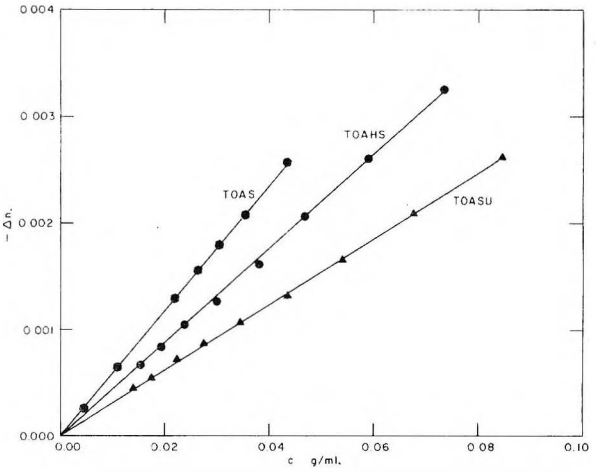

Fig. 1.—Refractive index increments of the tri-*n*-octylamine sulfate, bisulfate and uranyl sulfate complex forms *vs.* concentration in benzene.

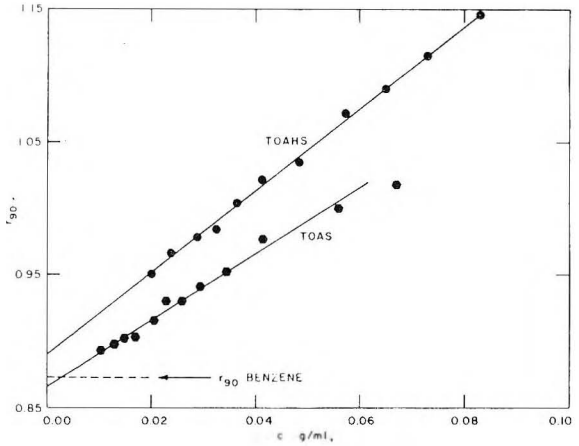

Fig. 2.—Scattering ratios of tri-*n*-octylamine bisulfate and sulfate *vs.* concentration in benzene.

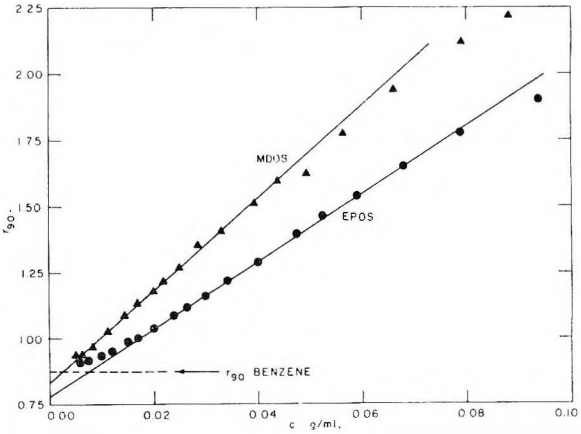

Fig. 3.—Scattering ratios of methyl di-*n*-octylamine sulfate and 1,3-ethylpentyl-4-ethyloctylamine sulfate *vs.* concentration in benzene.

(7) C. A. Kraus, *Ann. N. Y. Acad. Sci.*, **51**, 789 (1949); C. H. Keith and C. A. Kraus, *Proc. Natl. Acad. Sci. U. S.*, **39**, 598 (1953); D. T. Copenhafer and C. A. Kraus, *J. Am. Chem. Soc.*, **73**, 4557 (1951); R. A. Rothrock and C. A. Kraus, *ibid.*, **59**, 1699 (1937); S. R. Palit and V. Venkataswarlu, *J. Chem. Soc.*, 2129 (1954); *Proc. Roy. Soc.*

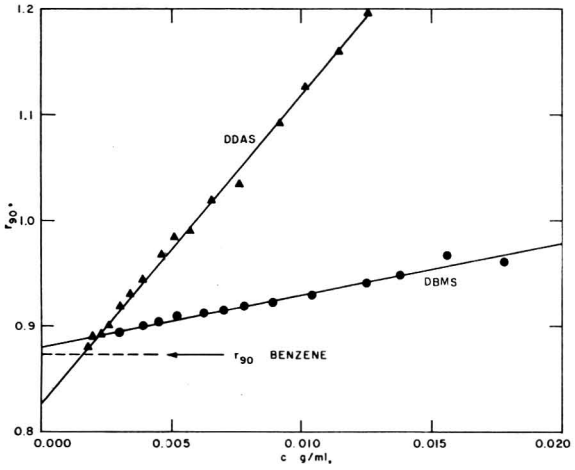

Fig. 4.—Scattering ratios of di-*n*-decylamine sulfate and di-1-isobutyl-3,5-dimethylhexylamine sulfate *vs.* concentration in benzene.

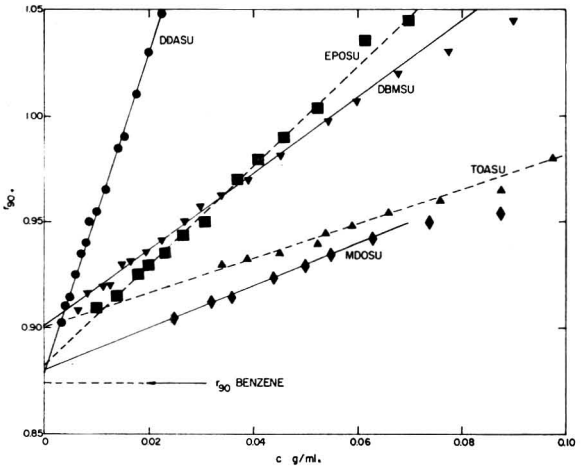

Fig. 5.—Scattering ratios of the uranyl sulfate complexes *vs.* concentration in benzene.

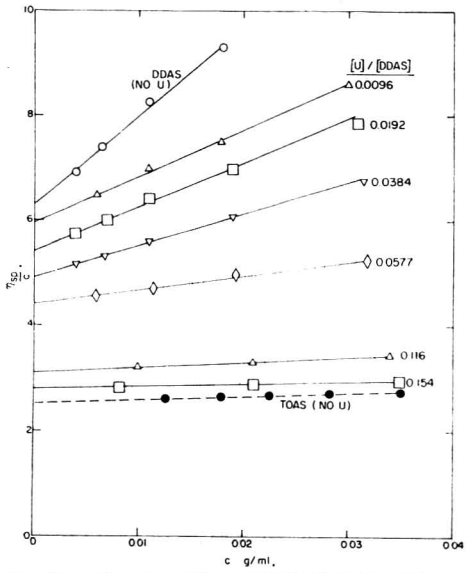

Fig. 6.—Specific viscosities of DDAS, DDASU at varying loadings, [U]/[DDAS] (moles of organic uranium per equivalent of di-*n*-decylamine sulfate), and TOAS as functions of concentration in benzene.

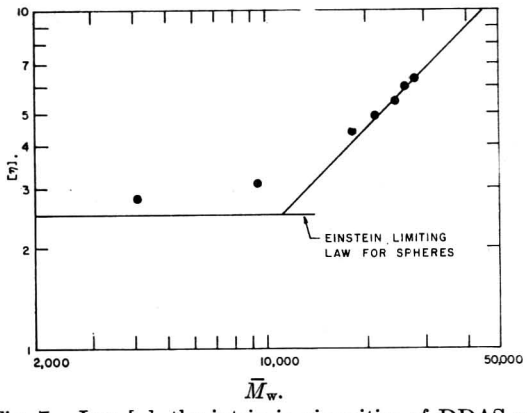

Fig. 7.—Log $[\eta]$, the intrinsic viscosities of DDAS solutions containing varying amounts of uranium, *vs.* log $\bar{M}_w$, the weight average molecular weights calculated for separate DDAS micelles and $(DDAS)_3 \cdot UO_2SO_4$ particles. The line through the points at low loading corresponds to $\alpha = 1$. The Einstein limiting law for hydrodynamically ideal spheres predicts that the specific viscosity should be $^5/_2$ times the volume fraction of solute. Thus, since the solute densities here are close to unity, we have $\eta_{sp}/c = [\eta] = 2.5$ from the limiting law.

TABLE IV

MOLECULAR WEIGHTS OF THE AMINE SULFATE–URANYL SULFATE COMPLEXES

Solute	$-\frac{\partial n}{\partial c}$	$K \times 10^6$	$\left(\frac{R_{90}}{c}\right)_0 \times 10^6$	ρ	M	N
TOASU	0.0310	0.0080	15	0	1900	1
DBMSU	.0357	.0105	33	~0.5	(900)	(1)
MDOSU	.0346	.0100	18	0	1800	1
EPOSU	.0354	.0104	43	0	4100	2
DDASU	.0400	.0133	137	~0.8	(400)	(1)

from Henry's law would be just compensated by changes in the weight average molecular weights, the linear behavior of the scattering ratios suggests that the sulfates are monodisperse; apparently these structures are relatively stable. The large di-*n*-decylamine sulfate particle is probably an inverted Hartley micelle, with the sulfate heads and the associated waters on the inside of a roughly spherical configuration.

The tri-*n*-octylamine sulfate results were in disagreement with the inferences from the sulfuric acid equilibria,[2] and in addition they depended on large depolarization corrections. Estimating the maximum error in the observed values of ρ to be $\pm 20\%$, the spread in the weights of the TOA salts becomes 780–1000 for the sulfate, and 650–1300 for the bisulfate. Thus, while any significant degree of aggregation is still ruled out, isopiestic measurements were made on TOAS as an additional check.[8] These results confirmed the monomeric weight to within a few per cent. The apparent depolarization ratio shown by the di-*n*-decylamine–uranyl sulfate complex was so anomalously high as to reduce the computed particle weight to less than 20% of that of the monomer, which is impossible. This solute was also checked in the isopiestic apparatus and found to be monomeric.[8]

Additional evidence was obtained from a series of viscosity measurements run on DDAS as a function of uranium loading. The resulting specific

(*London*), **A208**, 542 (1951); Ayao Kitahara, *J. Colloid Sci.*, **12**, 342 (1957); C. R. Singleterry, *J. Am. Oil Chemist's Soc.*, **32**, 446 (1955).

(8) C. F. Baes, Jr., private communication.

viscosities are shown in Fig. 6, together with those for tri-*n*-octylamine sulfate solutions for comparison. It is apparent here that the introduction of uranium causes de-aggregation, even at very low loadings. These results were further correlated using the empirical relation[9]

$$[\eta] = k(\bar{M}_w)^{\alpha}$$

where

$$[\eta] = \operatorname{Lim}_{c \to 0} \frac{\eta_{sp}}{c}$$

and computing $\bar{M}_w$, the weight average molecular weight of the DDAS–DDASU complex mixture, on the basis of a six to one amine–uranium ratio.[10]

(9) P. J. Flory, "Principles of Polymer Chemistry," Cornell University Press, Ithaca, New York, 1953, pp. 310–311; this equation is not ordinarily applied in systems of non-linear polymers; it is used here only in the most empirical sense as a correlative device.

(10) The weight-average molecular weight $\bar{M}w$ of a mixture of DDAS particles of weight M_1 and $(DDAS)_5UO_2SO_4$ particles of weight M_1 is given to a very good approximation by the formula

$$\bar{M}_w = M_1 + (M_2 - M_1)\frac{1 - 6x}{1 + x}$$

where x is the ratio, [U]/[ΣR] of organic uranium per equivalent of amine sulfate as used in Fig. 6. M_2 was taken as 28,000 from Table III, and since the six to one species is probably predominant at the low loadings of interest here (W. J. McDowell and C. F. Baes, Jr., THIS JOURNAL, **62**, 777 (1958)), M_1 was taken as 2400 instead of the monomeric weight computed for the fully loaded solute as shown in Table II.

The extraction mechanism for the DDASU system mentioned in the introduction depended on the observed first power dependence of the uranium extraction coefficients, $[U]_o/[U]_a$, on the free DDAS concentrations, over a considerable range. This is consistent with a large DDAS aggregate only if the resulting metal complex is incorporated into the micelles without significant size changes. The existence of the complex as a separate monomeric particle would imply that the extraction coefficient should be independent of the free DDAS concentration.

It is apparent from Fig. 7 that the resulting intrinsic viscosity molecular weight relationship is of the expected form for a separate complex, monomeric with respect to uranium.

Construction of a Hirschfelder molecular model of the tri-*n*-octylamine sulfate molecule showed that the six octyl chains would indeed sterically hinder the close grouping of additional sulfates. On the other hand, a model of the di-*n*-decylamine sulfate molecule folded nicely into a compact configuration with the four chains aligned, providing considerable methylene–methylene "zippering," and with the sulfate protruding at one end, allowing the formation of the inverted Hartley sphere referred to above. The progressive increases in the sizes of the intermediate amine sulfates can be seen from the structures in Table I to show at least qualitative consistency with this trend.

Acknowledgments.—The author is indebted to G. N. Case for technical assistance, and to C. F. Coleman for helpful discussions throughout the work.

AN ELECTROCHEMICAL METHOD FOR THE DETERMINATION OF THE SATURATION PRESSURE AND HEAT OF SOLUTION OF HYDROGEN IN A TWO-PHASE Pd–H ALLOY[1]

BY ROBERT J. RATCHFORD AND GILBERT W. CASTELLAN

Department of Chemistry, The Catholic University of America, Washington, D. C.

Received June 5, 1958

The potential–temperature dependence of saturated α-palladium in a hydrogen-stirred solution compared to a Pt/H_2 electrode in the same solution is given by $E = 0.06309 - 0.0005057(T - 273.16)$. The value of 9280 ± 100 cal./mole H_2 is calculated for the standard heat of absorption of hydrogen, and $\log p_s(\text{mm.}) = 7.9776 - 2028.2/T$ expresses the saturation pressure of hydrogen over the saturated α-palladium electrode. Factors governing the stability of this potential are discussed.

Introduction

Extensive electrochemical investigations of the palladium–hydrogen electrode[2-7] have shown that in 2 N H_2SO_4 solution saturated with hydrogen gas the potential-determining reaction on a palladium electrode of low hydrogen content (α-Pd–H alloy) is $H^+ + e^- \rightleftarrows H\alpha$. $H\alpha$ symbolizes a hydrogen atom in the α-phase Pd–H alloy. The potential exhibited by the Pd H electrode is consequently a function of the composition of the alloy, but is independent of composition over at least part of the two-phase ($\alpha+\beta$) region.[6] This potential of the α-Pd alloy when at least a little β-phase (hydrogen-rich phase) is present has a value at room temperature of approximately 0.050 v. positive (more noble) to a $Pt–H_2$ electrode in the same acid solution if the ambient H_2 pressure is 1 atm. This 0.050 v. potential is clearly equal to the potential of an ordinary hydrogen electrode under a pressure, p_s, the saturation pressure of hydrogen over the two-phase alloy. This suggests an electrochemical method for determining these saturation pressures at ordinary temperatures. The present investigation of the potential–temperature dependence of the saturated α-Pd–H electrode was undertaken in order to compare the electrochemically-deter-

(1) From a dissertation submitted by Robert J. Ratchford to the Faculty of the Graduate School of Arts and Science of The Catholic University of America in partial fulfillment of the requirements for the degree of Doctor of Philosophy.

(2) J. P. Hoare and S. Schuldiner, *J. Electrochem. Soc.*, **102**, 485 (1955).

(3) (a) S. Schuldiner and J. P. Hoare, *ibid.* **103**, 178 (1956); (b) J. P. Hoare and S. Schuldiner, *ibid.*, **104**, 564 (1957).

(4) J. P. Hoare and S. Schuldiner, THIS JOURNAL, **61**, 399 (1957).

(5) S. Schuldiner, G. W. Castellan and J. P. Hoare, *J. Chem. Phys.*, **28**, 16 (1958).

(6) G. W. Castellan, J. P. Hoare and S. Schuldiner, *ibid.*, **28**, 20 (1958).

(7) J. P. Hoare, S. Schuldiner and G. W. Castellan, *ibid.*, **28**, 22 (1958).

mined values of the saturation pressure and the heat of solution with those values obtained from the direct studies of the gas–solid equilibrium.

Experimental Method

Reagents.—The hydrogen was electrolytic grade, chemically purified by passage through a train and brought to thermal equilibrium by passage through a saturator containing 2 *N* sulfuric acid which was immersed in a thermostat maintained to ±0.05°. For flexibility, short pieces of virgin polyethylene tubing were used for some of the connections in the train. A mass spectrographic analysis of the hydrogen showed only the presence of hydrogen and water vapor. The cell electrolyte was 2 *N* sulfuric acid. The water used for the preparation of solutions and for the rinsing of the electrodes and cells was triply distilled. The second distillation was from alkaline permanganate, and the third was from a sulfuric acid solution. The water was stored in aged polyethylene containers of liter capacity. The water had a specific conductivity of about 4×10^{-6} mhos/cm. A roll of platinum gauze was suspended in the electrolyte and water containers to remove impurities by adsorption. The containers were subjected to constant gentle agitation by a shaker, and the gauzes were flamed and cleaned in concentrated nitric acid daily.

Cells and Electrodes.—The first cells used were constructed of glass or polyethylene. However, for several months an extremely unstable α-palladium potential was obtained, and trace impurities slowly leaching from these cells to contaminate the electrodes were thought to be the cause. Therefore, following closely the work of Hoare and Schuldiner,[2] we machined the cells from a solid 1⅝″ rod of Teflon. The cavity was 2″ deep and 1″ in diameter and contained about 20 ml. of 2 *N* sulfuric acid. A Teflon cap, machined to fit the cavity, was fitted with a ⅛″ tube extending to the bottom of the cell for the hydrogen inlet and a ¼″ tube for an exhaust. Both tubes were Teflon. The cell accommodated four electrodes. Two reference electrodes were made from fine, bright platinum gauze welded to 10 mil platinum wire. The larger was placed against the cell wall with the lead extending through the wall, and the smaller was suspended deep in the cell cavity with the lead extending through the cap. A 40 mil platinum wire for anodic cleaning of the electrodes prior to a run was inserted through a small hole in the cap. The palladium electrodes were 5 and 10 mil wires; 1, 3 and 5 mil foils; and beads prepared by melting the wires or foils; all welded to 10 mil platinum wires. The spectrographic analysis of one batch of the sheet palladium was 99.6% pure, with gold comprising half of the impurity, and a later batch was reported 99.8% pure.

Procedure.—The cell was periodically cleaned with hot concentrated nitric acid and thoroughly rinsed with triply distilled water. The time required for the references to achieve equilibrium after starting the hydrogen flow was taken as an indication of the purity of the electrodes. The shorter the time, the less impurity present. The palladium electrode was cleaned by repeated plunging in concentrated nitric acid and flaming in a Meker burner. Then the platinum lead and the weld area were coated with polyethylene to prevent solution contact, and the electrode was suspended from the cap so that the electrolyte covered the entire palladium surface. Pre-electrolysis at 5–10 ma. was carried out with the palladium and the platinum reference electrodes as anodes, and the removable platinum wire as cathode. All potentials were measured with a Leeds and Northrup K-2 potentiometer against the large platinum reference electrode, whose equilibrium potential was repeatedly checked against the smaller platinum electrode. On approximately half of the runs a chart recorder was employed to yield a permanent time–potential curve. However, only values measured with the potentiometer were used in the calculations.

Hydrogen Analysis.—The hydrogen content of the palladium electrodes was determined by analysis with ceric ion.[3] The weighed electrode was dropped into a 250-ml. erlenmeyer flask containing 1 ml. of standardized 0.1 *N* ceric ammonium sulfate in 1 *N* sulfuric acid. The flask was placed on a shaker, and further 1-ml. amounts of ceric solution were pipetted into the flask until the yellow color of the ceric ion persisted for at least six hours. With one drop of 0.025 *N* ferroin indicator, the excess ceric ion was titrated with a standard solution of 0.1 *N* ferrous ammonium sulfate, using a Gilmont microburet which could be read to 0.001 ml. Two blanks were run simultaneously to give a check on the normality of the ferrous solution, which decreased about 0.0005 *N* daily.

(8) F. A. Lewis and A. R. Ubbelohde, *J. Chem. Soc.*, 1710 (1954).

Experimental Results

It was evident after a first series of experiments that the presence of impurities poisoning the electrode reaction by surface adsorption was far more troublesome than possible solution contact with the platinum. Use of the Teflon cell with its large reference electrode and small volume of solution, greater caution in the handling and preparation of electrodes and solutions, and anodic pre-electrolysis were factors that led to more consistent results.

In general, the potential–time plot at a given temperature for the hydrogen-free palladium electrode in a hydrogen-stirred 2 *N* sulfuric acid solution was similar to that obtained by Hoare and Schuldiner.[4] However, a remarkable feature was detected that has not been reported previously. Instead of directly leveling from the high positive potential to the plateau value, the potential invariably fell below and then recovered to the plateau. This effect was followed by direct potentiometric readings, and later was observed on the potential–time traces. The time for recovery from this minimum was variable, but seldom exceeded one hour, while the minimum ranged from 1–5 mv. below the plateau. Figure 1 is the plot of a typical run.

The duration of the plateau was never predictable and varied from a mere inflection to six days. In several cases when the temperature was changed for a new series of runs, the potential adjusted to the new plateau after 24 hours on the previous temperature plateau. The plots bear a striking similarity to cooling curves where the dip below the plateau corresponds to a supersaturation effect, and the plateau to a nearly reversible phase change. Analogously, the minimum in the potential corresponds to supersaturation of the α-phase, and the plateau to the slow growth of the β-phase. Just as the plateau in a cooling curve lies slightly below the equilibrium freezing temperature because of the flow of heat from the system, so here the plateau lies slightly below the reversible e.m.f. because of the slow addition of hydrogen to the alloy. The plateau length of the cooling curve can be increased with proper insulation, and the plateau length of the potential curve can be increased by regulating the rate of sorption of hydrogen causing the growth of the β-phase. Factors that enhance this rate or retard it, as the case may be, will be discussed later. Since the dissolution of hydrogen is slow, therefore long in time compared to the time of measurement, a near-equilibrium situation obtains, and the use of the plateau potentials to evaluate thermodynamic quantities is permissible.

The averages and probable errors of the plateau potentials from 25 to 60° are given in Table I.

The potential readings for a given run qualified to be included in the average if the time–potential plot showed a definite plateau length of at least two hours. The fact that out of 199 experiments con-

TABLE I

Temp., °C.	Potential, mv.	Electrode used	No. of expt.
25.00	50.42 ± 0.06	wire	6
29.85	47.72 ± .66	wire, bead, foil	13
35.00	45.51 ± .25	wire	6
39.92	43.41 ± .40	wire, bead, foil	13[a]
44.95	40.01 ± .19	foil	9
50.00	38.14 ± .49	foil, bead	15[a]
55.15	34.80 ± .23	foil	9
60.30	32.70 ± .07	foil	8[b]

[a] One run rejected using Chauvenet's criterion.[9] [b] Two runs similarly rejected.

ducted over this temperature range, 121 were plotted, and of these only 79 qualified for the averages, indicates the degree of success, roughly 40%, that can be expected in random experimentation. *Cf.* the discussion of the factors governing the stability. Even though eight runs were stopped after two hours, the average plateau length for the 79 experiments was 6.5 hours. An average of four potentiometric measurements determined the plateau potential.

The potential of the hydrogen reference electrode is sensitive to the partial pressure of hydrogen maintained at its surface, and the potential must be corrected for the vapor pressure of water; this correction varies from +0.4 to 3.14 mv. for the 25 to 60° range. However, experiments without the saturator in the purification train failed to show any potential change greater than the experimental error. Apparently the gas passing through the saturator did not come to equilibrium with the solution in the saturator. Further, during the course of these experiments, the ambient pressure varied in the range 760 ± 20 mm. but the corresponding variation of the potential was within the limit of reproducibility of the experiment.

Temperature Coefficient of the Saturated α-Palladium–Hydrogen Potential.—By the method of least squares, a linear equation was determined from the potential–temperature data in Table I

$$E = 0.06309 - 0.0005057(T - 273.16) \text{ volts} \quad (1)$$

The probable error in the intercept and slope expressed in mv. is: 63.09 ± 0.32 or 0.5%, and 0.5057 ± 0.0073 or 1.4%, respectively.

Nylén[10] reported the potential of a palladium black electrode at three temperatures. However, the original paper[11] giving the technique points out two significant differences from the present investigation. His electrodes were platinum covered with a velvety-black coating of palladium, and they were charged with hydrogen either by cathodic polarization or by immersion in a formic acid solution, and then placed in buffer solutions not saturated with hydrogen. He reports that the potential rose from about the reversible hydrogen potential to a reproducible positive value where it remained constant. The time on this plateau was dependent on the presence of oxidizing agents in the solution which slowly deprived the electrode of its hydrogen. Finally the potential rose to a second less stable plateau value when the hydrogen was depleted. The observed plateau values are comparable to "anodic" or desorption potentials exhibited as the electrode loses hydrogen and makes the transition from the two-phase region to the α-phase. As will be seen, this "anodic" potential is expected to be high.

(9) J. W. Mellor, "Higher Mathematics for Students of Chemistry and Physics," Dover Press, New York, N. Y., 1955, p. 563, 623.

(10) P. Nylén, *Z. Elektrochem.*, **43**, 915 (1937).

(11) P. Nylén, *Svensk. Kem. Tid.*, **48**, 76 (1936).

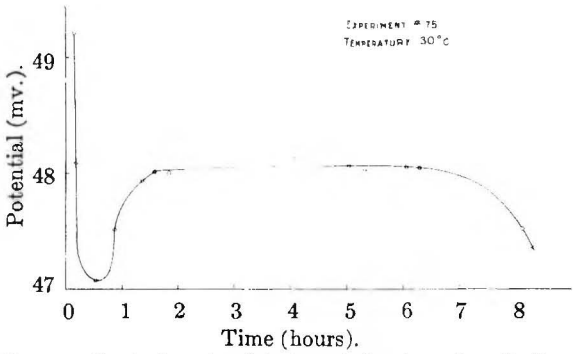

Fig. 1.—Typical potential–time behavior of palladium–hydrogen electrode.

Federova and Frumkin[12] reported values of the potential of a palladium electrode in aqueous sulfuric acid saturated with hydrogen. However, these potentials were obtained by polarization and are not open-circuit potentials as given here. On anodization they found that the potential rose linearly with decreasing H/Pd atom ratio from the reversible value of zero volts to a plateau value (region of phase transition), then rapidly increased when almost all of the occluded hydrogen was consumed. On cathodic polarization, the potential retraced the anodic curve in all regions save the plateau region, where the potential was 8 mv. lower. This is the fact that may account for the higher values of Nylén. These experimental differences should be kept in mind when comparing the values listed in Table II.

The open circuit values given here are "slightly cathodic" values since addition of hydrogen to the alloy is taking place continuously, although the rate of addition is very slight compared to the rate with a current flowing. Comparison with the cathodic values of Federova and Frumkin shows that the open-circuit values are definitely less cathodic and consequently approach the reversible value more closely.

TABLE II

POTENTIAL–TEMPERATURE VALUES

Temp., °C.	Potential in mv. Present research eq. 1	Nylén	Federova and Frumkin Anodic	Federova and Frumkin Cathodic
20	52.98	59.6	60	52
25	50.45			
30	47.92			
35	45.39	52.2		
40	42.86		47	39
45	40.34			
50	37.81			
55	35.28			
60	32.75		34	26

The Standard Heat of Solution.—The temperature coefficient of the α-palladium potential is

(12) A. L. Federova and A. N. Frumkin, *Zhur. Fiz. Khim.*, **27**, 247 (1953).

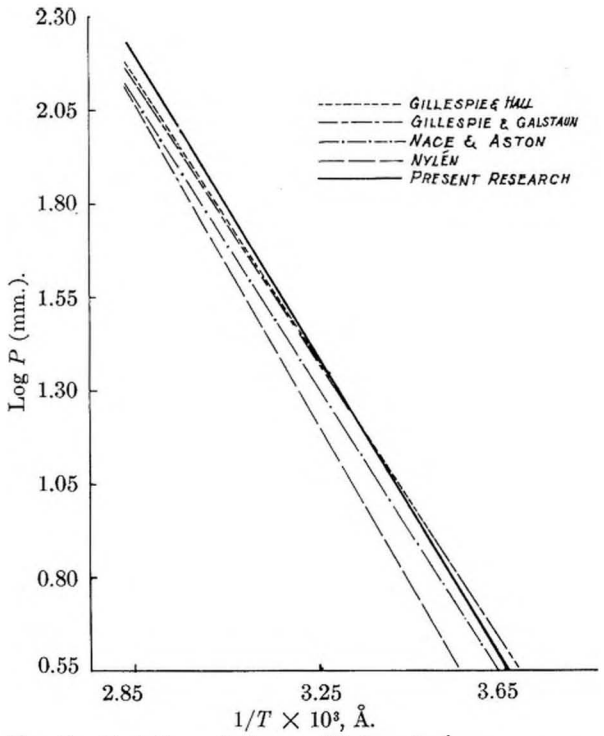

Fig. 2.—Variation of the equilibrium hydrogen pressure over palladium with temperature.

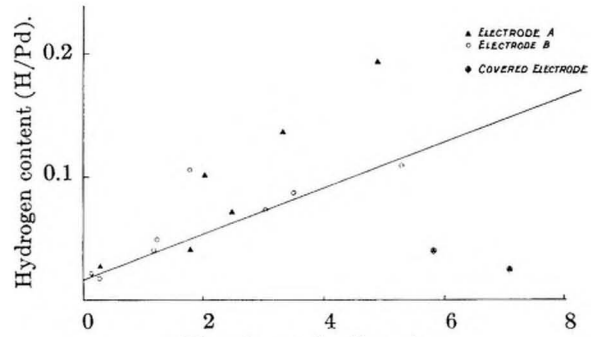

Fig. 3.—Variation in hydrogen content of palladium electrode with time.

related to the standard heat of solution ΔH_s by the Gibbs–Helmholtz relation

$$\left[\frac{\partial(E/T)}{\partial(1/T)}\right]_P = \frac{-\Delta H_s}{nF}$$

where E is the potential in volts, T is the Kelvin temperature, n is the number of electrons involved in the reaction and F is the faraday. For the reaction $H_2 \rightarrow 2H$ (in Pd), n is 2, and we obtain 9280 ± 100 cal./mole H_2 as the standard heat of solution of hydrogen in saturated α-palladium over the temperature range 25–60°. Some literature values are given in Table III.

Pressure-Temperature Relationship.—To calculate the saturation pressure of hydrogen p_s over the two-phase alloy from the cell potential, the cell reaction is written

$$^1/_2H_2 \text{ (gas, 1 atm.)} \rightleftarrows H_{\alpha-sat}$$

The Nernst equation for the cell is

$$E = E^0_{\alpha-sat} - \frac{RT}{F} \ln \frac{a_{\alpha-s}}{p^{1/2}} \qquad (2)$$

Table III

Comparison of Values of Standard Heat of Solution

Investigator	ΔH_s, cal./mole H_2	Remarks
Favre[13]	9102	Calorimetric
Mond, *et al.*[14]	9362	Calorimetric, 22°, Pd black
Gillespie and Hall[15]	8700	30°, fine Pd black
	8450	80°, fine Pd black
Nace and Aston[16]	8870, 9440	Desorption, 45–75°, Pd black
	9330, 9640, and 10300	Isosteric method, 55–75°
		Calorimetric method:
	8948	α-Phase, 30° absorption
	9605	$\alpha + \beta$-Phase, 30° absorption
	9304, 10280	$\alpha + \beta$-Phase, 68° desorption
Nylén[10]	9490	Electrochemical, 20–35°
Present research	9280	Electrochemical, 25–60°

where $a_{\alpha-s}$ is the activity of hydrogen atoms in the saturated α-alloy, p is the pressure of hydrogen in the cell in equilibrium with H^+ ion at the platinum electrode. The Sieverts' law constant K is related to $a_{\alpha-s}$ and $E^0_{\alpha-sat}$ by the equations

$$K = \frac{a_{\alpha-s}}{p_s^{1/2}}$$

$$E^0_{\alpha-sat} = \frac{RT}{F} \ln K$$

Combination of these equations with eq. 2 yields

$$E = -\frac{RT}{F} \ln \left[\frac{p_s}{p}\right]^{1/2} \qquad (3)$$

Since p = 1 atm., we obtain $\log p_s = -10079\,(E/T)$. Using eq. 1 for the potential–temperature dependence, the saturation pressure p_s is given by

$$\log p_s \text{ (atm.)} = 5.0968 - \frac{2028.2}{T}$$

or

$$\log p_s \text{ (mm.)} = 7.9776 - \frac{2028.2}{T} \qquad (4)$$

Equation 4 is plotted in Fig. 2 together with data from some earlier investigations.[10,15–17]

Hydrogen Content Determinations.—The hydrogen content of two palladium electrodes was determined by titration with ceric ion. The cell and electrode were prepared for a run in the usual manner, and the potential was measured with time against the Pt/H_2 electrode. All experiments were carried out at 25.7 ± 0.1°. Since the initial oxide coating on the electrode surface may differ from one experiment to the next, for consistency the time interval before analysis was measured from the time when the minimum potential reading was attained. The electrode was removed from the cell and analyzed after it exhibited the plateau potential for a definite time interval. The trend of these determinations is shown in Fig. 3. The line in Fig. 3 is the least squares line for electrode B.

Since the potentials recorded for these experi-

(13) P. A. Favre, *Compt. rend.*, **77**, 649 (1873).
(14) L. Mond, W. Ramsay and J. Shields, *Trans. Roy. Soc. (London)*, **A191**, 105 (1898).
(15) L. J. Gillespie and F. P. Hall, *J. Am. Chem. Soc.*, **48**, 1207 (1926).
(16) D. M. Nace and J. G. Aston, *ibid.*, **79**, 3619 (1957).
(17) L. J. Gillespie and L. S. Galstaun, *ibid.*, **58**, 2565 (1936).

ments were within 0.6 mv. of the plateau value for 25.7°, it is clear that the potential-determining reaction for the saturated α-palladium extends into the two-phase region as reported by Schuldiner, Castellan and Hoare.[5,6] In further agreement with their work, the H/Pd atom ratio of about 0.65, corresponding to the β-palladium, was found for two runs when the analysis was made after the potential had fallen to zero volts. After 18 and 49 hours, both electrodes showed approximately the same hydrogen content, 0.649 and 0.662, respectively.

In all cases the palladium electrode was welded to a platinum wire which was coated with polyethylene from the welded area to the lid of the cell, and for the analysis the entire electrode was dropped into the flask containing the ceric solution. Therefore a series of checks was made to determine the effect of platinum and polyethylene on the analytical method. Both platinum and polyethylene reduce the ceric ion, possibly due to adsorbed hydrogen or some other reducing agent present. In six determinations the error ranged from 0.005 - 0.0010 meq. of hydrogen. This affects the reported H/Pd atom ratios in the third place, about a 2% error. The error in the method based on the accuracy of weighing, standardization procedure, pipet and buret delivery amounts to about 1%.

Stability of the α-Palladium Potential. The unpredictable plateau length of the potential and the results of the hydrogen analysis which indicated a nearly linear increase in the hydrogen content of the electrode with time differ with the findings of Schuldiner, Castellan and Hoare,[5-7] who report a stable potential if impurities are absent, and if solution contact with the platinum lead is eliminated. Nylén,[10,11] Stout,[18] and Hitzler, Knorr and Mertens,[19,20] who also reported the positive potential of the palladium–hydrogen system, either make no mention of its stability or employed methods such that stability was not possible.

Certainly purity of the system is of utmost importance, since trace impurities can poison the electrode surface and cause the potential to become less noble and approach zero volts.[5] However, other factors influence the system. Palladium shows a marked difference in appearance and behavior after repeated use. When the hydrogen is removed by flaming, profound bending and twisting of the foil is noticed, and gradually the once shiny smooth surface becomes dull, gray and rough. Electrode B in the hydrogen content study was such a conditioned electrode. It absorbed hydrogen at a lower rate than electrode A, hence it would have had a longer plateau length in a potential–time run.

Finally, it is natural to expect electrodes such as beads with a small surface-to-volume ratio to exhibit a longer plateau potential. Two runs in Fig. 3 indicate the effect of restricting the entry of hydrogen by covering all but a corner of a palladium electrode with polyethylene. In the same time interval the hydrogen content attained a value about $^1/_{10}$ as great as that of a comparable uncovered electrode.

Acknowledgment.—We gratefully acknowledge the interest and advice of J. P. Hoare of Ford Motor Co., S. Schuldiner and J. C. White of the Electrochemistry Branch of the Naval Research Laboratory.

(18) H. P. Stout, *Disc. Faraday Soc.*, **1**, 107 (1947).

(19) M. Hitzler, C. A. Knorr and F. R. Mertens, *Z. Elektrochem.* **53**, 228 (1949).

(20) M. Hitzler and C. A. Knorr, *ibid.*, **53**, 233 (1949).

HEATS OF DILUTION OF THE POLYISOBUTYLENE–BENZENE SYSTEM[1]

BY M. A. KABAYAMA AND H. DAOUST

Département de Chimie, Université de Montréal, Montreal, Canada

Received June 11, 1958

The calorimetric measurements of the heats of dilution of the polyisobutylene–benzene system at 25° have been carried out by using a Tian Calvet microcalorimeter. The measurements have been done with four fractions having molecular weights ranging from 34,000 to 392,000. Within the experimental errors, no variation of the enthalpy parameter has been found with the molecular weight. Furthermore, the results show that the partial molar heat of dilution for the system under investigation cannot be represented by the simple Van Laar–Scatchard equation but by a series expansion of the form $\Delta\bar{H}_1 = RT\kappa_1\varphi^2 + RT\kappa_2\varphi^3 + RT\kappa_3\varphi^4 + \ldots$ where $\kappa_1 = 0.21$, $\kappa_2 = 0.46$ and $\kappa_3 = 0.09$. These results, combined with the results of Flory and Daoust on the free energy of dilution of the same system, give data for the entropy of dilution which are compared with the Miller Guggenheim theory.

Introduction

The thermodynamic properties of the polyisobutylene–benzene system have been studied over the entire concentration range by different workers using different methods.[2-7] The results in the moderate[6] and high concentration ranges[5,7] show that the Flory–Huggins relation for the free energy of dilution of a high polymer solution is not followed if a single interaction parameter is used to characterize this system. A new semi-empirical equation for the free energy of dilution has been discussed by Orofino and Flory.[8] The proposed equation is

$$\Delta\bar{F}_1 = RT[\ln(1-\varphi) + (1-1/x)\varphi + \sum_{i=1}(\chi_i)\varphi^{i+1}] \quad (1)$$

(1) This paper has been presented in part at the 132nd Meeting of the American Chemical Society at New York City, N. Y., September 8–13, 1957.

(2) T. G. Fox, Jr., and P. J. Flory, THIS JOURNAL, **53**, 197 (1949).

(3) T. G. Fox, Jr., and P. J. Flory, *J. Am. Chem. Soc.*, **73**, 1909 (1951).

(4) W. R. Krigbaum and P. J. Flory, *ibid.*, **75**, 5254 (1953).

(5) C. E. H. Bawn and R. D. Patel, *Trans. Faraday Soc.*, **52**, 1664 (1956).

(6) P. J. Flory and H. Daoust, *J. Polymer Sci.*, **25**, 429 (1957).

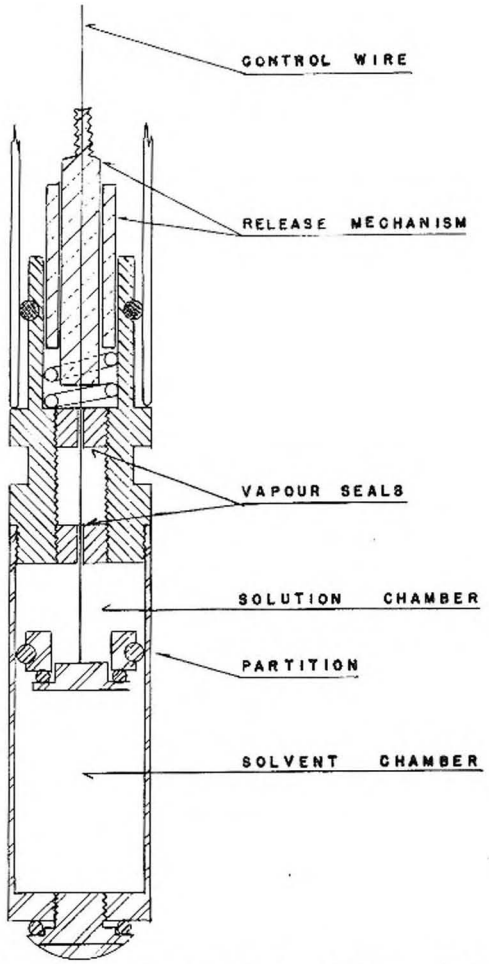

Fig. 1.—Dilution cell; scale: horizontal 2:1; vertical 1.5:1.

where φ is the volume fraction of the polymer and x, the ratio of the molar volumes of the polymer and the solvent. Each parameter χ_i in the power series is assumed to be a constant for a given system and might be temperature dependent. From eq. 1, through the use of standard thermodynamic equations, the heat of dilution may be shown to be given by

$$\Delta\bar{H}_1 = -T^2[\partial(\Delta\bar{F}_1/T)/\partial T]_p \qquad (2)$$

or

$$\Delta\bar{H}_1 = RT\kappa_1\varphi^2 + RT\kappa_2\varphi^3 + \ldots \qquad (3)$$

where

$$\kappa_i = -T(\partial\chi_i/\partial T) \qquad (4)$$

A few direct calorimetric measurements of heats of dilution of polymer–solvent systems in the concentration range we have investigated are reported in the literature,[9-11] but none of them can be used in testing eq. 3. The present investigation has been carried out to check the applicability of this equation to the polyisobutylene–benzene pair.

Experimental

Materials.—The polymer fractions PF-2 ($\bar{M}_v$ = 82,000) and PF-5 ($\bar{M}_v$ = 34,000) have been obtained from a fractionation of commercial Vistanex LM-MH-225 having a viscosity average molecular weight of about 60,000. The polymer fractions PD-5 ($\bar{M}_v \approx$ 392,000) and PD-6 ($\bar{M}_v$ = 252,000) have been obtained from a double fractionation of commercial Vistanex L-100 having a viscosity average molecular weight of about 1.36×10^5. Both commercial polymer samples have been generously supplied by Enjay Co. Inc. The fractionations have been carried out in accordance with previous procedures[12] and the molecular weights determined by the usual viscosity treatment of cyclohexane solutions. The reagent grade benzene was purified in a high efficiency distilling column (80 theoretical plates) and stored over sodium wire. The solutions were made gravimetrically assuming complete additivity of volumes.[13]

Apparatus.—The calorimetric measurements of the heats of dilution have been carried out using a Tian–Calvet microcalorimeter, a differential isothermal type which has been adequately described elsewhere.[14,15] In our installation, a photopen recorder follows the spot of light reflected from the galvanometer mirror. The apparatus is calibrated electrically, and the measurement of the area under the curve gives the heat developed during the course of the reaction. This apparatus is sensitive to a heat effect of 0.001 cal./hr. and is designed especially to follow a reaction over a long period of time.

Dilution Cells.—The cell shown in Fig. 1 was designed for the more fluid solutions. It will be noted that the apparatus has been designed in such a way that it can be filled without any vapor space and develops a small heat of friction during the opening. Teflon "O"-rings are used to seal the fixed part of the partition to the cell wall and to seal the movable part to the fixed one. All the parts in contact with the polymer solution are made of stainless steel, Teflon or nylon. Two cells of three and nine ml. capacity were made, and in each one, the ratio of the volumes of the two chambers can be changed at will by displacement of the partition. Since the solution is slightly denser, it was placed in the upper chamber while the solvent was placed into the lower. To speed up the mixing in some cases, mercury has been placed in the solution chamber in large enough quantity to force up the whole volume of solvent into the solution. Following the attainment of thermal equilibrium, the partition was opened by releasing the spring and pushing down on the control wire. Stirring was furnished by moving the movable part of the partition up and down six times. After the experiment had terminated, the stirring operation was repeated several times in order to determine the heat generated by friction. For the very viscous solutions which do not flow, a different procedure was employed. A stainless steel mesh cage attached to a stainless steel wire was filled with the polymer and introduced into a test-tube containing a certain amount of solvent in the bottom. Solvent vapor was absorbed by the dry polymer until a given concentration was obtained. The cage was then immersed under a quantity of mercury in a stainless steel cell, a weighed amount of solvent was added and the cell tightly stoppered. After thermal equilibrium was attained, this cage was then raised into the solvent and the thermal phenomenon measured as in the other case.

Results

The treatment of the data has been done in a way similar to that used by Tompa[9,16] and many others. The integral heat of dilution ΔH_d evolved when a solution containing n_1 moles of solvent and n_2 moles of solute is diluted to a solution containing $n_1' = (n_1 + dn_1)$ moles of solvent is defined by the relation

$$\Delta H_d = \int_{n_1}^{n_1'} \Delta\bar{H}_1\, dn_1 \qquad (5)$$

(7) R. S. Jessup, *J. Research Natl. Bur. Standards*, **60**, 47 (1958).
(8) T. A. Orofino and P. J. Flory, *J. Chem. Phys.*, **26**, 1067 (1957).
(9) H. Tompa, *J. Polymer Sci.*, **8**, 51 (1952).
(10) K. Amaya and R. Fujishiro, *Bull. Chem. Soc. Japan*, **29**, 270, 361, 830 (1956).
(11) E. Jenckel and K. Gorke, *Z. Elektrochem.*, **60**, 579 (1956).
(12) P. J. Flory, *J. Am. Chem. Soc.*, **65**, 372 (1943).
(13) A. Horth, Ph.D. thesis, University of Montreal, Montreal, 1957.
(14) E. Calvet in Rossini's "Experimental Thermochemistry," Chap. 12, Interscience Publishers, New York, N. Y., 1956.
(15) E. Calvet and H. Prat, "Microcalorimétrie; applications physico-chimiques et biologiques," Masson & Cie, Paris, 1956.
(16) H. Tompa, "Polymer Solutions," Butterworths, London, 1956.

By introducing the value of $\Delta\bar{H}_1$ as given by (3), ΔH_d may be shown to be given by

$$\Delta H_d = RT\kappa_1 n_2 x(\varphi - \varphi') + RT'\kappa_2 n_2 x(\varphi^2 - \varphi'^2)/2 + RT\kappa_3 n_2 x(\varphi^3 - \varphi'^3)/3 + \ldots \quad (6)$$

where $\varphi = n_2x/(n_1 + n_2x)$ and $\varphi' = n_2x/(n_1' + n_2x)$. If we keep only the first three terms of the series expansion and if we approximate $(\varphi^3 - \varphi'^3)/3$ by $\varphi_a^2(\varphi - \varphi')$, equation 6 may be written as

$$\Delta H_d/RT'n_2x(\varphi - \varphi') = \kappa_1 + \kappa_2\varphi_a + \kappa_3\varphi_a^2 \quad (7)$$

where φ_a is the average volume fraction of the polymer. The quantity on the left hand side of equation 7 is called the apparent enthalpy parameter "κ_a." Table I shows the data of the heats of dilution at 25° for the four different fractions of polyisobutylene. The variation of κ_a with the average volume fraction of the polymer is shown in Fig. 2. The scatter of the data is inevitable when working with such concentrated polymer solutions but it is evident from the results that κ_a cannot be averaged to a constant value. The statistical analysis of the data gives values for the first three enthalpy parameters: $\kappa_1 = 0.21$; $\kappa_2 = 0.46$; $\kappa_3 = 0.09$.

In a few cases, the value of ΔH_d has been obtained from long range dilution, and in such cases the value of κ_a is averaged over a wide concentration range. Short range dilutions of the very concentrated solutions are technically very difficult to obtain but the data of Bawn and Patel[5] on the heat of dilution of the polyisobutylene–benzene system obtained from vapor pressure measurements on very concentrated solutions ($\varphi = 0.48$ and above) seem to indicate a strong positive variation of κ_a with concentration.

The data also show that within the experimental errors, there is no variation of the heat parameter with molecular weight. It should be noted here that the results are very sensitive to the presence of traces of water since the measurements have been done very close to the Flory temperature which is 24.5° for this system.[3,4] In fact, a series of measurements which gave much lower values for the enthalpy parameters ($\kappa_1 = 0.14, \kappa_2 = 0.14$) have been rejected since it was proven that the benzene used contained traces of water (0.02 molar).

Discussion

The value 0.21 found for κ_1 compares favorably with those obtained by indirect methods. It is higher than the value of 0.15 found from the viscosity measurements of Fox and Flory[2,3] at 25° and close to the value of 0.19 found by Flory and Daoust.[6] The value of the second parameter, κ_2, if compared with that calculated from eq. 4 using the value of χ_2 obtained by Flory and Daoust at 24.5 and 50°, is about twice as large. However, it should be noted that a slight variation in the values of χ_2 at both temperatures will introduce a large error on κ_2.

The physical meaning of each enthalpy parameter is not known and following Orofino and Flory's point of view, each parameter should be regarded as purely empirical.

The results obtained in this investigation, combined with the data for the free energy of dilution obtained by Flory and Daoust for the same system at 25°, can be used to calculate the total entropy of dilution $\Delta\bar{S}_1$ which is a quantity that can give another test for any theory on higher polymer solutions. The data are summarized in Table II. The values of the entropy of dilution as given in this

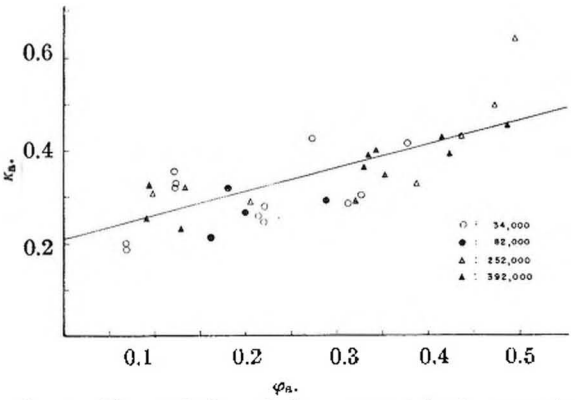

Fig. 2.—The variation of the apparent heat parameter with the average volume fraction of polyisobutylene in benzene at 25°.

TABLE I

HEATS OF DILUTION DATA AT 25°

$n_2x \times 10^3$	$\varphi \times 10^2$	$\varphi_a \times 10^2$	ΔH_d, cal.	κ_a
		$\bar{M}_v$ = 34,000		
1.727	8.36	6.87	0.006	0.20
1.889	8.36	6.93	.006	.19
5.881	15.91	12.10	.085	.32
5.909	15.91	12.14	.095	.35
6.417	15.91	12.27	.092	.33
10.463	28.07	21.37	.213	.26
5.168	28.07	21.98	.091	.24
12.192	28.07	22.01	.243	.28
15.087	34.32	27.17	.545	.43
4.799	43.78	31.49	.199	.29
14.831	43.78	32.64	.592	.30
9.801	43.78	37.59	.297	.42
		$\bar{M}_v$ = 82,000		
3.580	20.15	15.72	0.039	0.21
15.913	20.15	15.97	.133	.32
5.018	27.68	19.92	.094	.26
6.469	36.35	28.79	.134	.29
		$\bar{M}_v$ = 252,000		
4.805	12.70	9.78	0.051	0.31
10.010	26.56	20.51	.207	.29
3.583	72.51	38.72	.467	.33
3.633	82.17	43.58	.721	.43
3.641	89.45	47.26	.906	.50
3.744	93.57	49.36	1.269	.65
		$\bar{M}_v$ = 392,000		
3.777	14.20	9.02	0.059	0.25
3.777	14.20	9.34	.071	.33
5.904	18.90	12.82	.100	.23
8.485	18.90	13.28	.179	.32
1.842	61.80	32.19	.186	.29
1.153	64.20	32.95	.156	.37
1.282	65.10	33.45	.186	.39
1.251	66.20	34.22	.189	.40
1.159	68.80	35.23	.158	.34
2.190	79.70	41.37	.428	.43
1.783	82.20	42.36	.332	.40

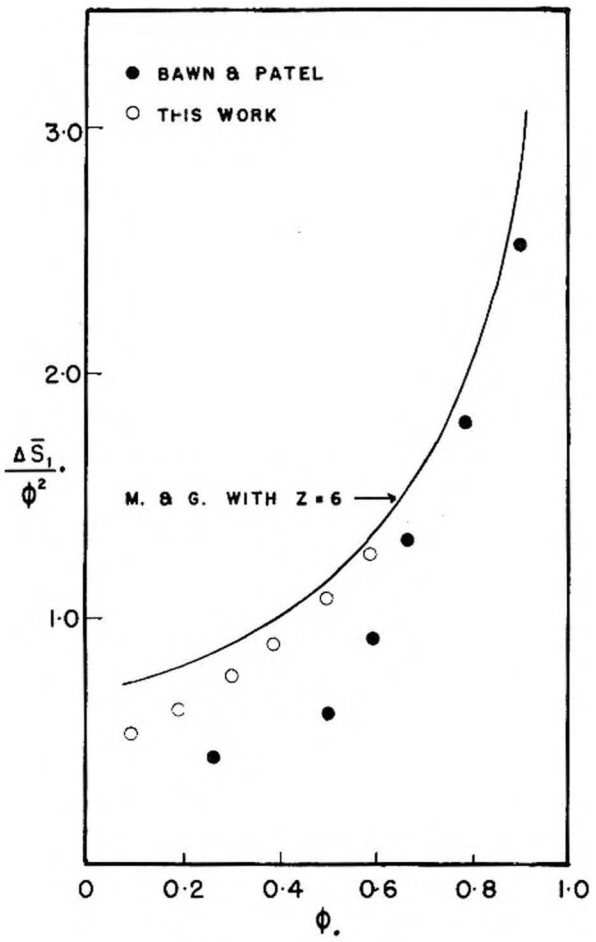

Fig. 3.—The variation of the partial molar entropy of dilution of polyisobutylene with benzene with the volume fraction of the polymer at 25°.

table contain both the configurational entropy of dilution and the contribution from the specific interaction between the polymer and the solvent. The comparison between experimental data and the theory is difficult since only the configurational entropy can be calculated from the Flory or Guggenheim type of theories. However, it is interesting to make this comparison and Fig. 3 shows the variation of $\Delta S/\varphi^2$ with φ as given in Table II, along with the data obtained by Bawn and Patel, and the values calculated from the Miller[17] and Guggenheim[18] relation setting the lattice coördination number $z = 6$.

(17) A. R. Miller, *Proc. Cambridge Phil. Soc.*, **39**, 54, 151 (1943); **43**, 442 (1947).

(18) E. A. Guggenheim, *Proc. Roy. Soc. (London)*, **A180**, 203 (1944).

TABLE II

THERMODYNAMIC FUNCTIONS OF THE POLYISOBUTYLENE-BENZENE SYSTEM AT 25°

φ	$\Delta\bar{F}_1$,[a] cal./mole	$\Delta\bar{H}_1$,[b] cal./mole	$\Delta\bar{S}_1$, e.u.
0.1	−0.02	1.50	0.0051
.2	−0.28	7.25	.025
.3	−1.11	19.1	.068
.4	−3.81	39.1	.144
.5	−10.99	68.9	.268

[a] Calculated according to the relation $\Delta\bar{F}_1 = RT[\ln(1-\varphi) + (1-1/x)\varphi + 0.50\,\varphi^2 + 0.31\,\varphi^3 + 0.17\,\varphi^4]$. (See ref. 6). [b] Calculated according to the relation $\Delta\bar{H}_1 = 0.21RT\varphi^2 + 0.46RT\varphi^3 + 0.09RT\varphi^4$.

The discrepancy between the two sets of data is probably due to the lack of sensitivity of the vapor pressure measurements in the low concentration range where the values reported for the solvent activity are much too high. There are two reasons to set $z = 6$: first, this is the lowest value having physical significance and second, this is the value estimated from the relation given by Orofino and Flory for the free energy parameter χ_i

$$\chi_i = (z\Delta w_{12}/kT)i(1 - 2/z)(2/z)^{i-1} \qquad (8)$$

where Δw_{12} is the average free energy change for the formation of one polymer segment solvent contact in solution. Setting the maximum values for χ_1 (= 0.50) and χ_2 (= 0.33), $z = 6$ according to the relation 8. As φ increases, the experimental data reported in this work approach the theoretical curve, but in the medium and low concentration ranges values of $z = 5$ and $z = 4$ would fit better than $z = 6$. If z is assumed to be a constant, the decrease of the entropy of dilution might be due to some specific interactions between the polymer and the solvent and to the self-coiling or back-coiling of the polymer. Some theoretical derivations[19-21] take care of these two factors, but the relationships thus obtained for the entropy of dilution can explain the experimental data only qualitatively. The back-coiling of the polymeric chain might also explain the decrease in $\Delta\bar{H}_1/\varphi^2$ upon dilution, since the number of polymer segment–solvent contacts is reduced when the number of intramolecular contacts increases.

Acknowledgment.—We wish to thank the National Research Council of Canada for the generous financial assistance in this investigation and for the award of a studentship to M.A.K. while doing this research.

(19) A. J. Staverman, *Rec. trav. chim.*, **69**, 163 (1950).

(20) A. Münster, *Trans. Faraday Soc.*, **49**, 1 (1953).

(21) M. L. Huggins, *J. Polymer Sci.*, **16**, 209 (1955).

THE KINETICS OF GROWTH OF COLLOIDAL COBALT PARTICLES IN MERCURY

BY F. E. LUBORSKY

Instrument Department, General Electric Co., West Lynn, Mass.

Received June 20, 1958

The growth of cobalt particles in mercury from 75 to 300 Å. radius as followed by the measurement of their magnetic coercive force, obeys the relation $\log r/r_0 \approx 0.0971\ t + 1.02 - 500/T$. The growth is diffusion controlled, the driving force being provided by the particle size distribution. The slower growth rate of the cobalt particles as compared to the iron particles previously studied is thus attributed to their smaller size distribution. The dependence of the particle radius on time of growth for both iron and cobalt falls in the range predicted by theory.

The kinetics of growth of colloidal metallic particles in molten metals is of fundamental importance in our work concerned with the development of single magnetic domain particles for permanent magnets.[1-3] In a previous paper[4] the kinetics of growth of spherical iron crystallites in mercury was presented in some detail and the mechanism of growth deduced. It is the purpose of this paper to present kinetic data on the growth of spherical cobalt particles in mercury. This work supports and clarifies the growth mechanism previously postulated for the iron particles.

Experimental Method and Results

Colloidal cobalt particles in mercury were prepared by electrodeposition and their growth followed as previously described[4] for iron by measurement of their magnetic coercive force. The correlation between the coercive force of the cobalt particles made in this way and their radius has been reported[5] previously and has been verified in this work at one particle size by means of an electron micrograph at 100,000×. The particle shape was essentially spherical.

The results of the measurements on the cobalt particles growing from 75 to 300 Å. radius at 100, 150 and 200° can be accurately summarized by

$$\log \frac{r}{r_0} = 0.0971 \log t + F = 0.0971 \log t + 1.02 - \frac{500}{T} \quad (1)$$

where r is the particle radius in cm. at any time t in sec. and T is the absolute temperature. These results are compared in Fig. 1 to the growth of iron particles. The rate constant, calculated from the data on the basis of the simple diffusion controlled growth model as developed for iron,[4] exhibits a temperature dependence given by

$$\log k = -\frac{7750}{2.3RT} + \log 1.05 \times 10^{-14} \quad (2)$$

This equation is compared in Fig. 2 to the results previously obtained for iron.

Discussion

The growth of iron particles in mercury is 2.3 times faster than the growth of cobalt particles as measured by the slope of the growth equations shown in Fig. 1. The temperature dependent term in these growth equations is 2.8 times larger for iron than for cobalt. The apparent "activation energy" for cobalt from equation 2 is 2.1 times larger for iron than for cobalt as measured by the slopes of the curves in Fig. 2.

To account for these differences in the growth of iron and cobalt, let us first consider the rate constant

$$k = \frac{2DM(c - c_0)}{N\rho(1 - p^{1/3})} \quad (3)$$

as derived previously,[4] where D is the diffusion constant, M the atomic weight, $c - c_0$ the supersaturation, ρ the density of the solid phase, N Avogadro's number and p the concentration of particles. From the value of the constants in this equation, as listed in Table I, we obtain the ratio

$$k_{Fe}/k_{Co} = 1.04(c - c_0)_{Fe}/(c - c_0)_{Co} \quad (4)$$

Thus, the supersaturation which exists in the two systems will be the determining factor in their growth rates. It must be concluded from (4) and the results shown in Fig. 2, that at a growth temperature of about 80° when $k_{Fe} = k_{Co}$ the supersaturation present in the cobalt dispersion is the same as in the iron dispersion. Since the supersaturation maintained in these systems is due to the particle size distribution, which is controlled by the particle solubility we can further conclude that at this same temperature the particle size distribution and the solubilities will be the same. At temperatures greater than 80° when k_{Fe} is greater than k_{Co}

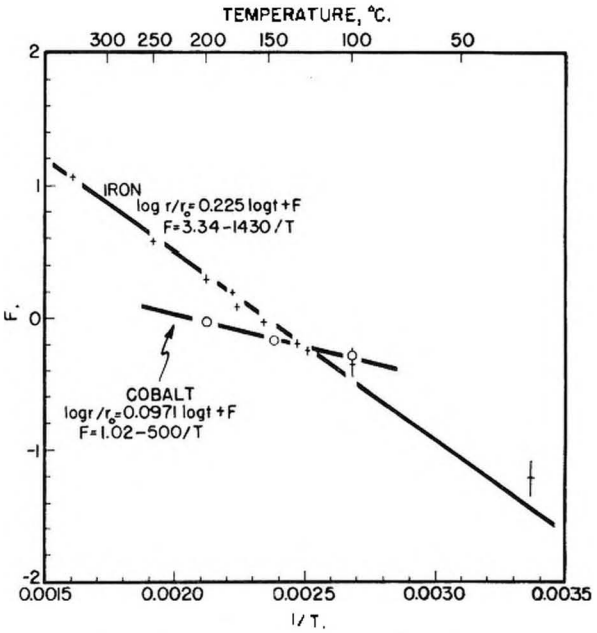

Fig. 1.- Experimental temperature dependence of the growth of iron and cobalt particles in mercury.

(1) T. O. Paine, L. I. Mendelsohn and F. E. Luborsky, *Phys. Rev.*, **100**, 1055 (1955).

(2) L. I. Mendelsohn, F. E. Luborsky and T. O. Paine, *J. Appl. Phys.*, **26**, 1274 (1955).

(3) F. E. Luborsky, L. I. Mendelsohn and T. O. Paine, *ibid.*, **28**, 344 (1957).

(4) F. E. Luborsky, THIS JOURNAL, **61**, 1336 (1957).

(5) W. H. Meiklejohn, *Rev. Modern Phys.*, **25**, 302 (1953).

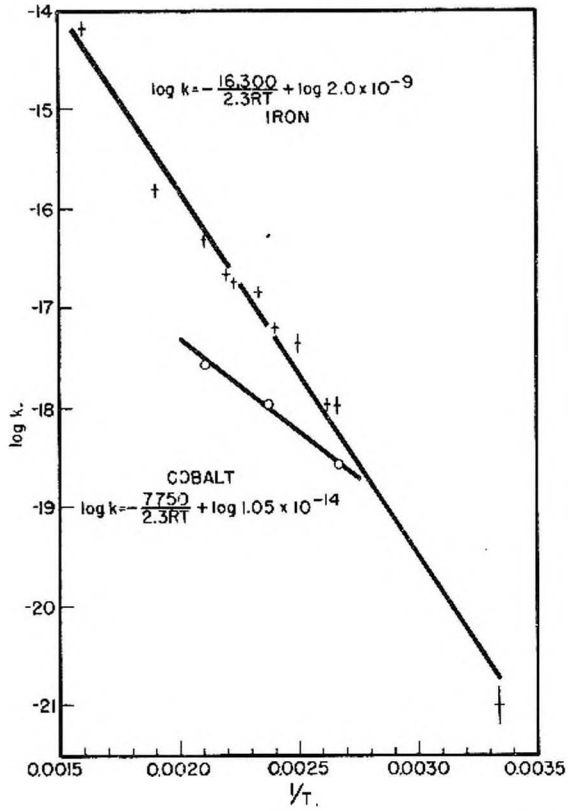

Fig. 2.—The rate constant according to the simple diffusion controlled growth model for iron and cobalt particles in mercury.

the supersaturation, and thus the particle size distribution, in the iron sample will be greater than in the cobalt sample. The particle size distribution of the iron particles grown at 175° to a mean particle radius of 75 Å. has a symmetric distribution with a standard deviation of 17 Å. For cobalt grown at both 150 and 175° to radii of 75 and 100 Å. the standard deviation was considerably smaller, in agreement with the above analysis. The solubilities of iron and cobalt reported in the literature[6,7] show considerable variation. However, it appears that at room temperature the solubility of cobalt in mercury is greater than that of iron as expected from the growth rates. There are insufficient data at higher temperatures to make this comparison.

Greenwood[8] has shown, as discussed for the case of the iron dispersions,[4] that the maximum rate of growth for polydispersed particles corresponds to a radial dependence on time of $t^{1/3}$. This maximum rate is attained only by the particles with a radius twice that of the mean radius. As the particle size distribution decreases, the driving force decreases and thus the growth dependence approaches a constant, $t^{1/\infty} = 1$. These theoretical limits for the polydispersed system are compared to the experimental results in Table II. In the case of the monodispersed particles the system must be initially supersaturated to show growth. The observed rate dependences for both iron and cobalt do fall between the maximum and minimum predicted for the polydispersed system of particles.

(6) J. F. de Wet and R. A. Haul, *Z. anorg. allgem. Chem.*, **277**, 96 (1954).

(7) A. Marshall, L. Epstein and F. Norton, *J. Am. Chem. Soc.*, **72**, 3514 (1950).

(8) G. W. Greenwood, *Acta Met.*, **4**, 243 (1956).

TABLE I

COMPARISON OF CONSTANTS FOR IRON AND COBALT AT 25°

	Iron	Cobalt
D, cm.²/sec.[4]	1.8×10^{-6}	1.8×10^{-6}
M, g./g. atom	55.85	58.94
ρ, g./cc.	7.86	8.90
p, cc. metal/cc. Hg	0.025	0.031
c_0, atoms/cc.[6,7]	$\sim 1 \times 10^{15}$	$\sim 2 \times 10^{15}$

TABLE II

THEORETICAL AND EXPERIMENTAL COMPARISON OF DIFFUSION CONTROLLED GROWTH

		Radius proportional to
Monodispersed		$t^{0.50}$
Polydispersed	Maximum rate	$t^{0.33}$
	Minimum rate	t^{0}
Experimental	Iron	$t^{0.225}$
	Cobalt	$t^{0.0971}$

Conclusions

The growth of colloidal cobalt particles in mercury has been shown to be very similar to the growth of iron where the diffusion process was considered to be the rate limiting step. The driving force in both cases is the supersaturation provided by the distribution of particle sizes present. The slower growth of cobalt is attributed to the smaller size distribution, but the growth dependence of both iron and cobalt particles is in the range predicted by theory.

The substantial difference in the growth rate of particles as similar as cobalt and iron and the examination of micrographs of particles at various stages of growth further substantiates the fact that a coagulation mechanism is not a major factor in the growth of these particles.

KINETICS OF THE AQUEOUS REVERSION OF PYROPHOSPHATE

BY R. KEITH OSTERHELD[1]

Contribution from the Department of Chemistry, Cornell University, Ithaca, N. Y., and the Department of Chemistry, Montana State University, Missoula, Montana

Received June 23, 1958

The rate of reversion of sodium pyrophosphate has been studied in aqueous solution at 60.03° over the *p*H range 0.38 to 6.74 at ionic strength about 0.44. The acid ionization constants assigned to the species $H_5P_2O_7^+$, $H_4P_2O_7$, $H_3P_2O_7^-$, $H_2P_2O_7^{-2}$ and $HP_2O_7^{-3}$ under these conditions are $\geq 1 \times 10^2$, 1×10^{-1}, 1×10^{-2}, 2.5×10^{-6} and 4×10^{-10}, respectively. The first-order rate constants for the hydrolysis of the same species are, respectively, ≥ 115, 0.037, 0.024, 0.0112 and 0.00036 hr.$^{-1}$ It was necessary to postulate the participation of an $H_5P_2O_7^+$ species to account for the rapid change in over-all rate constant over the *p*H range 0.38 to 1.79. Alternatives to this are discussed.

The kinetics of the aqueous reversion of pyrophosphate to orthophosphate have been the subject of many investigations. The reaction has been shown to be first order in pyrophosphate concentration when studied at constant *p*H in dilute aqueous solution.[2] For some time[3] it has been evident that the dependence of the kinetics on *p*H results from the dependence on *p*H of the relative concentrations of the various acid pyrophosphate species, the rate constant being different for each of the species. The over-all observed rate constant at a particular *p*H is then the average of the rate constants for the individual species, weighted on the basis of the relative abundance of the various acid pyrophosphate species.

$$k_{obsd} = k_4x_4 + k_3x_3 + k_2x_2 + k_1x_1 + k_0x_0 \quad (1)$$

where k represents a rate constant, x represents a mole fraction of the total pyrophosphate in solution, and the subscripts 4, 3, 2, 1 and 0 refer to the species $H_4P_2O_7$, $H_3P_2O_7^-$, $H_2P_2O_7^{-2}$, $HP_2O_7^{-3}$ and $P_2O_7^{-4}$, respectively.

If the rate constants for the individual species differ sufficiently and systematically a plot of observed rate constant values as a function of *p*H should resemble a titration curve for pyrophosphoric acid over the same *p*H range. This is of interest as the kinetics of this reaction have commonly been studied at temperatures of 50° or higher, temperatures at which reliable ionization constants are unavailable for pyrophosphoric acid. In principle, one should be able to obtain from the kinetic data both the rate constants and the ionization constants for the individual pyrophosphoric acid species. The fact that a plot of the observed rate constant for this reaction *vs.* *p*H shows a stepped shape has not previously been emphasized, the kinetics having been studied over a relatively narrow *p*H range[2-4] or at a few widely separated values.[5-8] Campbell and Kilpatrick[9] presented data from which the stepped shape of this curve could be inferred. In that work, however, for different ranges of acidity different ionic strengths or buffers were used. In the *p*H ranges over which experimental conditions were uniform no complete steps appeared.

Experimental

In designing a run the pyrophosphoric acid ionization constants determined by Abbott and Bray[10] at 18° were assumed to be correct at 60°. On this basis were calculated the amount of hydrochloric acid required to give the desired *p*H and the amount of sodium chloride necessary to produce an ionic strength of 0.50. Recalculating on the basis of the results of the present work, the initial ionic strengths were found to be actually 0.41–0.46, generally close to 0.44. The ionic strength in a given run no doubt changed slightly as the reversion of pyrophosphate to orthophosphate proceeded.

To prepare for a run three flasks were brought to 60.03 ± 0.03°: (1) a volumetric flask containing the calculated amounts of hydrochloric acid and sodium chloride, (2) a flask containing a freshly prepared solution of reagent grade sodium pyrophosphate decahydrate, and (3) a flask of water. The run was started by pipetting into the first flask enough of the pyrophosphate solution to make the pyrophosphate concentration 0.033 *M*, adding enough of the water to make the solution up to the mark, and mixing the resulting solution.

Immediately and at intervals thereafter samples were withdrawn for determination of *p*H and of pyrophosphate concentration. Samples for *p*H determination were transferred to a cell in the constant temperature bath and the *p*H determined at 60.03° with a Beckman Model "G" *p*H meter, correcting for the elevated temperature. Aliquots taken for pyrophosphate determination were cooled rapidly to below room temperature and the *p*H was made >4.5 if the acidity of the sample was not already that low. Pyrophosphate analyses were carried out by the Bell method,[11] employing corrections empirically determined by analysis of a series of synthetic mixtures representing various stages in the reversion of a sample. Pipets used at bath temperature were preheated in a well in the bath. Where necessary, volumetric equipment was recalibrated at the bath temperature.

No attempt was made to control the *p*H during a run. Over the *p*H range 0.38 through 1.37 the *p*H and the observed rate constant did not change during a run within experimental error. From *p*H 1.73 through *p*H 5.67 the *p*H increased during a run and the rate constant decreased, the latter being only slightly affected in the *p*H range 3.23–4.96, however. At *p*H 6.01 the *p*H and rate constant did not change during the run. At *p*H 6.71–6.74 the *p*H decreased and the rate constant increased. For those runs producing a curved plot of log *M* *vs.* time the slope of the tangent to the curve at a given time was used to calculate the rate constant for the *p*H prevailing in the solution at that time.

Results and Discussion

The observed first-order rate constants appear in Table I. By means of successive approximations values were assigned to the ionization constants and

(1) Department of Chemistry, Montana State University, Missoula, Montana.

(2) H. Giran, *Ann. chim. phys.*, [VII], **30**, 203 (1903); G. A. Abbott, *J. Am. Chem. Soc.*, **31**, 763 (1909); and S. J. Kiehl and E. Claussen, *ibid.*, **57**, 2284 (1935).

(3) J. Muus, *Z. physik. Chem.*, **159A**, 268 (1932).

(4) S. L. Friess, *J. Am. Chem. Soc.*, **74**, 4027 (1952).

(5) J. R. Van Wazer, E. J. Griffith and J. F. McCullough, *ibid.*, **74**, 4977 (1952); **77**, 287 (1955).

(6) J. D. McGilvery and J. P. Crowther, *Can. J. Chem.*, **32**, 174 (1954).

(7) J. P. Crowther and A. E. R. Westman, *ibid.*, **32**, 42 (1954).

(8) L. M. Postnikov, *Vestnik Moskov. Univ.*, **6**, No. 5. Ser. Fiz-Mat. i. Estest. Nauk No. 3. 63 (1950).

(9) D. O. Campbell and M. L. Kilpatrick, *J. Am. Chem. Soc.*, **76**, 893 (1954).

(10) G. A. Abbott and W. C. Bray, *ibid.*, **31**, 729 (1909).

(11) R. N. Bell, *Anal. Chem.*, **19**, 97 (1947).

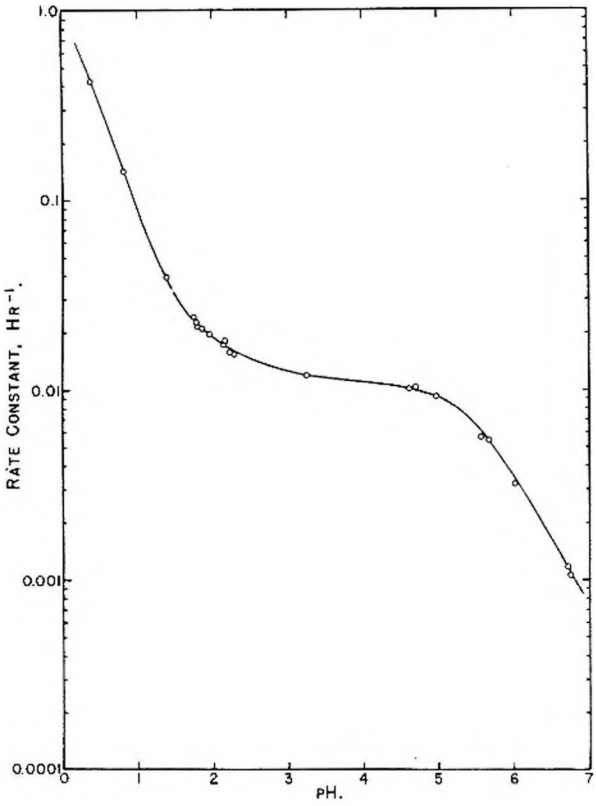

Fig. 1.

reversion rate constants for the various acid pyrophosphate species. In the *p*H range studied the concentration of the $P_2O_7^{-4}$ ion is negligibly small. Although it would appear that the remaining eight parameters of equation 1 should permit a fit to almost any curve, it proved impossible to fit the rapid change in the observed rate constant over the *p*H range 0.38–1.79 and the rest of the data simultaneously without introducing an additional species, the $H_5P_2O_7^+$ ion. Then

$$k_{obsd} = k_6x_5 + k_4x_4 + k_3x_3 + k_2x_2 + k_1x_1 + k_0x_0 \quad (2)$$

Attempts to fit the data in the highly acid region without the assumption of the participation of an $H_5P_2O_7^+$ ion forced the assignment of unacceptable values to various parameters of equation 1. Some of these unacceptable alternatives were, depending upon the approach to the calculation, (1) a negative value for the ionization constant of $H_4P_2O_7$, (2) a value for the ionization constant of $H_3P_2O_7^-$ greater than that of $H_4P_2O_7$, and (3) a negative value for the rate constant for reversion of $H_3P_2O_7^-$. Actually, only the last of these permits a close fit to the data.

The values obtained for the various constants appear in Table II. In Table I over-all rate constants calculated from the assigned parameters and equation 2 are compared with the observed values. Agreement between the observed and calculated rate constants is generally well within the limitations imposed by the low precision of *p*H measurements. The fit to the observations is not sensitive to small changes in the ionization constants for $H_4P_2O_7$ and $H_3P_2O_7^-$. The ionization constant given for $H_5P_2O_7^+$ is the minimum value that will

TABLE I

PYROPHOSPHATE REVERSION AT 60.03°, OBSERVED FIRST-ORDER RATE CONSTANTS, HR.$^{-1}$

*p*H	$k_{obsd.}$	$k_{calcd.}$	*p*H	$k_{obsd.}$	$k_{calcd.}$
0.38	0.424	0.424	4.61	0.01010	0.01025
0.80	.1411	.141	4.69	.01038	.01002
1.37	.0392	.0383	4.96	.00924	.00923
1.73	.0242	.0239	5.57	.00567	.00599
1.77	.0226	.0229	5.59	.00563	.00589
1.79	.0216	.0222	5.62	.00556	.00567
1.85	.0210	.0212	5.64	.00553	.00555
1.95	.0197	.0196	5.67	.00549	.00531
2.13	.0171	.0176	6.01	.00322	.00341
2.14	.0181	.0175	6.71	.001177	.00116
2.21	.0158	.0168	6.72	.001149	.00112
2.28	.0153	.0161	6.74	.00107	.001085
3.23	.01199	.0119			

fit the observations. A fit can also be obtained by assigning to $H_5P_2O_7^+$ any ionization constant greater than 100, which then necessitates a corresponding increase in the reversion rate constant for this species, but no other adjustment. With the values here assigned to the parameters the percentages of the observed rate constant attributed to the $H_5P_2O_7^+$ ion at *p*H values of 0.38, 0.80, 1.37, 1.73 and 1.85 are 92, 78, 33, 11 and 6%, respectively. The permissible changes in the ionization and rate constants mentioned above for the $H_5P_2O_7^+$ ion do not affect these percentages.

The stepwise dependence of the kinetics of this reaction on acidity in the *p*H range studied is evident in Fig. 1. Some experimental points, but no extreme ones, have been omitted from Fig. 1 for clarity. The solid line represents the curve generated by equation 2 using the assigned parameters. The stepped curve of Fig. 1 is distinctly different from the smooth curve presented by McGilvery and Crowther[6] and by Crowther and Westman.[7] The two interpolations made by McGilvery and Crowther in calculating rate constants for the individual pyrophosphate species were then unjustified, and their derived rate constants are questionable. The rapid change in rate constant in the highly acid region was noted by Campbell and Kilpatrick,[9] who preferred to explain it in terms of a second-order reaction of $H_4P_2O_7$ with hydronium ion. Their data, however, did not permit quantitative treatment of the kinetics in this region.

Because of the interrelationship of the hydrogen ion concentration, the hydroxide ion concentration, and the relative abundance of the various pyrophosphate species, for the first-order rate constant derived for a particular pyrophosphate species two corresponding second-order rate constants could equally well be calculated, one for reaction of the next less acid pyrophosphate species with hydronium ion, the other for reaction of the next more acid pyrophosphate species with hydroxide ion. These second-order rate constants can be simply derived from the values listed in Table II by use of the ionization constants of the acid pyrophosphate species and of water.

Since it is mathematically impossible from kinetic data such as these to make a choice of mechanism for this reaction we more or less arbitrarily chose to consider the reversion a first-order reaction

TABLE II

IONIZATION CONSTANTS AND FIRST-ORDER REVERSION RATE CONSTANTS FOR PYROPHOSPHATE SPECIES

	This work	Campbell and Kilpatrick[9]	McGilvery and Crowther[6]	Abbott and Bray[10]
Temp., °C.	60.03	59.87	65.5	18
Ionic strength	0.44	0.15		0.026
Ionization constants:				
$H_5P_2O_7^+$	$\geq 1 \times 10^2$			
$H_4P_2O_7$	1×10^{-1}		1.07×10^{-1}	1.4×10^{-3}
$H_3P_2O_7^-$	1×10^{-2}	$0.2\text{–}1 \times 10^{-2}$	7.58×10^{-3}	1.1×10^{-3}
$H_2P_2O_7^{-2}$	2.5×10^{-6}	$1.5\text{–}2.5 \times 10^{-6}$	1.45×10^{-6}	2.9×10^{-7}
$HP_2O_7^{-3}$	4×10^{-10}	4×10^{-10}	9.81×10^{-9}	3.6×10^{-9}
Rate constants, $hr.^{-1}$:				
$H_5P_2O_7^+$	≥ 115			
$H_4P_2O_7$	0.037		0.23	
$H_3P_2O_7^-$	0.024	0.0120	0.044	
$H_2P_2O_7^{-2}$	0.0112	0.00956	0.017	
$HP_2O_7^{-3}$	0.00036		0.00315	
$P_2O_7^{-4}$			0.00028	

over the *p*H range studied here. The arithmetic is simpler on this basis. Experimental evidence in support of this viewpoint includes the observation that the rate of the first-order hydrolysis of the P–O–P bond of tetraethyl pyrophosphate is relatively insensitive to acidity over the *p*H range 1 to 7.[12,13] Oxygen tracer studies of the hydrolysis of acetyl phosphate have shown that whereas the C–O bond is broken in basic solution, the P–O bond is broken in acidic solution.[14] This is consistent with a mechanism assuming nucleophilic attack of the phosphorus by water, the phosphorus atom of a phosphate species being rendered more positive in acidic solution by formation of un-ionized acid species. The possibility exists, of course, that more than one mechanism is involved in these examples or even in the inorganic system studied in the present work.

(12) S. A. Hall and M. Jacobson, *Ind. Eng. Chem.*, **40**, 694 (1948).

(13) J. A. A. Ketelaar and A. H. Bloksma, *Rec. trav. chim.*, **67**, No. 11, 665 (1948).

(14) R. Bentley, *J. Am. Chem. Soc.*, **71**, 2765 (1949).

NOTES

ON THE ABSENCE OF COMPLEX IONS IN SOLUTIONS OF CALCIUM AND MAGNESIUM BICARBONATES

BY FRANZ HALLA AND RENÉ VAN TASSEL

Société d'Etudes, de Recherches et d'Applications pour l'Industrie, 1091 Chaussée d'Alsemberg, Brussels

Institut Royal des Sciences Naturelles, 31, rue Vautier, Brussels

Received December 28, 1957

Greenwald[1] suggested on the basis of *p*H determinations that complex ions, formed according to

$$Me^{++} + HCO_3^- \rightleftarrows MeHCO_3^+ \qquad (1)$$

are present in bicarbonate solutions (Me = Ca or Mg) at comparatively high ionic strength ($\mu = 0.16$). We found no evidence, at least in more dilute solutions, for the formation of such complexes; our *p*H determinations were carried out under constant carbon dioxide partial pressure ($p_{CO_2} \sim 1$ atm.).

Experimental

The standard solutions A (175 mmole of magnesium per liter) and B (9 mmole calcium per liter) were prepared by passing a current of purified carbon dioxide through aqueous suspensions of MgO and $CaCO_3$, respectively. Water saturated with carbon dioxide was used throughout the experiments.

The *p*H measurements were made in an especially constructed *p*H meter of high impedance. The calibration error, determined with a commercial buffer, was 0.04 *p*H unit.

The experimental results are shown in Table I.

TABLE I

*p*H of aqueous solutions of $Mg(HCO_3)_2$ and $Ca(HCO_3)_2$ saturated with carbon dioxide (p_{CO_2} = 726.0 mm. at 28.4°).

Solute	c = mmole/L. Mg or Ca	*p*H	$(H^+) \times 10^7$	$\kappa/(H^+)$	$2c - \kappa/(H^+)$
$Mg(HCO_3)_2$	9.6	6.33	4.68	30.5	−11.3
	4.8	6.07	8.52	16.7	− 7.1
	2.4	5.68	20.9	6.8	− 2.0
	1.2	5.25	56.2	2.5	− 0.1
	0.6	4.91	125	1.14	− 0.06
$Ca(HCO_3)_2$	9.3	6.15	7.07	29.2	− 1.6
	4.65	5.84	14.5	9.8	− 0.5
	2.33	5.57	29.9	5.3	− 0.6
	1.16	5.28	52.6	2.7	− 0.38
	0.58	4.99	102	1.4	− 0.24

For such bicarbonate solutions the *p*H is given by

$$pH = pK_1' + \log \frac{[HCO_3^-]}{[CO_2]} + \log \frac{[f_{HCO_3^-}]}{f_{CO_2}} \qquad (2)$$

(1) I. Greenwald, *J. Biol. Chem.*, **141**, 789 (1941).

as long as the pH < 7; K_1' is the first apparent dissociation constant of carbonic acid.

If we make $[MeHCO_3^+] = x$, $[Me^{++}] = y$, and $[HCO_3^-] = v$, then $c = x + y$ and $2y + x = v$. The constant for the formation of a complex according to (1) is then

$$K = \frac{(MeHCO_3^+)}{(Me^{2+})(HCO_3^-)} = \frac{2c - v}{v(v - c)} \times \frac{f_x}{f_a f_v} \quad (3)$$

For infinite dilutions this gives

$$K = \lim_{c=0} \frac{2c - v}{v(v - c)} \quad (4)$$

Introducing $\kappa = K_1'[CO_2]_{sat} = 4.63 \times 10^{-7} \times 0.0308 = 1.425 \times 10^{-8}$ at 28.4° as a new constant,[2] we obtain according to (2)

$$v = \kappa f_{CO_2}/(H^+)f_a \quad (5)$$

and (4) becomes

$$K = \lim_{c=0} \frac{2c - \kappa/(H^+)}{[\kappa/(H^+) - c]\kappa/(H^+)} \quad (6)$$

Table I shows that $2c - \kappa/(H^+)$ and with it K, converge from negative values toward zero with decreasing c for both bicarbonates. Therefore, complex formation does not occur at these ionic strengths.

The pH of mixed bicarbonate solutions (Mg:Ca = 4:1, 3:2, 1:1 and *vice versa*) was measured at values of μ ranging from 2.8×10^{-2} to 1.75×10^{-4}. The finding that the pH is independent of the Mg:Ca ratio for a given value of μ indicates that there is no strong specific ionic interaction at these concentrations.

pH determinations were made on a series of solutions made up by dilution of A with increasing volumes of B in the pH meter. The plot of the pH values *vs.* the volume ratios occasionally showed a maximum, a finding which is inconsistent with the above conclusion.

TABLE II

DENSITIES d OF DIFFERENT MIXED SOLUTIONS OF $Mg(HCO_3)_2$ AND $Ca(HCO_3)_2$ IN WATER SATURATED WITH CO_2 ($p \sim 1$ ATM.)

Mg, mmole/l.	Ca, mmole/l.	Total Mg + Ca	d_{19}
163.5	0.00	163.5	1.0199
130.8	2.03	132.8	148
98.1	4.06	102.2	116
82.5	5.08	87.6	100
65.4	6.09	71.5	82
32.7	8.12	40.8	52
0.0	10.15	10.15	19

This anomaly proved to be due to the adsorption of calcium and magnesium ions on the surface of the electrode; an equilibrium was not established between the more dilute solution and the adsorbed ions. The anomaly was never observed if the electrode was washed thoroughly between experiments, with highly diluted hydrochloric acid and distilled water, a precaution which was followed through our work.

(2) Values of K_1', which were taken from H. S. Harned and B. B. Owen, "The Physical Chemistry of Electrolytic Solutions," Reinhold Publ. Corp., New York, N. Y., 1956, were interpolated. The dependence of the $[CO_2]_{sat.}$ on c is within the experimental error; see A. Seidell, "Solubilities," Vol. 1, D. Van Nostrand Co., New York, N. Y., 1940, pp. 221, 226.

Acknowledgments.—The pH meter used was designed by Mr. Van Aerschodt and built in our workshop.

THE CONDUCTANCE OF CONCENTRATED AQUEOUS SOLUTIONS OF POTASSIUM IODIDE AT 25° AND OF POTASSIUM AND SODIUM CHLORIDES AT 50°

BY J. F. CHAMBERS[1]

Chemistry Department, University of Western Australia, Nedlands, Australia

Received January 20, 1958

This paper continues the report of work carried out in the research program outlined in a previous paper.[2] The aim, briefly, is to provide some precise experimental data of the conductance and viscosity of concentrated aqueous solutions of simple salts for study in the light of recent theoretical developments.[3-5]

Experimental

The apparatus and the experimental procedure used in the measurement of the present data are the same as described in ref. 2. The results presented in that paper, for aqueous solutions of sodium and potassium chlorides, agreed within 0.02% with the results of Shedlovsky, *et al.*[6] The purity of the stock of these two salts used in the present work was several times checked by a determination of the equivalent conductance of an aqueous solution at 25°. These values were always in excellent agreement with those in ref. 2. Sodium chloride was A.R. grade, purified by precipitation from conductance water by hydrogen chloride gas. It was then given a preliminary drying at 110° and before use was heated at 400° for 48 hours. Potassium chloride was A.R. grade, purified by precipitation from conductance water, then given a preliminary drying at 110°. Before use it was heated at 400° for 48 hours. Potassium iodide was A.R. grade, recrystallized twice from conductance water, dehydrated over calcium chloride under vacuum for a week, then finally heated at 150° in air for four days. The stock so prepared was used within a week or two. Regular check solutions of the salt so prepared occasionally were found to have conductances which were up to 0.3% high. In such cases the whole procedure was repeated until the conductances agreed with the data recorded in Table I. Conductance water was the laboratory distilled water redistilled through Pyrex and stored in polythene bottles. It had a specific conductance of about 1.2×10^{-6} int. ohms^{-1} cm.$^{-1}$ at 25° and about 2.5×10^{-6} int. ohm^{-1} cm.$^{-1}$ at 50°. A solvent correction was always made to the measured specific conductance of the solutions. Densities were taken from the International Critical Tables,[7] and vacuum corrections were used throughout. Molecular weights used in computing the molarities were: KCl, 74.553; NaCl, 58.454; KI, 166.02. Temperatures were maintained constant in oil bath thermostats at 25 and 50° to within ±0.002° by the use of calorimeter thermometers, whose true reading was found on a platinum resistance thermometer to within ±0.01°. The actual measurements at 50° were made at temperatures up to 0.09° low and later corrected to 50.00°. The Pyrex glass cells were as described in the first paper[2] and had cell constants from 0.5 to 459

(1) Electrolytic Zinc Company Research Fellow, 1955.

(2) J. F. Chambers, Jean M. Stokes and R. H. Stokes, THIS JOURNAL, 60, 985 (1956).

(3) H. Falkenhagen, M. Leist and G. Kelbg, *Ann. physik.*, [6] 11, 51 (1952); H. Falkenhagen and M. Leist, *Naturwiss.*, 41, 570 (1954).

(4) R. M. Fuoss and L. Onsager, *Proc. Natl. Acad. Sci., U. S.*, 41, 274 (1955).

(5) B. F. Wishaw and R. H. Stokes, *J. Am. Chem. Soc.*, 76, 2065 (1954).

(6) T. Shedlovsky, A. S. Brown and D. A. MacInnes, *Trans. Electrochem. Soc.*, 66, 165 (1934).

(7) "International Critical Tables," Vol. III, McGraw-Hill Book Co., Inc., New York, N. Y.

cm.$^{-1}$. The cells were calibrated at 25° with the Jones and Bradshaw 1 and 0.1 D potassium chloride solutions.[8] For use at 50° the cells were regarded simply as long narrow glass tubes in order to derive the expression for the cell constants: $a_{50} = a_{25}[1 - (t - 25)\alpha_Q]$ where α_Q is the coefficient of linear expansion of Pyrex glass. This is undoubtedly a gross simplification for some of the cells used but is in agreement with previous workers.[9] The resistance measurements were made with a Leeds and Northrup Jones conductivity bridge at two frequencies, 1000 and 2000 c.p.s., and the resistances extrapolated to infinite frequency as recommended by Jones and Christian.[10] The correction rarely exceeded 0.03% of the resistance.

TABLE I

EQUIVALENT CONDUCTANCES OF KCl, NaCl AT 50° AND OF KI AT 25°

(Λ given as Int. ohm^{-1} cm.^{2} mole^{-1})

KI 25°		KCl 50°		NaCl 50°	
C, mole l.$^{-1}$	Λ	C, mole l.$^{-1}$	Λ	C, mole l.$^{-1}$	Λ
0.010492	142.03	0.012171	213.93	0.009626	184.89
.012307	141.45	.024636	208.63	.019176	180.35
.015422	140.55	.045221	203.18	.030925	176.61
.019939	139.49	.062498	199.80	.048570	172.61
.024356	138.56	.078744	197.35	.068474	169.29
.056218	134.32	.098784	194.73	.11379	163.75
.068089	133.23	.14151	190.62	.14556	160.84
.084311	132.05	.20104	186.29	.18299	157.98
.13956	129.08	.29904	181.17	.27966	152.27
.14665	128.75	.35732	178.86	.37615	147.92
.17548	127.71	.41241	176.83	.50448	143.26
.22634	126.19	.55951	172.53	.65880	138.64
.36896	123.32	.76679	167.79	.80532	134.87
.49333	121.66	.98528	163.86	1.0007	130.44
.65169	120.08	1.4074	157.65	1.2063	126.29
.72161	119.51	1.8187	152.47	1.4934	121.07
.97751	117.74	2.2922	147.08	1.6744	118 02
1.2310	116.27	2.7382	142.30	2.0900	111.58
1.6595	114.06	2.8882	140.72	2.2154	109.78
2.0837	111.86	3.3107	136.28	2.3643	107.62
2.3417	110.45	3.6385	132.83	2.5153	105.51
2.7879	107.87	4.3948	124.87	2.9739	99.41
2.9347	106.94			3.2748	95.62
3.6492	101.95			3.9907	87.07
4.1946	97.62			4.5035	81.26
4.6550	93.34			5.0776	75.11
5.5041	85.31				
5.6916	83.40				

Results

The experimental concentrations and equivalent conductances are listed in Table I. The concentrations are in moles per liter at the temperature of measurement and the equivalent conductances are in international ohm^{-1} cm.^{2} mole^{-1} units. The 25° results are as actually recorded but the 50° results have been adjusted from the actual experimental temperature to the 50.00° values utilizing separately determined temperature coefficients of conductance. At 50°, (100/Λ) (dΛ/dt) varied from 1.46% at $C = 0$ to 1.14% at $C = 4\ M$ for potassium chloride and from 1.55% at $C = 0$ to 1.48% at $C = 4\ M$ for sodium chloride. The magnitude of the adjustment to the equivalent conductance did not exceed 0.03% for sodium chloride or 0.1% for potassium chloride. By means of large scale graphs of the deviation function $x = \Lambda + A\sqrt{C}$, where A is chosen to give as flat a curve as possible, the results were plotted and the data at round concentrations were interpolated and are presented in Table II. At 25° the limits of possible error are ±0.03%. At 50°, the limits of possible error are ±0.07%.

TABLE II

EQUIVALENT CONDUCTANCES AT ROUND CONCENTRATIONS

C, mole l.$^{-1}$	ΛKI 25°	ΛKCl 50°	ΛNaCl 50°
0.05	134.97	202.14	172.35
.10	131.11	194.59	165.26
.15	128.69	189.93	160.48
.20	126.89	186.35	156.66
.25	125.57	183.51	153.86
.30	124.51	181.13	151.27
.40	122.68	177.28	146.98
.50	121.58	174.14	143.41
.60	120.53	171.50	140.29
.70	119.68	169.18	137.52
.80	118.92	167.14	135.00
.90	118.24	165.31	132.65
1.0	117.61	163.63	130.46
1.2	116.43	160.57	126.42
1.4	115.37	157.76	122.71
1.6	114.35	155.14	119.26
1.8	113.34	152.69	116.00
2.0	112.30	150.35	112.94
2.5	109.55	144.82	105.72
3.0	106.47	139.55	99.08
3.5	103.04	134.31	92.88
4.0	99.17	128.80	86.96
4.5	94.84	....	81.30
5.0	90.12	....	75.92
5.5	85.34	....	....

Comparison with Previous Results.—With the exception of the potassium iodide data, the method of checking these results with previous work was to insert the values for Λ into a theoretical equation giving Λ^0 in terms of Λ and a parameter $\mathring{a}$ and to vary $\mathring{a}$ to give the best constancy for Λ^0 from data at concentrations up to 0.03 M. This is the method used by Robinson and Stokes,[11] but instead of their equation, one was used in which the term for the relaxation effect was that derived by Falkenhagen and Leist,[3] which also corresponds to the first-order term in the expression due to Pitts.[12]

Potassium Iodide at 25°.—The Λ values agree to within ±0.01% with the data of Jervis, *et al.*,[13] and with the data of Longsworth[14] and these data are incorporated in the deviation function graphs.

Potassium Chloride at 50°.—The use of $\mathring{a} = 2.58$ Å. gives Λ^0 = 228.95 from the data up to 0.03 M. Harned and Owen[15] give 228.92 ± 0.04 and the re-

(8) G. Jones and B. C. Bradshaw, *J. Am. Chem. Soc.*, **55**, 1780 (1933).

(9) B. B. Owen and F. H. Sweeton, *ibid.*, **63**, 2811 (1941).

(10) G. Jones and S. M. Christian, *ibid.*, **57**, 272 (1935).

(11) R. A. Robinson and R. H. Stokes, *ibid.*, **76**, 1991 (1954).

(12) E. Pitts, *Proc. Roy. Soc.* (*London*), **A217**, 43 (1953).

(13) R. E. Jervis, D. R. Muir, J. P. Butler and A. R. Gordon, *J. Am. Chem. Soc.*, **75**, 2855 (1953).

(14) L. G. Longsworth, reported in D. A. MacInnes, "Principles of Electrochemistry," Reinhold Publ. Corp., New York, N. Y., 1939, p. 339.

(15) H. S. Harned and B. B. Owen, "The Physical Chemistry of Electrolytic Solutions," 2nd ed., Reinhold Publ. Corp., New York, N. Y., 1950, p. 589.

calculations by Robinson and Stokes[11] of the data due to Benson and Gordon[16] and to Owen and Zeldes[17] lead to 228.83 ± 0.05.

Sodium Chloride at 50°.—The use of δ = 2.55 Å. gives A° = 197.81 from the data up to 0.02 *M*. Harned and Owen[15] give 197.77 ± 0.05.

Acknowledgments.—The author wishes to express his thanks to the Electrolytic Zinc Company for receipt of their Fellowship in Electrochemistry and to Professor R. H. Stokes for much helpful advice and assistance.

(16) G. C. Benson and A. R. Gordon, *J. Chem. Phys.*, **13**, 473 (1945).
(17) B. B. Owen and H. Zeldes, *ibid.*, **18**, 1083 (1950).

PHENANTHRENE–ISOBUTANE: BINARY HYDROCARBON SYSTEM HAVING TWO LIQUID PHASES[1]

BY J. G. ROOF AND N. W. CRAWFORD, JR.

Shell Development Company, Houston, Texas

Received March 13, 1958

During the course of an investigation on the phase behavior of hydrocarbon systems, we have made observations on the phenanthrene–isobutane system. Mixtures of these two hydrocarbons exhibit a behavior unusual to binary hydrocarbon systems in that two liquid phases are found to coexist over a considerable range of pressure and temperature. In 1950 it was stated[2] that the literature seemed to contain no description of a system consisting of only two hydrocarbons that separates into two liquid phases. The present system is the first to come to the authors' attention.

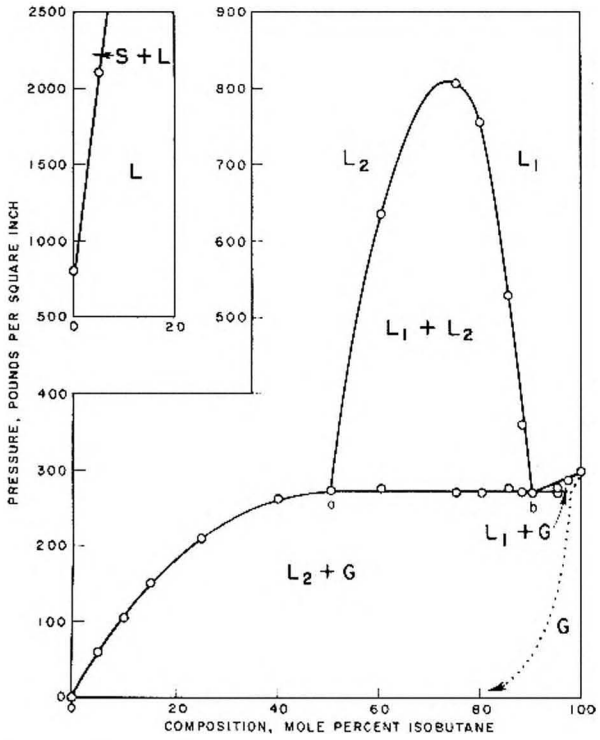

Fig. 1.—Phase behavior in the phenanthrene–isobutane system at 101°.

Multiple fluid phases have been obtained[3] upon addition of methane and propane to a natural crude petroleum. The two liquid phases so obtained were certainly multicomponent and probably did not consist only of hydrocarbons, since it is unlikely that all of the sulfur-, nitrogen- and oxygen-containing compounds in the oil were precipitated into the asphaltic solid phase.

The isobutane used in the present study had a minimum purity of 99% (Phillips Petroleum, research grade). The phenanthrene was Eastman Kodak Co. white label product; its melting point was observed to be 99.5°. The materials were used without further purification.

The major item of equipment used was a pressure cell with internal window[4] that permitted visual observation on the volumetric and phase behavior at pressures up to 500 atmospheres and temperatures as high as 150°. The phenanthrene was placed in an auxiliary vessel, melted and degassed before being transferred through a heated line into the evacuated windowed cell. The quantity of phenanthrene so introduced was determined by observation of the volume occupied by the liquid in the cell. The density of liquid phenanthrene was determined by pycnometer to be 1.066 g./cm.^{3} at 101°. Known amounts of isobutane were then introduced by volumetric metering from a vessel at known temperature and pressure. Density of the isobutane is available from the literature.[5]

Results of the observations on phase behavior in this system at 101° are given in Fig. 1. Experimental points are shown by circles. Phase boundaries so established are shown by solid lines. *S*, *L*, and *G* designate solid, liquid, and gas, respectively. The less dense liquid is designated by L_1, the more dense by L_2. It was not practical to expand samples sufficiently to establish the dew-point locus, which is shown only schematically by the dotted line. No attempt was made to determine compositions of coexistent phases; hence, it is not known whether the solid phase is pure phenanthrene or a solid solution of isobutane in phenanthrene. If solid solutions do exist, an *S* area should be shown to the left of the $S + L$ area.

Within the $L_1 + L_2$ area there are two liquids whose bubble point occurs at the pressure shown by the horizontal line ab. The liquid–liquid miscibility gap is of considerable size at temperatures slightly above the normal melting point of phenanthrene. A single observation at a higher temperature (120°) indicated that the gap decreases rapidly with temperature and probably would disappear below 150°.

Perhaps the lack of complete miscibility between these two hydrocarbons should not be surprising when one considers the differences in shape and

(1) Publication No. 158, Exploration and Production Research Division, Shell Development Company.
(2) A. W. Francis, Chapter 7 in "Physical Chemistry of the Hydrocarbons," edited by A. Farkas, Academic Press, New York, N. Y., 1950.
(3) D. J. Vink, A. M. Ames, R. A. David and D. L. Katz, *Oil and Gas J.*, **39**, No. 28, 34 (1940).
(4) F. W. Wells and J. G. Roof, *Rev. Sci. Instr.*, **26**, 403 (1955).
(5) (a) R. H. Sage and W. N. Lacey, *Ind. Eng. Chem.*, **30**, 673 (1938); (b) "Thermodynamic Properties of the Lighter Hydrocarbons and Nitrogen," American Petroleum Institute, New York, N. Y., 1950.

size of the molecules and in other physical properties. The dissimilarity is pointed up by the large difference in the Hildebrand solubility parameters at 25° as given below.[6]

Hydrocarbon	δ_{298}
Phenanthrene	9.8
Isobutane	6.25
Neopentane	6.25
Butane	6.7
Isopentane	6.75

The solubility parameter is a function of both temperature and pressure, but in this system the dissimilarity is great enough to cause incomplete miscibility at 101° at moderate pressure. From the other values in the table one might expect neopentane to give two liquid phases with phenanthrene at 101°, whereas predictions about butane or isopentane would be subject to more uncertainty.

(6) J. H. Hildebrand and R. L. Scott, "The Solubility of Nonelectrolytes," Third Edition, Reinhold Publ. Corp., New York, N. Y., 1950, p. 436.

THE "THERMAL REGENERATION" OF NICKEL, COPPER AND COBALT AFTER LOW TEMPERATURE OXIDATION

BY R. M. DELL

Houdry Process Corporation, Marcus Hook, Pa.

Received April 9, 1958

It has been known since the early studies of Russell and Bacon[1] that when a reduced nickel or copper powder is saturated with oxygen at 0° and then heated *in vacuo* at a suitably high temperature (200–400°), it is able subsequently to adsorb a further quantity of oxygen at 0°, even though no gas was desorbed during the thermal treatment. This effect, known as "thermal regeneration" has been the subject of investigation by Zettlemoyer and co-workers in a recent series of papers concerned with the low temperature oxidation of cobalt, copper and nickel powders.[2-4] The over-all phenomenon has been discussed by these authors in terms of a mechanism involving three steps: (1) initial formation on the reduced metal at low temperatures of a thin oxide film which, in turn, chemisorbs a monolayer of O-anions causing a potential gradient to be set up across the oxide film; (2) incorporation of the adsorbed oxygen ions into the metal oxide lattice during thermal activation *in vacuo;* under the influence of the potential gradient, cations diffuse outwards from the metal/oxide interface, by way of vacancies in the oxide lattice, and react with the adsorbed anions; (3) subsequent adsorption of further oxygen ions at 0° on the bare oxide surface thus regenerated.

While this reaction scheme may be correct in some instances and is almost certainly the manner in which chemisorbed oxygen is incorporated into a *thick* oxide layer present on a metal, nevertheless, it is possible to envisage at least two alternate mechanisms for the thermal regeneration of a metal surface covered by a *thin* oxide film formed at room temperature or below, *viz.:* (b) disappearance of the surface oxide film into the bulk of the metal, either by the formation of a homogeneous solution of oxygen in the metal or by the incorporation of oxide particles into the metal matrix; (c) recrystallization of the surface oxide film into discrete crystallites of appreciable thickness covering a fraction of the surface; these oxide crystallites may form preferentially on certain crystal planes of the metal. Either of these two mechanisms of regeneration would give rise to exposed metal surface capable of adsorbing more oxygen at 0°. The object of this note is to draw attention to the fact that a substantial body of experimental data exists from which it may be inferred that mechanism (c) probably plays an important role in the regeneration process for each of these three metals.

Nickel.—Before considering the thermal regeneration of nickel, it is pertinent to mention briefly some recent experiments concerned with the interaction of a nickel surface with oxygen at low temperatures. Exposure of a reduced nickel powder to oxygen at room temperature results in the formation of a surface oxide film several layers thick. The heat of oxidation, 95 ± 5 kcal./mole O_2,[1,5] is rather less than the heat of formation of nickel oxide (116 kcal./mole O_2). Experiments with evaporated films[5,6] have shown that provided the heat of chemisorption is adequately dissipated, nickel is capable of chemisorbing only a single monolayer of oxygen atoms at 20°. With nickel powder, however, heat dissipation is generally poor, resulting in high temperatures locally and encouraging further oxidation. The heat of adsorption of oxygen on an evaporated nickel film (~140 kcal./mole) is considerably higher than for a powder; this result may be attributed to the release of internal "strain energy" of the unsintered metal film during chemisorption. Both powders and films exhibit a relatively constant heat of oxygen uptake over a wide range of coverage. It appears that as successive increments of oxygen are admitted, chemisorption (and oxidation where appropriate) occurs on the fraction of the metal surface first encountered by the incoming gas. Succeeding increments of oxygen penetrate further into the powder (or porous film), oxidizing regions of the nickel surface more remote from the gas inlet tube.[6] Similar effects have been demonstrated experimentally for copper.[7] As a result of this non-selective oxygen uptake, any heterogeneity of adsorption potential over the nickel surface is masked in the heat–coverage curve. It may be concluded that the measured heat of oxygen uptake on a thin evaporated film represents the heat of chemisorption on a site of 'average" adsorption potential (together

(1) W. W. Russell and O. C. Bacon, *J. Am. Chem. Soc.*, **54**, 54 (1932).

(2) Y. F. Yu, J. J. Chessick and A. C. Zettlemoyer, *Advances in Catalysis*, **9**, 415, 492 (1957).

(3) A. C. Zettlemoyer, Y. F. Yu, J. J. Chessick and F. H. Healey, THIS JOURNAL, **61**, 1319 (1957).

(4) J. J. Chessick, Y. F. Yu and A. C. Zettlemoyer, "Proceedings of Second World Congress on Surface Activity," London, 1957.

(5) R. M. Dell, D. F. Klemperer and F. S. Stone, THIS JOURNAL, **60**, 1586 (1956).

(6) D. F. Klemperer and F. S. Stone, *Proc. Roy. Soc. (London)*, **A243**, 375 (1958).

(7) W. W. Russell and L. G. Ghering, *J. Am. Chem. Soc.*, **57**, 2544 (1935).

with a contribution from strain energy), while the constant heat observed with a nickel powder is a composite value containing contributions from the average heat of oxygen chemisorption on bare metal, the heat of oxidation of nickel and the heat of adsorption of oxygen on nickel oxide (60–50 kcal./mole).[8]

With these calorimetric data and their interpretation in mind, measurements of the heat of sorption of oxygen on a "regenerated" metal surface assume considerable significance. For nickel, Russell and Bacon[1] have shown that such a surface takes up oxygen with a heat of 93-91 kcal./mole. This agrees well with the heat observed on a freshly reduced and evacuated nickel powder and is markedly greater than the heat of adsorption of oxygen on nickel oxide. Likewise, the heat of oxygen uptake on a regenerated nickel film is as high as 120 kcal./mole.[6] Such high heats of adsorption make it most probable that free nickel metal is present in the surface. Further evidence for this view will now be summarized.

Schlier and Farnsworth[9] report that the electron diffraction pattern arising from an oxide layer present on the (100) face of a single crystal of nickel after exposure to oxygen disappears on heating *in vacuo* at 250–300° for 60 hours. It seems that the surface oxide has either dissolved in the metal lattice or recrystallized to form a new oxide phase covering only a fraction of the metal surface. However, the studies of both Russell[1] and Zettlemoyer[3] on nickel powder have shown that the extent of oxygen chemisorption after regeneration is less than 50% of the initial uptake; it appears therefore that an appreciable fraction of the surface remains covered with oxide, as might be expected for a recrystallization phenomenon. With the single crystals used by Schlier, the fraction of the surface covered with oxide after regeneration may well be much smaller, as the thermal conditions prevailing during oxidation undoubtedly will have resulted in a considerably thinner oxide film than is normally formed on powders.

Field emission microscopy has been used by Gomer[10] to study adsorption of oxygen on polyhedral nickel surfaces. The patterns obtained seem to demonstrate directly that when a surface saturated with oxygen at room temperature is heated to 400°, recrystallization of the adsorbed film occurs and nickel oxide crystallites assume preferred orientations on certain crystal planes.

A beautiful visual demonstration that at high temperatures a very thin oxide layer on nickel consists of finite crystallites of NiO scattered over the metal surface has been provided by Martius.[11] Nickel crystals were exposed to an hydrogen atmosphere containing a trace of water vapor at 1100°; photomicrographic study showed clearly the presence of small NiO crystallites distributed over the surface and separated by relatively large areas of unoxidized or sparingly oxidized metal.

Copper.—For copper, the molar heat of oxygen chemisorption after regeneration (69–62 kcal.)[1] is rather less than the heat of oxidation of a freshly reduced powder (82–76 kcal./mole O_2)[1,12] although still greater than the heat of adsorption of oxygen on cuprous oxide (56 kcal./mole).[13] We conclude that oxygen uptake on a regenerated copper surface is probably a composite process of chemisorption on the oxide and oxidation of exposed metal. In comparison with nickel oxide, it may be recalled that Cu_2O chemisorbs more oxygen per unit surface area and, owing to a higher mobility of cations in the surface region, incorporates chemisorbed oxygen into the lattice more readily.[14] The failure of Zettlemoyer, *et al.*,[3] to observe appreciable chemisorption on copper at −195° after regeneration may be ascribed to the rather mild thermal treatment employed (2 hours at 200°), which apparently did not lead to recrystallization of the oxide layer and exposure of underlying metal. Oxygen chemisorption on cuprous oxide has a marked activation energy (7 kcal./mole)[13] and would not be expected to proceed readily at −195°.

Both Gwathmey[15,16] and Rhodin[17] have shown that during the initial stages of oxidation of a single crystal of copper, the thickness and orientation of the surface oxide film depend upon the crystal face under study. Oxidation proceeds most readily on the (100) face. The stability of the oxide layer formed on a particular crystal face will be determined by the reduction in surface free energy which might be achieved by migration and recrystallization; this, in turn, will depend upon the degree of correspondence of the lattice parameters of the metal face and the oriented oxide layer as well as the interfacial surface tensions. Obviously these properties will be quite variable from one crystal plane to another and it is not at all unreasonable that an oxide film formed at low temperatures should recrystallize under thermal treatment. Similar considerations presumably apply to the other metals, although comparable experimental studies with single crystals are lacking.

Cobalt.—Yu, Chessick and Zettlemoyer[2] have measured oxygen uptake on reduced cobalt powder at various temperatures (26 to 78°) and also after successive regenerations for 2 hours at 375°. An attempt was made to fit the data to the equation of Cabrera and Mott[18] for low temperature oxidation of metals. When, after n oxidations, the calculated *total* oxide film thickness was substituted in this equation, the value deduced for the electrical potential across the oxide film was nonsensical; however, reasonable values were obtained using the *incremental* film thickness developed in each single oxidation. Rather than assume the Cabrera and Mott theory to be inapplicable to the oxidation of cobalt, it seems more plausible that

(8) R. M. Dell and F. S. Stone, *Trans. Faraday Soc.*, **50**, 501 (1954).
(9) R. E. Schlier and H. E. Farnsworth, *Advances in Catalysis*, **9**, 434 (1957).
(10) R. Gomer, *J. Chem. Phys.*, **21**, 293 (1953).
(11) U. Martius, *Canad. J. Phys.*, **33**, 466 (1955).
(12) R. M. Dell, F. S. Stone and P. F. Tiley, *Trans. Faraday Soc.*, **49**, 195 (1953).
(13) W. E. Garner, F. S. Stone and P. F. Tiley, *Proc. Roy. Soc. (London)*, **A211**, 472 (1952).
(14) R. Rudham and F. S. Stone, "Chemisorption," Ed. W. E. Garner, Butterworths, 1957, p. 205.
(15) F. W. Young, J. V. Cathcart and A. T. Gwathmey, *Acta Metal.*, **4**, 145 (1956).
(16) K. R. Lawless and A. T. Gwathmey, *ibid.*, **4**, 153 (1956).
(17) T. N. Rhodin, *J. Am. Chem. Soc.*, **73**, 3143 (1951).
(18) N. Cabrera and N. F. Mott, *Repts. Prog. Phys.*, **12**, 163 (1949).

this result is indicative of the presence of exposed cobalt surface after each regeneration; this new surface is then oxidized *ab initio*. Moreover, it seems clear just from the quantity of oxygen taken up (which for adsorption at 26° after one regeneration would correspond to at least five monolayers of oxygen on cobalt oxide[19]) that recrystallization of the oxide phase must occur at 375° *in vacuo*.

This inference is substantiated by recently published calorimetric data for cobalt.[2] Like copper, the initial heat of adsorption of oxygen on a regenerated powder surface (95 kcal./mole) is less than the heat of oxidation of the reduced metal (120 kcal./mole) but significantly greater than the heat of chemisorption of oxygen on CoO (60–55 kcal./mole).[14] Again a composite process is envisaged, in keeping with the known similarity of CoO and Cu_2O toward adsorption and incorporation of oxygen.[14] The shape of the heat–coverage curve indicates that the extent of exposed cobalt surface after regeneration at 375° is strictly limited. Raising the regeneration temperature from 375 to 425° led to a doubling of the subsequent oxygen uptake, presumably due to more extensive recrystallization.[4]

The conclusion to be drawn from these various experiments is that recrystallization of the thin oxide film formed on these metals at low temperatures plays a significant role in their thermal regeneration, being perhaps more important for nickel than for copper or cobalt. The nature and extent of this recrystallization will undoubtedly depend upon the metal and severity of the thermal treatment, ranging possibly from mere cracking of the coherent oxide film under the influence of internal stresses to bulk migration and crystal growth upon a more favorable metal plane.

In general, the ability of a supported oxide film to reduce its surface free energy by recrystallization may be regarded as the driving force in the regeneration process. Such recrystallization will be confined to thin oriented oxide films (~10–20 Å.) formed at low temperatures; thicker oxide films prepared at elevated temperatures are stable and "regenerate" only by incorporation of adsorbed oxygen through the cation vacancy diffusion mechanism.

(19) Calculated using the value of Rudham and Stone[14] for the monolayer coverage of oxygen on CoO (0.197 cc./m.²) and the density of CoO (6.47).

POTENTIALS OF NOBLE METAL AND PALLADIUM ALLOY HYDROGEN ELECTRODES

BY JAMES P. HOARE, GILBERT W. CASTELLAN AND SIGMUND SCHULDINER

U. S. Naval Research Laboratory, Washington 25, D. C.

Received April 11, 1958

A series of gold-palladium alloys of Au/Pd atomic ratios 0.12, 0.24, 0.43, 0.88 and 2.70 together with pure palladium and a silver–palladium alloy of composition Ag/Pd = 0.64 were cleaned in nitric acid, heated white-hot and then placed in highly purified, pre-electrolyzed 2 *N* sulfuric acid solution stirred with hydrogen. An anodic followed by a cathodic polarizing current (40 ma. for 1000 sec. each) was applied to each electrode. The circuit then was opened and the potential on each of these alloys slowly came to a steady value. The same steady potentials were obtained after anodic polarization only. The steady, open-circuit potential of each of these metals is shown in Fig. 1. The temperature was 30 ± 1°.

These results aroused interest in the equilibrium potentials of noble metal/H_2 systems. The equilibrium potentials of platinum, gold, rhodium, iridium and ruthenium/H_2 electrodes *vs.* a Pt/H_2 electrode in 2*N* sulfuric acid solution (*p*H 0) and under a hydrogen pressure of one atmosphere were determined. In all cases, the measured potential differences were equal to zero.

Previously reported work[1] has indicated that a palladium electrode in acid solution stirred with hydrogen would form the saturated α-Pd–H alloy and that the reversible open-circuit potential of this alloy *vs.* a Pt/H_2 electrode was 0.05 volt. It was further shown that the potential-determining reaction on the α-Pd was not the same as on the Pt/H_2 electrode. It was demonstrated that this reaction was

$$H^+ + e^- \overset{Pd}{\rightleftharpoons} (Pd\text{–}H)\alpha \qquad (1)$$

It was also shown that on the β-Pd–H alloy the potential-determining reaction was the same as on the Pt/H_2 electrode, namely

$$H^+ + e^- \rightleftharpoons 1/2\ H_2 \qquad (2)$$

The authors[1] showed that when the α- and β-phases of the Pd–H system coexisted a mixed potential arises because different potential-determining reactions occur on each phase. The over-all potential will be determined by the relative areas of each phase and will be between zero and 0.05 volt. In the case of the Au- and Ag–Pd alloys shown in Fig. 1 (Me/Pd < 1), the potential (solid line) may either be determined by a complex mixed potential system which results from the ternary

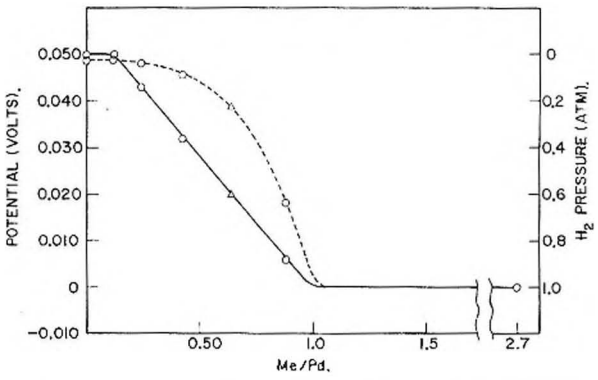

Fig. 1.—Open circuit potentials of Au- and Ag–Pd alloys in hydrogen-saturated 2 *N* sulfuric acid solution (solid line). Broken line, calculated equilibrium hydrogen pressures of the Me–Pd–H alloys in the two (α and β) phase region. Circles are Au–Pd alloys. Triangles are for Ag–Pd alloy.

alloys, Au–Pd–H or Ag–Pd–H, or they may be the potentials owing to the formation of a single phase in the Me–Pd–H alloys which is analogous to α-Pd–H and for which the potential determining

(1) S. Schuldiner, G. W. Castellan and J. P. Hoare, *J. Chem. Phys.*, **28**, 16 (1958).

reaction involves an equilibrium between hydrogen ions in solution and hydrogen atoms dissolved in the metal (reaction 1).

The experimental results of Mundt[2] showed that Au–Pd alloys to a composition of about 45 weight % Au (atomic ratio Au/Pd $\sim$ 0.45) did form a two-phase system with hydrogen which was similar to the α- and β-phases for the Pd-H system. Similarly, Krüger and Gehm[3] showed that for the Ag–Pd–H system two phases existed for Ag–Pd alloys up to about an Ag/Pd atomic ratio of 0.79. Bénard and Talbot,[4] on the other hand, from an investigation of Au–Pd–H alloys came to the conclusion that at room temperature this was a single phase system only.

The experimental results shown in Fig. 1 agree with the contention of Mundt[2] and Krüger and Gehm[3] that a two phase Au–Pd–H and Ag–Pd–H system analogous to the α- and β-Pd–H system can exist at room temperature. These results indicate that the two-phase system in alloys with Au/Pd $\sim$ 1 may exist. Berry[5] has shown that hydrogen is soluble in Au–Pd alloys up to a weight per cent. of about 75% Au (atomic ratio Au/Pd $\sim$ 1.6). Hence the two-phase system could exist over a large part of the hydrogen solubility range.

If the two-phase system does exist for these alloys, and if the potentials of other than zero value, shown in Fig. 1, are reversible potentials of potential-determining reaction 1 then the ternary alloys (Me/Pd < 1) exhibiting these potentials would either be in the saturated α-phase or have α- and β-phases coexisting with the α-phase determining the potential. In this event, the equilibrium pressures over the two-phase alloy can be calculated for the various Me/Pd ratios from the Nernst equation

$$E = -(RT/F) \ln p_{H_2}^{1/2}$$

The pressure *vs.* Me/Pd curve so calculated is shown as a broken line in Fig. 1.

For the Au/Pd = 2.7 alloy, the solubility of hydrogen in the metal would be negligible and this alloy would behave as a normal hydrogen electrode.

Of the pure noble metals investigated, α-Pd is unique in establishing a different potential-determining hydrogen reaction. This potential-determining reaction also may occur on the analogous Au- and Ag–Pd alloys.

(2) H. Mundt, *Ann. Physik*, [5] **19**, 721 (1934).
(3) F. Krüger and G. Gehm, *ibid.*, [5] **16**, 190 (1933).
(4) J. Bénard and J. Talbot, *Compt. rend.*, **222**, 493 (1946).
(5) A. J. Berry, *J. Chem. Soc.*, **99**, 463 (1911).

SURFACE TENSIONS OF THE $AgNO_3$–$NaNO_3$ AND $AgNO_3$–KNO_3 SYSTEMS

BY JUNE LOMNES DAHL AND FREDERICK R. DUKE

Institute for Atomic Research and Department of Chemistry, Iowa State College, Ames, Iowa. Work was performed in the Ames Laboratory of the U. S. Atomic Energy Commission

Received April 19, 1958

The surface tensions of the binary fused salt systems $AgNO_3$–$NaNO_3$ and $AgNO_3$–KNO_3 have been measured by the maximum bubble pressure method. These systems were investigated to supplement transference measurements carried out in this Laboratory.[1] Details of the experimental procedure and calculations involved are presented in a publication on the surface tensions of binary systems containing $PbCl_2$ and the alkali metal chlorides.[2]

TABLE I

SURFACE TENSION IN THE SYSTEM $AgNO_3$–$NaNO_3$[a]

Mole % $NaNO_3$	Temp., °C.	Surface tension (dynes/cm.)	Mole % $NaNO_3$	Temp., °C.	Surface tension (dynes/cm.)
0.00	222	147.9	57.13	302	126.0
	223	149.2		305	125.6
	226	148.8		326	124.7
	232	149.1		326	124.4
	232	148.0		328	124.3
	242	147.3			
	245	146.6	80.00	316	122.2
	248	147.5			
	253	147.2		317	121.8
	268	146.3		319	121.4
	269	146.7		319	121.7
	274	145.7		344	120.4
	278	146.5		344	120.4
	294	144.3		368	118.5
	299	143.9		368	118.4
	318	143.1			
	322	142.3	86.33	322	120.7
	344	140.7		322	120.3
	349	142.5		352	118.3
	352	140.2		352	118.9
				376	117.2
9.52	302	137.0		376	117.3
	324	137.0		390	115.8
	309	137.3		398	115.6
	327	136.1			
	327	135.9	100.00	316	119.6
	328	136.3		317	119.6
	352	134.6		319	119.0
	354	134.5		320	119.3
				338	117.3
18.16	248	140.5		344	117.7
	250	138.9		345	117.6
	254	138.9		349	117.2
	296	135.0		369	115.7
	300	135.9		372	116.3
	300	135.9		376	115.7
	303	135.9		399	114.5
	303	135.9		399	114.7
	325	134.1		400	114.9
	328	134.3		420	113.0
	329	134.1		424	113.0
	356	132.3		463	109.7
				474	109.7
40.00	269	131.7		528	106.4
	271	132.8		530	106.3
	272	133.4		593	102.5
	302	129.4		596	102.2
	302	129.6			
	328	128.6			
	329	128.5			

[a] The density data used in calculating these surface tensions were those given by Byrne, Fleming and Wetmore.[3]

(1) F. R. Duke and R. Owens, *J. Electrochem. Soc.*, **105**, 476 (1958).
(2) J. L. Dahl and F. R. Duke, THIS JOURNAL, in press.

The results of the surface tension measurements on the two binary nitrate melts are given in Tables I and II. Surface tension isotherms were plotted and compared with isotherms calculated from Guggenheim's equation for the dependence of the surface tension of an ideal binary mixture on its composition.[3] The surface tension isotherms for these systems show small, negative deviations from ideality. These deviations are greater for $AgNO_3$–KNO_3 than for $AgNO_3$–$NaNO_3$, in agreement with previous findings that the surface tensions of binary mixtures of salts with a common anion show increasing deviations from ideality with increasing difference in the size of the replacing cations.[4,5]

TABLE II

SURFACE TENSION IN THE SYSTEM $AgNO_3$–KNO_3[a]

Mole % KNO_3	Temp., °C.	Surface tension (dynes/cm.)	Mole % KNO_3	Temp., °C.	Surface tension (dynes/cm.)
8.12	252	139.7	87.05	324	115.1
	252	138.9		324	115.8
	256	138.5		325	114.8
	304	135.3		326	114.6
	306	135.5		351	112.6
	324	134.8		352	113.5
	325	133.8		352	112.3
	326	134.3		353	112.3
	356	132.8			
			100.00	358	111.9
29.58	254	132.0		358	111.8
	254	132.3		398	109.6
	300	125.4		398	108.7
	302	125.0		419	106.9
	328	124.0		420	107.0
				454	104.2
52.83	254	123.9		454	104.3
	256	123.9		473	102.9
	276	122.7		473	102.9
	276	122.5		494	101.5
	296	120.7		496	101.3
	298	120.7		546	97.0
	324	118.7		546	97.6
	324	118.7		594	93.8
	354	116.9		595	93.8
71.60	276	119.3			
	276	119.4			
	298	117.4			
	302	117.4			
	302	117.8			
	322	115.9			
	323	115.6			
	325	116.3			
	355	114.0			

[a] Density data given by Bloom and Rhodes.[6]

The surface tension data, the additivity of molar volumes,[6,7] the small, negative deviations from additivity of conductivity[7,8] and molar refractivity[6] and the proportionality of transference numbers to mole fraction[1] all substantiate the idea that little or no ionic association takes place in these melts.

It is interesting to compare the surface tensions of the three pure nitrate melts at corresponding temperatures above their melting points. The surface tensions of the pure alkali metal nitrates and chlorides decrease regularly with increase in size of the alkali metal ion.[9] Silver nitrate does not fit into this pattern since its surface tension is higher than that of $NaNO_3$ despite the fact that the ionic sizes are comparable. This is indicative of stronger ionic interactions in a $AgNO_3$ melt compared to a $NaNO_3$ melt. This can be attributed to (a) smaller interionic separation in a $AgNO_3$ melt compared to a $NaNO_3$ melt despite the fact that the radii of the ions are approximately the same in the solid state, and (b) increased covalent character in the interactions in a $AgNO_3$ melt compared to a $NaNO_3$ melt attributed in part to the 18-electron shell of a transition type ion like Ag^+ being more easily deformed (polarized) than is the inert gas-type shell.

The maximum probable error in γ is $\pm$ 0.2 dyne/cm., except at high mole % $AgNO_3$ where peculiar bubble formation always became a problem, probably as a result of a high viscosity; the error here may be as much as $\pm$ 1 dyne/cm.

(3) E. A. Guggenheim, *Trans. Faraday Soc.*, **41**, 150 (1945).

(4) N. K. Boardman, A. R. Palmer and E. Heymann, *Trans. Faraday Soc.*, **51**, 277 (1955).

(5) V. K. Semenchenko and L. P. Shikhobalova, *Zhur. Fiz. Khim.*, **21**, 612 (1947).

(6) H. Bloom and D. C. Rhodes, THIS JOURNAL, **60**, 791 (1956).

(7) J. Byrne, H. Fleming and F. E. W. Wetmore, *Can. J. Chem.*, **30**, 922 (1952).

(8) F. R. Duke and R. Fleming, *J. Electrochem. Soc.*, in press.

(9) F. M. Jaeger, *Z. anorg. Chem.*, **101**, 1 (1917).

VAPOR PRESSURE OF THORIUM TETRAFLUORIDE[1]

BY A. J. DARNELL AND F. J. KENESHEA, JR.

Contribution from the Research Department of Atomics International Canoga Park, Cal.

Received April 26, 1958

No experimental determination of the vapor pressure of thorium tetrafluoride is reported in the literature although an estimate has been made by Brewer.[2]

In the present work, the Knudsen[3] effusion method was used to determine the vapor pressure of the solid and the quasi-static method of Rodebush and Dixon[4] was used to determine the vapor pressure of the liquid. These two methods were used to extend the measurements over as wide a range as practicable in the solid and liquid states in order to obtain values for the heats of sublimation and vaporization of ThF_4.

A mass spectrographic analysis was made to determine the gaseous species vaporizing from ThF_4.

Experimental

The ThF_4 used in these experiments was obtained from the A. D. Mackay Company. An X-ray diffraction pattern of the sample showed only ThF_4 lines. Chemical analysis of the salt gave a value of 75.3 $\pm$ 0.2 weight % thorium,

(1) This investigation was supported by the U. S. Atomic Energy Commission, under Contract AT(11-1)-GEN-8.

(2) L. Brewer, "The Fusion and Vaporization Data of the Halides," Paper 7 in "Chemistry and Metallurgy of Miscellaneous Materials: Thermodynamics," Ed. by L. Quill, McGraw-Hill Book Co., New York, N. Y., 1950.

(3) M. Knudsen, *Ann. Physik*, **29**, 179 (1909).

(4) W. H. Rodebush and A. L. Dixon, *Phys. Rev.*, **26**, 851 (1925).

(theoretical 75.33). Weight loss experiments also showed less than 0.2% volatile impurities. The melting point was determined by thermal analysis to be 1110 ± 2° which is to be compared with a literature value[5] of 1111°.

Temperature measurements were made with Pt–Pt, 10% Rh thermocouples calibrated at the melting point of recrystallized sodium chloride. The temperature of the ThF_4 was held constant during vapor pressure determinations by means of a Leeds and Northrup potentiometric type controller-recorder.

Nickel cells were used to contain the ThF_4 in the effusion and quasistatic experiments. A corrosion test with molten ThF_4 showed less than 0.005% Ni contamination from the crucible.

Effusion Method.—The effusion cell was fitted with a screw cap and interchangeable thin lids with various orifice diameters. The inside dimensions of the cell were ½ inch by 1 inch. The cell was heated by a Marshall tube furnace adjusted to obtain a uniform temperature (±2°) region extending 1 inch beyond the ends of the cell. The error in the effusion time was kept below 1% by maintaining the heat-up and cool-off intervals of the cell short in comparison to the total time of the run.

The quantity of material effused was determined from the weight loss of the cell during an experiment. In one run, the effusate was collected on a cylindrical tantalum collector; within experimental accuracy, the amount collected was equal to the weight loss of the cell. The effusate was analyzed by X-ray diffraction and chemical analysis and was found to be ThF_4.

Quasi-static Method.—The quasi-static method in essence yields the pressure at which the salt boils for a given temperature. This method is described by Rodebush and Dixon[4] and was used by Fiock and Rodebush[6] to measure the vapor pressure of some of the alkali halides. The nickel cell used here is similar to the quartz cell used by Fiock and Rodebush.[6] The nickel tubes were welded into the top of the cell to hold the reflux capillaries. The upper end of one of these tubes was connected to a vacuum system through a stopcock. The upper end of the other tube was connected to an absolute manometer filled with H_2SO_4. A differential manometer containing Amoil-5 was connected between the two tubes. Two thermocouple wells were placed in the cell: one immersed in the liquid salt and the other in the vapor immediately above the liquid. The temperature of the liquid and vapor always agreed within 3° and values obtained for the liquid were used in the calculations.

The nickel cell was enclosed in an evacuated porcelain tube to prevent collapse of the cell. This was necessary because at the temperatures used, nickel does not have sufficient mechanical strength to withstand an external pressure of one atmosphere. The cell and protection tube were mounted vertically in a Hoskins Model FHS-304 tube furnace.

Vapor pressure measurements were made by starting with an inert gas pressure greater than the vapor pressure of the salt, then reducing the pressure in the system by small increments until the first "permanent difference" was obtained in the differential manometer. At this condition, the vapor pressure of the salt was equal to the pressure of the inert gas at the absolute manometer.

Mass Spectrometric Investigation of Vapor.—The vapor effusing from an inductively heated Knudsen cell containing ThF_4 was examined with a Bendix time-of-flight mass spectrometer using 75-volt electrons. The nickel cell containing the salt was mounted in a manifold so that the vapor would pass into the ionizing region of the mass spectrometer. This system was connected to a conventional vacuum pump which provided a background pressure of less than 5×10^{-5} mm. The temperature of the salt was determined by "sighting" into the cell orifice with an optical pyrometer. Inspection of the positive ion fragments formed from ThF_4 vapor was made over the temperature range 900 to 1200°.

Results and Discussion

The experimental data obtained from the effusion experiments are presented in Table I. The pressure was calculated from the Knudsen effusion equation

$$P_{(atm)} = \frac{0.02255g}{Kat}\sqrt{\frac{T}{M}} \qquad (1)$$

where

g = grams of material effused
K = Clausing[7] factor
a = area of orifice in cm.²
t = time interval in sec.
T = temperature, °K.
M = molecular weight of vapor

Three orifices were used with area ratios of approximately 1 to 4 to 8. The pressures obtained were independent of hole size within the experimental accuracy of the determination, indicating that the vapor was at equilibrium with the solid. Effusion experiments were performed up to pressures of 0.1 mm.; above this pressure, the viscous flow contribution complicates the treatment of the effusion data.

TABLE I

VAPOR PRESSURE OF SOLID THORIUM TETRAFLUORIDE BY KNUDSEN EFFUSION METHOD

Temp., °K.	Wt. loss, g.	Time, sec.	Orifice[a]	Pressure, atm.
1055	0.0150	3.32×10^5	c	1.21×10^{-7}
1066	.0259	3.38×10^5	c	2.06×10^{-7}
1077	.0295	2.42×10^4	c	3.31×10^{-7}
1113	.0066	2.35×10^5	a	8.55×10^{-7}
1113	.0724	2.38×10^5	c	8.36×10^{-7}
1166	.0212	1.52×10^5	a	4.33×10^{-6}
1184	.0256	1.20×10^4	c	6.08×10^{-6}
1186	.1651	6.35×10^4	c	7.41×10^{-6}
1212	.0386	1.30×10^5	a	1.39×10^{-5}
1214	.0354	6.02×10^4	a	1.87×10^{-5}
1218	.0480	6.22×10^4	a	2.47×10^{-5}
1225	.0515	1.35×10^4	b	2.38×10^{-5}
1277	.0393	1.70×10^4	a	7.54×10^{-5}
1297	.0552	1.47×10^4	a	1.23×10^{-4}

[a] Orifice areas (cm.²) and Clausing correction factors (K) were, respectively, a, 0.00196, 0.65; b, 0.00815, 0.82; c, 0.0164, 0.86.

The data from the quasi-static experiments are given in Table II. This method has been used by Fiock and Rodebush[6] in the pressure range 6 to 55 mm. To check the applicability of the method below 6 mm., measurements were made on sodium chloride; the results down to 1.5 mm. agreed with those in the literature.[6,8] Below this pressure, the quasi-static method gave low and erratic results. This probably was due to effusion of the inert gas through the vapor tubes at these low pressures making it difficult to detect the "permanent difference" in pressure between the two legs of the cell. The upper limit of the quasi-static pressure measurements was set by the loss of mechanical strength of the nickel cell at high temperatures.

The results from the two methods are plotted in Fig. 1. Equations for the vapor pressure of the solid and of the liquid were obtained by least

(5) W. J. Asker, E. R. Segnit and A. W. Wylie, *J. Chem. Soc.*, 4470 (1952).

(6) E. F. Fiock and W. H. Rodebush, *J. Am. Chem. Soc.*, **48**, 2523 (1926).

(7) (a) R. Clausing, *Ann. Physik*, **12**, 961 (1932); (b) S. Dushman, "Scientific Foundations of Vacuum Technique," John Wiley and Sons Inc., New York, N. Y., 1949, p. 96.

(8) K. K. Kelley, U. S. Bureau of Mines Bulletin 383, Washington, D. C., 1935.

TABLE II

VAPOR PRESSURE OF LIQUID THORIUM TETRAFLUORIDE BY THE QUASI-STATIC METHOD

Temp., °K.	Pressure, atm.	Temp., °K.	Pressure, atm.
1437	2.03×10^{-3}	1501	6.07×10^{-3}
1459	3.15×10^{-3}	1529	9.34×10^{-3}
1466	3.07×10^{-3}	1532	8.77×10^{-3}
1466	2.64×10^{-3}	1535	9.71×10^{-3}
1469	3.91×10^{-3}	1555	1.33×10^{-2}
1470	3.96×10^{-3}	1575	1.72×10^{-2}
1477	4.09×10^{-3}	1575	1.71×10^{-2}
1484	5.03×10^{-3}	1595	2.44×10^{-2}
1499	5.88×10^{-3}		

squares treatments of the log P *vs.* $1/T$ data. The equations are

sublimation

$$\log P_{(atm)} = -\frac{(16{,}860 \pm 190)}{T} + (9.105 \pm 0.160), (1055\text{–}1297°K.) \quad (2)$$

vaporization

$$\log P_{(atm)} = -\frac{(15{,}270 \pm 310)}{T} + (7.940 \pm 0.206), (1427\text{–}1595°K.) \quad (3)$$

Vapor pressure measurements were not carried out at the melting point because neither method is applicable in this pressure range. Comparison of the results was made by extrapolating equations 2 and 3 to the melting point (1383°K.); vapor pressures of 8.2×10^{-4} and 7.9×10^{-4} atmosphere, respectively, were obtained.

The heats of sublimation and vaporization at the mid-temperatures in each set of experimental data are

$$\Delta H_{1176}(\text{subl}) = 77.1 \pm 0.9 \text{ kcal./mole} \quad (4)$$
$$\Delta H_{1515}(\text{vap}) = 69.9 \pm 1.5 \text{ kcal./mole} \quad (5)$$

The ΔC_p of vaporization (−19 cal./deg./mole) estimated for the other tetrahalides of thorium by L. Brewer, and reported in N.B.S. Circular 500,[9] was used in the free energy of vaporization equation

$$\Delta F°_T = \Delta H_0 - \Delta C_p T \ln T + IT \quad (6)$$

The constants ΔH_0 and I are evaluated from (3) as 98,660 and −194.50, respectively. Equation 6 gives a normal boiling point of 1953°K. for ThF_4. Application of this ΔC_p correction to (5) yields $\Delta H_{1953}(\text{vap}) = 61.6$ kcal./mole, $\Delta S_{1953}(\text{vap}) = 31.5$ cal./deg./mole.

Some conclusions may be drawn regarding the vapor species of ThF_4 by comparing the vapor pressure data from the two methods. The quasi-static method gives the total pressure above the salt. The results from the effusion method were calculated by assuming the salt vaporized as the monomer. The agreement of the two sets of data on extrapolation to the melting point represents good evidence that ThF_4 vaporizes as the monomer. This conclusion is substantiated by mass spectrographic studies made on ThF_4 effusing from a Knudsen cell. The predominant peak was due to mass 289; smaller peaks representing masses of 270, 251 and 232 also were observed. These masses are attributed to ionization of $ThF_{4(g)}$ to ThF_3^+, ThF_2^+, ThF^+ and Th^+. Corresponding peaks for the dimer of ThF_4 were not observed over the temperature range of these measurements.

(9) F. D. Rossini, D. D. Wagman, W. H. Evans, S. Levine and I. Jaffe, Selected Values of Chemical Thermodynamic Properties, National Bureau of Standards, Circular 500 (1952).

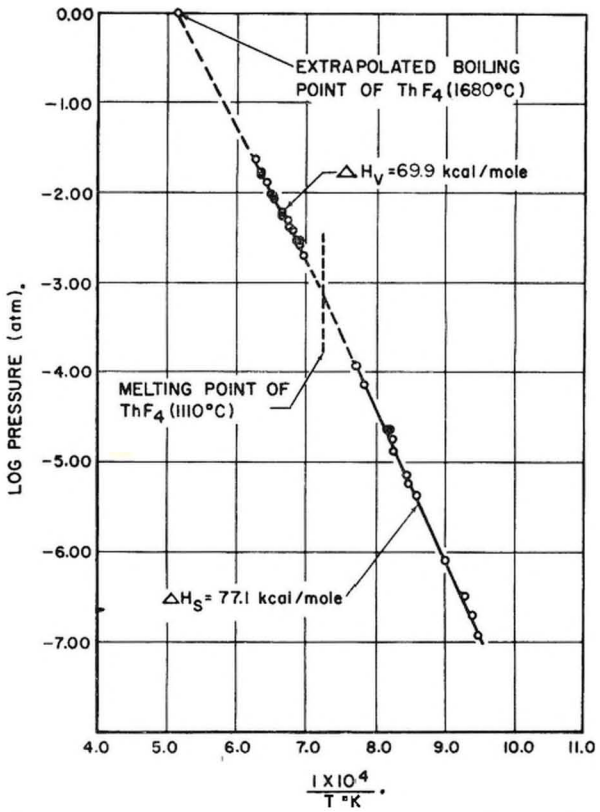

Fig. 1.—Plot of log P *vs.* $1/T$ for thorium tetrafluoride.

Acknowledgments.—The authors wish to thank Dr. T. A. Milne and Dr. S. J. Yosim for the helpful discussions concerning these results, Mr. W. A. McCollum for assistance in performing the experiments and Mr. L. Silverman for carrying out the chemical analyses.

THE ABSORPTION SPECTRUM OF THE TITANIUM(IV)–HYDROGEN PEROXIDE COMPLEX

BY DAVID LEWIS

Department of Chemistry, The City College, New York 31, N. Y.

Received March 26, 1958

The colored complex formed by the reaction of Ti(IV) and hydrogen peroxide in strong acid solution, usually M sulfuric acid, is characterized by an absorption band with a maximum at 405–10 mμ and a molar absorptivity of *ca.* 730. Most measurements of this spectrum have been made on solutions $10^{-3}M$ or less in Ti(IV), since this is the analytically useful range of the colored complex. Reeves and Jonassen[1] have examined the spectral behavior of more concentrated solutions; they report that above a concentration of $1.2 \times 10^{-3}M$ Ti(IV) the maximum shifts progressively toward

(1) R. E. Reeves and H. B. Jonassen, *J. Am. Chem. Soc.*, **76**, 5354 (1954).

lower wave lengths and lower molar absorptivities with increasing concentration of the complex.

Results obtained in this Laboratory on solutions in the same concentration range studied by Reeves and Jonassen show no change in the maximum wave length and only a slight decrease –3.5%—in molar absorptivity compared to the value for more dilute solutions. The curves in Fig. 1 show the

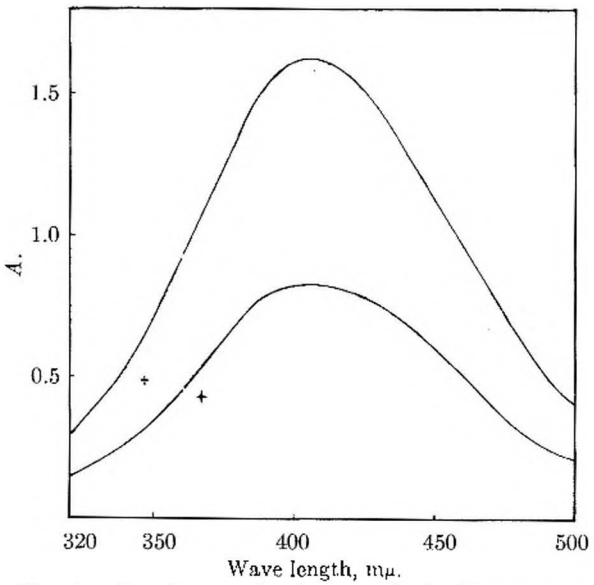

Fig. 1.—Absorbance of solutions of the Ti(IV)–H_2O_2 complex in M H_2SO_4 and 0.20 M H_2O_2: upper curve, 2.28×10^{-2} M Ti: lower curve 1.14×10^{-2} M Ti. Crosses (+) indicate location of maxima reported by Reeves and Jonassen.

spectra for two solutions, the upper curve corresponding to the highest concentration reported by Reeves and Jonassen. The data are plotted on an absorbance scale; on the molar absorptivity scale used by Reeves and Jonassen the two curves would be identical within experimental error. The crosses indicate the location of the maxima estimated from their data. This region was examined at 2 mμ intervals but no evidence of any discontinuity in the curve was found. The spectra were obtained with a Beckman DU Spectrophotometer using 1.00 cm. cells and inserts to give a 1.00 mm. path length. Replicate measurements gave for the maximum a = 705 ± 1, 707 ± 5, λ 405 10 mμ, 405–10mμ for the $2.28 \times 10^{-2}M$ Ti(IV) and for the 1.14×10^{-2} M Ti(IV) solutions, respectively.

The only significant difference in the experimental procedure of Reeves and Jonassen and that reported here lies in the method of preparing the Ti(IV) solutions. The former hydrolyzed tetraisopropyl titanate with cold 5 N sulfuric acid and used the resulting hydrolysis mixture for their measurements; in this work titanium metal sponge (du Pont, assay 99.63%) was dissolved by boiling with concentrated sulfuric acid and the addition, at intervals, of 30% hydrogen peroxide to oxidize the accumulated Ti(III) salts to Ti(IV). Since the latter solutions gave identical spectra with hydrogen peroxide in the entire concentration range investigated, it must be concluded that the varying spectra obtained by Reeves and Jonassen reflect the behavior of their mixture of hydrolysis products rather than of Ti(IV) when treated with hydrogen peroxide. The simplest explanation of their results would be to attribute the decrease in molar absorptivity to incomplete complex formation; and, since uncomplexed Ti(IV) does not absorb in the spectral region reported, the shift in the maximum wave length would be due to the increasing contribution of the organic species to the spectrum.

A THERMODYNAMIC INVESTIGATION OF DIBORON TETRACHLORIDE

BY MILTON J. LINEVSKY AND THOMAS WARTIK

Contribution from The Pennsylvania State University, College of Chemistry and Physics, Department of Chemistry, University Park, Penna.

Received May 2, 1958

Diboron tetrachloride is one of the relatively few boron compounds which contain a boron-to-boron single bond. Although reasonable progress has been made toward its chemical characterization[1–3] and although its structure has been determined by X-ray diffraction[4] and by spectroscopic analysis,[5] its thermodynamic properties have not previously been investigated. The principal deterrent to its thermodynamic investigation is its low stability. Although decomposition in the vapor phase is apparently not too rapid, liquid B_2Cl_4 begins to decompose almost immediately at room temperature.

The authors have measured heat capacities of B_2Cl_4 in the region from 13.42 to 214.51°K., in which range no abnormalities were observed. The heat of fusion was found to be 2579 ± 4 cal. per mole, and, using a correction for liquid-soluble, solid-insoluble impurities, the temperature of fusion of pure B_2Cl_4 was estimated to be 180.21°K.

Preparation and Purification of B_2Cl_4.—B_2Cl_4 was prepared by the method of Wartik, Moore and Schlesinger,[1] and was purified by fractional distillation in a low temperature column similar to that described by Simons.[6] With the pressure in the column at about 10 mm., distillation occurred at −20°. The vapor pressure of the compound at 0° agreed with the reported value of 44 mm. By this method, 19.7 g. of purified B_2Cl_4 was obtained and kept in an ampoule at −78.5° until ready for use.

To eliminate the effects of the inevitable decomposition which occurred during the weighing of the sample, the latter was weighed after, instead of before, the heat capacities were measured. Through careful handling and rapid transfers, a purity of 98.50 mole % was realized in the sample studied. This purity, although far below that usually achieved in this Laboratory, is probably close to the maximum which can be expected in view of the fact that the sample had to be introduced into the calorimeter through a relatively long filling tube of very small diameter.

Measurement of the Heat Capacities.—The heat capacities of B_2Cl_4 were measured in isothermal calorimeter "C" (with thermocouples S_4 and S_7) of the Cryogenic Laboratories. The apparatus, method, and temperature scale were as described by Messerly and Aston.[7] One defined calorie was taken as equal to 4.1833 international joules. Before the sample was introduced, the calorimeter was exposed

(1) T. Wartik, R. Moore and H. I. Schlesinger, *J. Am. Chem. Soc.*, **71**, 3265 (1949).

(2) G. Urry, T. Wartik, R. Moore and H. I. Schlesinger, *ibid.*, **76**, 5293 (1954).

(3) A. Stock, G. Brandt and A. Fisher, *Ber.*, **58**, 653 (1925).

(4) A. Atoji, W. Lipscomb and R. Wheatley, *J. Chem. Phys.*, **23**, 1176 (1955).

(5) D. E. Mann and L. Fano, *ibid.*, **26**, 1665 (1957).

(6) J. H. Simons, *Ind. Eng. Chem., Anal. Ed.*, **10**, 29 (1938).

(7) J. G. Aston and G. Messerly, *J. Am. Chem. Soc.*, **58**, 2354 (1937); **62**, 886 (1940).

TABLE I

THE HEAT CAPACITY OF DIBORON TETRACHLORIDE

Mol. wt., 163.468; 0.12069 mole in calorimeter; 0°C. = 273.16°K.

T (°K.)	C_p (cal./deg./mole)	Approximate rise, (°K.)
	Series II	
13.42	1.591	1.04
14.56	1.810	0.87
15.50	2.138	0.73
16.26	2.568	0.63
17.19	3.064	0.88
18.87	3.637	2.26
21.18	4.173	2.22
23.46	5.099	2.15
26.19	6.244	2.03
28.14	7.242	1.77
31.23	8.094	4.15
34.32	8.586	1.88
42.18	10.590	4.25
46.28	11.432	3.62
50.16	12.181	3.80
54.36	12.594	4.51
58.89	13.099	4.51
	Series III	
60.70	13.331	4.24
65.40	13.950	4.75
70.43	14.674	4.26
75.10	15.361	3.88
79.91	16.018	4.27
	Series I	
92.50	17.114	4.08
97.68	17.794	4.27
102.60	18.232	4.47
107.63	18.737	4.21
113.39	19.306	4.35
118.20	19.700	4.14
123.17	20.165	1.29
128.43	20.395	4.38
134.12	20.897	4.75
139.28	21.546	4.52
144.31	22.092	4.22
149.16	22.589	4.14
153.85	24.043	3.92
158.38	24.586	4.24
163.52	29.724	4.69
163.79	29.808	4.64
168.64	35.730	3.85
173.43	Fusion	
	Series V	
183.27	32.878	2.28
189.47	32.958	4.42
194.62	32.849	4.31
199.52	32.990	4.20
204.37	32.846	4.11
209.24	32.775	4.03
214.51	32.869	4.42
	Series IV	
80.76	15.892	4.22
85.98	16.441	4.52
98.65	17.844	4.52
123.11	19.982	4.75
128.00	20.277	4.55

to trichloroborane to remove all trace of water which might otherwise have reacted with the compound being studied. B_2Cl_4 (19.7284 g. or 0.12069 mole) was condensed into the calorimeter from a −22.9° bath (melting carbon tetrachloride). (This precaution prevented liquid B_2Cl_4 from exposure to room temperature during the relatively long period required for introduction into the calorimeter.) The heat capacity measurements, taken from 13.42 to 214.51°K., are listed in Table I. As a result of the relatively small sample used, the accuracy was less than is usual with the calorimeter employed; it is estimated that the heat capacities are accurate to ±0.5%. Table II gives the values of the heat capacities interpolated from the data for rounded values of the absolute temperature.

TABLE II

ROUNDED VALUES OF THE HEAT CAPACITIES OF DIBORON TETRACHLORIDE

T (°K.)	C_p (cal./deg./mole)	T (°K.)	C_p (cal./deg./mole)
12	1.150	90	16.955
14	1.730	95	17.470
16	2.400	100	17.965
18	3.140	105	18.445
20	3.910	110	18.915
22	4.700	115	19.355
24	5.490	120	19.760
26	6.250	125	20.160
28	6.970	130	20.565
30	7.630	135	21.010
32	8.250	140	21.490
34	8.815	145	21.985
36	9.330	150	22.490
38	9.815	155	23.000
40	10.255	160	23.525
42	10.670	165	24.010
44	11.055	170	24.480
46	11.400	175	24.945
48	11.730	180	32.945
50	12.030	185	32.935
55	12.695	190	32.930
60	13.310	195	32.930
65	13.930	200	32.915
70	14.590	205	32.895
75	15.230	210	32.865
80	15.840	215	32.860
85	16.410	220	32.860

The Heat of Fusion.—The data were taken with the same sample in the same calorimeter using the usual methods. Results are presented in Table III.

The Melting Point and Purity. The melting point and purity of the sample were determined in the conventional manner. The equilibrium temperatures of solid and liquid B_2Cl_4 were observed over a period of ten hours with various fractions of the sample melted, as estimated from the heat input and heat of fusion. The concentration of liquid-soluble, solid-insoluble impurity was found to be 1.50 mole %. Table IV summarizes the data on the melting point, which was estimated as 180.21°K.

TABLE III

HEAT OF FUSION OF DIBORON TETRACHLORIDE

(0.12069 mole used)

Temp. interval (°K.)	Heat input (cal.)	Correction (cal.)	ΔH fusion (cal./mole)
172.419 to 183.025	392.065	81.403	2574.1
173.527 to 182.085	369.617	57.545	2585.8
173.424 to 182.274	372.540	61.569	2576.7
173.218 to 181.848	371.000	59.409	2581.9

Av. = 2579 ± 4 cal./mole

TABLE IV

MELTING POINT OF DIBORON TETRACHLORIDE

Total time (min.)	Heat input (cal.)	$\int C_p\,dT$	% Melted	T, °K.
18	36.03	28.16	5.9	174.817
58	37.31	19.56	11.6	177.008
109	36.97	11.38	19.9	178.315
156	44.65	6.52	32.1	179.044
242	45.52	3.29	45.7	179.400
364	52.56	1.91	62.0	179.605
580	56.84	1.21	79.8	179.752

Estimated m.p. = 180.21°K.
Purity = 98.50 mole %

Acknowledgment.—The authors are grateful to Professor J. G. Aston for making available the calorimetric apparatus used in this research and for his coöperation and assistance in carrying out the investigations. The support of the Office of Scientific Research, Air Research and Development Command, is also gratefully acknowledged.

THE MERCURY PHOTOSENSITIZED DECOMPOSITION OF ETHYLENIMINE[1]

BY C. LUNER[2] AND H. GESSER

Contribution from the Department of Chemistry, Illinois Institute of Technology, Chicago, Illinois, and Department of Chemistry, University of Manitoba, Winnipeg, Canada

Received May 5, 1958

The reaction of methyl radicals with ethylenimine[3] has shown that the abstraction reaction

$$CH_3 + CH_2{-}CH_2 \longrightarrow CH_4 + CH_2{-}CH_2 \quad (1)$$
$$\qquad\quad \diagdown\,\diagup \qquad\qquad\qquad\quad \diagdown\,\diagup$$
$$\qquad\quad NH \qquad\qquad\qquad\quad N$$

has a very low (4.8 kcal./mole) activation energy. The reactions postulated for the disappearance of the ethylenimino radical were

$$2CH_2{-}CH_2 \longrightarrow 2C_2H_4 + N_2 \quad (2)$$
$$\qquad\quad \diagdown\,\diagup$$
$$\qquad\quad N$$

$$2CH_2{-}CH_2 \longrightarrow (CH_2)_2NN(CH_2)_2 \quad (3)$$
$$\qquad\quad \diagdown\,\diagup$$
$$\qquad\quad N$$

The present work was undertaken since it was thought that the mercury photosensitized decomposition of ethylenimine would permit a study of some of the reactions of the ethylenimino radical.

The apparatus was of the conventional high vacuum type, with an ultimate vacuum of about 2×10^{-6} mm. The cell was cylindrical in form, 80 mm. long and 50 mm. in diameter, and was constructed of fused quartz and plane parallel quartz windows 2 mm. thick. A mercury reservoir, attached to the cell, was kept at room temperature. The gas was circulated by means of a glass enclosed iron propeller driven by a magnetic stirrer.

A mercury rare gas resonance lamp was used as the light source. The lamp was enclosed in a box and was operated by a 6000 V neon sign transformer with a variable transformer in the primary circuit. A constant voltage transformer also was used in the primary circuit to minimize line fluctuations. The light beam was roughly collimated and filtered by a Corning filter No. 9863. The effective radiation was restricted to the 2537 Å. resonance line. The incident intensity was determined to be 2.2×10^{-6} einsteins/min. using propane as the actinometer.[4]

The reaction system consisted of a cell, mercury reservoir kept at room temperature and a small U-trap. The reaction system was isolated from the apparatus by two mercury cut-offs, one of which led to a Le Roy[5] still and a calibrated volume which was used to measure the products condensable at the temperature of liquid nitrogen. The second cut-off led to an automatic toepler pump and a second calibrated volume to measure the products non-condensable at liquid nitrogen temperature.

The ethylenimine was prepared by Dr. Paul Fanta of this Laboratory and had a b.p. range of 55.5–55.7°. Mass spectrometric analysis indicated that it contained 99.0% ethylenimine, 0.8% propylenimine and 0.2% butylenimine. The ethylenimine was degassed prior to each use and was isolated from the apparatus by a mercury cut-off, and entered the reaction cell through a Fugassi valve. The initial pressure of the ethylenimine in the cell was measured with a mercury manometer.

The products were fractionated, measured and then analyzed by a Consolidated Mass Spectrometer.

Results and Discussion

The products obtained from the mercury photosensitized decomposition of ethylenimine were mainly hydrogen (70-75 mole %) and nitrogen (20-30 mole %) with smaller amounts (2-3 mole %) of methane in the fraction non-condensable at liquid nitrogen temperature and essentially ethylene (93-97 mole %) with small amounts of ethane, propane, acetylene and butene in the condensable fraction volatile above −100°.

The rates of formation of the principal products volatile above −100° at 123 mm. pressure of ethylenimine were within experimental error essentially independent of reaction time. These results are recorded in Table I.

TABLE I

THE PHOTOSENSITIZED DECOMPOSITION OF ETHYLENIMINE

Pressure of ethylenimine, 123 ± 2 mm.

Time, min.	$R_{C_2H_4}$	$R_{C_2H_6}$	$R_{C_3H_8}$	$R_{C_2H_2}$	R_{N_2}	R_{H_2}	R_{CH_4}
			micromoles per min.				
3.0	0.83	0.011		0.0057	0.197	1.23	0.028
6.0	1.12	.020	.0070	.0058	.28	1.10	.026
7.5	1.17	.027	.006	.0073			
10.5	1.14	.026	.0047	.0024			
15.0	1.37	.045	.0114	.0042	.346	1.03	.031
15.0	1.11	.037	.0082	.0012	.376	1.00	.032

The results showing the effect of pressure on the rates of formation of the principal products, nitrogen, hydrogen and ethylene are shown in Fig. 1. The data for reactant pressures of 25, 123 and 185 mm. are each the average of two experiments.

During the course of a reaction, a white opaque non-volatile material was deposited on the walls of the cell. This polymer was soluble in water and acetone and was removed prior to each experiment.

The results of a few experiments at 175° showed no appreciable difference in the products from those obtained at 27°.

Mass spectrometric analysis of the liquid reactant and products showed the presence of ammonia, hydrogen cyanide and a mass peak of 84 which is attributed to the dimer of the ethylenimino radical. The yields of these products ranged from 0.5 to 3

(1) This work was performed at the Illinois Institute of Technology and supported by Contract N7onr32912 with the Office of Naval Research, United States Navy.

(2) United States Steel Corporation, Applied Research Laboratory, Monroeville, Pennsylvania.

(3) R. K. Brinton and D. H. Volman, *J. Chem. Phys.*, **20**, 25 (1952).

(4) S. Bywater and E. W. R. Steacie, *ibid.*, **19**, 319 (1951).

(5) D. J. Le Roy, *Can. J. Res.*, **B28**, 492 (1950).

mole %. The total extent of decomposition was of the order of 3%, indicating that these products may be of principal importance.

Two experiments in a flow system at 125 mm. pressure of ethylenimine gave distribution of products similar to that obtained in the static system.

The fact that both ethylene and hydrogen are major products would seem to indicate that they are formed in the primary photodecomposition process. The approximate equality of the rates of formation of these two products is difficult to account for stoichiometrically. Energetically, some of the more probable primary processes are

$$\begin{array}{l}CH_2{-}CH_2 \\ \quad\diagdown\diagup \\ \quad NH\end{array} + Hg(^3P_1) \longrightarrow \begin{array}{l}CH_2{-}CH_2 \\ \quad\diagdown\diagup \\ \quad\ N\end{array} + H + Hg(^1P_0) \quad (4)$$

$$\begin{array}{l}CH_2{-}CH_2 \\ \quad\diagdown\diagup \\ \quad NH\end{array} + Hg(^3P_1) \longrightarrow CH_2{=}CH_2 + NH + Hg(^1P_0) \quad (5)$$

$$\begin{array}{l}CH_2{-}CH \\ \quad\diagdown\diagup \\ \quad NH\end{array} + Hg(^3P_1) \longrightarrow \begin{array}{l}CH_2{-}CH \\ \quad\diagdown\diagup \\ \quad\ NH\end{array} + H + Hg(^1P_0) \quad (6)$$

A primary split at the N–H bond has been postulated[6] for both the photolysis and mercury photosensitized decomposition of methylamine, and together with reaction 6 can account for the presence of hydrogen by the reaction

$$\begin{array}{l}CH_2{-}CH_2 \\ \quad\diagdown\diagup \\ \quad NH\end{array} + H \longrightarrow \begin{array}{l}CH_2{-}CH_2 \\ \quad\diagdown\diagup \\ \quad\ N\end{array} + H_2 \quad (7)$$

or

$$\begin{array}{l}CH_2{-}CH_2 \\ \quad\diagdown\diagup \\ \quad NH\end{array} + H \longrightarrow \begin{array}{l}CH_2{-}CH \\ \quad\diagdown\diagup \\ \quad\ NH\end{array} + H_2 \quad (7a)$$

Reaction 5 may possibly occur in two steps

$$\begin{array}{l}CH_2{-}CH_2 \\ \quad\diagdown\diagup \\ \quad NH\end{array} + Hg(^3P_1) \longrightarrow CH_2{-}CH_2{-}NH + Hg(^1P_0)$$

$$CH_2{-}CH_2{-}NH \longrightarrow CH_2{=}CH_2 + NH$$

The presence of ammonia indicates that reaction 5 occurs. Ammonia probably is formed by the consecutive hydrogen abstraction by the imine radical since the reaction of the imine radical with ethylene[7] has shown the prevalence of a hydrogen abstraction reaction.

Both hydrogen cyanide and methane were obtained as the principal products of the reaction of hydrogen atoms with ethylenimine.[8] The reaction sequence proposed to account for these products was reaction 7 followed by

$$\begin{array}{l}CH_2{-}CH_2 \\ \quad\diagdown\diagup \\ \quad\ N\end{array} \longrightarrow HCN + CH_3 \quad (8)$$

and methane is formed by the subsequent hydrogen abstraction reaction by the methyl radical, such as reaction 1. This is consistent with the results obtained in the present investigation.

The ethylene, nitrogen and ethylenimine dimer can be adequately accounted for by reactions 2, 3 and 5. The polymer probably is formed by radical addition reactions to ethylenimine.

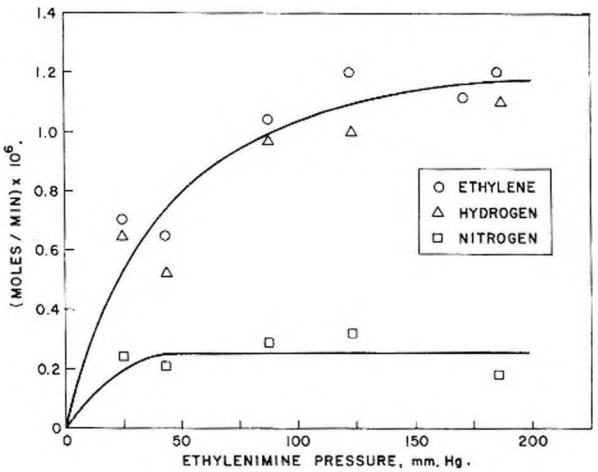

Fig. 1.—Effect of pressure on the rate of formation of ethylene, hydrogen and nitrogen.

(6) O. C. Whetmore and H. A. Taylor, *J. Chem. Phys.*, **12**, 61 (1944); J. S. Watson and B. de B. Darwent, *ibid.*, **20**, 1041 (1952); C. I. Johnson and H. A. Taylor, *ibid.*, **19**, 613 (1951).

(7) F. O. Rice and M. Freamo, *J. Am. Chem. Soc.*, **73**, 5529 (1951).

(8) J. W. S. Jamieson and C. A. Winkler, THIS JOURNAL, **60**, 1542 (1956).

EVIDENCE ON THE NATURE OF BISMUTH (I) CHLORIDE FORMED BY SOLUTION OF BISMUTH IN BISMUTH(III) CHLORIDE[1]

BY JOHN D. CORBETT

Institute for Atomic Research and Department of Chemistry, Iowa State College, Ames, Iowa

Received May 8, 1958

The Bi-$BiCl_3$ system has been a subject of considerable interest with regard to the phenomena of the apparent solution of certain metals in their molten halides.[2-5] An interpretation of these solutions has been presented in terms of the formation of slightly stable subhalides in dilute solution,[5] and in some cases such lower halides have been isolated as complexes with a strong Lewis acid.[6] The Bi-$BiCl_3$ system, however, represents a case in which the lower halide is sufficiently stable to separate as a solid phase; the phase diagram shows the new compound is stable up to about 323°, at which temperature it decomposes into two liquid phases of the approximate compositions $BiCl_{1.64}$ and $BiCl_{0.075}$.[7] This subhalide recently has been isolated and identified as bismuth(I) chloride.[8] Furthermore, the relatively small depression of the freezing point of $BiCl_3$ by added metal[7] can be accounted for very well if the solute is taken to be $(BiCl)_4$.[8]

(1) Contribution No. 640. Work was performed in the Ames Laboratory of the U. S. Atomic Energy Commission.

(2) D. D. Cubicciotti and C. D. Thurmond, *J. Am. Chem. Soc.*, **71**, 2149 (1949).

(3) D. Cubicciotti, *ibid.*, **74**, 1198 (1952).

(4) J. D. Corbett and S. von Winbush, *ibid.*, **77**, 3964 (1955).

(5) J. D. Corbett, S. von Winbush and F. C. Albers, *ibid.*, **79**, 3020 (1957).

(6) J. D. Corbett and R. K. McMullan, *ibid.*, **78**, 2906 (1956).

(7) T. I. Sokolova, *Issest. Sektora Fiz-Khim. Anal., Inst. Obshchei Neorg. Khim., Akad. Nauk SSSR*, **21**, 159 (1952), AEC translation No. 3168.

(8) J. D. Corbett, *J. Am. Chem. Soc.*, **80**, 4757 (1958).

Unpublished freezing point depression measurements on these solutions[9] are in substantial agreement with the phase diagram.

Recently Cubicciotti, Keneshea and Kelley[10] have reported data on the vapor pressure of $BiCl_3$ over Bi–$BiCl_3$ solutions as a function of composition at 301, 356 and 392°. From the temperature dependence of trichloride activity (P/P_0) at constant composition and the activity, and without any presumption as to the nature of the solute, the solvent was found to behave nearly ideally in the concentration range of zero to greater than 0.2 mole fraction of added bismuth. This is indicated by the fact that the calculated partial molar enthalpies and entropies of the trichloride, relative to the pure liquid, were less than 100 cal. and 0.15 e.u., respectively, over this range.[11] However, marked positive deviations from Raoult's law were found when the activities of the solvent were compared to those calculated for a monatomic solution of metal.[12] Although it was noted that the data could by explained by the assumption of a mixture of polymers of Bi (or Bi^+ or Bi^{+2}) these possibilities were discarded; rather the deviations were considered reasonable in view of the fact that the Bi–$BiCl_3$ system shows a considerable area of immiscibility (in the metal-rich region). However, this explanation avoids the reasons for the rather large apparent solubility of metal in the molten trichloride and directly contradicts the separation of a solid monochloride below about 323°, since in this case the solvent should show negative deviation on the basis of a simple solution of the components.

It is actually possible to explain the reported vapor pressure data at the lower temperatures in terms of a much simpler system, the formation of essentially ideal solutions of Bi_4Cl_4 in $BiCl_3$. Table I shows the excellent agreement between the mole fraction $BiCl_3$ calculated on this basis and the observed activity of $BiCl_3$ at 301°. The vapor pressure data were taken directly from the curve drawn through the experimental points[10]; the data are less certain in the region corresponding to the last composition. The differences are well within the reported experimental errors; deviations from ideality seven times larger are found if the solute is taken to be the BiCl trimer. The data at 356° can be treated in a similar manner if the point at $N_{Bi} = 0.26$ is taken to be in error. The results at the highest temperature, 392°, are not fit as well; this may not be too surprising since, as suggested by Yosim,[13] a different solution process probably must be invoked ultimately in order to account for the complete miscibility present in the system at higher temperatures. However, at lower temperatures the system can be interpreted as a solution of $(BiCl)_4$ in $BiCl_3$, essentially ideal with respect to the trichloride, in agreement with the observed solution thermodynamics. The possibility that bismuth–bismuth bonds may account for the dia magnetism of the monochloride[5,6] is currently being investigated.

TABLE I

ACTIVITY *vs.* MOLE FRACTION OF $BiCl_3$ BASED ON THE SOLUTE Bi_4Cl_4

Apparent N_{BiCl_3}	Vapor pressure mm., 301°	Obsd. activity p/p_0	Calcd. N_{BiCl_3}
1.000	31.8	(1.00)	(1.00)
0.950	31.0	0.97_5	0.980
.900	30.4	$.95_6$	.958
.850	29.7	$.93_4$	.932
.800	28.8	$.90_6$	.903
.750	27.6_5	$.87_0$	.870
.700	25.9	$.81_4$	.830

(9) S. J. Yosim and S. W. Mayer, U. S. Atomic Energy Commission Report No. NAA-SR-2124, Semiannual Progress Report, Jan.–June 1957, p. 19. ADDED IN PROOF.—The molar heat of fusion used[8] (2.6 kcal.) may be quite low (S. Yosim, private communication). If so, the degree of polymerization of BiCl will be lower, and the solvent will show slight positive deviation.

(10) D. Cubicciotti, F. J. Keneshea and C. M. Kelley, THIS JOURNAL, **62**, 463 (1958). A copy of the original manuscript was kindly furnished by Dr. Dan Cubicciotti.

(11) Ref. 10, Figs. 4 and 5. A consideration of the ideal entropy of mixing depends on the nature of the solute.

(12) Ref. 10, Fig. 3.

(13) S. Yosim, A. Darnell and W. Gehman, Abstracts of Papers, ACS Meeting, New York, N. Y., Sept. 1957, p. 8-N.

THE SYSTEM OF 2-PYRROLIDONE–WATER

BY L. JAY LOHR[1]

Contribution from the Central Research Laboratory of General Aniline and Film Corporation, Easton, Pennsylvania

Received May 19, 1958

It was observed in this Laboratory that certain concentrations of aqueous 2-pyrrolidone have a higher freezing point than pure 2-pyrrolidone. Tafel and Stern[2] found that 2-pyrrolidone forms a monohydrate which has a melting point of 29.3–30.6° and a freezing point of 29.7–29.9° but report that another observer found these constants to be 35°. A complete phase study was undertaken to confirm the formation of a monohydrate of 2-pyrrolidone and to determine whether 2-pyrrolidone forms hydrates other than the monohydrate.

Experimental

Material.—The 2-pyrrolidone for this phase study was purified by fractional distillation and repeated crystallization until its freezing point could not be increased. After purification, the product contained negligible water and analyzed 100%. The purified sample was analyzed by basic hydrolysis with a known quantity of excess, standard, aqueous sodium hydroxide and titration of the unreacted,

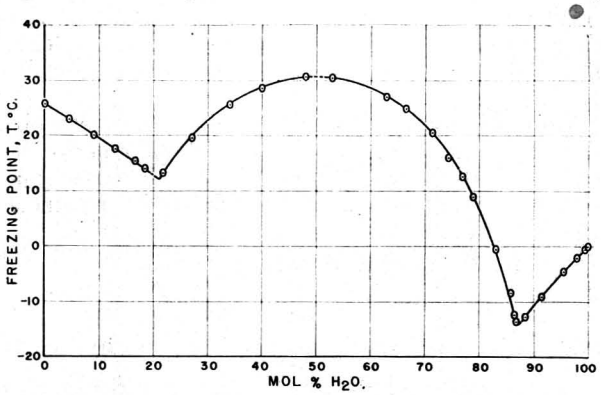

Fig. 1.—Phase diagram 2-pyrrolidone–H_2O.

(1) E. I. du Pont de Nemours & Co., Eastern Laboratory, Gibbstown, New Jersey.

(2) J. Tafel and M. Stern, *Ber.*, **33**, 2224 (1900).

excess base. The purity of the sample was calculated from the moles of sodium hydroxide consumed in the hydrolysis.

Anal. Calcd. for C_4H_7ON: C, 56.44; H, 8.30; N, 16.46. Found: C, 56.51; H, 8.42; N, 16.44.

Apparatus.—The freezing points were determined in a conventional apparatus which is described elsewhere.[3] The temperatures were measured with a ten-junction, calibrated thermopile[4] and were recorded automatically. Calibration of the thermopile itself[5] and calibration of the thermopile and recording device at the freezing point of triple-distilled mercury indicate that the instrument is accurate to about 0.03°. Actual freezing points of aqueous pyrrolidone solutions given in Table I are accurate to ±0.1° and the extrapolated eutectic points (Fig. 1) are estimated to be accurate to ±1°. The freezing points of 2-pyrrolidone and pyrrolidone monohydrate are estimated to be accurate to ±0.1°.

2-Pyrrolidone–Water Solutions.—The various solutions were made by weighing to the nearest milligram the 2-pyrrolidone and the water. Approximately 50 ml. of the known solution was transferred to the cell for the freezing point determination. The freezing points and mole % H_2O of the various solutions are given in Table I and a plot of the data is shown in Fig. 1.

TABLE I

FREEZING POINTS OF AQUEOUS PYRROLIDONE SOLUTIONS

F.p., °C.	Mole % H_2O	F.p., °C.	Mole % H_2O
25.57	0.0	20.3	71.3
22.8	4.6	16.0	74.4
20.0	9.1	12.6	76.9
17.6	13.0	8.8	78.9
15.2	16.7	− 0.5	83.1
13.9	18.5	− 8.5	85.7
13.1	21.7	−12.4	86.4
19.5	27.2	−13.7	86.9
25.4	34.0	−12.8	88.5
28.4	39.9	− 9.1	91.4
30.4	48.1	− 4.4	95.5
30.3	52.8	− 2.0	98.0
26.9	62.9	− 0.5	99.6
24.7	66.5	0.0	100.0

Discussion

The phase diagram (Fig. 1) shows that 2-pyrrolidone and water form only a monohydrate confirming the work of Tafel and Stern.[2] The freezing point of the monohydrate is 30.4°, and the eutectic points of the phase system are estimated to be 12 and −14°.

Acknowledgment.—I am indebted to Dr. L. T. Hallett who encouraged me to undertake this study and to Mr. R. C. Rheinhart who made the solutions and determined their freezing points.

(3) A. R. Glasgow, Jr., A. J. Streiff and F. D. Rossini, *J. Research Natl. Bur. Standards*, **35**, 355 (1945).

(4) J. B. Hickman, *J. Chem. Educ.*, **25**, 163 (1948).

(5) R. B. Scott, "Temperature, Its Measurement and Control in Science and Industry," American Institute of Physics, Reinhold Publ. Corp., New York, N. Y., 1941, p. 212 ff.

PROTON NUCLEAR RESONANCE SPECTROSCOPY. I. RELIABLE SHIELDING VALUES BY "INTERNAL REFERENCING" WITH TETRAMETHYLSILANE

BY GEORGE VAN DYKE TIERS

Contribution No. 182, Central Research Dept., Minnesota Mining and Manufacturing Co., St. Paul 6, Minnesota

Received June 16, 1958

Tetramethylsilane, a highly soluble volatile liquid which is magnetically isotropic, non-associative and chemically unreactive, appears particularly suitable as a homogeneous "internal reference" for proton nuclear spin resonance (n.s.r.) spectroscopy. Its sharp peak falls beyond the usual spectral region (more shielded) and is readily identified. Shielding values ("chemical shifts") so measured in CCl_4 solution are highly reproducible, are commonly independent of temperature or concentration and agree closely with the most precise and reliable published "externally referenced" measurements, the latter having been obtained by extrapolation to infinite dilution in CCl_4.[1,2] In Table I the equivalence of the two techniques is made clear.[3]

TABLE I

A DEMONSTRATION OF THE EQUIVALENCE OF "SINGLE PHASE" AND "EXTRAPOLATED TWO PHASE"[a] REFERENCING TECHNIQUES FOR THE PRECISE MEASUREMENT OF THE PROTON NUCLEAR RESONANCE SHIELDING VALUE, τ[b]

Compound	"Extrapolated two-phase"[a] τ (p.p.m.)[b]	"Single-phase" τ (p.p.m.)[b]	Vol. % concn. in CCl_4
Benzene	2.74[c]	2.734 ± 0.003	2.0
$C_6H_5C_2H_5$	2.89[c]	2.888 ± .002	5
$(C_6H_5CH_2)_2$	2.89[c]	2.893 ± .001	5
p-$C_6H_4(CH_3)_2$	3.05[c]	3.053 ± .003	5
Cycloöctatetraene	4.26[c]	4.309 ± .004	3.0
CH_3NO_2	5.69[d]	5.720 ± .002	2.0
$C_6H_5OCH_3$	6.31[d]	6.266 ± .002	6.0
CH_3OH	6.60[d]	6.622 ± .002	1.0
$(C_6H_5CH_2)_2$	7.13[c]	7.129 ± .001	5
$C_6H_5CH_2CH_3$	7.42[c]	7.382 ± .003	5
$C_6H_5CH_3$	7.67[d]	7.663 ± .003	2.0
Acetic anhydride	7.81[d]	7.809 ± .003	3.0
Methyl iodide	7.81[d]	7.843 ± .004	2.0
Acetone	7.91[d]	7.915 ± .003	3.0
CH_3CO_2H	7.90[d]	7.930 ± .004	6.0
Acetonitrile	8.10[d]	8.026 ± .002	3.0
Cyclohexane	8.51[e]	8.564 ± .002	1.0

[a] Shielding-value measurements made at two or more concentrations in CCl_4 are extrapolated to zero concentration. By this procedure the magnetic susceptibility correction is rendered constant. [b] τ (in p.p.m.) = [10.000 − 10^6 $(\nu_{obs.} - \nu_{Me_4Si})/\nu_{Me_4Si}$] = [10.000 − 10^6 $(H_{Me_4Si} - H_{obs.})/H_{Me_4Si}$]. Increasing values of τ signify increasing shielding of the proton. Error values are standard deviations for the measurements. [c] Data of ref. 1, converted to τ-values by sign reversal and addition of 5.24 p.p.m.; error (standard deviation) is ±0.033 p.p.m. for eight remeasured values. [d] Data of ref. 2, expressed in p.p.m. (40.00 mc./sec. frequency assumed) and converted to τ-values by addition of 5.21 p.p.m.; error (standard deviation) is ±0.036 p.p.m. for nine remeasured values.

Conventional n.s.r. equipment was employed, namely, a Varian V-4300-2 40.00 mc./sec. spectrometer with flux stabilizer, sample spinner, audio-oscillator, Hewlett-Packard 522-B frequency counter, and Varian recorder. Sample solutions (½ ml.) containing 1 vol. % Me_4Si (pure grade, Anderson Laboratories, Inc., Weston, Mich.) were sealed in ordinary 5 mm. o.d. "Pyrex" tubes. The sweep was such that 1.0 p.p.m. occupied approx. 100 mm. of chart; peak positions were measured to the nearest tenth of a mm.

(1) J. S. Waugh and R. W. Fessenden, *J. Am. Chem. Soc.*, **79**, 846 (1957).

(2) A. L. Allred and E. G. Rochow, *ibid.*, **79**, 5361 (1957).

(3) For highest reproducibility, shielding value measurements referenced externally by H_2O must be corrected for temperature, about 0.005 p.p.m. being added per 1° rise. Measurements such as those of refs. 1 and 2, if made at 23.0°, are converted to τ-values by addition of 5.207 p.p.m.

relative to "side-band" peaks produced in the recorded spectrum by the audio-oscillator. The frequency separation of the "side-band" from its "parent-peak" was obtained, by direct counting, to ±0.05 c.p.s. The "side-band" from the Me_4Si "parent-peak" thus may be brought very close to the "parent-peak" of the compound under study (or *vice versa*); a separation of 0.3 to 0.5 p.p.m. is convenient. The novel feature of this technique, not previously described, is that after sweeping through a Me_4Si "side-band" and then through the "parent-peak" of the compound, the "side-band" frequency can be changed suddenly to a new value such that a new "side-band" peak is produced in the *same sweep* but on the *other* side of the compound "parent-peak." The peak position is then obtained by simple interpolation between two such Me_4Si "side-band" peaks which are separated by *ca.* 1 p.p.m. Each τ-value reported in this communication is the average of four to twelve interpolations, the sweep direction being routinely alternated to preclude directed error.

Internally referenced measurements made on binary mixtures or on very concentrated solutions appear to be only slightly less reliable.[4] Shielding values so obtained for seventeen sharp peaks[4] were remeasured in dilute CCl_4 solution to ±0.003 by the present technique. The reported values[4] were found to average 0.024 p.p.m. low, with a standard deviation of ±0.045.

In the present research several of the compounds of Table I were re-examined as pure liquids, to which 3% by volume of Me_4Si had been added to provide the internal reference. The values for τ so measured were: CH_3OH, 6.653 ± 0.004; acetone, 7.909 ± 0.003; CH_3CO_2H, 7.934 ± 0.004; CH_3CN, 8.033 ± 0.004; cyclohexane, 8.544 ± 0.004; C_6H_6, 2.841 ± 0.004. In the last-mentioned case the τ-value is significantly higher than that of Table I; such specific medium effects are encountered when aromatic molecules are present in high concentration.[5] Pure nitromethane so studied had τ = 5.640 ± 0.002, the displacement toward lower shielding being attributable to weak hydrogen-bonding; similar effects have been noted for chloroform.[6,7]

Internal referencing is particularly suitable[6] for the study of weak solvent effects, since external referencing requires the making of highly precise magnetic susceptibility corrections; volume susceptibilities are not usually known with the needed accuracy,[5-7] and even when known require an empirical proportionality constant rather than the theoretically-predicted one.[5] Temperature corrections[3] do not appear to be required for measurements referenced internally; for $(C_6H_6CH_2)_2$, upon 20° elevation of temperature, $\tau(CH_2)$ was found to be 7.127 ± 0.006.

The significant advantages of the tetramethylsilane internal referencing technique are enumerated below.

(1) Reliable, temperature-independent τ-values are obtained from a single sample; extrapolation to infinite dilution is not required.

(2) The τ-value definition of spectral position is simple, precise and operational, and is independent of field strength.

(3) The τ-values are positive in sign for virtually all non-acidic protons, and are not complicated by conflicting definitions.[2,4]

(4) Special sample cells are unnecessary.

(5) The tetramethylsilane reference peak lies outside the usual spectral region and is readily identified.

(6) With good precision, τ-values can be obtained in any solvent, or in the absence of solvent (exception: Me_4Si is insoluble in D_2O).

(7) Other precise measurements[1,2,4] are readily converted to τ-values.[3]

(8) Even very small differences in τ-value (*ca.* 0.01 p.p.m.) can be established accurately; examples include distant-group effects and complex formation.

Unfortunately, several recent and otherwise excellent papers have employed unreliable or non-convertible systems of shielding values.[8-11] Such measurements, even though made with great care, cannot be used satisfactorily as reliable shielding values.

An important conclusion to be drawn is that all subsequently reported proton n.s.r. data *should and can easily* be presented in a truly interconvertible system of units; the author prefers τ-values but welcomes data such as those of refs. 1, 2 and 4.

The author thanks George N. Filipovich for excellent maintenance and operation of the n.s.r. equipment.

(4) A. A. Bothner-By and C. Naar-Colin, *J. Am. Chem. Soc.*, **80**, 1728 (1958).

(5) A. A. Bothner-By and R. E. Glick, *J. Chem. Phys.*, **26**, 1647, 1651 (1957).

(6) G. J. Korinek and W. G. Schneider, *Can. J. Chem.*, **35**, 1157 (1957).

(7) L. W. Reeves and W. G. Schneider, *ibid.*, **35**, 251 (1957).

(8) E. J. Corey, *et al.*, *J. Am. Chem. Soc.*, **80**, 1204 (1958).

(9) W. D. Kumler, J. N. Shoolery and F. V. Brutcher, Jr., *ibid.*, **80**, 2533 (1958). Had extrapolation to infinite dilution been done, addition of 3.51 p.p.m. would convert the data exactly to τ-values.

(10) K. L. Rinehart, Jr., *et al.*, *ibid.*, **80**, 503 (1958).

(11) P. Yates and C. D. Anderson, *ibid.*, **80**, 1265 (1958).

AZEOTROPIC DATA

-- Advances in Chemistry Series Volume No. 6

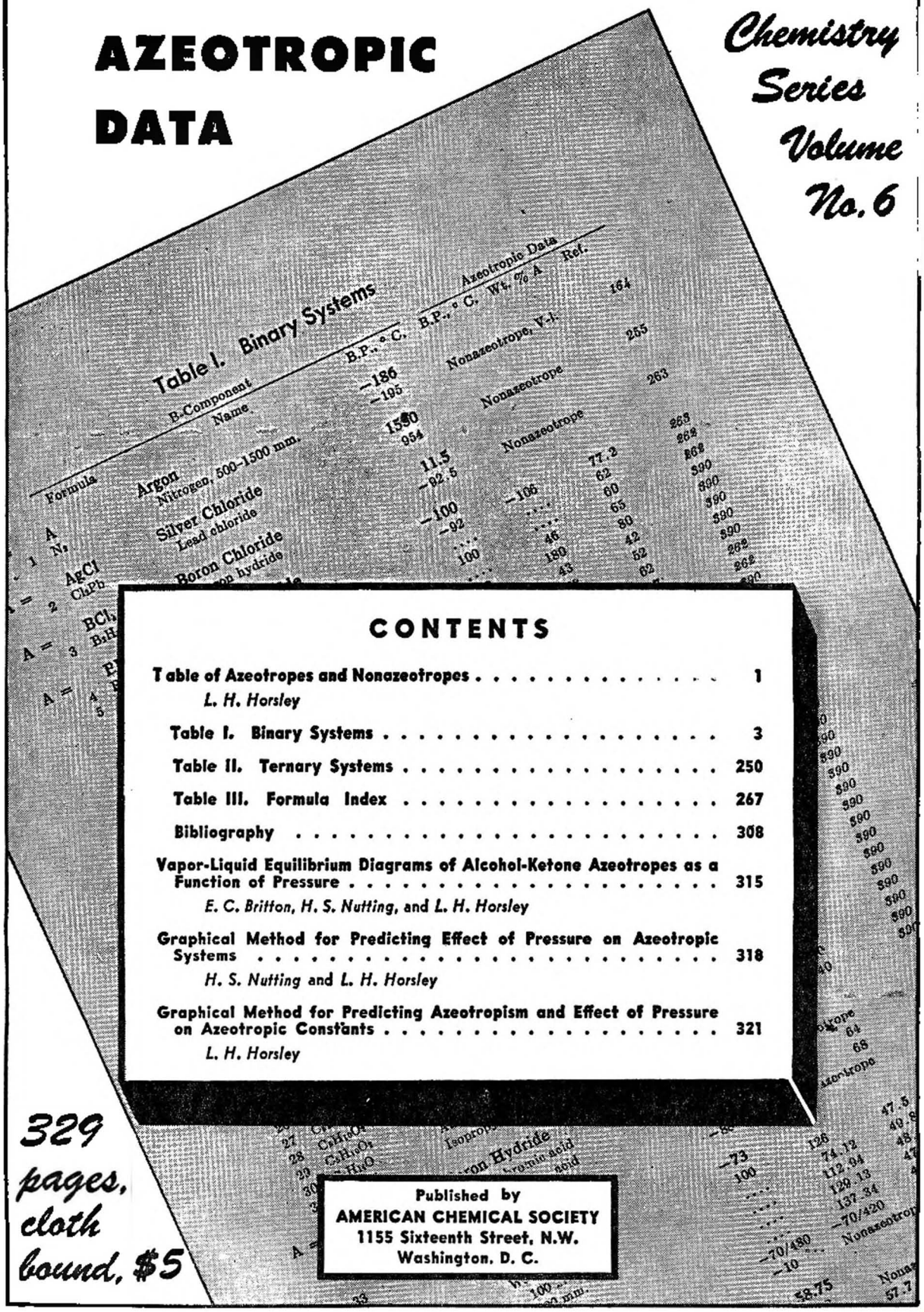

CONTENTS

329 pages, cloth bound, $5

Published by
AMERICAN CHEMICAL SOCIETY
1155 Sixteenth Street, N.W.
Washington, D. C.